UNIVERSIDADE DA BEIRA INTERIOR
Ciências

Study of 3D tumor spheroids for biomedical applications

Elisabete Cristina da Rocha Costa

Tese para obtenção do Grau de Doutor em
Bioquímica
(3º ciclo de estudos)

Orientador: Prof. Doutor Ilídio Joaquim Sobreira Correia

Covilhã, dezembro de 2019

Dedicatory

"Wir halten zusammen
Wir halten einander aus
Wir halten zu einander
Niemand hält uns auf"
Rammstein

To everyone that made a difference in my life…

Acknowledgments

First of all, I would like to thank my supervisor, Dr. Ilídio J. Correia, for the support, guidance and knowledge that I received since the beginning of my master thesis until now, which contributed to improve myself as a person and as a researcher.

I would like to also thank to my work colleagues, especially to the other PhD students (André Moreira, Duarte Diogo and Sónia Miguel) for the friendship, as well as for the support and help. I hope that we will have the time to take coffee in the future.

Furthermore, I would like to thank my family, especially to my parents and sister, and also my friends, for the continuous support, love, care and forgiveness during the last years. I apologize for my absence and distance.

To João Boga, I want to thank deeply for his friendship and love. No matter what, we will be always here for each other. “I look at you and I know it's gonna be a lovely day”.

Moreover, I would like to acknowledge the University of Beira Interior (UBI), in particular the Health Sciences Research Centre (Centro de Investigação em Ciências da Saúde da UBI (CICS-UBI)), for providing me the facilities, the equipment and the resources required to perform this PhD thesis.

Lastly, I would like to express my gratitude to Fundação para a Ciência e a Tecnologia (FCT) for the financial support through the individual PhD fellowship (SFRH/BD/103507/2014), and to the funding from the projects POCI-01-0145-FEDER-007491 and UID/Multi/00709/2013. The funding from CENTRO-01-0145-FEDER-028989 and POCI-01-0145-FEDER-031462 is also acknowledged.

List of Publications

Articles published in peer-reviewed international journals included in this Doctoral thesis

I. **3D tumor spheroids: an overview on the tools and techniques used for their analysis**
Elisabete C. Costa, André F. Moreira, Duarte de Melo-Diogo, Vítor M. Gaspar, Marco P. Carvalho and Ilídio J. Correia
Biotechnology Advances, 2016, 34(8): 1427-1441
DOI: 10.1016/j.biotechadv.2016.11.002
Impact Factor: 12.831
Rank: Q1 and TOP10 Biotechnology & Applied Microbiology (5/162)
Citations: ISI Web of Knowledge: 56; Google Scholar: 74; Scopus: 59

II. **Spheroids Formation on Non-Adhesive Surfaces by Liquid Overlay Technique: Considerations and Practical Approaches**
Elisabete C. Costa, Duarte de Melo-Diogo, André F. Moreira, Marco P. Carvalho and Ilídio J. Correia
Biotechnology Journal, 2017, 13(1): 1700417
DOI: 10.1002/biot.201700417
Impact Factor: 3.543
Rank: Q1 Biochemical Research Methods (18/79); Q2 Biotechnology & Applied Microbiology (46/162)
Citations: ISI Web of Knowledge: 8; Google Scholar: 10: Scopus: 7

III. **Polyethylene glycol molecular weight influences the Clear^{T2} optical clearing method for spheroids imaging by confocal laser scanning microscopy**
Elisabete C. Costa, André F. Moreira, Duarte de Melo-Diogo and Ilídio J. Correia
Journal of Biomedical Optics, 2018, 23(5): 1-11
DOI: 10.1117/1.JBO.23.5.055003
Impact Factor: 2.555
Rank: Q2 Biochemical Research Methods (35/79); Q2 Optics (37/95); Q2 Radiology, Nuclear Medicine & Medical Imaging (52/129)
Citations: ISI Web of Knowledge: 2; Scopus: 2; Google Scholar: 3

IV. **Clear^{T} immersion optical clearing method for intact 3D spheroids imaging through confocal laser scanning microscopy**
Elisabete C. Costa, André F. Moreira, Duarte de Melo-Diogo and Ilídio J. Correia
Optics & Laser Technology, 2018, 106: 94-99
DOI: 10.1016/j.optlastec.2018.04.002
Impact Factor: 3.319
Rank: Q1 Optics (21/95); Q2 Physics, Applied (38/148)
Citations: ISI Web of Knowledge: 5; Scopus: 5; Google Scholar: 5

V. **3D tumor spheroids as in vitro models to mimic in vivo human solid tumors resistance to therapeutic drugs**
Ana S. Nunes*, Andreia S. Barros*, Elisabete C. Costa*, André F. Moreira and Ilídio J. Correia
*Authors contributed equally to the work
Biotechnology and Bioengineering, 2018, 116(1): 206–226
DOI: 10.1002/bit.26845
Impact Factor: 4.260
Rank: Q1 Biotechnology & Applied Microbiology (30/162)
Citations: ISI Web of Knowledge: 2; Scopus: 2; Google Scholar: 3

VI. **Optical clearing methods: an overview of the techniques used for the imaging of 3D spheroids**
Elisabete C. Costa*, Daniel N. Silva*, André F. Moreira and Ilídio J. Correia
*Authors contributed equally to the work
Biotechnology and Bioengineering, 2019, 116: 2742– 2763
Impact Factor: 4.260
Rank: Q1 Biotechnology & Applied Microbiology (30/162)
Citations: ISI Web of Knowledge: 0; Scopus: 0; Google Scholar: 0

Articles published in peer-reviewed international journals not included in this Doctoral thesis

I. **Evaluation of Nanoparticle Uptake in Co-culture Cancer Models**
Elisabete C. Costa, Vítor M. Gaspar, João G. Marques, Paula Coutinho and Ilídio J. Correia
PLOS ONE, 2013, 8(7): e70072
DOI: 10.1371/journal.pone.0070072
Impact Factor: 2.776
Rank: Q2 Multidisciplinary Sciences (24/69)
Citations: ISI Web of Knowledge: 27; Scopus: 26; Google Scholar: 37

II. **Synthesis and characterization of micelles as carriers of non-steroidal anti-inflammatory drugs (NSAID) for application in breast cancer therapy**
João G. Marques, Vítor M. Gaspar, Elisabete C. Costa, Catarina M. Paquete and Ilídio J. Correia
Colloids and Surfaces B: Biointerfaces, 2014, 113: 375-383
DOI: 10.1016/j.colsurfb.2013.09.037
Impact Factor: 3.973
Rank: Q1 Biophysics (15/72); Q2 Chemistry, Physical (49/148); Q2 Materials Science, Biomaterials (11/32)
Citations: ISI Web of Knowledge: 14; Scopus: 16; Google Scholar: 24

III. **Optimization of Liquid Overlay Technique to Formulate Heterogenic 3D Co-Cultures Models**
Elisabete C. Costa, Vítor M. Gaspar, Paula Coutinho and Ilídio J. Correia
Biotechnology and Bioengineering, 2014, 111(8): 1672-1685
DOI: 10.1002/bit.25210
Impact Factor: 4.260
Rank: Q1 Biotechnology & Applied Microbiology (30/162)
Citations: ISI Web of Knowledge: 40; Scopus: 40; Google Scholar: 52

IV. **Co-delivery of Sildenafil (Viagra ®) and Crizotinib for Synergistic and Improved Anti-tumoral Therapy**
João G. Marques, Vítor M. Gaspar, David Markl, Elisabete C. Costa, Eugénia Gallard and Ilídio J. Correia
Pharmaceutical Research, 2014, 31(9): 2516–2528
DOI: 10.1007/s11095-014-1347-x
Impact Factor: 3.896
Rank: Q1 Pharmacology & Pharmacy (54/267); Q2 Chemistry, Multidisciplinary (52/172)
Citations: ISI Web of Knowledge: 14; Scopus: 15; Google Scholar: 19

V. **Poly (2-ethyl-2-oxazoline)-PLA-g-PEI Amphiphilic Triblock Micelles for Co-delivery of Minicircle DNA and Chemotherapeutics**
Vítor M. Gaspar, Cristine Gonçalves, Duarte de Melo-Diogo, Elisabete C. Costa, João A. Queiroz, Chantal Pichon, Fani Sousa and Ilídio J.Correia
Journal of Controlled Release, 2014, 189: 90-104
DOI: 10.1016/j.jconrel.2014.06.040
Impact Factor: 7.901
Rank: Q1 Chemistry, Multidisciplinary (22/172); Q1 and TOP10 Pharmacology & Pharmacy (9/267)
Citations: ISI Web of Knowledge: 56; Scopus: 60; Google Scholar: 69

VI. **Preparation of end-capped pH-sensitive mesoporous silica nanocarriers for on-demand drug delivery**

André F. Moreira, Vítor M. Gaspar, Elisabete C. Costa, Duarte de Melo-Diogo, Paulo Machado, Catarina M. Paquete and Ilídio J. Correia

European Journal of Pharmaceutics and Biopharmaceutics, 2014, 88(3): 1012-1025

DOI: 10.1016/j.ejpb.2014.09.002

Impact Factor: 4.708

Rank: Q1 Pharmacology & Pharmacy (28/267)

Citations: ISI Web of Knowledge: 26; Scopus: 30; Google Scholar: 32

VII. **Combinatorial delivery of Crizotinib-Palbociclib-Sildenafil using TPGS-PLA micelles for improved cancer treatment**

Duarte de Melo-Diogo, Vítor M. Gaspar, Elisabete C. Costa, André F. Moreira, David Oppolzer, Eugénia Gallardo and Ilídio J. Correia

European Journal of Pharmaceutics and Biopharmaceutics, 2014, 88(3): 718-729

DOI: 10.1016/j.ejpb.2014.09.013

Impact Factor: 4.708

Rank: Q1 Pharmacology & Pharmacy (28/267)

Citations: ISI Web of Knowledge: 29; Scopus: 34; Google Scholar: 38

VIII. **Folate-Targeted Multifunctional Amino Acid-Chitosan Nanoparticles for Improved Cancer Therapy**

Vítor M. Gaspar, Elisabete C. Costa, João A. Queiroz, Chantal Pichon, Fani Sousa and Ilídio J. Correia

Pharmaceutical Research, 2015, 32(2): 562-577

DOI: 10.1007/s11095-014-1486-0

Impact Factor: 3.896

Rank: Q1 Pharmacology & Pharmacy (54/267); Q2 Chemistry, Multidisciplinary (52/172)

Citations: ISI Web of Knowledge: 33; Scopus: 34; Google Scholar: 39

IX. **Bioreducible poly(2-ethyl-2-oxazoline)-PLA-PEI-SS triblock copolymer micelles for co-delivery of DNA minicircles and Doxorubicin**

Vítor M. Gaspar, Patrick Baril, Elisabete C. Costa, Duarte de Melo-Diogo, Frédéric Foucher, João A. Queiroz, Fani Sousa, Chantal Pichon and Ilídio J. Correia

Journal of Controlled Release, 2015, 213: 175-191

DOI: 10.1016/j.jconrel.2015.07.011

Impact Factor: 7.901

Rank: Q1 Chemistry, Multidisciplinary (22/172); Q1 and TOP10 Pharmacology & Pharmacy (9/267)

Citations: ISI Web of Knowledge: 42; Scopus: 46; Google Scholar: 53

X. **Gas-generating TPGS-PLGA microspheres loaded with nanoparticles (NIMPS) for co-delivery of minicircle DNA and anti-tumoral drugs**
Vítor M. Gaspar, André F. Moreira, Elisabete C. Costa, João A. Queiroz, Fani Sousa, Chantal Pichon and Ilídio J. Correia
Colloids and Surfaces B: Biointerfaces, 2015, 134: 287-294
DOI: 10.1016/j.colsurfb.2015.07.004
Impact Factor: 3.973
Rank: Q1 Biophysics (15/72); Q2 Chemistry, Physical (49/148); Q2 Materials Science, Biomaterials (11/32)
Citations: ISI Web of Knowledge: 26; Scopus: 29; Google Scholar: 31

XI. **Minicircle DNA Vectors for Gene Therapy: Advances and Applications**
Vítor M. Gaspar, Duarte de Melo-Diogo, Elisabete C. Costa, André F. Moreira, João A. Queiroz, Chantal Pichon, Ilídio Correia and Fani Sousa
Expert Opinion on Biological Therapy, 2014, 15(3): 353-379
DOI: 10.1517/14712598.2015.996544
Impact Factor: 3.585
Rank: Q2 Medicine, Research & Experimental (51/136); Q2 Biotechnology & Applied Microbiology (44/162)
Citations: ISI Web of Knowledge: 26; Scopus: 28; Google Scholar: 40

XII. **Tumor spheroid assembly on hyaluronic acid-based structures: A review**
Marco P. Carvalho, Elisabete C. Costa, Sónia P. Miguel and Ilídio J. Correia
Carbohydrate Polymers, 2016, 150: 139-148
DOI: 10.1016/j.carbpol.2016.05.005
Impact Factor: 6.044
Rank: Q1 and TOP10 Chemistry, Applied (2/71); Q1 and TOP10 Chemistry, Organic (3/57); Q1 and TOP10 Polymer Science (4/87)
Citations: ISI Web of Knowledge: 15; Scopus: 18; Google Scholar: 21

XIII. **D-α-tocopheryl polyethylene glycol 1000 succinate functionalized nanographene oxide for cancer therapy**
Duarte de Melo-Diogo, Cleide Pais-Silva, Elisabete C. Costa, Ricardo O. Louro and Ilídio J. Correia
Nanomedicine, 2017, 12(5): 443-456
DOI: 10.2217/nnm-2016-0384
Impact Factor: 4.717
Rank: Q1 Biotechnology & Applied Microbiology (23/162); Q2 Nanoscience & Nanotechnology (31/94)
Citations: ISI Web of Knowledge: 11; Scopus: 12; Google Scholar: 12

XIV. **Thermo- and pH-responsive nano-in-micro particles for combinatorial drug delivery to cancer cells**
André F. Moreira, Diana R. Dias, Elisabete C. Costa and Ilídio J. Correia
European Journal of Pharmaceutical Sciences, 2017, 104: 42-51
DOI: 10.1016/j.ejps.2017.03.033
Impact Factor: 3.532
Rank: Q2 Pharmacology & Pharmacy (71/267)
Citations: ISI Web of Knowledge: 14; Scopus: 15; Google Scholar: 15

XV. **Assembly of breast cancer heterotypic spheroids on hyaluronic acid coated surfaces**
Marco P. Carvalho, Elisabete C. Costa and Ilídio J. Correia
Biotechnology Progress, 2017, 33(5): 1346-1357
DOI: 10.1002/btpr.2497
Impact Factor: 2.406
Rank: Q3 Biotechnology & Applied Microbiology (83/162); Q2 Food Science & Technology (47/135)
Citations: ISI Web of Knowledge: 5; Scopus: 5; Google Scholar: 5

XVI. **Development of poly-2-ethyl-2-oxazoline coated gold-core silica shell nanorods for cancer chemo-photothermal therapy**
André F. Moreira, Carolina F. Rodrigues, Catarina A. Reis, Elisabete C. Costa, Paula Ferreira and Ilídio J. Correia
Nanomedicine, 2018, 13(20): 2611-2627
DOI: 10.2217/nnm-2018-0179
Impact Factor: 4.717
Rank: Q1 Biotechnology & Applied Microbiology (23/162); Q2 Nanoscience & Nanotechnology (31/94)
Citations: ISI Web of Knowledge: 1; Scopus: 3; Google Scholar: 3

XVII. **Towards the development of electrospun mats from poly(ε-caprolactone)/poly(ester amide)s miscible blends**
Miguel L. Lamas, Mafalda S. Lima, Ana C. Pinho, David Tugushi, Ramaz Katsarava, Elisabete C. Costa, Ilídio J. Correia, Arménio C. Serra, Jorge F. J. Coelho and Ana C. Fonseca
Polymer, 2018, 150: 343-359
DOI: 1 10.1016/j.polymer.2018.07.050
Impact Factor: 3.771
Rank: Q1 Polymer Science (13/87)
Citations: ISI Web of Knowledge: 1; Scopus: 1; Google Scholar: 0

XVIII. **Comparative study of the therapeutic effect of Doxorubicin and Resveratrol combination on 2D and 3D (spheroids) cell culture models**
Andreia S. Barros, Elisabete C. Costa, Ana S. Nunes, Duarte de Melo-Diogo and Ilídio J. Correia
International Journal of Pharmaceutics, 2018, 551(1-2): 76-83
DOI: 10.1016/j.ijpharm.2018.09.016
Impact Factor: 4.213
Rank: Q1 Pharmacology & Pharmacy (44/267)
Citations: ISI Web of Knowledge: 2; Scopus: 2; Google Scholar: 3

XIX. **Establishment of 2D Cell Cultures Derived From 3D MCF-7 Spheroids Displaying a Doxorubicin Resistant Profile**
Ana S. Nunes, Elisabete C. Costa, Andreia S. Barros, Duarte de Melo-Diogo and Ilídio J. Correia
Biotechnology Journal, 2018, 14(4): e1800268
DOI: 10.1002/biot.201800268
Impact Factor: 3.543
Rank: Q1 Biochemical Research Methods (18/79); Q1 Biotechnology & Applied Microbiology (46/162)
Citations: ISI Web of Knowledge: 0; Scopus: 0; Google Scholar: 0

XX. **POxylated graphene oxide nanomaterials for combination chemo-phototherapy of breast cancer cells**
Duarte de Melo-Diogo, Elisabete C. Costa, Cátia G. Alves, Rita Lima-Sousa, Ricardo O. Louro and Ilídio J. Correia
European Journal of Pharmaceutics and Biopharmaceutics, 2018, 131: 162-169
DOI: 10.1016/j.ejpb.2018.08.008
Impact Factor: 4.708
Rank: Q1 Pharmacology & Pharmacy (28/267)
Citations: ISI Web of Knowledge: 4; Scopus: 4; Google Scholar: 4

XXI. **Gold-Core Silica Shell Nanoparticles Application in Imaging and Therapy: A Review**
André F. Moreira, Carolina F. Rodrigues, Catarina A. Reis, Elisabete C. Costa and Ilídio J. Correia
Microporous and Mesoporous Materials, 2018, 270: 168-179
DOI: 10.1016/j.micromeso.2018.05.022
Impact Factor: 4.182
Rank: Q1 Chemistry, Applied (12/71); Q2 Chemistry, Physical (46/148); Q2 Nanoscience & Nanotechnology (37/94); Q1 Materials Science, Multidisciplinary (63/293)
Citations: ISI Web of Knowledge: 7; Scopus: 7; Google Scholar: 7

XXII. Functionalization of graphene family nanomaterials for application in cancer therapy

Duarte de Melo-Diogo, Rita Lima-Sousa, Cátia G. Alves, Elisabete C. Costa, Ricardo O. Louro and Ilídio J. Correia

Colloids and Surfaces B: Biointerfaces, 2018, 171: 260-275

DOI: 10.1016/j.colsurfb.2018.07.030

Impact Factor: 3.973

Rank: Q1 Biophysics (15/72); Q2 Chemistry, Physical (49/148); Q2 Materials Science, Biomaterials (11/32)

Citations: ISI Web of Knowledge: 6; Scopus: 7; Google Scholar: 8

XXIII. Hyaluronic acid functionalized green reduced graphene oxide for targeted cancer photothermal therapy

Rita Lima-Sousa, Duarte de Melo-Diogo, Cátia G. Alves, Elisabete C. Costa, Paula Ferreira, Ricardo O. Louro and Ilídio J. Correia

Carbohydrate Polymers, 2018, 200: 93-99

DOI: 10.1016/j.carbpol.2018.07.066

Impact Factor: 6.044

Rank: Q1 and TOP10 Chemistry, Applied (2/71); Q1 and TOP10 Chemistry, Organic (3/57); Q1 and TOP10 Polymer Science (4/87)

Citations: ISI Web of Knowledge: 9; Scopus: 9; Google Scholar: 11

XXIV. Functionalization of AuMSS nanorods towards more effective cancer therapies

Carolina F. Rodrigues, Telma A. Jacinto, André F. Moreira, Elisabete C. Costa, Sónia P. Miguel and Ilídio J. Correia

Nano Research, 2019, 12(4): 719–732

DOI: 10.1007/s12274-019-2286-y

Impact Factor: 8.515

Rank: Q1 Chemistry, Physical (23/148); Q1 Nanoscience & Nanotechnology (15/94); Q1 Materials Science, Multidisciplinary (26/293); Q1 Physics, Applied (13/148)

Citations: ISI Web of Knowledge: 0; Scopus: 0; Google Scholar: 0

XXV. Hyaluronic acid functionalized nanoparticles loaded with IR780 and DOX for cancer chemo-photothermal therapy

Cátia G. Alves, Duarte de Melo-Diogo, Rita Lima-Sousa, Elisabete C. Costa and Ilídio J. Correia

European Journal of Pharmaceutics and Biopharmaceutics, 2019, 137: 86-94

DOI: 10.1016/j.ejpb.2019.02.016

Impact Factor: 4.708

Rank: Q1 Pharmacology & Pharmacy (28/267)

Citations: ISI Web of Knowledge: 0; Scopus: 1; Google Scholar: 1

Manuscripts submitted for publication in peer-reviewed international journals not included in this Doctoral thesis

I. **Microneedles Mediated Chemotherapy and Photothermal Therapy for the Treatment of Cancer**
André F. Moreira, Carolina F. Rodrigues, Telma A. Jacinta, Sónia P. Miguel, Elisabete C. Costa and Ilídio J. Correia
Submitted for publication.

II. **AuMSS nanorods coated with TPGS and HA for cancer targeted photothermal therapy**
Telma A. Jacinto, Paula Ferreira, André F. Moreira, Carolina F. Rodrigues, Sónia P. Miguel, Elisabete C. Costa and Ilídio J. Correia
Submitted for publication.

III. **Optimization of *Clear^{T}* and *Clear^{T2}* conditions for the fluorescence imaging of PI-stained spheroids**
Daniel N. Silva, Elisabete C. Costa, André F. Moreira and Ilídio J. Correia
Submitted for publication.

Book chapters in peer-reviewed scientific books published by international publishers not included in this Doctoral thesis

I. **Chapter 6 - Multifunctional Nanocarriers for Codelivery of Nucleic Acids and Chemotherapeutics to Cancer Cells**
Vítor M. Gaspar, André F. Moreira, Duarte de Melo-Diogo, Elisabete C. Costa, João A. Queiroz, Fani Sousa, Chantal Pichon and Ilídio J. Correia
Nanobiomaterials in Medical Imaging – Volume VIII, Edited by Alexandru M. Grumezescu, Published by Elsevier (2016)
DOI: 10.1016/B978-0-323-41736-5.00006-6
Citations: ISI Web of Knowledge: 0; Scopus: 1; Google Scholar: 1

List of Scientific Communications

Oral scientific communications

I. Vítor M. Gaspar, Elisabete C. Costa, Ricardo O. Louro, João A. Queiroz, Fani Sousa and Ilídio J. Correia, *Nanomaterials for Delivery of Biomolecules with Application in Cancer Therapy*, V Jornadas em Ciências Biomédicas, 13th to 15th of March of 2014, Faculdade de Ciências da Saúde (FCS), Covilhã, Portugal.

II. Elisabete C. Costa, Vítor M. Gaspar, João F.G. Marques, Paula Coutinho and Ilídio J. Correia, *Mimicking Cancer Microenvironment with 2D and 3D In Vitro Coculture Models to Evaluate Nanoparticles Uptake*, II Encontro Nacional de Estudantes de Química (II ENEQUI), 28th to 30th of March of 2014, Universidade da Beira Interior (UBI), Covilhã, Portugal. **(invited speaker)**

III. Vítor M. Gaspar, Elisabete C. Costa, João G. Marques, Ricardo O. Louro, João A. Queiroz, Fani Sousa and Ilídio J. Correia, *Development of Nanosystems for Delivery of Bioactive Molecules with Application in Cancer Therapy*, Sessão Clínica, 22nd of May of 2014, Centro Hospitalar Cova da Beira (CHCB), Covilhã, Portugal.

IV. Vítor M. Gaspar, Cristine Gonçalves, Duarte de Melo-Diogo, Elisabete C. Costa, João A. Queiroz, Chantal Pichon, Fani Sousa and Ilídio J. Correia, *Simultaneous Delivery of Drugs and Genes by Multi-block Polymeric Nanomicelles for Synergistic Cancer Therapy*, Nanoscience and Nanotechnology International Conference - NanoPT, 11th to 13th of February of 2015, Porto, Portugal.

V. Vítor M. Gaspar, Cristine Gonçalves, Duarte de Melo-Diogo, Elisabete C. Costa, João A. Queiroz, Chantal Pichon, Fani Sousa and Ilídio J. Correia, *Polymeric Nanocarriers for Delivery of Multiple Bioactive Molecules to Breast Cancer Cells*, Biochemistry Symposium, 6th and 7th of May of 2015, Universidade da Beira Interior (UBI), Covilhã, Portugal. **(invited speaker)**

VI. Duarte de Melo-Diogo, Cleide Pais-Silva, Elisabete C. Costa, Cátia G. Alves, Rita Lima-Sousa, Ricardo O. Louro and Ilídio J. Correia, *Near infrared light responsive nanomaterials for cancer therapy*, XVI Portuguese Conference on Fracture, 23rd and 24th of April of 2018, TRYP Dona Maria Hotel, Covilhã, Portugal.

VII. Elisabete C. Costa, Marco P. Carvalho, André F. Moreira, Duarte de Melo-Diogo and Ilídio J. Correia, *Agarose and Hyaluronic Acid (HA) application in 3D cell culture of breast cancer cells*, XVI Portuguese Conference on Fracture, 23rd and 24th of April of 2018, TRYP Dona Maria Hotel, Covilhã, Portugal.

VIII. Duarte de Melo-Diogo, Cleide Pais-Silva, Elisabete C. Costa, Cátia G. Alves, Rita Lima-Sousa, Ricardo O. Louro and Ilídio J. Correia, *Near infrared light responsive nanomaterials for cancer therapy*, VI Jornadas de Bioengenharia, 2nd and 3rd of May of 2018, Universidade da Beira Interior (UBI), Covilhã, Portugal. **(invited speaker)**

Poster presentations

I. Elisabete C. Costa, Vítor M. Gaspar, João G. Marques, Paula Coutinho and Ilídio J. Correia, *Mimicking Breast Cancer Microenvironment with In Vitro Co-culture Models*, VI Jornadas sobre Tecnologia e Saúde, 3rd of May of 2013, Instituto Politécnico da Guarda (IPG), Guarda, Portugal. **(best poster award)**

II. João G. Marques, Vítor M. Gaspar, Elisabete C. Costa, Catarina M. Paquete and Ilídio J. Correia, *Development of Micelles as Carriers of Non-steroidal Anti-inflammatory Drugs (NSAID) for Application in Breast Cancer Therapy*, VIII Annual CICS Symposium, 1st and 2nd of July of 2013, Faculdade de Ciências da Saúde (FCS), Covilhã, Portugal.

III. Vítor M. Gaspar, Elisabete C. Costa, João G. Marques, João A. Queiroz, Chantal Pichon, Fani Sousa and Ilídio Correia, *Evaluation of Targeted Gene Delivery to Cancer Cells Trough High Throughput Fluorescence Microscopy*, 1st POLARIS Workshop International Conference, 7th to 9th of October of 2013, Palácio Congress Hotel & Spa, Porto, Portugal.

IV. David Oppolzer, João G. Marques, Duarte de Melo-Diogo, Vítor M. Gaspar, Elisabete C. Costa, Eugenia Gallardo and Ilídio J. Correia, *Simultaneos Determination of Sildenafil and Crizotinib using HPLC-DAD*, 8º Encontro Nacional de Cromatografia, 2nd to 4th of December of 2013, Faculdade de Ciências da Saúde (FCS), Covilhã, Portugal.

V. André F. Moreira, Vítor M. Gaspar, Elisabete C. Costa, Duarte de Melo-Diogo, Paulo Machado, Catarina M. Paquete and Ilídio J. Correia, *Synthesis and Characterization of MCM-41 type Silica Nanoparticles by a Stöber Modified Method*, Encontro Bienal das Divisões Técnicas da Sociedade Portuguesa de Materiais (SPM), 4th of May of 2014, Universidade da Beira Interior (UBI), Covilhã, Portugal.

VI. Elisabete C. Costa, Vítor M. Gaspar, Duarte de Melo-Diogo, André F. Moreira, João G. Marques, Paula Coutinho and Ilídio J. Correia, *Evaluation of nanoparticles uptake in breast cancer co-cultures,* Encontro Bienal das Divisões Técnicas da Sociedade Portuguesa de Materiais (SPM), 4th of May of 2014, UBI, Universidade da Beira Interior (UBI), Covilhã, Portugal.

VII. Vítor M. Gaspar, Elisabete C. Costa, João A. Queiroz, Chantal Pichon, Fani Sousa and Ilídio Correia, *Evaluation of Targeted Gene Delivery to Cancer Cells Trough High Throughput Fluorescence Microscopy*, Encontro Bienal das Divisões Técnicas da Sociedade Portuguesa de Materiais (SPM), 4th of May of 2014, Universidade da Beira Interior (UBI), Covilhã, Portugal.

VIII. André F. Moreira, Vitor M. Gaspar, Elisabete C. Costa, Duarte de Melo-Diogo, Paulo Machado, Catarina M. Paquete and Ilídio J. Correia, *Development of Mesoporous Silica Nanoparticles for Drug Delivery to Cancer Cells*, IX Annual CICS Symposium, 30th of June and 1st of July of 2014, Faculdade de Ciências da Saúde (FCS), Covilhã, Portugal.

IX. Elisabete C. Costa, Vítor M. Gaspar, Duarte de Melo-Diogo, André F. Moreira, João G. Marques, Paula Coutinho and Ilídio J. Correia, *Co-cultures for Nanoparticles Uptake Analysis*, IX Annual CICS Symposium, 30th of May and 1st of July of 2014, Faculdade de Ciências da Saúde (FCS), Covilhã, Portugal.

X. João G. Marques, Vítor M. Gaspar, David Markl, Elisabete C. Costa, Duarte de Melo-Diogo, André F. Moreira, Eugénia Gallardo and Ilídio J. Correia, *Co-delivery of a Dual Drug Combination in Polymeric Nanovehicles for Improved Anticancer Therapy*, IX Annual CICS Symposium, 30th of May and 1st of July of 2014, Faculdade de Ciências da Saúde (FCS), Covilhã, Portugal.

XI. André F. Moreira, Vítor M. Gaspar, Elisabete C. Costa, Duarte de Melo-Diogo, Paulo Machado, Catarina M. Paquete and Ilídio J. Correia, *pH-sensitive mesoporous silica nanoparticles for drug delivery to prostate cancer cells*, Semana da Ciência, 28th of November of 2014, Universidade da Beira Interior (UBI), Covilhã, Portugal.

XII. Duarte de Melo-Diogo, Vítor M. Gaspar, Elisabete C. Costa, André F. Moreira, David Oppolzer, Eugénia Gallardo and Ilídio J. Correia, *Triple drug loaded polymeric micelles for improved lung cancer therapy*, Semana da Ciência, 28th of November of 2014, Universidade da Beira Interior (UBI), Covilhã, Portugal.

XIII. Elisabete C. Costa, Vítor M. Gaspar, Duarte de Melo-Diogo, André F. Moreira, Paula Coutinho and Ilídio J. Correia, *Liquid Overlay Technique (LOT) optimizations for spheroids 3D cell culture*, Semana da Ciência, 28th of November of 2014, Universidade da Beira Interior (UBI), Covilhã, Portugal.

XIV. André F. Moreira, Vítor M. Gaspar, Elisabete C. Costa, Duarte de Melo-Diogo, Paulo Machado, Catarina M. Paquete and Ilídio J. Correia, *Calcium carbonate coated nanoparticles for pH-responsive drug co-delivery to prostate cancer cells*, VIII Jornadas sobre Tecnologia e Saúde, 17th of April of 2015, Instituto Politécnico da Guarda (IPG), Guarda, Portugal.

XV. Duarte de Melo-Diogo, D., Vítor M. Gaspar, Elisabete C. Costa, André F. Moreira, David Oppolzer, Eugénia Gallardo and Ilídio J. Correia, *Triple-drug co-delivery by TPGS-PLA micelles for lung cancer therapy*, VIII Jornadas sobre Tecnologia e Saúde, 17th of April of 2015, Instituto Politécnico da Guarda (IPG), Guarda, Portugal.

XVI. Elisabete C. Costa, Vítor M. Gaspar, Duarte de Melo-Diogo, André F. Moreira, João G. Marques, Paula Coutinho, Ilídio J. Correia, *Optimization of Liquid Overlay Technique (LOT) to produce 3D Breast and Cervical Co-Culture Models*, VIII Jornadas sobre Tecnologia e Saúde, 17th of April of 2015, Instituto Politécnico da Guarda (IPG), Guarda, Portugal. (**best poster award**)

XVII. Marco P. Carvalho, Elisabete C. Costa and Ilídio J. Correia, *Assembly of breast cancer spheroids*, XI Annual CICS-UBI Symposium, 30th June and 1st July of 2016, Faculdade de Ciências da Saúde (FCS), Covilhã, Portugal. (**best poster award**)

XVIII. André F. Moreira, Vítor M. Gaspar, Elisabete C. Costa, Duarte de Melo-Diogo, Paulo Machado, Catarina M. Paquete and Ilídio J. Correia, *Calcium carbonate coated nanoparticles for pH responsive drug co-delivery to prostate cancer cells*, Encontro com a Ciência e Tecnologia 2016, 4th to 6th of July of 2016, Centro de Congressos de Lisboa, Lisboa, Portugal.

XIX. Marco P. Carvalho, Elisabete C. Costa and Ilídio J. Correia, *Hyaluronic acid biomaterial application in breast cancer spheroids assembly*, V Encontro de Estudantes de Materiais (ENEM), 29th and 30th of September of 2016, Universidade da Beira Interior (UBI), Covilhã, Portugal.

XX. Duarte de Melo-Diogo, Cleide Pais-Silva, Elisabete C. Costa, Ricardo O. Louro and Ilídio J. Correia, *Functionalization of graphene oxide for anticancer applications*, V Ciclo de Conferências da Faculdade de Ciências, 21st of January of 2017, Faculdade de Ciências da Saúde (FCS), Covilhã, Portugal. (**best poster award**)

XXI. André F. Moreira, Diana R. Dias, Elisabete C. Costa and Ilídio J. Correia, *Nano-in-micro particles for stimuli responsive drug delivery to cancer cells*, II International Congress in Health Sciences Research Towards Innovation and Entrepreneurship: Trends in Biotechnology for Biomedical Applications, 17th to 20th of May of 2017, Faculdade de Ciências da Saúde (FCS), Covilhã, Portugal.

XXII. Duarte de Melo-Diogo, Cleide Pais-Silva, Elisabete C. Costa, Ricardo O. Louro and Ilídio J. Correia, *PEGylated Vitamin E functionalized nanographene oxide for breast cancer therapy*, II International Congress in Health Sciences Research Towards Innovation and Entrepreneurship: Trends in Biotechnology for Biomedical Applications, 17th to 20th of May of 2017, Faculdade de Ciências da Saúde (FCS), Covilhã, Portugal.

XXIII. Elisabete C. Costa, Marco P. Carvalho, Duarte de Melo-Diogo, André F. Moreira and Ilídio J. Correia, *Mimicking Breast Cancer Microenvironment with in vitro 3D Co-culture Models*, II International Congress in Health Sciences Research Towards Innovation and Entrepreneurship: Trends in Biotechnology for Biomedical Applications, 17th to 20th of May of 2017, Faculdade de Ciências da Saúde (FCS), Covilhã, Portugal.

XXIV. André F. Moreira, Diana R. Dias, Elisabete C. Costa and Ilídio J. Correia, *Dual-stimuli responsive nano-in-micro drug delivery systems for cancer therapy*, Encontro com a Ciência e Tecnologia 2017, 3rd to 5th of July of 2017, Centro de Congressos de Lisboa, Lisboa, Portugal.

XXV. Duarte de Melo-Diogo, Cleide Pais-Silva, Elisabete C. Costa, Ricardo O. Louro and Ilídio J. Correia, *Nanographene oxide functionalized with PEGylated Vitamin E for breast cancer therapy*, Encontro com a Ciência e Tecnologia 2017, 3rd to 5th of July of 2017, Centro de Congressos de Lisboa, Lisboa, Portugal.

XXVI. Elisabete C. Costa, Marco P. Carvalho, Duarte de Melo-Diogo, André F. Moreira and Ilídio J. Correia, *Mimicking breast cancer microenvironment with in vitro 3D heterotypic spheroids*, Encontro com a Ciência e Tecnologia 2017, 3rd to 5th of July of 2017, Centro de Congressos de Lisboa, Lisboa, Portugal.

XXVII. André F. Moreira, Diana R. Dias, Carolina F. Rodrigues, Catarina A. Reis, Elisabete C. Costa and Ilídio J. Correia, *Nano-in-micro spheres for pH- and thermo-responsive drug delivery to cancer cells*, Encontro com a Ciência e Tecnologia 2018, 2sd to 4th of July of 2018, Centro de Congressos de Lisboa, Lisboa, Portugal.

XXVIII. Ana S. Barros, Elisabete C. Costa, Ana S. Nunes, Duarte de Melo-Diogo and Ilídio J. Correia, *Comparative study of the therapeutic effect of Doxorubicin and Resveratrol combination on 2D and 3D (spheroids) cell culture models*, XIII Annual CICS-UBI Symposium, 5th and 6th July of 2018, Faculdade de Ciências da Saúde (FCS), Covilhã, Portugal.

XXIX. Ana S. Nunes, Elisabete C. Costa, Ana S. Barros, Duarte de Melo-Diogo and Ilídio J. Correia, *Gathering 2D cell cultures derived from 3D MCF-7 spheroids displaying a Doxorubicin resistant profile*, XIII Annual CICS-UBI Symposium, 5th and 6th July of 2018, Faculdade de Ciências da Saúde (FCS), Covilhã, Portugal.

XXX. Cátia G. Alves, Duarte de Melo-Diogo, Rita Lima-Sousa, Elisabete C. Costa and Ilídio J. Correia, *Formulation of hyaluronic acid-based micelles loaded with IR780 for cancer therapy*, XIII Annual CICS-UBI Symposium, 5th and 6th July of 2018, Faculdade de Ciências da Saúde (FCS), Covilhã, Portugal.

XXXI. Rita Lima-Sousa, Duarte de Melo-Diogo, Cátia G. Alves, Elisabete C. Costa, Ricardo O. Louro and Ilídio J. Correia, *Environmentally-friendly reduction and functionalization of graphene oxide based nanomaterials for cancer therapy*, XIII Annual CICS-UBI Symposium, 5th and 6th July of 2018, Faculdade de Ciências da Saúde (FCS), Covilhã, Portugal.

XXXII. Cátia G. Alves, Duarte de Melo-Diogo, Rita Lima-Sousa, Elisabete C. Costa and Ilídio J. Correia, *IR780 and DOX Loaded Hyaluronic Acid-based Micelles for Targeted Cancer Chemo-Phototherapy*, 6th IEEE Portuguese Meeting on Bioengineering, 22nd and 23th of February of 2019, Instituto Superior de Engenharia de Lisboa (ISEL), Lisboa, Portugal.

XXXIII. Daniel N. Silva, Elisabete C. Costa, André F. Moreira, Duarte de Melo-Diogo and Ilídio J. Correia, *Optical clearing techniques for the imaging of 3D spheroids*, 6th IEEE Portuguese Meeting on Bioengineering, 22nd and 23th of February of 2019, Instituto Superior de Engenharia de Lisboa (ISEL), Lisboa, Portugal.

XXXIV. Rita Lima-Sousa, Duarte de Melo-Diogo, Cátia G. Alves, Elisabete C. Costa and Ilídio J. Correia, Targeted cancer photothermal therapy using hyaluronic acid functionalized green reduced graphene oxide, 6th IEEE Portuguese Meeting on Bioengineering, 22nd and 23th of February of 2019, Instituto Superior de Engenharia de Lisboa (ISEL), Lisboa, Portugal.

Conference Organizing Committees

Member of the organizing committee of scientific conferences

I. XVI Portuguese Conference on Fracture, TRYP Dona Maria, 23rd and 24th of April of 2018, TRYP Dona Maria Hotel, Covilhã, Portugal

Resumo Alargado

O cancro é atualmente uma das doenças com maior incidência na população mundial, sendo que uma em cada seis mortes ocorre como consequência desta doença, de acordo com os dados da Organização Mundial de Saúde (2018). Nos países desenvolvidos, esta doença é a segunda maior causa de morte, sendo apenas superada pelas doenças cardiovasculares (p.ex. cardiopatia isquémica). A elevada taxa de mortalidade associada ao cancro advém da reduzida eficácia e das limitações das terapias normalmente utilizadas na clínica, nomeadamente a quimioterapia, radioterapia e cirurgia. As limitações destas abordagens terapêuticas têm despoletado junto da indústria farmacêutica, da comunidade médica e científica a necessidade de desenvolver novos agentes anticancerígenos.

Todos os compostos desenvolvidos para aplicações terapêuticas devem ser cuidadosamente estudados e avaliados de acordo com as normas das agências reguladoras, tais como *Food and Drug Administration (FDA)* e a Agência Europeia de Medicamentos (EMA), antes de poderem ser usados em meio clínico. Para atingir este objetivo, os compostos são primeiramente avaliados em ensaios pré-clínicos, onde são usados modelos *in vitro* (células) e *in vivo* (animais), e posteriormente em ensaios clínicos (humanos). Neste contexto, os modelos *in vitro* são fundamentais numa fase inicial para se proceder à avaliação da eficácia terapêutica dos compostos, assim como para reduzir o número de animais utilizados em laboratório, que é uma das principais reivindicações de diferentes organizações, nomeadamente da *European Partnership for Alternative Approaches to Animal Testing (EPAA)*.

O modelo *in vitro* mais usado para a avaliação da eficácia terapêutica de novos compostos é a cultura de células em 2D, *i.e.* o crescimento de células em monocamada sobre uma superfície plana de plástico (p. ex. poliestireno). Este tipo de cultura celular é atrativo devido ao seu fácil manuseamento, reduzido custo e elevada reprodutibilidade. Contudo, as culturas celulares 2D não conseguem prever com exatidão a ação dos fármacos nos tumores. Deste modo, uma grande percentagem dos compostos que apresentam resultados promissores nos ensaios *in vitro* não demonstram a mesma eficácia terapêutica nos ensaios *in vivo*. Estes resultados são explicados pelo facto destes modelos celulares não conseguirem mimetizar a organização estrutural e funcional dos tumores.

Com o intuito de ultrapassar as limitações das culturas celulares 2D, durante as últimas décadas, a proliferação de células em 3D tem sido um dos tópicos mais investigado. Na atualidade, este tipo de cultura é realizado em estruturas artificiais que reproduzem a matriz extracelular dos tecidos humanos. Para além disso, a cultura de células em 3D pode também ser efetuada sob a forma de agregados celulares, usando técnicas como a *Liquid Overlay*

Technique (LOT) e *Hanging Drop Technique*. Estes agregados celulares são conhecidos por esferoides e vários estudos têm demonstrado que estes mimetizam de uma forma aproximada as características dos tumores que afetam os seres humanos, nomeadamente os tumores sólidos. À semelhança do que ocorre nestes tumores, os esferoides apresentam um gradiente de gases e nutrientes. As células que se encontram na camada exterior do esferoide têm acesso facilitado a nutrientes e a oxigénio, enquanto que as células presentes nas regiões mais internas possuem um acesso limitado (hipóxia). Deste modo, a taxa de proliferação das células diminui da periferia para o interior do esferoide, sendo o interior destes agregados constituído por células necróticas. Em comparação com as culturas celulares 2D, os esferoides apresentam ainda um maior número de interações célula-célula, célula-matriz e uma elevada deposição de proteínas da matriz extracelular.

Apesar dos diferentes estudos já efetuados, as culturas celulares 3D têm tido uma contribuição marginal para o desenvolvimento de novos fármacos anticancerígenos. Este facto deve-se à necessidade de otimizar os métodos de produção de esferoides de forma a obter agregados celulares de forma reprodutível e em larga escala. Por outro lado, a maioria dos protocolos e equipamentos usados na avaliação de compostos em culturas celulares estão apenas otimizados para a análise de células cultivadas em monocamada.

A avaliação da eficácia terapêutica de compostos nos esferoides tem sido essencialmente monitorizada através de microscopia ótica, microscopia de fluorescência, citometria de fluxo, *western blot*, entre outras técnicas. A microscopia de fluorescência tem sido uma das técnicas mais usadas para efetuar este tipo de análise, no entanto, alguns dos microscópios de fluorescência não possuem as características adequadas para a visualização dos esferoides. Por outro lado, a microscopia confocal de fluorescência não permite a aquisição de imagens de amostras com elevada espessura. Este facto deve-se à dispersão da luz que ocorre quando esta atravessa os constituintes celulares e não celulares dos esferoides (p.ex. água, proteínas, lípidos, entre outros), que possuem índices de refração diferentes. Em consequência deste fenómeno, a luz usada para excitar a amostra é dispersa e não atinge todas as partes do esferoide, como o seu interior.

O plano de trabalhos desenvolvido durante o meu doutoramento teve como objetivo melhorar a aquisição de imagens dos esferoides por microscopia de confocal de fluorescência. Para tal, foram usados métodos de clareamento ótico, nomeadamente o *Clear^{T}* e o *Clear^{T2}*. Estes métodos permitem reduzir a dispersão da luz nos esferoides através da homogeneização do índice de refração dos seus constituintes. Após o processo de clareamento, os esferoides tornam-se mais transparentes, o que permite uma maior penetração da luz e, simultaneamente, a aquisição de imagens mais completas dos esferoides.

No primeiro estudo experimental realizado no âmbito do meu doutoramento, foi utilizado pela primeira vez o método *Clear^{T}* para efetuar o clareamento ótico dos esferoides. Este método

envolveu a imersão dos agregados celulares em soluções de concentração crescente de formamida. Os resultados obtidos demonstraram que o método *Clear^{T}* permite tornar os esferoides mais transparentes sem influenciar a sua estrutura, uma vez que o tamanho dos esferoides não é significativamente alterado após o seu clareamento. Por outro lado, a aplicação do método *Clear^{T}* não diminui significativamente a intensidade de fluorescência do iodeto de propídio comparativamente com os esferoides não clareados. Simultaneamente, a profundidade da deteção do sinal do iodeto de propídio no eixo do Z foi melhorada em cerca de 43%. Para além disso, foram ainda registadas melhorias na deteção de fluorescência no interior dos esferoides, sendo que a uma distância de 100 µm no eixo do Z foi possível detetar mais 47% do sinal de iodeto de propídio.

No segundo estudo realizado, procedeu-se à otimização do método *Clear^{T2}* para a análise de esferoides. Este método baseia-se na imersão das amostras em soluções aquosas com concentrações crescentes de formamida e polietilenoglicol (PEG). Para alcançar os objetivos definidos foram realizados os métodos denominados por *Clear^{T2}/4*, *Clear^{T2}/8* e *Clear^{T2}/10* usando PEG com 4000, 8000 e 10000 Da, com o intuito de determinar qual destes é o mais eficiente para alcançar o clareamento ótico dos esferoides. Os resultados obtidos demonstraram que independentemente do peso molecular do PEG, todas as variações do método *Clear^{T2}* permitiram obter esferoides transparentes sem que o tamanho original destes fosse afetado. Para além disto, todas as variantes do método *Clear^{T2}* permitiram que a intensidade de sinal do iodeto de propídio não fosse reduzida após a aplicação do processo de clareamento. Em particular, o método *Clear^{T2}/4* permitiu incrementar significativamente a intensidade de fluorescência proveniente dos esferoides marcados com iodeto de propídio (a intensidade de fluorescência foi incrementada em cerca de 120% comparativamente com os esferoides não clareados). Para além disto, o método *Clear^{T2}/4* foi aquele que permitiu obter imagens dos esferoides a uma maior profundidade no eixo Z (até 212 µm), assim como um sinal de fluorescência mais intenso no interior dos esferoides (26%).

Com base nos resultados obtidos pode concluir-se que ambos os métodos *Clear^{T}* e *Clear^{T2}* podem ser usados para melhorar a aquisição de imagens de esferoides marcados com iodeto de propídio através de microscopia confocal de fluorescência. Por outro lado, estes métodos poderão contribuir para o desenvolvimento de novos agentes anticancerígenos, uma vez que estes podem ser usados para permitir a avaliação da morte celular em esferoides após a administração de agentes anticancerígenos. Adicionalmente, estes métodos poderão também permitir a análise da penetração e distribuição de fármacos ou nanopartículas, assim como avaliar a expressão de proteínas específicas nos esferoides através de microscopia de fluorescência.

Palavras-chave

Clear^{T}, *Clear*^{T2}, esferoides, microscopia confocal de fluorescência, iodeto de propídio.

Abstract

Cancer is a major health issue for the worldwide population. It is the second most common cause of death in developed countries. According to the World Health Organization (WHO; 2018), 1 in 6 deaths occurs as a result of this disease. This scenario occurs due to the limited effectiveness of the currently available treatments, namely chemotherapy, radiotherapy and surgery. To overcome such drawbacks, the medical/scientific community as well as the pharmaceutical companies have been effortfully pursuing the development of new cancer treatments exhibiting a higher efficacy.

Before the new drugs can be used in the clinic, they must fulfill all the requirements established by the regulatory agencies, namely by the Food and Drug Administration (FDA) and the European Medicine Agency (EMA). The initial assessment of anticancer agents' efficacy is performed through *in vitro* and *in vivo* assays (preclinical studies). This preclinical stage includes physicochemical and biological characterization of the compounds as well as their safety and toxic profile, by using cells and animals.

The 2D cell cultures, *i.e.* cells grown as a monolayer on artificial flat plastic surfaces, are the most common *in vitro* model used for drug development purposes. These cell culture models are easy to handle, cost-effective and display a good reproducibility. However, they are unable to fully predict the effect of therapeutic agents in *in vivo* tumors. Due to that, a huge number of compounds showing effectiveness in 2D cell culture models fail when tested in *in vivo* models. This drawback leads to an over-use of animals in experimentation, and also contributes to increase the time and the overall cost of the drug development process.

The limitations presented by 2D cell cultures result from their inability to mimic the characteristics of the *in vivo* tumor tissues, specially their cellular organization and function. Therefore, it is crucial to screen anticancer agents in *in vitro* models that can better represent the features of solid tumors affecting humans. Sphere-like tightly bound cellular aggregates, known as spheroids, are *in vitro* 3D cell culture models that reproduce closely the complexity of cancerous human tissues. Such is owed to the fact that spheroids display inherent metabolic (oxygen, carbon dioxide, nutrients and waste) gradients like those found in poorly vascularized tumors. Such gradients endow spheroids a cellular similar organization to that exhibited by solid tumors, *i.e.* three main cellular layers composed of an external layer of proliferative cells, an intermediate layer formed by quiescence cells and an inner acidic and hypoxic layer comprised of necrotic cells. On the other hand, compared to 2D cell cultures, spheroids demonstrate increased cell-cell interactions, as well as ECM proteins deposition and cell-ECM interactions.

Despite of the potential of 3D tumor spheroids for drug screening purposes, their use is still scarce. In one hand, spheroids' production techniques that can be used to form spheroids (*e.g.* Liquid Overlay Technique (LOT) and Hanging Drop Technique) demand optimization for allowing the production of spheroids under highly reproducible conditions. On the other hand, the analysis of the therapeutics' effect on spheroids is still challenging, due to the limited availability of protocols, techniques and equipment required to perform such assays. Particularly, although the fluorescence microscopy is one of the most used techniques to assess the therapeutics distribution within the spheroids or the cellular death in response to a potential therapeutic, some fluorescence microscopes are not suitable for the imaging of spheroids.

The imaging of spheroids by confocal fluorescence microscopy modalities is challenging due to spheroids' thickness and to the light scattering phenomenon. When light cross a biological sample, it is scattered due to the refractive index (RI) mismatches between acellular and cellular constituents. Due to this fact, the excitation light is dispersed through the sample, thus limiting its penetration into the deepest regions of spheroids. Therefore, it is challenging to obtain high-resolution images of intact spheroids, specially from their interior.

Having this in mind, the main objective of this thesis' work plan was to address the limitations of spheroids imaging by confocal laser scanning microscopy (CLSM). To achieve this goal, optical clearing methods, namely *Clear*^{T} and *Clear*^{T2}, that were previously applied for the imaging of animals' biological samples, were optimized for spheroids analysis. These methods were used to reduce the light scattering phenomenon in the spheroids by performing the homogenization of the spheroids overall RI, to accomplish an improved spheroids' transparency and a light penetration depth.

In the first experimental study that was performed within the scope of this thesis, the *Clear*^{T} optical clear method was, from the best of my knowledge, used for the first time for spheroids' analysis. To accomplish that, spheroids were cleared by immersing them on solutions with increasing concentrations of formamide. The obtained results demonstrated that the *Clear*^{T} method did not affect the structure of the spheroids and improved the PI signal penetration depth by about 43%. Additionally, *Clear*^{T} also enhanced the cells imaging within the spheroid by increasing the imaging cross-section depth by 47% (at 100 µm of depth in the Z-axis).

In the second study, the *Clear*^{T2} optical clearing method was investigated and optimized for the analysis of spheroids. The *Clear*^{T2} protocol involves the immersion of the samples in aqueous solutions with increasing concentrations of formamide and polyethylene glycol (PEG). Herein, it was investigated for the first time the influence of PEG molecular weight on *Clear*^{T2} method ability to clear spheroids. For this purpose, several PEG molecular weights were investigated, namely 4000, 8000 and 10000 Da. The obtained results demonstrated that the *Clear*^{T2} method enhances spheroids' transparency and contributes to preserve the PI fluorescence intensity for

all the PEG MW used. Further, the *Clear*^{T2} method performed using PEG 4000 Da allowed a better PI signal penetration depth (up to 212 μm in the Z-axis) and an enhanced of the cross-section depth (about 26% more than that of the non-cleared spheroids at a penetration depth of 100 μm).

Overall, the obtained results demonstrate that the *Clear*^{T} and *Clear*^{T2} methods were able to improve the CLSM imaging of PI stained spheroids. Furthermore, these methods may also contribute for the development of new anticancer treatments, since they may be used for the evaluation of the cellular death within spheroids prompted by therapeutics and even for the analysis of drugs distribution and dispersion within spheroids as well as to perform the analysis of the expression of specific fluorescent proteins in spheroids.

Keywords

Clear^{T}, *Clear*^{T2}, spheroids, confocal microscopy, propidium iodide.

Thesis Overview

This Doctoral thesis is organized into 8 chapters.

The first chapter presents the general and specific aims established for the work plan of this PhD thesis.

The second, third, fourth and fifth chapters enclose the introductory section. Chapter 2 gives an overview of the 3D tumor spheroids properties as well as of their similarities with the solid tumors that affect human beings. Chapter 3 comprises a revision of the methods used to produce 3D tumor spheroids, highlighting the spheroids formation on non-adhesive surfaces. Chapter 4 provides an overview of the tools and techniques used for spheroids analysis. Chapter 5 is focused on the optical clearing methods used for spheroids imaging.

The sixth and seventh chapters present the results obtained in the experimental work developed during this PhD thesis:

- Chapter 6 - Research Work 1:
  - *Clear*^{T} immersion optical clearing method for intact 3D spheroids imaging through confocal laser scanning microscopy.

- Chapter 7 - Research Work 2:
  - Polyethylene glycol molecular weight influences the *Clear*^{T2} optical clearing method for spheroids imaging by confocal laser scanning microscopy.

Finally, Chapter 8 contains the concluding remarks, making a summary of the results obtained during this PhD thesis and provides future directions concerning spheroids imaging and their application in drug development.

Index

List of Figures

Chapter 5 - Introduction (part D)

Chapter 6 - Research Work 1

Chapter 7 - Research Work 2

List of Tables

Abbreviations

2D	Two-Dimensional
2PM	Two-Photon Microscopy
3D	Three-Dimensional
5-FU	5-Fluorouracil
3DISCO	3D Imaging of Solvent-Cleared Organs
ABC	ATP-Binding Cassette
ALDH	Aldehyde Dehydrogenase
APH	Acid Phosphatase
ATP	Adenosine Triphosphate
BABB	Benzyl Alcohol/Benzyl Benzoate
BrdU	5-Bromo-2'-Deoxyuridine
CAF	Cancer-Associated Fibroblast
Cal AM	Calcein AM
CD	Cluster of Differentiation
CLARITY	Clear Lipid-Exchanged Acrylamide-Hybridized Rigid Imaging/Immunostaining/*In Situ* Hybridization-Compatible Tissue-Hydrogel
CLSM	Confocal Laser Scanning Microscopy
CSC	Cancer Stem Cell
CSF-1	Colony Stimulating Factor
CTCF	Corrected Total Cell Fluorescence
CUBIC	Clear, Unobstructed Brain/Body Imaging Cocktails and Computational Analysis
DAPI	4′,6-Diamidino-2-Phenylindole
DIC	Differential Interference Contrast
DiI	1,1'-Dioctadecyl-3,3,3',3'-Tetramethylindocarbocyanine Perchlorate
DMEM-F12	Dulbecco's Modified Eagle's Medium F-12
DMSO	Dimethyl Sulfoxide
DOX	Doxorubicin
DRAQ5	Deep Red Anthraquinone 5
ECM	Extracellular Matrix
EDTA	Ethylenediaminetetraacetate
EdU	5-Ethynyl-2'-Deoxyuridine

EGF	Epidermal Growth Factor
EMA	European Medicine Agency
EPAA	European Partnership for Alternative Approaches to Animal Testing
ESC	Embryonic Stem Cells
EtBr	Ethidium Bromide
EthD-1	Ethidium Homodimer-1
FAK	Focal Adhesion Kinase
FAP	Fibroblast Activation Protein
FBS	Fetal Bovine Serum
FDA	Food and Drug Administration
FDISCO	3D Imaging of Solvent-Cleared Organs with Superior Fluorescence Preserving Capability
FGF	Fibroblast Growth Factor
FITC	Fluorescein Isothiocyanate
FTIR	Fourier Transform Infrared
Fucci	Fluorescent Ubiquitination-Based Cell Cycle Indicator
GFP	Green Fluorescent Protein
GLUT	Glucose Transporter
H&E	Hematoxylin ad Eosin
HA	Hyaluronic Acid
HAPS	Hypoxia-Activated Pro-Drug
hASC	Human Derived Adipose Stem Cell
HDME	Human Dermal Microvascular Endothelial Cell
HGF	Hepatocyte Growth Factor
HIF	Hypoxia-Inducible Factor
HOB	Human Osteoblast
HTS	High-Throughput Screening
HUVEC	Human Umbilical Vein Endothelial Cell
IC_{50}	Half-Maximum Inhibitory Concentration
ID	Integrated Density
iDISCO	Immunolabeling-Enabled 3D Imaging of Solvent-Cleared Organs
IFP	Interstitial Fluid Pressure
IGF	Insulin-Like Growth Factor
IL	Interleukin
iPSC	Induced Pluripotent Stem Cell

Klf	Kruppel-Like Factor
LDH	Lactate Dehydrogenase
LIF	Leukemia Inhibitory Factor
LOT	Liquid Overlay Technique
LSFM	Light Sheet Fluorescence Microscopy
MCT	Masson's Trichrome
MDR	Multidrug Resistance
mDSLM	Monolithic Digital LSFM
MFB	Mean Fluorescence of The Background
MMP	Matrix Metalloproteinase
MPM	Multi-Photon Microscopy
MRP	Multidrug Resistance-Associated Protein
MSC	Mesenchymal Stem Cell
MTC	Monocarboxylate Transporter
MTS	3-(4,5-Dimethylthiazol-2-Yl)-5-(3-Carboxymethoxyphenyl)-2-(4-Sulfophenyl)-2H-Tetrazolium
MTT	3-(4,5-Dimethyl-2-Thiazolyl)-2, 5-Diphenyl-2H-Tetrazolium Bromide
MEF	Murine Embryonic Fibroblast
MW	Molecular Weight
n.s.	Non-Significant
NADH	Reduced Nicotinamide Adenine Dinucleotide
NHDF	Normal Human Dermal Fibroblast
NSC	Neural Stem Cell
Oct	Octamer-Binding Transcription Factor
p27-ASON	P27-Antisense Oligodeoxynucleotide
PACT	Passive Clarity Technique
PARS	Perfusion-Assisted Agent Release *In Situ*
PBS	Phosphate-Buffered Saline
PDGF	Platelet-Derived Growth Factor
PDGFR	Platelet-Derived Growth Factor Receptor
PDMS	Polymethylsiloxane
PEG	Polyethylene Glycol
PFA	Paraformaldehyde
P-gp	P-Glycoprotein
PI	Propidium Iodide
PIXE	Proton Induced X-Ray Emission

poly-HEMA	Poly(2-Hydroxyethyl Methacrylate)
qRT-PCR	Quantitative Real-Time Reverse Transcription Polymerase Chain Reaction
rBM	Reconstituted Basement Membrane
REF	Reference
RI	Refractive Index
RIMS	Refractive Index Matching Solution
ROS	Reactive Oxygen Species
RPM	Rotations per Minute
RT	Room Temperature
SA	Selected area
SD	Standard Deviation
SDS	Sodium Dodecyl Sulfate
SeeDB	See Deep Brain
SEM	Scanning Electron Microscopy
SPIM	Single (or Selective) Plane Illumination Microscopy
TB	Toluidine Blue
TDE	2,2′-Thiodiethanol
TDS	Tissue Dynamic Spectroscopy
TEM	Transmission Electron Microscopy
TGF	Transforming Growth Factor
THF	Tetrahydrofuran
TNF	Tumor Necrosis Factor
uDISCO	Ultimate 3D Imaging of Solvent-Cleared Organs
UV	Ultraviolet
VCAM	Vascular Cell Adhesion Molecule
VEGF	Vascular Endothelial Growth Factor
WGA	Wheat Germ Agglutinin
WHO	World Health Organization
WST-8	2-(2-Methoxy-4-Nitrophenyl)-3-(4-Nitrophenyl)-5-(2,4-Disulfophenyl)-2-Tetrazolium

Chapter 1

Global Aims

Global Aims

Spheroids are the *in vitro* 3D cell culture model that closely represent the properties of the tumors found in humans. Nevertheless, the analysis of the spheroids by using fluorescence microscopy, such as CLSM, is still limited by the low penetration of the light within the spheroids due to the light scattering phenomenon. In order to improve the imaging of spheroids, optical clearing methods can be used to homogenize the RI across the cellular and acellular spheroids constituent and consequently enhance the penetration of the light. Having this in mind, the main objective of this thesis was to investigate and optimize the application of *Clear*^{T} and *Clear*^{T2}.

The specific aims of this thesis were:

- Application of the *Clear*^{T} optical clearing method on PI-stained spheroids;
- Optimization of the *Clear*^{T2} optical clearing method application on PI-stained spheroids;
- Image of the non-cleared and cleared spheroids by optical and fluorescence microscopy, namely CLSM;
- Analysis of the optical and CLSM images;
- Comparison of the results obtained for non-cleared and cleared spheroids.

Chapter 2

Introduction (part A)

3D tumor spheroids as *in vitro* models to mimic *in vivo* human solid tumors resistance to therapeutic drugs

This chapter is based on the publication entitled: 3D tumor spheroids as *in vitro* models to mimic *in vivo* human solid tumors resistance to therapeutic drugs, Biotechnology and Bioengineering, 2018, 116(1): 206–226.

2.1. Abstract

Three-dimensional (3D) cell culture models, such as spheroids, can be used in the process of development of new anticancer agents, since they are able to closely mimic the main features of human solid tumors, namely their structural organization, cellular layered assembling, hypoxia and nutrient gradients. These properties imprint to the spheroids an anticancer therapeutics resistance profile, which is similar to that displayed by human solid tumors. In this chapter, an overview of 3D tumor spheroids properties and drug resistance mechanisms are provided. Further, comparisons between the therapeutics resistance profile exhibited by spheroids and two-dimensional (2D) cell cultures are presented. Lastly, examples of the therapeutic approaches that have been developed to surpass the drug resistance mechanisms exhibited by spheroids are described.

Keywords: drugs; drug resistance; *in vitro* models; solid tumors; spheroids.

2.2. Introduction

Cancer still remains as one of the deadliest diseases affecting the worldwide population [1]. Chemotherapy (administration of compounds such as drugs), among other anticancer treatments such as surgery (removal of cancer tissue from the body) and radiotherapy (administration of radiation), is the most used clinical treatment approach toward cancer related diseases since 1940 [2]. However, chemotherapeutic agents are often unspecific, rapidly cleared from circulation and present a low accumulation at the tumor site [3]. Moreover, cancer cells can develop resistance to anticancer drugs in the beginning of the treatment or after several administrations of the drugs. Consequently, cancer cells will be able to avoid the drugs action leading to a decreased therapeutic effectiveness [4]. This increased resistance of the cancer cells helps to understand why the progression-free survival of patients after the second-line of chemotherapy is lower than that of first-line treatment [5].

Therefore, the scientific community and the pharmaceutical industry have been investing in the development of more effective anticancer therapeutics aimed to fight the solid tumors resistance [6, 7]. Still, these compounds must fulfill the requirements established by the regulatory agencies, like Food and Drug Administration (FDA) and the European Medicine Agency (EMA), before they can be applied in the clinic. For that purpose, all the anticancer therapeutics candidates must be evaluated on *in vitro* and *in vivo* assays (preclinical stage of drug development process), and further in humans (clinical trials) [8].

Up to now, the 2D cell cultures (Figure 2.1), initially developed by Harrison in the early 19 century [9], remain as the most commonly used *in vitro* method for therapeutics screening due to its simplicity, reproducibility and low cost [10-12]. Nevertheless, flat 2D cell culture models are unable to reproduce the properties of *in vivo* solid tumors as well as their resistance to therapeutics. Consequently, a large number of ineffective drugs are able to proceed to the *in vivo* assays, which contributes to the over-use of animals in experimentation, as well as to the increase of the time and overall cost of the drug discovery process [9, 10, 13, 14].

Having this in mind, new and improved *in vitro* models, which are able to reproduce more closely the features of *in vivo* human tumors, have been investigated to improve the screening of the therapeutic candidates in early stages of the drug development and, consequently, reduce the number of animals used in laboratory [12, 13]. One important characteristic of the human solid tumors is their 3D architecture that provides optimal conditions for cellular organization, proliferation and differentiation. Taking this in consideration, *in vitro* 3D cell culture methodologies emerged in the recent decades as a viable intermediate step between standard 2D cancer cell cultures and *in vivo* animal experimentation for drug screening purposes (Figure 2.1).

In cancer research, spheroids are regarded as the main 3D cell culture model capable of reproducing a wide number of structural, physiological and biological features of solid tumors (*e.g.* oxygen, gases, nutrient and waste gradients; distribution of proliferative, senescent and necrotic cells; cellular heterogeneity and cell-cell signaling; extracellular matrix (ECM) proteins deposition and cell-ECM interactions; stem-like properties [15-18]) – Figure 2.1.

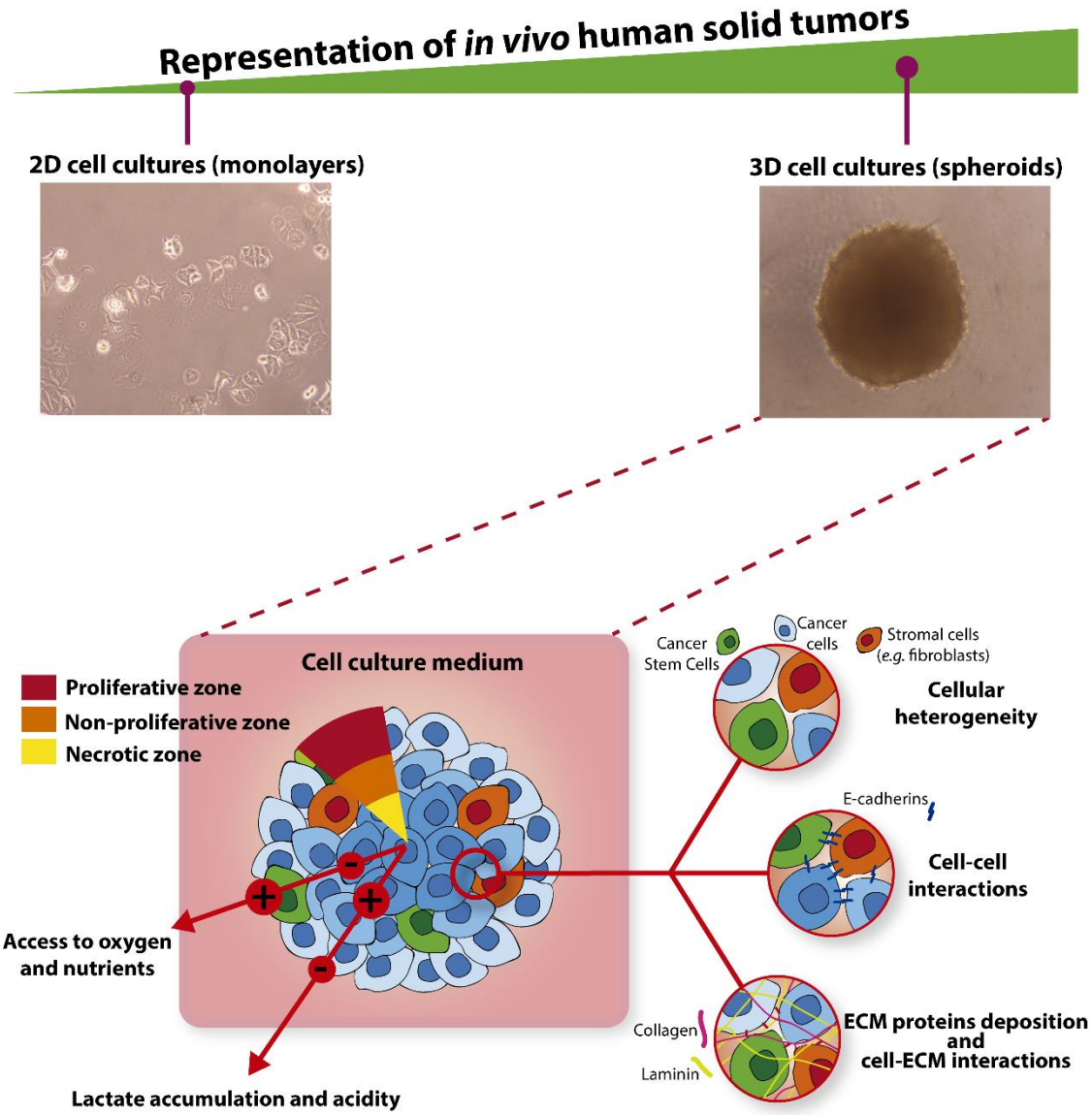

Figure 2.1. Overview of spheroids' properties that are similar to those found on human solid tumors.

These properties have prompted the spheroids application in the study of several aspects of basic tumor biology, such as: i) tumor growth kinetics; ii) cancer cells metabolism; iii) invasion and migration of cancer cells; iv) cancer stem cells and their niche; v) tumor microenvironment signaling crosstalk (reviewed in detail in [19]). On the other hand, spheroids are also capable of mimicking tumors evasion mechanisms to the anticancer treatments (discussed in detail in the following sections). Thus, they have been also widely used to investigate several anticancer treatment approaches, such as chemotherapy and combination chemotherapy [20, 21], drug

delivery systems [18, 21, 22], gene and oncolytic virus therapy [23], immunotherapy [24], photodynamic therapy [25, 26], phototherapy [27], photothermal therapy [28] and radiotherapy [26, 29]. Having this in mind, a better understanding of how the drug resistance mechanisms occur in spheroids may contribute for the development of more effective anticancer treatments.

Herein, the features of tumor spheroids that are similar to those found in human solid tumors will be discussed in detail, demonstrating how these properties contribute for the cells escape to therapeutics action. Further, examples of therapeutic approaches that can be used to act on these resistance mechanisms are also provided.

2.3. Spheroids' solid tumors-like properties and resistance against therapeutics

Large spheroids (> 500 μm in diameter) are capable of mimicking various properties of human solid tumors with sizes from 0.5 to 1 mm^3 [19]. These properties influence the therapeutic effect of various drugs and other pharmacological molecules on spheroids through similar mechanisms found in *in vivo* human solid tumors.

2.3.1. Lack of oxygen

In solid tumors, the oxygen delivery to the cells present in the inner regions of the tumor mass is frequently reduced due to the increased oxygen diffusion distances, *i.e.* distance between vasculature and cells [30]. Additionally, several tumor vessels irregularities (abnormal vessel walls, abnormal vascular architecture or abnormal vascular density) also contributes for the limited access to oxygen by the cells [30, 31]. Such leads to the establishment of a gradient of oxygen, *i.e.* cells in the external layer of the tumor have a high access to oxygen while those within the tumor (100 μm apart of the tumor vessels) are in hypoxia (reduced O_2 availability and decreased O_2 partial pressure) [30, 32]. During spheroids growth, a gradient of oxygen is also established (Figure 2.2), as demonstrated in several studies that measured the oxygen tension or content in spheroids by using O_2-sensitive microelectrodes or fiber-optic oxygen sensors [33-35]. The oxygen gradient in spheroids is explained by the proliferation of the cells in the external region of the spheroid during its growth resulting in a higher consumption of oxygen by these cells. At the same time, the oxygen diffusion distance also increases with the spheroid growth and, consequently, the oxygen availability and diffusion from the medium into the spheroid is reduced towards the spheroid center [33, 34, 36].

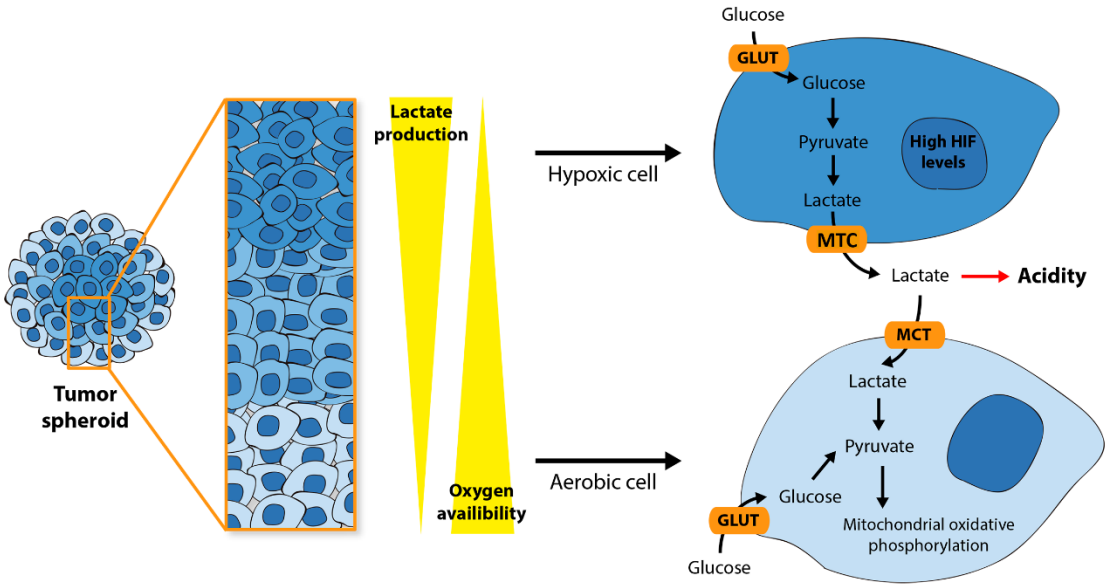

Figure 2.2. Oxygen distribution in tumor spheroids originating a hypoxia gradient that influences cells' metabolism.

As consequence of the hypoxic environment found in spheroids, cells display up-regulated expression of hypoxia-inducible factors (HIF). Tian and co-workers observed that the expression of HIF-1α protein occurred in Hela spheroids, while the same cells cultured in 2D did not show any HIF-1α expression [37]. Further, the expression of these factors by spheroid cells contributes for the establishment of various mechanisms of therapeutic resistance (reviewed in [38]). One of the main examples is the up-regulation of the multidrug resistance 1 gene (MDR1) that codifies the P-glycoprotein (P-gp; cell membrane protein that actively exports drugs or other molecules to the exterior of the cell). Wartenberg *et al.* reported that the expression of both HIF-1α and P-gp was up-regulated in DU-145 prostate tumor spheroids (994% and 388%, respectively) [39]. In another study, it was verified that the HIF-1 expression occurs in MCF-7 breast cancer spheroids contributing for the P-gp up-regulation, whereas no significant alterations were noticed in MCF-7 cells [40]. Moreover, this increased P-gp activity reduced the Doxorubicin (DOX) accumulation in the cells that form the spheroids [40].

The vascular endothelial growth factor (VEGF) can also have a crucial role in the cells' drug resistance and its expression can also be influenced by the HIF expression [41]. In fact, the data available in the literature demonstrates that VEGF is highly expressed in hypoxic regions of the spheroids [42, 43]. Terashima *et al.* noticed that the KYSE-70 esophageal cancer cells of spheroids, in comparison to those cells cultured in monolayers, present a 2-fold higher level of VEGF mRNA, which was mediated by the HIF-1α up-regulation [44]. Additionally, Qin and co-workers also observed that melanoma spheroids composed of A375 cells presented a higher HIF-1α and VEGF expression than the same cells cultured in 2D, and demonstrated that this metabolic variation can impact on cells sensitivity to Vemurafenib [43].

In literature, it was also reported that HIF-1 regulates the expression of several anti-apoptotic factors (*e.g.* Bak, Bax, Bcl-xL, Bcl-2, Bid, Mcl-1, NF-κB, p53 and survivin) [38, 45]. For instance, in a study performed by Khaitan *et al.* it was noticed that Bax, Bcl-2 and HIF-1α levels were up-regulated in glioma BMG-1 cultured as spheroids, that could lead to cells escape to cellular death prompted by anticancer therapeutics [46].

On the other side, the hypoxic environment found in spheroids can also support the development of the cancer cells resistance to therapeutics due to the fact that some compounds (*e.g.* 5-Fluorouracil (5-FU), Cisplatin, DOX and Irinotecan) need oxygen to induce an effective anticancer effect through the formation of reactive oxygen species (ROS) that damage cell's membrane and DNA [47, 48]. A decreased ROS formation in spheroids was already observed by Wartenberg and colleagues, which reported that DU-145 prostate tumor spheroids have reduced pericellular oxygen pressure and, consequently, a limited ROS generation [39].

This lack of oxygen within the spheroids has been also linked to a decrease in the cell damage mediated by radiation. In fact, the availability of the local molecular oxygen improves the efficacy of radiotherapy, as DNA lesions caused by ROS produced during water radiolysis react with oxygen to from stable DNA peroxides [49]. Having this in mind, the cancer cells that receive less oxygen, such as those from spheroids core, are typically more radioresistant [50, 51]. Khaitan *et al.* demonstrated that the BMG-1 cell monolayers were more affected by the 0-10 Gy-radiation than the spheroids, once the ROS production in the cells after the radiation was higher in the monolayers than in spheroids [46].

In order to surpass the chemoresistance resulting from the hypoxic environment found in solid tumors and spheroids, hypoxia-activated pro-drugs (HAPS) have been explored (Table 2.1). This type of drugs suffer a chemical reduction and become active when they are exposed to hypoxic environments, having no effect for cells in environments with normal oxygen levels [52].

Meng and colleagues evaluated HAPS, such as Tirapazamine and Evofosfamide (TH-302), in H460 lung cancer spheroids and concluded that the therapeutic effect of these drugs is dependent on the hypoxic environment found within spheroids [57]. In fact, the TH-302 IC_{50} (half-maximum inhibitory concentration) was 0.3 μM in 0.1% O_2 and 94 μM in 21% of O_2 [57]. In a recent study of Liu *et al.* it was demonstrated that the TH-302 increased the inhibitory effect of Sunitinib on 1205Lu melanoma spheroids and this combination also increased the survival of treated melanoma bearing genetically engineered mice (median survival of 112 *vs.* 75 days obtained for Sunitinib alone) [58].

Table 2.1. Hypoxia-activated pro-drugs (HAPS) that target regions of tumor hypoxia.

Drug/Compound	Action mechanism(s)	Status*	REF(s)
Apaziquone (EO9)	Generates DNA-damaging species (*e.g.* alkylating agents)	Clinical phase III	[53, 54]
Banoxantrone (AQ4N)	Inhibits Topoisomerase II	Clinical phase II	[53]
Evofosafamide (TH-302)	Generates DNA-damaging species (*e.g.* alkylating agents)	Clinical phase III	[53, 54]
Nimorazole	Generates DNA-damaging species (*e.g.* radical species)	Clinical phase III	[52]
Porfiromycin	Generate DNA-damaging species (*e.g.* radical species and alkylating agents)	Clinical phase III	[52]
PR-104	Generate DNA-damaging species (*e.g.* nitrogen mustard DNA crosslinking agents)	Clinical phase II	[53, 55]
Tarloxotinib (TH-4000)	Generate DNA-damaging species (*e.g.* nitro radical anion species)	Clinical phase II	[53, 54]
Tirapazamine (SR 4233)	Generate DNA-damaging species (*e.g.* radical species)	Clinical phase III	[53, 54, 56]

* Includes the trials were drugs were evaluated for cancer related diseases, data derived from clinicaltrials.gov (www.clinicaltrials.gov), accessed on 20th July, 2018.

On the other side, anticancer agents that inhibit HIF-1 activity have also been investigated, comprising those inhibitors of: i) HIF-1 mRNA expression (*e.g.* Aminoflavone, EZN-2698, PX-478 and Topotecan); ii) HIF-1 translation (*e.g.* Digoxin, Ouabain and Proscillaridin); iii) HIF-1 transcription (*e.g.* Bortezomib, Chetomin, Echinomycin, PX12 and PMX290); and iv) HIF-1 protein stability (*e.g.* 3-(5'-hydroxymethyl-2'-furyl)-1-benzylindazole (YC-1), Apigenin and Geldanamycins) - reviewed in detail in [38, 45, 59-61]. A study performed by Doublier and co-workers demonstrated that the administration of HIF-1α inhibitors (3-(5'-hydroxymethyl-2'-furyl)-1-benzylindazole and siRNA for HIF-1α) significantly reduced the expression of P-gp, leading to an increased intracellular accumulation of DOX in MCF-7 breast cancer spheroids, as well as an enhanced activity of the caspase-9 activity, which plays an essential role in cell apoptosis [40].

2.3.2. Variations in cells energy metabolism

Under normal oxygen conditions, cells obtain their energy through mitochondrial oxidative phosphorylation. In solid tumors, due to the reduced oxygen content available in the inner regions of the tissue (as discussed in the previous section), cells obtain energy through the anaerobic metabolism of glucose that have lactate as a by-product - Warburg effect [62]. This altered energy metabolism presented by human solid tumors is also found in tumor spheroids

(Figure 2.2). Longati *et al.* observed that the mRNA expression ratio of glucose transporter-1 (GLUT-1; predominant glucose transporter in many types of cancer) and lactate dehydrogenase (LDH; enzyme that is responsible for the lactate production) on the PANC-1 pancreatic cancer cells cultured in 2D/3D was approximately 3.5 and 7.5, respectively [63]. Similarly, Pereira *et al.* also demonstrated that GLUT-1 expression was 0.5-fold higher in MCF-7 breast cancer spheroids in comparison to the monolayer cultures [64]. Additionally, Khaitan *et al.* denoted that the glucose consumption and lactate production were 2- up to 3-folds higher in BMG-1 glioma spheroids than in BMG-1 monolayer cell cultures [46]. In the literature it has been reported that the increase of GLUT-1 and lactate production due to the high glycolytic rate of the cancer cells can lead to drug resistance through the altered expression of the multidrug resistance-associated protein 1 (MRP1) and P-gp [65].

In order to reduce the impact of the drug resistance mechanisms related to the altered energy metabolism, researchers have been exploring the utilization of therapeutics that reduce the glucose transport and inhibits the glycolytic rate displayed by cancer cells (Table 2.2). For instance, Wartenberg and colleagues demonstrated that the downregulation of glycolysis by the administration of Iodoacetate or 2-Deoxyglucose reduced the P-gp expression in DU-145 prostate cancer and Gli36 glioma spheroids and thus increased the DOX retention in the cells [66].

2.3.3. Acidic microenvironment

In human solid tumors the increased production of lactate by oxygen deprived cells originates an acidic environment (pH of 6.5-7.2) [31]. In spheroids, the lactate production also promotes the acidification of its core [79] - Figure 2.2. Carlsson *et al.* observed that spheroids (*e.g.* HT29 colon carcinoma, U-251 MG glioma and HTh-7 thyroid carcinoma spheroids) display a low pH within their structure, *i.e.* the spheroids deepest regions presented lower pH values [80]. These low pH values have an impact on drugs efficiency by affecting their cellular uptake [18, 81]. In particular, weak basic drugs with a dissociation constant of 7.5-9.5 (*e.g.* DOX, Mitoxantrone, Vincristine, Vinblastine, anthraquinones and vinca alkaloids) are protonated in acidic environments. As result, the cellular uptake of these drugs is reduced, since charged drugs are less effective in transposing cellular membrane [81, 82]. This influence of spheroids pH in drugs uptake was initially verified by Swietach *et al.* [83]. These authors showed that the DOX uptake decreased proportionally to the HCT116 colon cancer spheroid-depth, *i.e.* the deepest and acidic regions of the spheroids presented the lowest cellular drug uptake (1.7-fold lower at pH = 6.4 than at pH = 7.4) [83]. Consequently, the IC_{50} of DOX was higher at pH = 6.4 [83].

Moreover, inhibitors of sodium-driven bicarbonate transporters have been also evaluated in spheroids to reduce or overcome the pH-dependent therapeutic resistance. For instance, Mclntyre *et al.* demonstrated that the administration of S0859 in spheroids comprising tumor cells, colon (Ls174T), breast (MDA-MB-231) or glioma (U87), resulted in the pH stabilization and

further increased the cellular apoptosis in the spheroids core (verified through the analysis of caspase-3 activity) [84].

Table 2.2. List of molecules that inhibit glucose transport or glucose metabolism.

Target	Drug/Compound	Status*	REF(s)
Glucose transport (*e.g.* GLUT-1) inhibitor	Apigenin	Clinical phase II	[67]
	BAY-876	Preclinical	[68]
	Fasentin	Preclinical	[69, 70]
	Genistein	Clinical phase III	[67]
	Glufosfamide	Clinical phase III	[71]
	Hesperetin	Preclinical	[67]
	Naringenin	Clinical early phase I	[68]
	Phloretin	Preclinical	[68, 70, 72]
	Resveratrol	Clinical phase II	[68]
	STF-31	Preclinical	[68, 73]
	Silybin	Clinical phase I	[68, 72]
	WZB117	Preclinical	[74]
Hexokinase	2-Deoxyglucose	Clinical phase IV	[69, 70, 72, 75]
	3-Bromopyruvate	Preclinical	[69, 70, 72, 75]
	Clotrimazole	Preclinical	[70]
	Imatinib	FDA-approved	[75]
	Lonidamine	Clinical phase III	[69, 75]
	Methyl jasmonate	Preclinical	[67]
Glucose-6-phosphate dehydrogenase	6-aminonicotinamide	Preclinical	[69]
	Imatinib	FDA-approved	[75]
Glyceraldehyde 3-phosphate dehydrogenase	Iodoacetamide	Preclinical	[76]
	Iodoacetate	Preclinical	[70, 72]
Enolase	Fluoride	Clinical phase II	[70]
Pyruvate kinase	Alkannin	Preclinical	[67]
	Shikonin	Preclinical	[69]
	TT-232	Preclinical	[69]
Lactate dehydrogenase	Dichloroacetate	Clinical phase II	[70, 72]
	FX11	Preclinical	[70, 72]
	Galloflavin	Preclinical	[77]
	Gossypol (AT-101)	Clinical phase III	[77]
	NHI-1	Preclinical	[78]
	NHI-2	Preclinical	[78]

* Includes the trials were drugs were evaluated for cancer related diseases, data derived from clinicaltrials.gov (www.clinicaltrials.gov), accessed 20th July, 2018.

On the other side, compounds that target LDH, enzyme responsible for the lactate production, have been explored to overcome the acidic environment created by the highly glycolytic cells [77] - Table 2.2. A study performed by Maftouh and colleagues demonstrated that the administration of NHI-1 and NHI-2 LDH inhibitors in combination with Gemcitabine to PANC-1 and LPC006 pancreatic cancer spheroids significantly contributed for the disintegration of the spheroids as well as to the reduction of their sizes when compared with the untreated spheroids [78].

Alternatively, inhibitors of the transporters involved in lactate transportation across the cellular membrane, namely monocarboxylate transporter (MTC; *e.g.* MCT1 and MCT4), can be used to regulate the lactate accumulation and acidification of the tissue. Examples of these MTC inhibitors are the α-cyano-4-hydroxycinnamate, AZD3965, Luteolin, Morin, Phloretin and Quercetin [72, 85, 86].

2.3.4. Cell cycle arrest

The acidic pH, in association with the lack of oxygen and nutrients induces a dormant state, *i.e.* quiescence or senescence, on cells present in solid tumors or in spheroids [87]. Despite that, these cells are able to express cytokines, chemokines and growth factors involved in tumorigenesis and therapeutics resistance profile (reviewed in [87]). Barrera-Rodríguez and Fuentes suggested that INER-37 and INER-51 lung cancer spheroids are more resistance towards Camptothecin, DOX, Etoposide and Teniposide when compared to 2D cell cultures, a result that was associated to the quiescent cell subpopulation found in the spheroids [88]. In a different study, Gong *et al.* analyzed the cell cycle of MCF-7 breast cancer cells cultured in monolayer or spheroids through flow cytometry [42]. The data obtained revealed that spheroids possess an increased number of cells in quiescence, *i.e.* spheroids presented 58.48% of the cells trapped in G0-G1 phase of cell cycle, contrasting with the 40.76% of the cells cultured in 2D [42]. Accordingly, when incubated with DOX, the MCF-7 cells cultured in monolayers presented an increased cellular death, *i.e.* the IC_{50} of this drug was approximately 50-, 60- and 80-fold higher for spheroids with 300, 400 and 500 μm diameter, respectively [42].

The non-proliferative state of cells within spheroids can also be responsible for a poor therapeutic efficacy of drugs that are more efficient in proliferative cells, such as Carboplatin, Cisplatin, DOX, Oxaliplatin, Methotrexate and Paclitaxel [89]. Usually, the cytotoxic effect mediated by this type of drugs depends on their covalent or noncovalent interaction with the DNA during the process of cellular replication [89]. Having this in mind, Imamura *et al.* evaluated the expression of Ki-67 (a proliferative biomarker) and the effect of Paclitaxel in 2D cell cultures and spheroids of BT-474, BT-549 and T-47D cells [90]. The results demonstrated that, as example, the BT-549 cells presented 84% of Ki-67 positive cells when cultured in 2D, whereas this value decreased to 46.5% when in spheroids, suggesting that the spheroids had a greater G0-dormant subpopulation that was responsible for its resistance to Paclitaxel [90].

To surpass the drugs poor therapeutic effect on dormant cells, Xing and colleagues administrated p27-ASON (a p27-antisense oligodeoxynucleotide) that mediated the decrease of the p27 expression (a cyclin-dependent kinase inhibitor that prompted cellular senescence) on A2780 and CAOV3 ovarian cancer spheroids [91]. Consequently, the number of A2780 and CAOV3 cells in the S-G2 phase of cell cycle increased, which led to an improved Paclitaxel toxicity (drug mediated apoptosis rate in A2780 spheroids non-treated with ASON corresponded to 16.11% while 34.22% for ASON treated spheroids) [91].

2.3.5. Heterogenic cellular constitution

Nowadays, it is well known that solid tumors have a heterogenic cellular constitution, *i.e.* these tissues are not only composed of cancer cells, but also by stromal cells like adipocytes, fibroblasts (also known as cancer-associated fibroblasts (CAF)), immune cells (*e.g.* lymphocytes and macrophages), lymphatic endothelial cells, vascular endothelial cells and pericytes [92, 93]. Despite of these cells being non-malignant, their interactions with each other and with the cancer cells through the secretion of cytokines and growth factors (*e.g.* interleukin 1 (IL-1), IL-6, fibroblast growth factors (FGF), insulin-like growth factor (IGF) and hepatocyte growth factor (HGF)) – Figure 2.3, promote events such as tumor angiogenesis, proliferation, invasion, metastasis, as well as mediate mechanisms of therapeutic resistance (reviewed in [94-97]).

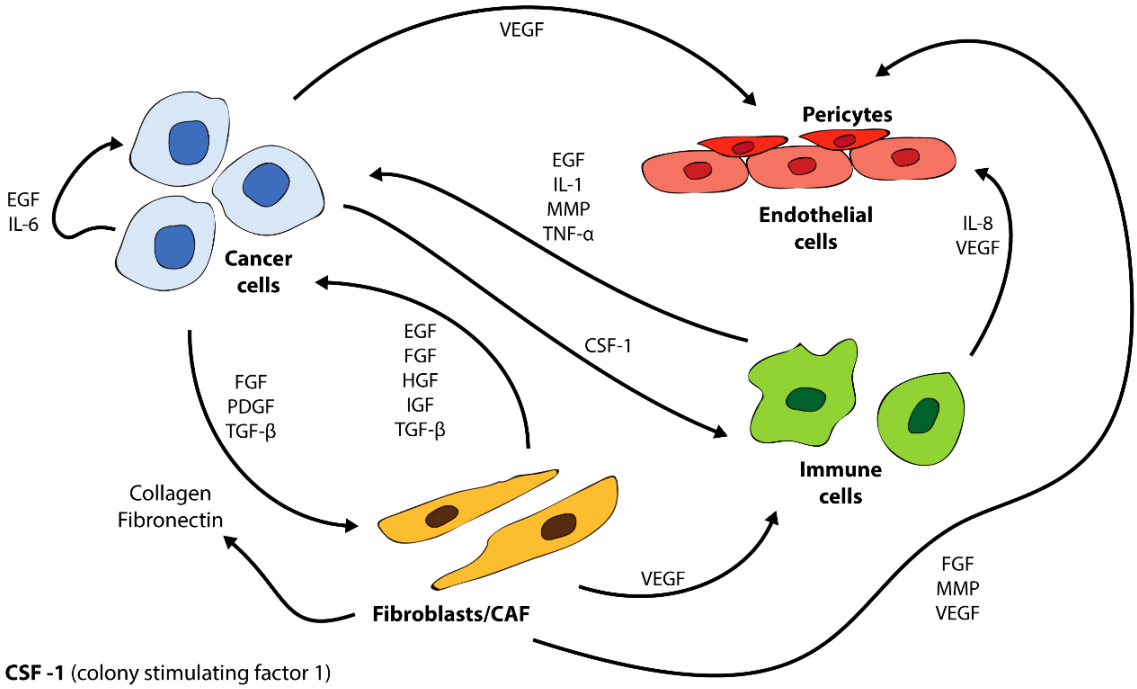

CSF -1 (colony stimulating factor 1)
EGF (epidermal growth factor)
FGF (fibroblast growth factor)
HGF (hepatocyte growth factor)
IGF (insulin-like growth factor)
IL-1, -6, -8 (interleukin 1, 6, 8)
MMP (matrix metalloproteinases)
PDGF (platelet-derived growth factor)
VEGF (vascular endothelial growth factor)
TGF-β (transforming growth factor beta)
TNF-α (tumor necrosis factor alpha)

Figure 2.3. Overview of the cancer cells cross-talk with the major stromal cells through the secretion of cytokines and growth factors.

The 3D tumor spheroids have been also optimized in order to mimic the cellular heterogeneity of the solid tumors, as well as the resistance mediated by the tumor-stromal cell interactions by the production of spheroids using a co-culture of cancer and stromal cells (heterotypic spheroids). For instance, Majety *et al*. produced spheroids composed of cancer cells (pancreatic, breast or lung) and fibroblasts that demonstrated an increased cell proliferation [98]. This improved proliferation of the cells was attributed to the increased secretion of epidermal growth factor (EGF), HGF and IL-6, when cells were maintained in co-culture [98]. Also, authors observed that the increased expression of soluble factors contributed for cancer cells resistance, once pancreatic cancer cells (Bxpc3) in monoculture demonstrated approximately 50% survival to treatment with Erbitux, while Bxpc3 cells in spheroids co-culture with fibroblasts (MRC5 lung fibroblasts or LT2 pancreatic fibroblasts) demonstrated approximately 75% survival to the same treatment [98]. Lee *et al.*, in a recent study, demonstrated that the co-cultivation of the cancer cells with CAF improved spheroids expression of proliferation and invasive markers, such as transforming growth factor beta 1 (TGF-β1), N-cadherin and vimentin, as well as their resistance to drugs [99]. In particular, more than 90% of head-and-neck cancer cells (HN3, HN4 and HN9), when cultured in 2D, died after being treated with < 5 μM Sorafenib or < 10 μM Cisplatin. On the other hand, when these cells were cultured as spheroids, they exhibited viability levels superior to 60% after their treatment with 10 μM Sorafenib or 20 μM Cisplatin, which further increased to more than 90% when they were co-cultivated with CAF cells [99]. Similar findings were observed in other studies, where heterotypic spheroids were produced with colorectal cancer cells (Caco-2) and CAF [100]; colorectal cancer cells (HT-29) and fibroblasts (CCD-18Co) [101]; prostate cancer cells (LNCaP and DuCaP) and CAF [102]; breast cancer cells (MDA-MB-231) and microvascular endothelial cells (HMEC-1) [103]; pancreatic cancer cells (PANC-1) and pancreatic stellate cells (myofibroblast-like cells) [104].

Since the stromal cells display a crucial role in tumor resistance, different tumor stroma cells-targeted therapeutic approaches have been investigated and are currently under evaluation, as reviewed in detail in [94, 95, 105-109]). Since CAF are one of the major cellular components of the tumor stroma, several therapeutics targeting the markers of these cells (*e.g.* fibroblast activation protein (FAP)) or their paracrine signaling pathways (*e.g.* platelet-derived growth factor receptor (PDGFR), HGF/MET receptor tyrosine kinase and TGF-β signaling pathways) are under investigation (Table 2.3). Likewise, other therapeutics that target stroma immune cells (*e.g.* Bindarit, CNTO 888, Ki20227 and JNJ-28312141 [108]), endothelial cells (*e.g.* Bevacizumab, Erlotinib and Gefitinib [108]) and pericytes (*e.g.* SU11248 and SU6668 [107]) have been also studied.

Table 2.3. Drugs/compounds targeting CAF or their paracrine signaling pathways.

Mechanism	Target	Drug/Compound	Status*	REF(s)
Targeting fibroblast markers directly	Fibroblast activation protein (FAP)	Rebimastat	Clinical phase III	[110]
		Ro6874813	Clinical phase I	[111]
		Ro6874281	Clinical phase II	[111]
		Sc40-fasl	Preclinical	[110]
		Sibrotuzumab	Clinical phase II	[107, 111, 112]
		Talabostat (PT-100)	Clinical phase III	[112, 113]
Targeting paracrine signaling of fibroblasts	HGF/MET signaling pathway	Cabozantinib (XL184)	FDA-approved	[113]
		Crizotinib	FDA-approved	[113]
		Ficlatuzumab	Clinical phase II	[113]
		Rilotumumab	Clinical phase III	[113]
		Tivantinib (ARQ197)	Clinical phase III	[113]
	PDGF/PDGFR signaling pathway	Apatinib (YN-968D1)	Clinical phase IV	[111]
		Crenolanib	Clinical phase III	[111]
		Dasatinib (BMS-354825)	FDA-approved	[111]
		Dovitinib	Clinical phase III	[109, 111]
		Famitinib	Clinical phase III	[111]
		Imatinib	FDA-approved	[107, 112]
		Masitinib (AB1010)	Clinical phase III	[111]
		Motesanib (AMG 706)	Clinical phase III	[111]
		Sorafenib (BAY 43-9006)	FDA-approved	[111]
		Sunitinib (Su11248)	FDA-approved	[113]
	TGF-β signaling	Fresolimumab (GC-1008)	Clinical phase II	[111]
		Galunisertib (LY2157299)	Clinical phase III	[111, 113]
		PF-03446962	Clinical phase II	[111]
		Tasisulam	Clinical phase III	[111]
		Trabedersen	Clinical phase III	[111]

* Includes the trials were drugs were evaluated for cancer related diseases, data derived from clinicaltrials.gov (www.clinicaltrials.gov), accessed 20th July, 2018.

2.3.6. Presence of a Cancer Stem Cells (CSC)

During the last years, the results obtained show the presence of a subpopulation of cancer cells with stem cell-like properties - Cancer Stem Cells (CSC) - in the mass of different tumors, such as breast, brain, colon, gastric, hepatic, lung, ovarian, pancreas, prostate and skin cancers [114, 115]. These cells exhibit unlimited self-renewal capacity and differentiation potential [116]. Additionally, studies have been demonstrating that CSC are resistant against chemotherapy and radiation, being capable to rebuilt the tumors following a treatment cycle [117]. The resistance of these cells is associated with three main mechanisms, namely: i) increased expression of aldehyde dehydrogenase (ALDH; enzyme capable of metabolizing drugs,

such as Cyclophosphamide); ii) enhanced DNA damage response; and iii) increased expression of ATP-binding cassette (ABC) transporters (*e.g.* ABCB1 (P-gp), ABCG2 and ABCB5) [118].

Nowadays, spheroids composed of CSC or cells with stem cell-related characteristics have been produced (Figure 2.4). For this purpose, spheroids are usually formed with cells isolated from tumor biopsies - Tumor-derived spheroids - since these cancerous tissues are rich in CSC or cells with stem cell-related characteristics. For instance, Todaro *et al.* produced spheroids with cells obtained from human colon adenocarcinoma tissue fragments and confirmed the expression of a CSC marker, *i.e.* CD133 [119]. Authors also observed that spheroids of CD133- cells showed a high sensitivity to treatments with 5-FU and Oxaliplatin, while the CD133+ cells were largely insensible to the drugs-induced apoptosis even at the highest dose of the tested concentrations [119]. For example, the 100 µM of Oxaliplatin reduced the CD133+ cell viability in only ≈ 10%, while the same treatment reduced the CD133- cell viability to ≈ 70% [119].

Optionally, spheroids can be produced with CSC obtained from cancer cell lines (Figure 2.4).

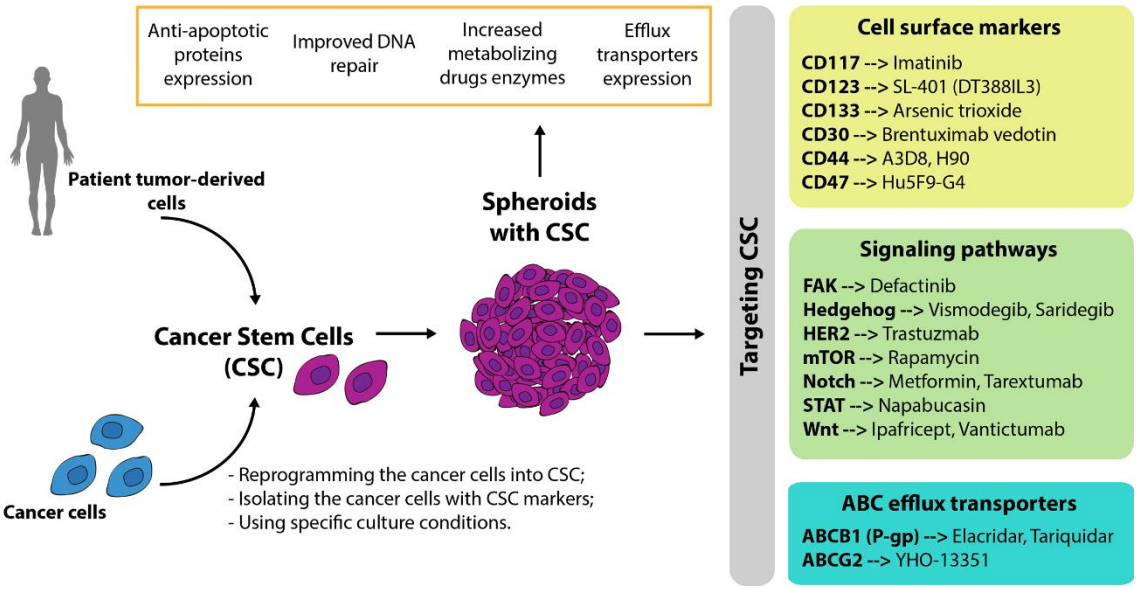

Figure 2.4. Formation of spheroids with CSC, respective properties and examples of therapeutics targeting CSC surface markers, signaling pathways and ABC efflux transporters.

These CSC are usually obtained by: i) reprogramming the cancer cells into CSC through exogenous forced expression of specific sets of transcription factors (*e.g.* octamer-binding transcription factor 4 (Oct4), Kruppel-like factor 4 (Klf4), c-Myc); ii) selecting and isolating the cancer cells with CSC markers within all the cancer cells; or iii) using specific culture conditions (*e.g.* repetitive cycles of hypoxia and reoxygenation, special cell culture media supplement with growth factors) (reviewed in detail in [115]). Bhuvanalakshmi *et al.* demonstrated that it is possible to obtain CSC from U87 and U373 cell lines by growing these glioma cells as spheroids in the absence of serum and supplementing the culture media with B27, EGF and leukemia inhibitory factor (LIF) [120]. Their results demonstrated that 94.12% of U87 spheroids and

83.91% of U373 spheroids were positive for CD133, whereas the monolayer culture resulted only in 63.56% and 67.6% positive cells for U87 and U373 cell lines, respectively [120]. Other studies showed that the spheroids produced with CSC obtained from cancer cell lines (*e.g.* BT474, GBM6, H1650 and MDA-MB-231) demonstrated a higher resistance towards different therapeutics (*e.g.* 5-FU, Camptothecin, Carmustine, Cisplatin, Gemcitabine, Lomustine, Paclitaxel, Temozolomide and Trastuzumab) than 2D cell cultures [121-124].

Since the resistance to chemotherapy and cancer relapse are major clinical challenges attributed to a subpopulation of CSC, several agents that target CSC-associated cell surface receptors (*e.g.* CD44), signaling pathways (*e.g.* Notch and Wnt) and ABC efflux transporters are now in clinical trials (reviewed in detail by several authors [115, 125-130]) – Figure 2.4. In spheroids, drugs that target CSC have been already explored. For example, Matsubara *et al.* observed that Rapamycin (FDA-approved mTOR inhibitor) reduced the viability of CD133+ pancreatic cancer cells spheroids [131]. In another study, Chao *et al.* observed that the treatment of SKOV-3 ovarian cancer spheroids that have stem like properties with an anti-CD44 antibody (A3D8) resulted in the inhibition of the cellular proliferation and enhanced the Cisplatin-induced apoptosis [132].

2.3.7. Cell-cell physical interactions

Cell-cell interactions are more pronounced in 3D cellular structures, such as solid tumors and spheroids, than in the 2D cells cultures. The increased number of cell-cell interactions established in spheroids can control cancer cells behavior, namely in their cell signaling, survival, proliferation and drug sensitivity. Among the cell-cell adhesion receptors, E-cadherins play an important role on tumor cells behavior [133]. E-cadherins are essential for the generation of a strong cellular cohesiveness and for the formation of breast cancer [134-137], hepatocyte [138], prostate cancer [139] and renal carcinoma spheroids [140]. Moreover, several studies already revealed that the expression of E-cadherins is more evident in spheroids than in 2D cultures [141-143]. For instance, E-cadherins expression was more than 5-folds higher in 14 days old spheroids, formed with carcinoma cells derived from differentiated hepatocytes (Huh7), than in their 2D cell cultures [141]. Xu *et al.* also demonstrated that the spheroids of ovarian cancer cells display increased E-cadherin expression, tighter cellular connections and longer survival times [142]. Additionally, authors also reported that the expression levels of E-cadherin influence the therapeutic response of the drugs [142]. In fact, Cisplatin was less effective in SK-H spheroids than in SK-N or OV-L spheroids (47.5, 60.3 and 58.0% of death, respectively), a fact attributed to the higher expression of E-cadherins in SK-H spheroids [142]. In different studies, the E-cadherins impact on spheroids drug resistance has been tackled through the utilization of agents that blocks E-cadherin function. Green *et al.* used an antiadhesive agent, namely SHE78-7 (anti-E-cadherin monoclonal antibody) to block the E-cadherins function [144]. The results obtained demonstrate that the administration of SHE78-7 improves the intracellular accumulation of the chemotherapeutics (5-FU, Etoposide, Paclitaxel

and Vinblastine) in HT29 human colorectal cancer spheroids [144]. For instance, spheroids treated with SHE78-7 displayed approximately a 300% higher accumulation of Vinblastine [144]. In a similar approach, Luebke-Wheeler and colleagues used an E-cadherin blocking antibody to inhibit the E-cadherin function on hepatocyte spheroids, which led to an improved cellular death through a caspase-independent mechanism [145]. Liang and colleagues also demonstrated that the E-cadherin knockdown in HCT116 colorectal cancer cells leads to a decrease on the MDR1 expression in spheroids [143]. This data indicates that E-cadherins can mediate the spheroids drug resistance due to their influence on MDR1 levels via HIF-1α [143].

During the last few years, ADH-1 (Exherin™) has been investigated in clinical trials to treat solid tumors, since it works as a competitive inhibitor of E-cadherins and, consequently, acts as an inhibitor of the cell-cell adhesion [146].

2.3.8. ECM proteins deposition

ECM is a non-cellular component present in all tissues, which is composed essentially by fibrous structural proteins (*e.g.* collagen, elastin, fibrillin), glycoproteins (*e.g.* fibronectin) and proteoglycans (*e.g.* glycosaminoglycan) [147]. ECM provides structural support for the cells within a tissue and plays key roles in the tissue maintenance and function. In tumors, the ECM dynamics often become abnormal and an increased deposition of ECM proteins, such as collagen and fibronectin, occurs [148, 149]. In tumors, the ECM cross-talk with cell surface receptors (*e.g.* discoidin receptors, syndecans and mainly integrins) can activate intracellular proliferation, differentiation and survival signaling pathways (reviewed in detail in [148-150]) – Figure 2.5. As example, the increased activation of the integrin signaling pathway (that activates focal adhesion kinase (FAK) via) can prompt the cells proliferation and survival by suppressing the p53-induced apoptosis [151]. In the other hand, cell adhesion to the ECM inactivates pro-apoptotic molecules such as Bax and induces expression of several anti-apoptotic genes (*e.g.* Bcl-2) favoring the cell survival [152].

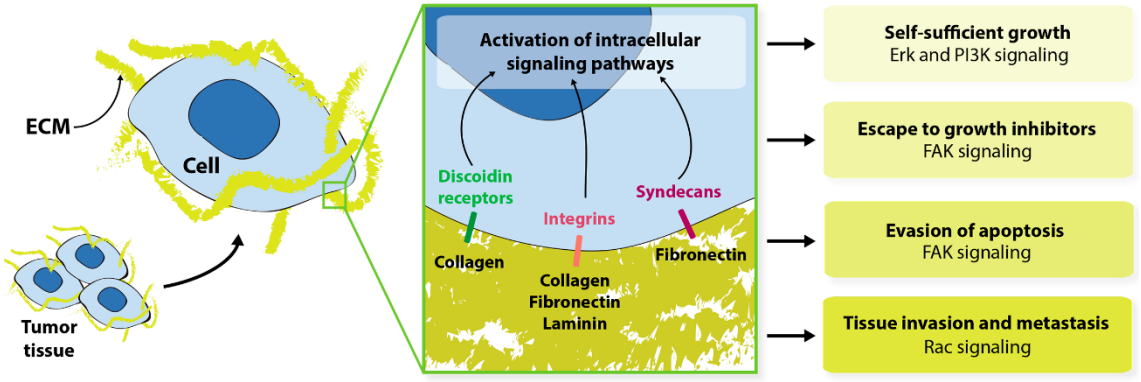

Figure 2.5. Interactions of ECM components with the cells in the tumor tissue that leads to the activation of several signaling pathways.

In a similar manner to the *in vivo* tumors, spheroids also display an increased expression of ECM proteins. Nederman *et al*. studied the presence and expression of ECM proteins in U-118 MG glioma and HTH-7 thyroid cancer spheroids and they noticed that spheroids were able to produce ECM components such as collagens (type I, III and V), fibronectin and laminin [153]. Subsequently, the same research group observed that the expression of ECM proteins (*e.g.* fibronectin) was more pronounced when glioma cell were cultured as spheroids than when the cells were maintained in 2D cultures [154]. Bjerkvig *et al*. also demonstrated that collagen type IV expression is upregulated in BT4C glioma tumor spheroids, whereas no significant expression was observed in monolayer cultures of BT4C cells [155].

Further studies showed that the increased deposition of ECM proteins in spheroids can influence the response of the cells to the therapeutics. Bai *et al*. verified that the increased expression of ECM proteins (*e.g.* collagen and fibronectin-1) in 3D cultures of soft sarcoma (HT1080, RD, SW872) and osteosarcoma (HOSS1) cell lines contributed for the establishment of a chemoresistant environment to DOX, Docetaxel and Gemcitabine [156]. In brief, the mRNA expression of COL1A1 (gene that encodes the major component of collagen type I) and FN1 (gene that encodes fibronectin) in HOSS1 cells were 2- and 4-folds higher in the spheroids than in 2D cell cultures, respectively [156]. Accordantly, the IC_{50} values of DOX, Gemcitabine an Docetaxel in HOSS1 cells were superior in spheroids (4.61, 23.55 and 103.2 μM, respectively) than in 2D cell cultures (0.078, 6.23 and 6.72 μM, respectively) [156].

To reduce the cell-ECM proteins interactions, Cheng *et al*. used an integrin-targeted chemotherapeutic drug (Cilengitide - synthetic peptide inhibitor of integrin αv heterodimer with high specificity for αvβ3 and αvβ5) to reduce the malignance behavior of malignant pleural mesothelioma cells (*e.g.* H28) spheroids [157]. Their results demonstrated that H28 cells viability was significantly reduced, since these cells display a high expression of Cilengitide target integrins. The H28 cells invasion capacity was also reduced when Cilengitide was administered [157]. Other examples of integrin-targeted chemotherapeutic drugs that can reduce the cell-ECM interactions are Etaracizumab, Intetumumab and Volociximab (reviewed in details in [108, 158]).

2.3.9. Physical barriers

In solid tumors, the deposition of ECM proteins, the cell-ECM and cell-cell interactions increase the tissue density and form a physical barrier that limits the penetration of the compounds and their delivery to cells - also known as limited mass transport effect [17, 32]. The deposition of ECM proteins and the close physical interactions among the cells also lead to an increased interstitial fluid pressure (IFP). This IFP contributes for the impaired penetration of pharmaceuticals by convection [17, 32].

The limited drug penetration prompted by the physical barrier was already demonstrated in spheroids [63, 159]. Longati *et al*. demonstrated that PANC-1 pancreatic cancer spheroids create a matrix-rich environment composed of various proteins (*e.g*. collagen type I, fibronectin-1 and lumican) that limits the drugs penetration increasing its resistance towards different therapeutics, like Gemcitabine [63]. In other study, Wang and colleagues demonstrated that DOX have a poor perfusion in SH-SY5Y neuroblastoma spheroids, being the drug penetration strictly limited to the cell layers present at the surface of the spheroids (≈ 70 μm from the periphery of the spheroids) [159]. In the literature, the penetration ability of the therapeutics in spheroids has been also described as being dependent on spheroids' size. Gong *et al*. observed that DOX has an increased penetration in spheroids with smaller sizes (diameters between 300-350 μm) than in spheroids with diameters from 450 to 500 μm [42]. Such result may be correlated with the lower number of cells and ECM deposition, and consequently less cell-cell and cell-ECM interactions that impairs the molecules penetration and distribution through the spheroid [42].

To improve the drugs penetration and distribution, proteases (collagenase, decorin, hyaluronidase, trypsin and relaxin) have been administered to the spheroids in order to reduce the ECM density by promoting its degradation [160]. Kohno *et al*. demonstrated that the administration of hyaluronidase contributed for increasing the penetration of DOX in HEp-2 laryngeal and PC-10 lung cancer spheroids and further reduction of the cells survival rate [161]. Further, other studies also demonstrated that the administration of this type of proteases in conjugation with nanomedicines can improve the nanoparticles penetration and distribution within the spheroids [162-164].

On the other hand, antifibrotic agents (*e.g*. Celecoxib, Diclofenac, Losartan, Indomethacin, Methylumbelliferone and Naproxen) that modulate the ECM proteins expression (*e.g*. collagen, fibronectin and hyaluronic acid) can be used in order to reduce the matrix-rich environment and improve the therapeutics penetration (reviewed in detail in [165]).

2.4. Conclusion and Outlook

Spheroids, in contrast with the scaffold-based 3D cell cultures, can be obtained by using various low cost, easy to handle and reproducible techniques that allow the production of cellular aggregates in large scale for high-throughput screening (HTS) purposes. Additionally, spheroids also reproduce the majority of the features exhibited by in vivo human solid tumors and, consequently, their resistance to therapeutics. Having this in mind, the understanding of the mechanisms that allow spheroids to present a drug resistance profile, may contribute for the development of new and more effective therapeutic compounds. Therefore, in this chapter,

the spheroids resistance mechanisms that result from the microtissue hypoxia, acidity, metabolic alterations, cell cycle arrest, ECM proteins deposition, cell-ECM and cell-cell interactions, as well as the establishment of physical barriers were highlighted. Moreover, some examples of therapeutic strategies tested in spheroids that target their resistance mechanisms were also presented. As a concluding remark, this chapter may contribute to further enhance the translation of the spheroids to the pharmaceutical industry, for gathering information that can prompt the development of new therapeutics to treat human solid tumors.

2.5. References

1. Siegel, R. L., Miller, K. D., and Jemal, A., *Cancer statistics, 2018.* CA: A Cancer Journal for Clinicians, 2018. 68: 7-30.

2. Chabner, B. A. and Roberts, T. G., Jr., *Timeline: Chemotherapy and the war on cancer.* Nature Reviews Cancer, 2005. 5: 65-72.

3. Moreira, A. F., Dias, D. R., and Correia, I. J., *Stimuli-responsive mesoporous silica nanoparticles for cancer therapy: A review.* Microporous and Mesoporous Materials, 2016. 236: 141-157.

4. Housman, G., *et al.*, *Drug Resistance in Cancer: An Overview.* Cancers, 2014. 6: 1769-1792.

5. Park, I. H., Lee, K. S., and Ro, J., *Effects of second and subsequent lines of chemotherapy for metastatic breast cancer.* Clinical Breast Cancer, 2015. 15: e55-62.

6. Nervi, C., De Marinis, E., and Codacci-Pisanelli, G., *Epigenetic treatment of solid tumours: a review of clinical trials.* Clinical Epigenetics, 2015. 7: 127.

7. Barnes, T. A., *et al.*, *Efficacy, safety, tolerability and price of newly approved drugs in solid tumors.* Cancer Treatment Reviews, 2017. 56: 1-7.

8. Singh, S., *et al.*, *Lead Phytochemicals for Anticancer Drug Development.* Frontiers in Plant Science, 2016. 7: 1667.

9. Breslin, S. and O'Driscoll, L., *Three-dimensional cell culture: the missing link in drug discovery.* Drug Discovery Today, 2013. 18: 240-249.

10. Zips, D., Thames, H. D., and Baumann, M., *New anticancer agents: in vitro and in vivo evaluation.* In Vivo, 2005. 19: 1-7.

11. Niu, N. and Wang, L., *In vitro human cell line models to predict clinical response to anticancer drugs.* Pharmacogenomics, 2015. 16: 273-285.

12. Chatzinikolaidou, M., *Cell spheroids: the new frontiers in in vitro models for cancer drug validation.* Drug Discovery Today, 2016. 21: 1553-1560.

13. Menshykau, D., *Emerging technologies for prediction of drug candidate efficacy in the preclinical pipeline.* Drug Discovery Today, 2017. 22: 1598-1603.

14. Doke, S. K. and Dhawale, S. C., *Alternatives to animal testing: A review.* Saudi Pharmaceutical Journal, 2015. 23: 223-229.

15. Conger, A. D. and Ziskin, M. C., *Growth of mammalian multicellular tumor spheroids.* Cancer Research, 1983. 43: 556-560.

16. Freyer, J. P., *Role of necrosis in regulating the growth saturation of multicellular spheroids.* Cancer Research, 1988. 48: 2432-2439.

17. Costa, E. C., *et al.*, *3D tumor spheroids: an overview on the tools and techniques used for their analysis.* Biotechnology Advances, 2016. 34: 1427-1441.

18. Mehta, G., *et al.*, *Opportunities and challenges for use of tumor spheroids as models to test drug delivery and efficacy.* Journal of Controlled Release, 2012. 164: 192-204.

19. Nath, S. and Devi, G. R., *Three-dimensional culture systems in cancer research: Focus on tumor spheroid model.* Pharmacology & Therapeutics, 2016. 163: 94-108.

20. LaBarbera, D. V., Reid, B. G., and Yoo, B. H., *The multicellular tumor spheroid model for high-throughput cancer drug discovery.* Expert Opinion on Drug Discovery, 2012. 7: 819-830.

21. Patel, N. R., *et al.*, *Cancer cell spheroids for screening of chemotherapeutics and drug-delivery systems.* Therapeutic Delivery, 2015. 6: 509-520.

22. Kim, T.-H., *et al.*, *The delivery of doxorubicin to 3-D multicellular spheroids and tumors in a murine xenograft model using tumor-penetrating triblock polymeric micelles.* Biomaterials, 2010. 31: 7386-7397.

23. Lamfers, M. L. and Hemminki, A., *Multicellular tumor spheroids in gene therapy and oncolytic virus therapy.* Current Opinion in Molecular Therapeutics, 2004. 6: 403-411.

24. Herter, S., *et al.*, *A novel three-dimensional heterotypic spheroid model for the assessment of the activity of cancer immunotherapy agents.* Cancer Immunology, Immunotherapy, 2017. 66: 129-140.

25. Evans, C. L., *Three-dimensional in vitro cancer spheroid models for photodynamic therapy: strengths and opportunities.* Frontiers in Physics, 2015. 3: 15.

26. Dubessy, C., *et al.*, *Spheroids in radiobiology and photodynamic therapy.* Critical Reviews in Oncology/Hematology, 2000. 36: 179-192.

27. Xiao, Z., *et al.*, *Distribution of photosensitizers in bladder cancer spheroids: implications for intravesical instillation of photosensitizers for photodynamic therapy of bladder cancer.* Journal of Pharmacy & Pharmaceutical Sciences, 2005. 8: 536-543.

28. Moreira, A. F., *et al.*, *Thermo- and pH-responsive nano-in-micro particles for combinatorial drug delivery to cancer cells.* European Journal of Pharmaceutical Sciences, 2017. 104: 42-51.

29. Schwachofer, J. H., *Multicellular tumor spheroids in radiotherapy research (review).* Anticancer Research, 1990. 10: 963-969.

30. Höckel, M. and Vaupel, P., *Tumor hypoxia: definitions and current clinical, biologic, and molecular aspects.* Journal of the National Cancer Institute, 2001. 93: 266-276.

31. Trédan, O., *et al.*, *Drug resistance and the solid tumor microenvironment.* Journal of the National Cancer Institute, 2007. 99: 1441-1454.

32. Minchinton, A. I. and Tannock, I. F., *Drug penetration in solid tumours.* Nature Reviews Cancer, 2006. 6: 583-592.

33. Mueller-Klieser, W., *Method for the determination of oxygen consumption rates and diffusion coefficients in multicellular spheroids.* Biophysical Journal, 1984. 46: 343-348.

34. Mueller-Klieser, W. F. and Sutherland, R. M., *Oxygen tensions in multicell spheroids of two cell lines.* British Journal of Cancer, 1982. 45: 256-264.

35. Grimes, D. R., *et al.*, *A method for estimating the oxygen consumption rate in multicellular tumour spheroids.* Journal of the Royal Society Interface, 2014. 11: 20131124.

36. Grimes, D. R., Fletcher, A. G., and Partridge, M., *Oxygen consumption dynamics in steady-state tumour models*. Royal Society Open Science, 2014. 1: 140080.

37. Tian, X., *et al.*, *Hypoxia-inducible factor-1a enhances the malignant phenotype of multicellular spheroid HeLa cells in vitro*. Oncology Letters, 2010. 1: 893-897.

38. Rohwer, N. and Cramer, T., *Hypoxia-mediated drug resistance: Novel insights on the functional interaction of HIFs and cell death pathways*. Drug Resistance Updates, 2011. 14: 191-201.

39. Wartenberg, M., *et al.*, *Regulation of the multidrug resistance transporter P-glycoprotein in multicellular tumor spheroids by hypoxia-inducible factor (HIF-1) and reactive oxygen species*. The FASEB Journal, 2003. 17: 503-505.

40. Doublier, S., *et al.*, *HIF-1 activation induces doxorubicin resistance in MCF7 3-D spheroids via P-glycoprotein expression: a potential model of the chemo-resistance of invasive micropapillary carcinoma of the breast*. BMC Cancer, 2012. 12: 4.

41. Krock, B. L., Skuli, N., and Simon, M. C., *Hypoxia-Induced Angiogenesis: Good and Evil*. Genes & Cancer, 2011. 2: 1117-1133.

42. Gong, X., *et al.*, *Generation of Multicellular Tumor Spheroids with Microwell-Based Agarose Scaffolds for Drug Testing*. PLOS ONE, 2015. 10: e0130348.

43. Qin, Y., *et al.*, *Hypoxia-Driven Mechanism of Vemurafenib Resistance in Melanoma*. Molecular Cancer Therapeutics, 2016. 15: 2442-2454.

44. Terashima, J., *et al.*, *VEGF expression is regulated by HIF-1alpha and ARNT in 3D KYSE-70, esophageal cancer cell spheroids*. Cell Biology International, 2016. 40: 1187-1194.

45. Masoud, G. N. and Li, W., *HIF-1a pathway: role, regulation and intervention for cancer therapy*. Acta Pharmaceutica Sinica B, 2015. 5: 378-389.

46. Khaitan, D., *et al.*, *Establishment and characterization of multicellular spheroids from a human glioma cell line; Implications for tumor therapy*. Journal of Translational Medicine, 2006. 4: 12-12.

47. Wigerup, C., Påhlman, S., and Bexell, D., *Therapeutic targeting of hypoxia and hypoxia-inducible factors in cancer*. Pharmacology & Therapeutics, 2016. 164: 152-169.

48. Deavall, D. G., *et al.*, *Drug-Induced Oxidative Stress and Toxicity*. Journal of Toxicology, 2012. 2012: 645460.

49. Sonveaux, P., *ROS and radiotherapy: more we care*. Oncotarget, 2017. 8: 35482-35483.

50. Gray, L. H., *et al.*, *The concentration of oxygen dissolved in tissues at the time of irradiation as a factor in radiotherapy*. The British Journal of Radiology, 1953. 26: 638-648.

51. Grimes, D. R. and Partridge, M., *A mechanistic investigation of the oxygen fixation hypothesis and oxygen enhancement ratio*. Biomedical Physics & Engineering Express, 2015. 1: 045209.

52. Mistry, I. N., *et al.*, *Clinical Advances of Hypoxia-Activated Prodrugs in Combination With Radiation Therapy*. International Journal of Radiation Oncology, Biology, Physics, 2017. 98: 1183-1196.

53. Phillips, R. M., *Targeting the hypoxic fraction of tumours using hypoxia-activated prodrugs*. Cancer Chemotherapy and Pharmacology, 2016. 77: 441-457.

54. Baran, N. and Konopleva, M., *Molecular Pathways: Hypoxia-Activated Prodrugs in Cancer Therapy.* Clinical Cancer Research, 2017. 23: 2382-2390.

55. Patterson, A. V., *et al.*, *Mechanism of action and preclinical antitumor activity of the novel hypoxia-activated DNA cross-linking agent PR-104.* Clinical Cancer Research, 2007. 13: 3922-3932.

56. Brown, J. M., *SR 4233 (tirapazamine): a new anticancer drug exploiting hypoxia in solid tumours.* British Journal of Cancer, 1993. 67: 1163-1170.

57. Meng, F., *et al.*, *Molecular and cellular pharmacology of the hypoxia-activated prodrug TH-302.* Molecular Cancer Therapeutics, 2012. 11: 740-751.

58. Liu, S., *et al.*, *Hypoxia-activated prodrug enhances therapeutic effect of sunitinib in melanoma.* Oncotarget, 2017. 8: 115140-115152.

59. Wilson, W. R. and Hay, M. P., *Targeting hypoxia in cancer therapy.* Nature Reviews Cancer, 2011. 11: 393-410.

60. Semenza, G. L., *Evaluation of HIF-1 inhibitors as anticancer agents.* Drug Discovery Today, 2007. 12: 853-859.

61. Hewitson, K. S. and Schofield, C. J., *The HIF pathway as a therapeutic target.* Drug Discovery Today, 2004. 9: 704-711.

62. Hirschhaeuser, F., Sattler, U. G. A., and Mueller-Klieser, W., *Lactate: A Metabolic Key Player in Cancer.* Cancer Research, 2011. 71: 6921-6925.

63. Longati, P., *et al.*, *3D pancreatic carcinoma spheroids induce a matrix-rich, chemoresistant phenotype offering a better model for drug testing.* BMC Cancer, 2013. 13: 95.

64. M. R. Pereira, P., *et al.*, *Cancer cell spheroids are a better screen for the photodynamic efficiency of glycosylated photosensitizers.* PLOS ONE, 2017. 12: e0177737.

65. Bergman, A. M., *et al.*, *Increased sensitivity to gemcitabine of P-glycoprotein and multidrug resistance-associated protein-overexpressing human cancer cell lines.* British Journal of Cancer, 2003. 88: 1963-1970.

66. Wartenberg, M., *et al.*, *Glycolytic pyruvate regulates P-Glycoprotein expression in multicellular tumor spheroids via modulation of the intracellular redox state.* Journal of Cellular Biochemistry, 2010. 109: 434-446.

67. Gao, J. L. and Chen, Y. G., *Natural compounds regulate glycolysis in hypoxic tumor microenvironment.* BioMed Research International, 2015. 2015: 354143.

68. Siebeneicher, H., *et al.*, *Identification and Optimization of the First Highly Selective GLUT1 Inhibitor BAY-876.* ChemMedChem, 2016. 11: 2261-2271.

69. Qian, Y., Wang, X., and Chen, X., *Inhibitors of glucose transport and glycolysis as novel anticancer therapeutics.* World Journal of Translational Medicine, 2014. 3: 37-57.

70. Zhang, Y. and Yang, J.-M., *Altered energy metabolism in cancer: A unique opportunity for therapeutic intervention.* Cancer Biology & Therapy, 2013. 14: 81-89.

71. Briasoulis, E., *et al.*, *Phase I trial of 6-hour infusion of glufosfamide, a new alkylating agent with potentially enhanced selectivity for tumors that overexpress transmembrane glucose transporters: a study of the European Organization for Research and Treatment of Cancer Early Clinical Studies Group.* Journal of Clinical Oncology, 2000. 18: 3535-3544.

72. Baltazar, F., *et al.*, *Monocarboxylate transporters as targets and mediators in cancer therapy response.* Histology and Histopathology, 2014. 29: 1511-1524.

73. Chan, D. A., *et al.*, *Targeting GLUT1 and the Warburg effect in renal cell carcinoma by chemical synthetic lethality.* Science Translational Medicine, 2011. 3: 94ra70.

74. Ganapathy-Kanniappan, S. and Geschwind, J.-F. H., *Tumor glycolysis as a target for cancer therapy: progress and prospects.* Molecular Cancer, 2013. 12: 152.

75. Pelicano, H., *et al.*, *Glycolysis inhibition for anticancer treatment.* Oncogene, 2006. 25: 4633-4646.

76. Schmidt, M. M. and Dringen, R., *Differential Effects of Iodoacetamide and Iodoacetate on Glycolysis and Glutathione Metabolism of Cultured Astrocytes.* Frontiers in Neuroenergetics, 2009. 1: 1.

77. Doherty, J. R. and Cleveland, J. L., *Targeting lactate metabolism for cancer therapeutics.* The Journal of Clinical Investigation, 2013. 123: 3685-3692.

78. Maftouh, M., *et al.*, *Synergistic interaction of novel lactate dehydrogenase inhibitors with gemcitabine against pancreatic cancer cells in hypoxia.* British Journal of Cancer, 2014. 110: 172-182.

79. Hirschhaeuser, F., *et al.*, *Multicellular tumor spheroids: An underestimated tool is catching up again.* Journal of Biotechnology, 2010. 148: 3-15.

80. Carlsson, J. and Acker, H., *Relations between pH, oxygen partial pressure and growth in cultured cell spheroids.* International Journal of Cancer, 1988. 42: 715-720.

81. Wojtkowiak, J. W., *et al.*, *Drug resistance and cellular adaptation to tumor acidic pH microenvironment.* Molecular Pharmaceutics, 2011. 8: 2032-2038.

82. Saggar, J. K., *et al.*, *The Tumor Microenvironment and Strategies to Improve Drug Distribution.* Frontiers in Oncology, 2013. 3: 154.

83. Swietach, P., *et al.*, *Importance of Intracellular pH in Determining the Uptake and Efficacy of the Weakly Basic Chemotherapeutic Drug, Doxorubicin.* PLOS ONE, 2012. 7: e35949.

84. McIntyre, A., *et al.*, *Disrupting Hypoxia-Induced Bicarbonate Transport Acidifies Tumor Cells and Suppresses Tumor Growth.* Cancer Research, 2016. 76: 3744-3755.

85. Kato, Y., *et al.*, *Acidic extracellular microenvironment and cancer.* Cancer Cell International, 2013. 13: 89.

86. Jones, R. S., Parker, M. D., and Morris, M. E., *Quercetin, Morin, Luteolin, and Phloretin Are Dietary Flavonoid Inhibitors of Monocarboxylate Transporter 6.* Molecular Pharmaceutics, 2017. 14: 2930-2936.

87. Lee, M. and Lee, J.-S., *Exploiting tumor cell senescence in anticancer therapy.* BMB Reports, 2014. 47: 51-59.

88. Barrera-Rodríguez, R. and Fuentes, J. M., *Multidrug resistance characterization in multicellular tumour spheroids from two human lung cancer cell lines*. Cancer Cell International, 2015. 15: 47.

89. Cheung-Ong, K., Giaever, G., and Nislow, C., *DNA-damaging agents in cancer chemotherapy: serendipity and chemical biology*. Cell Chemical Biology, 2013. 20: 648-659.

90. Imamura, Y., *et al.*, *Comparison of 2D- and 3D-culture models as drug-testing platforms in breast cancer*. Oncology Reports, 2015. 33: 1837-1843.

91. Xing, H., *et al.*, *Effect of the cyclin-dependent kinases inhibitor p27 on resistance of ovarian cancer multicellular spheroids to anticancer chemotherapy*. Journal of Cancer Research and Clinical Oncology, 2005. 131: 511-519.

92. Ham, S. L., *et al.*, *Liquid-based three-dimensional tumor models for cancer research and drug discovery*. Bulletin of Experimental Biology and Medicine, 2016. 241: 939-954.

93. Balkwill, F. R., Capasso, M., and Hagemann, T., *The tumor microenvironment at a glance*. Journal of Cell Science, 2012. 125: 5591-5596.

94. Mao, Y., *et al.*, *Stromal cells in tumor microenvironment and breast cancer*. Cancer and Metastasis Reviews, 2013. 32: 303-315.

95. Sun, Y., *Tumor microenvironment and cancer therapy resistance*. Cancer Letters, 2016. 380: 205-215.

96. Correia, A. L. and Bissell, M. J., *The tumor microenvironment is a dominant force in multidrug resistance*. Drug Resistance Updates, 2012. 15: 39-49.

97. Dalton, W. S., *The tumor microenvironment as a determinant of drug response and resistance*. Drug Resistance Updates, 1999. 2: 285-288.

98. Majety, M., *et al.*, *Fibroblasts Influence Survival and Therapeutic Response in a 3D Co-Culture Model*. PLOS ONE, 2015. 10: e0127948.

99. Lee, J., Shin, D., and Roh, J.-L., *Development of an in vitro cell-sheet cancer model for chemotherapeutic screening*. Theranostics, 2018. 8: 3964-3973.

100. Hoffmann, O. I., *et al.*, *Impact of the spheroid model complexity on drug response*. Journal of Biotechnology, 2015. 205: 14-23.

101. Jeong, S.-Y., *et al.*, *Co-Culture of Tumor Spheroids and Fibroblasts in a Collagen Matrix-Incorporated Microfluidic Chip Mimics Reciprocal Activation in Solid Tumor Microenvironment*. PLOS ONE, 2016. 11: e0159013.

102. Eder, T., *et al.*, *Cancer-Associated Fibroblasts Modify the Response of Prostate Cancer Cells to Androgen and Anti-Androgens in Three-Dimensional Spheroid Culture*. International Journal of Molecular Sciences, 2016. 17: E1458.

103. Kassim, Y. L., *et al.*, *Three Dimensional Tumor Engineering by Co-Culture of Breast Tumor and Endothelial Cells Using a Hyaluronic Acid Hydrogel Model*. Journal of Clinical & Experimental Oncology, 2017. 6: 1-8.

104. Lee, J.-H., *et al.*, *Microfluidic co-culture of pancreatic tumor spheroids with stellate cells as a novel 3D model for investigation of stroma-mediated cell motility and drug resistance*. Journal of Experimental & Clinical Cancer Research, 2018. 37: 4.

105. Zhang, J. and Liu, J., *Tumor stroma as targets for cancer therapy*. Pharmacology & Therapeutics, 2013. 137: 200-215.

106. Sounni, N. E. and Noel, A., *Targeting the tumor microenvironment for cancer therapy*. Clinical Chemistry, 2013. 59: 85-93.

107. Joyce, J. A., *Therapeutic targeting of the tumor microenvironment*. Cancer Cell, 2005. 7: 513-520.

108. Fang, H. and DeClerck, Y. A., *Targeting the Tumor Microenvironment: From Understanding Pathways to Effective Clinical Trials*. Cancer Research, 2013. 73: 4965-4977.

109. Bahrami, A. and Hassanian, S. M., *The Therapeutic Potential of Targeting Tumor Microenvironment in Breast Cancer: Rational Strategies and Recent Progress*. Journal of Cellular Biochemistry, 2018. 119: 111-122.

110. Xing, F., Saidou, J., and Watabe, K., *Cancer associated fibroblasts (CAFs) in tumor microenvironment*. Frontiers in Bioscience, 2010. 15: 166-179.

111. Gascard, P. and Tlsty, T. D., *Carcinoma-associated fibroblasts: orchestrating the composition of malignancy*. Genes & Development, 2016. 30: 1002-1019.

112. Togo, S., *et al.*, *Carcinoma-Associated Fibroblasts Are a Promising Therapeutic Target*. Cancers, 2013. 5: 149-169.

113. Tao, L., *et al.*, *Cancer associated fibroblasts: An essential role in the tumor microenvironment*. Oncology Letters, 2017. 14: 2611-2620.

114. Clevers, H., *The cancer stem cell: premises, promises and challenges*. Nature Medicine, 2011. 17: 313-319.

115. S. Franco, S., *et al.*, *In vitro models of cancer stem cells and clinical applications*. BMC Cancer, 2016. 16: 738.

116. Tirino, V., *et al.*, *Cancer stem cells in solid tumors: an overview and new approaches for their isolation and characterization*. The FASEB Journal, 2013. 27: 13-24.

117. Vidal, S. J., *et al.*, *Targeting cancer stem cells to suppress acquired chemotherapy resistance*. Oncogene, 2014. 33: 4451-4463.

118. Abdullah, L. N. and Chow, E. K.-H., *Mechanisms of chemoresistance in cancer stem cells*. Clinical and Translational Medicine, 2013. 2: 3.

119. Todaro, M., *et al.*, *Colon cancer stem cells dictate tumor growth and resist cell death by production of interleukin-4*. Cell Stem Cell, 2007. 1: 389-402.

120. Bhuvanalakshm, G., *et al.*, *Secreted Frizzled-Related Protein 4 Inhibits Glioma Stem-Like Cells by Reversing Epithelial to Mesenchymal Transition, Inducing Apoptosis and Decreasing Cancer Stem Cell Properties*. PLOS ONE, 2015. 10: e0127517.

121. Reynolds, D. S., *et al.*, *Breast Cancer Spheroids Reveal a Differential Cancer Stem Cell Response to Chemotherapeutic Treatment*. Scientific Reports, 2017. 7: 10382.

122. Rodriguez, C. E., *et al.*, *Breast cancer stem cells are involved in Trastuzumab resistance through the HER2 modulation in 3D culture*. Journal of Cellular Biochemistry, 2018. 119: 1381-1391.

123. Wang, K., *et al.*, *Culture on 3D Chitosan-Hyaluronic Acid Scaffolds Enhances Stem Cell Marker Expression and Drug Resistance in Human Glioblastoma Cancer Stem Cells.* Advanced Healthcare Materials, 2016. 5: 3173-3181.

124. Godugu, C., *et al.*, *AlgiMatrix™ Based 3D Cell Culture System as an In-Vitro Tumor Model for Anticancer Studies.* PLOS ONE, 2013. 8: e53708.

125. Kvinlaug, B. T. and Huntly, B. J., *Targeting cancer stem cells.* Expert Opinion on Therapeutic Targets, 2007. 11: 915-927.

126. Rosa, R., *et al.*, *Approaches for targeting cancer stem cells drug resistance.* Expert Opinion on Drug Discovery, 2016. 11: 1201-1212.

127. Pützer, B. M., Solanki, M., and Herchenröder, O., *Advances in cancer stem cell targeting: How to strike the evil at its root.* Advanced Drug Delivery Reviews, 2017. 120: 89-107.

128. Dragu, D. L., *et al.*, *Therapies targeting cancer stem cells: Current trends and future challenges.* World Journal of Stem Cells, 2015. 7: 1185-1201.

129. Khan, I. N., *et al.*, *Cancer stem cells: a challenging paradigm for designing targeted drug therapies.* Drug Discovery Today, 2015. 20: 1205-1216.

130. Kahlert, U. D., *et al.*, *Targeting cancer stem-like cells in glioblastoma and colorectal cancer through metabolic pathways.* International Journal of Cancer, 2017. 140: 10-22.

131. Matsubara, S., *et al.*, *mTOR plays critical roles in pancreatic cancer stem cells through specific and stemness-related functions.* Scientific Reports, 2013. 3: 3230.

132. Gu, C., *et al.*, *Anti-CD44 mAb remodels biological behaviors of spheroid cells with stemness from human ovarian cancer cell line SKOV-3.* Chinese Science Bulletin, 2012. 57: 1288-1297.

133. Jeanes, A., Gottardi, C. J., and Yap, A. S., *Cadherins and cancer: how does cadherin dysfunction promote tumor progression?* Oncogene, 2008. 27: 6920-6629.

134. Ivascu, A. and Kubbies, M., *Diversity of cell-mediated adhesions in breast cancer spheroids.* International Journal of Oncology, 2007. 31: 1403-1413.

135. Alpaugh, M. L., *et al.*, *Relationship of Sialyl-Lewis(x/a) Underexpression and E-Cadherin Overexpression in the Lymphovascular Embolus of Inflammatory Breast Carcinoma.* The American Journal of Pathology, 2002. 161: 619-628.

136. Tomlinson, J. S., Alpaugh, M. L., and Barsky, S. H., *An intact overexpressed E-cadherin/alpha,beta-catenin axis characterizes the lymphovascular emboli of inflammatory breast carcinoma.* Cancer Research, 2001. 61: 5231-5241.

137. Costa, E. C., *et al.*, *Optimization of liquid overlay technique to formulate heterogenic 3D co-cultures models.* Biotechnology and Bioengineering, 2014. 111: 1672-1685.

138. Takei, R., *et al.*, *Role of E-cadherin Molecules in Spheroid Formation of Hepatocytes Adhered on Galactose-Carrying Polymer as an Artificial Asialoglycoprotein Model.* Biotechnology Letters, 2005. 27: 1149-1156.

139. Enmon, R. M., *et al.*, *Aggregation kinetics of well and poorly differentiated human prostate cancer cells.* Biotechnology and Bioengineering, 2002. 80: 580-588.

140. Shimazui, T., *et al.*, *Role of complex cadherins in cell-cell adhesion evaluated by spheroid formation in renal cell carcinoma cell lines.* Oncology Reports, 2004. 11: 357-3560.

141. Jung, H.-R., *et al.*, *Cell Spheroids with Enhanced Aggressiveness to Mimic Human Liver Cancer In Vitro and In Vivo.* Scientific Reports, 2017. 7: 10499.

142. Xu, S., *et al.*, *Construction and characteristics of an E-cadherin-related three-dimensional suspension growth model of ovarian cancer.* Scientific Reports, 2014. 4: 5646.

143. Liang, X., *et al.*, *E-cadherin increasing multidrug resistance protein 1 via hypoxia-inducible factor-1a contributes to multicellular resistance in colorectal cancer.* Tumor Biology, 2016. 37: 425-435.

144. Green, S. K., *et al.*, *Antiadhesive antibodies targeting E-cadherin sensitize multicellular tumor spheroids to chemotherapy in vitro.* Molecular Cancer Therapeutics, 2004. 3: 149-159.

145. Luebke-Wheeler, J. L., *et al.*, *E-Cadherin Protects Primary Hepatocyte Spheroids From Cell Death by a Caspase-Independent Mechanism.* Cell Transplantation, 2009. 18: 1281-1287.

146. Yarom, N., *et al.*, *Phase I clinical trial of Exherin (ADH-1) in patients with advanced solid tumors.* Current Clinical Pharmacology, 2013. 8: 81-88.

147. Kular, J. K., Basu, S., and Sharma, R. I., *The extracellular matrix: Structure, composition, age-related differences, tools for analysis and applications for tissue engineering.* Journal of Tissue Engineering, 2014. 5: 2041731414557112.

148. Pickup, M. W., Mouw, J. K., and Weaver, V. M., *The extracellular matrix modulates the hallmarks of cancer.* EMBO Reports, 2014. 15: 1243-1253.

149. Xiong, G.-F. and Xu, R., *Function of cancer cell-derived extracellular matrix in tumor progression.* Journal of Cancer Metastasis and Treatment, 2016. 2: 357-264.

150. Lu, P., Weaver, V. M., and Werb, Z., *The extracellular matrix: a dynamic niche in cancer progression.* Journal of Cell Biology, 2012. 196: 395-406.

151. Frisch, S. M., *et al.*, *Control of adhesion-dependent cell survival by focal adhesion kinase.* Journal of Cell Biology, 1996. 134: 793-799.

152. Gilmore, A. P., *et al.*, *Integrin-mediated survival signals regulate the apoptotic function of Bax through its conformation and subcellular localization.* Journal of Cell Biology, 2000. 149: 431-446.

153. Nederman, T., *et al.*, *Demonstration of an extracellular matrix in multicellular tumor spheroids.* Cancer Research, 1984. 44: 3090-3097.

154. Glimelius, B., *et al.*, *Extracellular matrices in multicellular spheroids of human glioma origin: Increased incorporation of proteoglycans and flbronectin as compared to monolayer cultures.* Acta Pathologica, Microbiologica et Immunologica Scandinavica, 1988. 96: 433-444.

155. Bjerkvig, R., Laerum, O. D., and Rucklidge, G. J., *Immunocytochemical characterization of extracellular matrix proteins expressed by cultured glioma cells.* Cancer Research, 1989. 49: 5424-5428.

156. Bai, C., *et al.*, *Associations of chemo- and radio-resistant phenotypes with the gap junction, adhesion and extracellular matrix in a three-dimensional culture model of soft sarcoma.* Journal of Experimental & Clinical Cancer Research, 2015. 34: 58.

157. Cheng, N. C., van Zandwijk, N., and Reid, G., *Cilengitide Inhibits Attachment and Invasion of Malignant Pleural Mesothelioma Cells through Antagonism of Integrins avβ3 and avβ5.* PLOS ONE, 2014. 9: e90374.

158. Holle, A. W., Young, J. L., and Spatz, J. P., *In vitro cancer cell-ECM interactions inform in vivo cancer treatment.* Advanced Drug Delivery Reviews, 2016. 97: 270-279.

159. Wang, X., *et al.*, *Doxorubicin delivery to 3D multicellular spheroids and tumors based on boronic acid-rich chitosan nanoparticles.* Biomaterials, 2013. 34: 4667-4679.

160. Choi, I.-K., *et al.*, *Strategies to Increase Drug Penetration in Solid Tumors.* Frontiers in Oncology, 2013. 3: 193.

161. Kohno, N., Ohnuma, T., and Truog, P., *Effects of hyaluronidase on doxorubicin penetration into squamous carcinoma multicellular tumor spheroids and its cell lethality.* Journal of Cancer Research and Clinical Oncology, 1994. 120: 293-297.

162. Eikenes, L., *et al.*, *Effect of collagenase and hyaluronidase on free and anomalous diffusion in multicellular spheroids and xenografts.* Anticancer Research, 2010. 30: 359-368.

163. Goodman, T. T., Olive, P. L., and Pun, S. H., *Increased nanoparticle penetration in collagenase-treated multicellular spheroids.* International Journal of Nanomedicine, 2007. 2: 265-274.

164. Zhou, H., *et al.*, *Hyaluronidase embedded in nanocarrier PEG shell for enhanced tumor penetration and highly efficient antitumor efficacy.* Nano Letters, 2016. 16: 3268-3277.

165. Järveläinen, H., *et al.*, *Extracellular Matrix Molecules: Potential Targets in Pharmacotherapy.* Pharmacological Reviews, 2009. 61: 198-223.

Chapter 3

Introduction (part B)

Spheroids formation on non-adhesive surfaces by Liquid Overlay Technique: considerations and practical approaches

This chapter is based on the publication entitled: Spheroids Formation on Non-Adhesive Surfaces by Liquid Overlay Technique: Considerations and Practical Approaches, Biotechnology Journal, 2017, 13(1): 1700417.

3.1. Abstract

Scalable and reproducible production of three-dimensional (3D) cellular spheroids is highly demanded, by pharmaceutical companies, for drug screening purposes during the preclinical evaluation phase. These 3D cellular constructs, unlike the monolayer culture of cells, can mimic different features of human tissues, including cellular organization, cell-cell and cell-extracellular matrix (ECM) interactions. Up to now, different techniques (scaffold-based and scaffold-free) have been used for spheroids formation, being the *Liquid Overlay Technique (LOT)* one of the most explored methodologies, due to its low cost and easy handling. Additionally, during the last decades, this technique has been widely investigated in order to enhance its potential for being applied in high-throughput analysis. Herein, an overview of the LOT advances, practical approaches and troubleshooting is provided for those researchers that intend to produce spheroids using LOT, for drug screening purposes. Moreover, the advantages of the LOT over the other scaffold-free techniques used for the spheroids formation are also addressed.

Keywords: 3D cell culture; high-throughput screening; scaffold-free techniques; liquid overlay technique; tumor spheroids.

3.2. Introduction

Since the 50s, two-dimensional (2D) cell culture platforms remain as the gold standard approach for the *in vitro* testing of new therapeutic agents [1, 2]. These type of cultures are simple, cheap and compatible with the different equipment used for high-throughput screening (HTS) [3]. In the last decades, with the development of 2D cells co-cultures, these models gained the ability to better represent the cellular heterogeneity found in different human tissues. For instance, tumor cellular heterogeneity has been mimicked by seeding cancer cells along with stem-like cells [4], fibroblasts [5], macrophages [6], among others. Additionally, the central nervous system architecture has been reproduced by growing embryonic cortical neurons in the presence of cortical microglia [7], while hepatocyte/Kupffer cells co-cultures have been used to study immune-related responses to drugs [8]. Still, 2D cell cultures are not able to replicate the 3D architecture of human tissues, hindering their capacity to predict the effectiveness of therapeutic molecules aimed for human use. The limited relevance of physiological data gathered from 2D cell culture models was highlighted by Xu and co-workers which reported that only 50% of the acute hepatotoxic compounds under study were detected when screened on 2D monolayers cultures of hepatocytes [9]. These assays can lead to misleading and nonpredictive results that, in the majority of the cases, are used as the starting point to progress into the subsequent preclinical animal studies. Such limitations confine the rate of success of *in vivo* assays and are responsible for a huge waste of valuable resources [1, 3].

To surpass these limitations, researchers have been developing 3D *in vitro* cell culture systems. 3D sphere-like tightly bound cellular aggregates, known as spheroids, are an *in vitro* 3D cell culture models that represent more closely the complexity of different healthy and unhealthy human tissues, in comparison to 2D monolayers. For instance, Bell *et al*. observed that primary human hepatocyte spheroids can be used to mimic different liver pathologies, such as cholestasis, steatosis and viral hepatitis [10]. On the other side, Dingle and co-workers produced primary cortical spheroids that display several features of the *in vivo* cortical tissue (*e.g.* cell types, cell morphology, ECM production and mechanical properties) [11]. Moreover, spheroids have been also applied for the expansion and differentiation of pluripotent mesenchymal stem cells (MSC), embryonic stem cells (ESC) and induced pluripotent stem cells (iPSC), since the cellular aggregates constituted by these cells (embryoid bodies) are able to mimic many cell differentiation features of early embryogenesis and play an important role in the *in vitro* differentiation process of cells [12].

Notwithstanding, spheroids are also a valuable 3D cellular model to replicate the features of human solid tumors, as discussed in different reviews [13-15]. Such is owed to the fact that spheroids display inherent metabolic (oxygen, carbon dioxide, nutrients and wastes) gradients similarly to poorly vascularized tumors. These gradients lead to the establishment of three main cellular layers in the spheroids, namely an external layer composed of proliferative cells, an

intermediate layer constituted by quiescence cells and an inner acidic and hypoxic layer comprised of necrotic cells [13]. Some studies also demonstrated that spheroids, when compared to 2D cell culture models, show an enhanced production and deposition of tumor ECM proteins (*e.g.* collagen types IV and I, fibronectin, laminin and lumican) [16-18]. Lastly, spheroids can be composed of different types of cells as it occurs in the tumor microenvironment and therefore cell-cell signaling, through growth factors and cell-cell physical interactions (*e.g.* E-cadherins), is established [13, 19]. Due to these features, spheroids display an anticancer therapeutics resistance profile comparable to that found in *in vivo* tumors.

Therefore, in the last decades spheroids have been used for the *in vitro* biological evaluation of new anticancer therapeutics [18, 20-27]. Sutherland and co-workers, were pioneers to use spheroids (formed with chinese hamster V79 lung cells) to characterize the efficacy of ^{60}Co radiation in anticancer therapy [21]. Since then, spheroids began to be used to evaluate other anticancer treatments, like chemotherapy, gene therapy, photodynamic therapy and nanomedicines [13, 27-29]. Therefore, the ever-growing demand of spheroids for the evaluation of therapeutics prompted the development of different methodologies for spheroids production, such as scaffold-based and scaffold-free technologies.

3.2.1. Scaffold-based approaches and scaffold-free approaches for 3D spheroids production

3D culture of cells can be performed by seeding the cells on artificial matrices. These matrices are solid scaffolds (sponges or foams), hydrogels, fibers or beads which can be produced with different porosities and mechanical characteristics in order to mimic the ECM of *in vivo* tumors [13, 30]. When cells are placed on these artificial structures (by seeding them on the surface or within the matrix) they attach to the matrix and then they migrate to the interior of the structure, forming the microtissue in the interstices of the matrix [31].

The artificial matrices used for the formation of 3D spheroids are usually produced by using non-adhesive polymers (*e.g.* agarose and hyaluronic acid (HA)) or a blend of non-adhesive polymers with other biomaterials [32, 33]. The use of polymers with non-adhesive properties is essential to trigger the formation of spheroids. In this process, the adhesive forces among cells are more prominent than those established between the cells and the non-adhesive biomaterial, thus triggering the cellular aggregation. The use of polymeric structures for spheroids culture was demonstrated by Xu *et al.* that recreated the prostate cancer microenvironment by forming LNCaP spheroids on a HA-based hydrogel [33]. Moreover, Shin and co-workers also developed alginate/collagen/agarose hydrogels to growth spheroids of ovarian carcinoma (A2780), lymphoblast (EL4) and epithelial (1308.1) cells [32]. Polymers are the most used materials to produce scaffold-based materials for 3D cell culture, since their chemical and structural properties can be optimized to fulfill the required properties [34].

Still, despite of the wide variety of scaffolds available for 3D cell culture, matrix supported spheroids production is mainly used for tissue engineering purposes, since these scaffold-based methods have demonstrated several drawbacks when drug screening applications are intended. In fact, the techniques described for scaffolds construction, like electrospinning, melt molding and most of 3D printings-based methodologies, show low reproducibility, which leads to the production of matrices with some degree of variability from batch-to-batch [31]. Such drawback, hinders the production of 3D spheroids with reproducible features and has a direct impact on the accuracy of the results obtained during the drug screening assays. Also, some therapeutics can become adsorbed to the scaffolds, which may lead to a reduction of the amount of therapeutics that reach cancer cells and, consequently, disturb the therapeutic outcome [35]. Furthermore, some of the animal-sourced natural ECM extracts used for the production of matrices may contain residual growth factors and other undefined constituents that may affect spheroids formation, as well as cancer cells responsiveness to drugs [31].

Lastly, the analysis of spheroids that grew on artificial matrices can be difficult, since the imaging of the spheroids by optical and fluorescence techniques depends on the scaffold size and transparency. In addition, in some cases it can be difficult to extract and collect all the cells from the 3D scaffolds, which may compromise spheroids analysis through specific techniques, such as flow cytometry or western blot [31].

To surpass these limitations associated with scaffold-based methods, spheroids can be formed by using scaffold-free approaches (Figure 3.1.), where microtissues formation occurs by forcing cells to self-aggregate, in a process that comprises two main phases. Initially, single cells form loose cellular aggregates and then, an up-regulation of cell-cell adhesion molecules occurs (*e.g.* E-cadherins) leading to the formation of cohesive cellular aggregates. During this process, cells also produce and organize their own 3D ECM and therefore the matrix is completely endogenous.

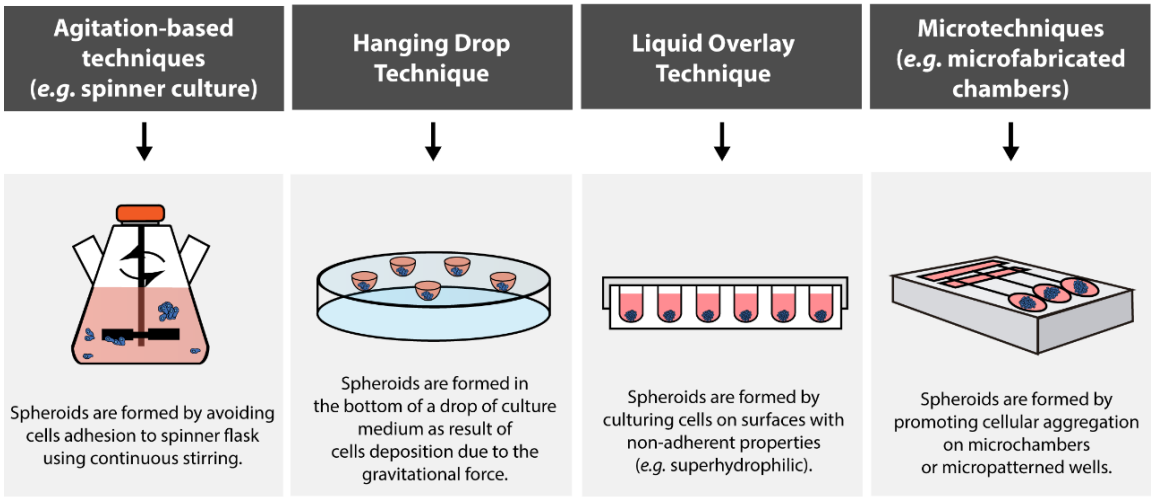

Figure 3.1. Scaffold-free techniques commonly used for spheroids formation for drug screening purposes.

The scaffold-free methods include agitation-based techniques, the Hanging Drop Technique, the LOT and micro-based techniques, as reviewed in detail by Lin and Chang [36], Breslin and O'Driscoll [3] and Mehta *et al*. [14] (Figure 3.1 and Table 3.1).

Table 3.1. Conventional scaffold-free techniques used for spheroids formation.

Technique	Advantages	Disadvantages	REF(s)
Agitation-based (*e.g.* spinner flasks and rotating systems)	- Production of a great number of spheroids; - Long term culture; - Dynamic control over the culture conditions (pH, nutrient concentration, glucose and oxygenation), when bioreactors are used (*e.g.* NASA bioreactor); - Easy access to spheroids; - Production of large spheroids.	- Variation in the size, shape and number of spheroids; - Require specialized equipment; - Cells are exposed to shear stress; - No individual compartment for each spheroid.	[3, 36-45]
Hanging Drop	- Cheap; - Does not require specialized equipment; - Good size and shape control; - Low shear stress.	- Low throughput; - Labor intensive; - Not stable; - Hard to scale-up; - Only allows cell culture for limited periods of time; - Limited applicability in drug screening; - Difficult to obtain large spheroids.	[3, 36, 45, 46]
Liquid Overlay	- Cheap; - Easy to handle; - Does not require specialized equipment; - Low shear stresses; - Long term cell culture; - Easy access to spheroids; - Compatible with HTS applications; - Allows the large-scale production of spheroids.	- Variation in size, shape and number of spheroids (when spheroids are formed on flat non-adhesive surfaces like Petri dishes); - Plate-coating procedure may be labor intensive when some non-adherent biomaterials are used (*e.g.* poly-HEMA).	[3, 36, 45, 47-49]
Microtechniques (*e.g.* microfabricated chambers)	- Good size and shape control of the spheroids; - Low shear stress; - Easy to apply in large-scale production of spheroids; - Highly reproducible.	- Expensive; - Require specialized laboratory settings; - Spheroids may be difficult to access; - Their application in HTS is limited due to instrumental constrains; - Material-drug interaction issues (hydrophobic compounds); - May not be able to sustain the cell culture for long periods of time; - The production of large spheroids is limited by the size of the chambers/microwells.	[3, 36, 45, 50, 51]

Among these, LOT arises as one of the simplest and cheapest scaffold-free techniques used for spheroids production [47-49]. Moreover, during the last decades, several modifications and optimizations of the LOT methodology have been made in order to improve its reproducibility, which is crucial for HTS purposes. In this chapter, the advantages of LOT and the different optimizations performed on this technique to improve spheroids formation, maintenance and growth will be addressed in the following sections.

3.3. Production of 3D spheroids by using LOT

Costăchel *et al*. [52] and Yuhas *et al*. [42] were the firsts authors to describe LOT in the 70s. This technique relies on the inhibition of cells adhesion to the materials' surfaces, where cells are usually seeded to be cultured. These surfaces have non-adherent properties (*e.g.* superhydrophilicity) and thus cell-cell interactions are more prominent than those established between the cells and the surface [30]. Consequently, cells aggregate leading to the formation of spheroids in 1-3 days, for the majority of the cell lines [53].

Spheroids produced through LOT can successfully represent the properties of human solid tumors. Mayer and co-workers demonstrated that 12 of the 17 gastric cancer cell lines were able to mimic the features of parental gastric carcinoma when cultured as spheroids using LOT [54]. Moreover, do Amaral *et al*. observed that MCF-7 breast cancer cells were able to grow as spheroids that mimic the tubular and acinar structures found in breast cancer [53]. Additionally, a wide number of studies have been showing the suitability of LOT for the production of spheroids aimed to evaluate the effect of different therapeutic agents, as resumed in Table 3.2.

3.3.1. Comparison of LOT with other scaffold-free techniques developed so far for spheroids production

The growth of cells in a spinner flask is an agitation-based method that has been used to produce spheroids. In this method, cells are maintained under continuous agitation, thus avoiding their adhesion [37, 41]. In comparison to LOT, this technique is also cost-effective, easy to handle and it is prone to be scale-up [40] - Table 3.1. However, the spheroids produced by using spinner flasks have a higher size and morphologic variability that can hinder their application in HTS [36]. Moreover, the high levels of shear fluid force used, in the agitation based techniques, may induce changes on cell physiology or even damage them, thus limiting the use of sensitive cell lines for spheroids production [40]. Further, the constant agitation makes the monitoring of spheroids size and growth overtime by optical microscopy very difficult [40].

Table 3.2. Overview of the therapeutics agents and compounds evaluated on spheroids produced by LOT.

Therapeutic agent	Spheroid model	Cell line	REF(s)
2-Methoxyestradiol	Glioblastoma	U87MG	[20]
5-Fluorouracil (5-FU)	Pancreatic cancer	MIAPaCa-2	[55]
		PANC-1	[55]
Mercaptopurine (6-MP)	Pancreatic cancer	PANC-1	[18]
Act16412			
Allicin			
Alvespimycin	Prostate cancer	LNCaP	[26]
		PC3	[26]
Amiodarone	Liver tissue	Hepatocytes obtained from patient	[10]
Arsenic trioxide	Colon cancer	HT-29	[56]
Axp-107-11 (genistein derivative)	Pancreatic cancer	PANC-1	[18]
Bosentan	Liver tissue	Hepatocytes obtained from patient	[10]
Cb5	Pancreatic cancer	PANC-1	[18]
Cb7			
Cb13			
Cisplatin	Breast cancer	EMT-6	[24]
	Endometrial cancer	Ishikawa	[25]
		RL95-2	[25]
		KLE	[25]
	Hypopharyngeal cancer	FaDu	[57]
	Ovarian cancer	OVCAR8	[58]
	Oral cancer	SCC25	[57]
		CAL27	[57]
Chlorimipramine	Glioma	C6	[59]
Cyclophosphamide	Breast cancer	EMT-6	[24]
Diclofenac	Liver tissue	Hepatocytes obtained from patient	[10]
	Hepatoma	C3A	[60]
Docetaxel	Cervical cancer	HeLa	[61]
	Colon cancer	HT29	[61]
Doxorubicin	Cervical cancer	HeLa	[62]
	Endometrial cancer	Ishikawa	[25]
		RL95-2	[25]
		KLE	[25]
	Hepatoma	C3A	[60]
		Huh7	[63]
	Lung cancer	A549	[64]

E-combretastatin A4	Melanoma	C8161	[65]
	Breast cancer	MDA 231	[65]
Elesclomol	Prostate cancer	LNCaP	[26]
		PC3	[26]
Fialuridine	Liver tissue	Hepatocytes obtained from patient	[10]
Fialuridine	Hepatoma	C3A	[60]
Gant61	Pancreatic cancer	PANC-1	[18]
Gemcitabine	Pancreatic cancer	MIAPaCa-2	[55]
		PANC-1	[18, 55]
Imatinib	Glioma	C6	[59]
Mitoxantrone	Colon cancer	HT-29	[66]
		HT-29	[67]
Mt100	Pancreatic cancer	PANC-1	[18]
Oxaliplatin	Colorectal cancer	HCT116	[68]
Olaparib	Prostate cancer	LNCaP	[26]
		PC3	[26]
Paracetamol	Hepatoma	C3A	[60]
Rucaparib	Prostate cancer	LNCaP	[26]
		PC3	[26]
Tamoxifen	Breast cancer	MCF-7	[69]
Tolcapone	Liver tissue	Hepatocytes obtained from patient	[10]
Trovafloxacin	Hepatoma	C3A	[60]

More recently, rotating systems and bioreactors have been developed to improve the conventional agitation-based approaches. Ingram and co-workers manufactured a new rotary cell culture system, termed as NASA, that allows a dynamic control over the spheroids culture conditions [70]. The NASA bioreactor allows the precise control over the pH of the culture medium and the concentration of nutrients and gases (*e.g.* glucose and oxygen, respectively) [38, 39]. However, the use of these complex systems increases the expenses associated to spheroids production and some of the shear forces drawbacks are not completely surpassed.

The Hanging Drop Technique was initially developed by Keller *et al.* to obtain embryonic stem cell aggregates, and up to now, this methodology has been extensively used for the production of tumor spheroids [71] – Table 3.1. In this technique, spheroids are produced by maintaining the cells in suspension inside 10-30 µL droplets of culture medium [46]. After some time, cells start to sediment, thus promoting cell-cell interaction and the formation of spheroids with similar sizes. The Hanging Drop Technique and LOT do not require specialized equipment or expensive materials, which renders them a huge potential for being applied in spheroids production [46, 47, 49, 53, 71] - Table 3.1. However, Hanging Drop method cannot be used for long periods, since the reduced volume of medium used to form the droplet is rapidly consumed

by the cells [45]. Additionally, as described by Metzger and colleagues, the Hanging Drop methodology has a limited applicability in HTS [49], since the instability of the culture medium droplets hinders the administration of the therapeutic compounds without the disruption of the spheroid.

Apart from these conventional techniques, the improvement and the development of microtechniques have prompted the emergence of new approaches for spheroids production (Table 3.1). These microtechniques comprise microfabricated micromolded wells or microchambers [72, 73]. Most of these devices are formed by casting agarose or polymethylsiloxane (PDMS) in a mold [51, 74]. These micromolded structures allow the production of spheroids in a highly reproducible manner, with a tailored shape and size [51, 74]. Moreover, some of the molds employed for spheroids formation are already commercially available (*e.g.* 3D Petri Dish®, Microtissues Inc. and AggreWell™ plates, STEMCELL Technologies Inc.) [75].

Regardless of the advantages of the application of microtechniques for 3D cell culture, the utilization of PDMS or similar materials may have some drawbacks like the binding of the anticancer drugs to the device, through hydrophobic interactions, which can affect the therapeutic outcome. Furthermore, the production of the microdevices demands cutting-edge equipment that is not available in all research facilities [50, 75]. In addition, microdevices are not compatible with the majority of the equipment used for drug HTS analysis.

3.4. Optimization of the methodology used to form 3D spheroids through LOT

An ideal method for the creation of 3D tumor spheroids should produce aggregates with a consistent size and uniform shape. Such are the prime requirements for spheroids use in HTS. In order to obtain spheroids with these properties, during the last decades researchers have been optimizing the formation of spheroids through LOT. The main optimizations, practical and troubleshooting approaches described in literature for this technique will be overviewed hereafter (Figure 3.2).

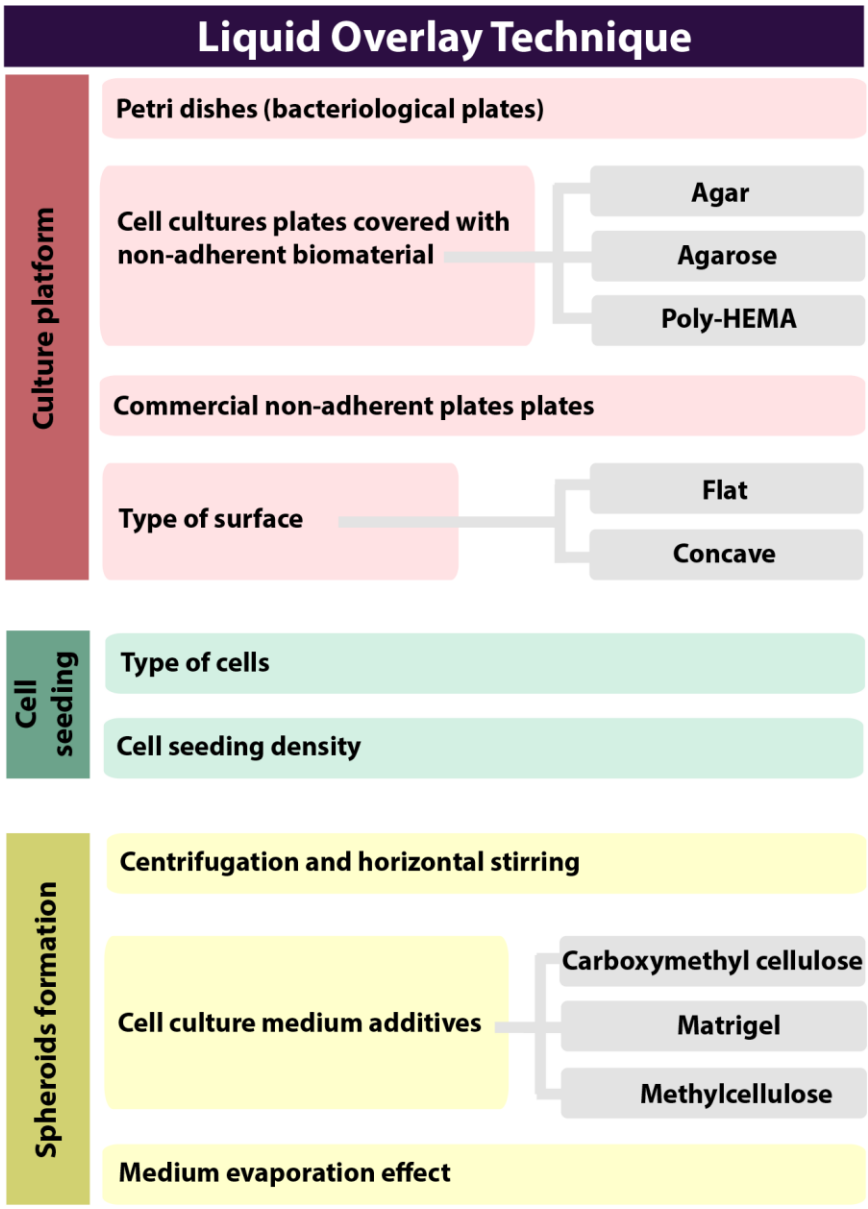

Figure 3.2. Overview of the variables studied for the production of spheroids through LOT.

3.4.1. Biomaterials used in the plate-coating procedure

Cells seeded on Petri dishes or bacteriological plates can form cellular aggregates [42]. Alternatively, spheroids can be obtained by placing cells on traditional cell culture plates pre-coated with biomaterials that prevent their adhesion. The majority of these biomaterials avoids cell adhesion by impairing the deposition of proteins from the culture medium [30, 76].

Agar and agarose were the first biomaterials applied for the growth of spheroids by LOT [15, 47, 49, 60, 62, 77-84]. Nowadays, these two materials are extensively used due to their low cost and easy manipulation, which reduces the time spent in the plate-coating procedure (Table 3.3).

Table 3.3. Overview of the advantages and disadvantages of the non-adherent biomaterials used to coat surfaces aimed for spheroids production through LOT.

Biomaterial	Advantages	Disadvantages	REFs
Agar	- Low cost; - Solutions can be prepared in water or in serum-free medium; - Easy sterilization by autoclave or ultraviolet (UV) radiation; - Plate-coating procedure is not time-consuming.	- Only soluble at high temperatures (usually, higher than 65 ºC); - Coated plates should only be stored during few days; - The remaining solution should not be reused; - Interferes with cells growth.	[49, 77-81, 85]
Agarose	- Low cost; - Solution can be prepared in water or in serum-free medium; - Easy sterilization by autoclave or UV radiation; - Plate-coating procedure is not time-consuming.	- Only soluble at high temperatures; - Coated plates should only be stored during few days; - The remaining solution cannot be reused.	[15, 47, 49, 60, 77, 82-84]
Poly-HEMA	- Easy sterilization (filtration through a 0.22 µm pore size membrane filter); - The remaining solution and coated plates can be stored at 4 ºC up to several months.	- Expensive; - Only soluble in ethanol 95%; - Solutions preparation is very time-consuming; - Plate-coating procedure is very time-consuming.	[19, 86-90]

For the preparation of agar or agarose coated plates, first the biomaterials are fully dissolved in water or serum-free medium and then they are sterilized by autoclave. Afterwards, the solutions are added to the bottom of the cell culture plate wells and then it takes only few minutes for the solutions to jellify at room temperature (RT). Researchers have been favoring the use of agarose coated plates instead of their agar equivalents since it was demonstrated that the sulfate groups of agar inhibit BHK 21 hamster fibroblasts growth [85].

The main handicap related to the application of agar and agarose in LOT is associated to the short storage time of the coated plates (Table 3.3). Metzger *et al.* noticed that the storage of coated plates at 4 ºC or in an incubator at 37 ºC during various days results in water evaporation, and, consequently, to the coating disruption, *i.e.* impairing the reproducible production of the spheroids [49]. Moreover, the storage of the remaining agar and agarose solutions is not recommended since these have to be heated before each application and such process may compromise biomaterials stability and the initial concentration of the solution, as previously reported [49, 77].

Poly(2-hydroxyethyl methacrylate) (poly-HEMA) is a non-adherent, soft and flexible plastic that has been recently applied as an alternative polymer to produce spheroids by LOT [91]. Poly-HEMA is usually dissolved in ethanol 95% (100% ethanol does not dissolve the polymer [90]) and then it is used to coat the materials surfaces [86-88]. Moreover, poly-HEMA is sterilized by filtering the sample solution with a 0.22 µm pore membrane filter. In contrast to the agar and

agarose solutions, sterile poly-HEMA solutions and poly-HEMA coated plates can be stored at 4 ºC, up to 2 months, before their used [90].

However, the utilization of poly-HEMA, as a non-adherent material for the production of spheroids through LOT, is a laborious procedure, since it takes several hours (5-7 h) to dissolve the polymer, at 37 ºC [90]. Furthermore, Phung *et al*. denoted that the complete evaporation of the ethanol from the poly-HEMA coated plates at RT (15-20 ºC) takes 1-2 weeks [89]. To surpass these drawbacks, Lawrenson *et al*. suggested to raise the temperature of the poly-HEMA solution (up to 65 ºC), in order to facilitate the polymer dissolution and to dry the coating inside a humidity free incubator at 37 ºC, for 48 h. Such procedure allows the creation of a uniform, solvent free plate coating [19].

Recently, in addition to the previous referred non-adhesive biomaterials, HA applicability to cover surfaces for spheroids formation has also been investigated by Lai and Tu [92] and by our lab [93]. HA is an ECM constituent found in normal, injured and tumor tissues and it demonstrates poor adhesive properties [94]. The attractiveness of the HA utilization as a coating for the spheroids formation resides on the fact that, contrasting to agar, agarose and poly-HEMA, it allows the establishment of cell-ECM interactions under *in vitro* conditions. This property plays an important role on the cancer cells behavior, tumor progression and also on the therapeutics resistance profile displayed by cancer cells [95].

Nevertheless, to reduce the time spent in the preparation of non-adherent cell culture surfaces, commercially available non-adherent plates can be used for the growth of spheroids (*e.g.* PrimeSurface® culture plates (Sumitomo Bakelite), Lipidure® COAT Plates (NOF Corporation) and Nunc®Low Cell Binding Surface 96-well plate (Thermofisher)) [3].

3.4.2. Improving cellular aggregates spherical-like shape by using concave non-adherent surfaces

The use of spheroids with similar sizes and with uniform spherical-like shapes is crucial to guarantee the correct assessment of therapeutics efficacy and the reproducibility of the obtained data. In fact, recent reports state that spheroids with a spherical shape are the most suitable to monitor different antitumoral therapeutics [47, 96]. The spherical organization of the cells originate a gradient of proliferative to necrotic cells resembling the *in vivo* conditions, which in the majority of the cases, is not found in non-spherical microtissues. Additionally, spherical-like cellular aggregates ensure an homogeneous distribution of the therapeutic molecules within the microtissue and the majority of the mathematical models applied to study drugs or other therapeutic agents effect on spheroids are optimized for round shaped spheroids [13].

Up to now, different studies have demonstrated that none or very few cellular aggregates with spherical shape are obtained by LOT when flat non-adherent surfaces (*e.g.* Petri dishes or flat cell culture plates covered with a thin layer of non-adherent biomaterial) are used [47, 48, 60] - Figure 3.3 A-E. In a previous work, our group noticed that HeLa cervical cancer cells seeded on non-adhesive flat bottom culture plates were only able to form disorganized or elongated compact cellular aggregates [47] - Figure 3.3 D and E. Moreover, other authors also showed that irregular cellular aggregates, loose discs of cells or single cell suspensions are attained when flat non-adherent surfaces are used (Figure 3.3 A-D). These cellular aggregates do not meet the requirements to be used in HTS, which hinders the translation of these technologies to the industry [48].

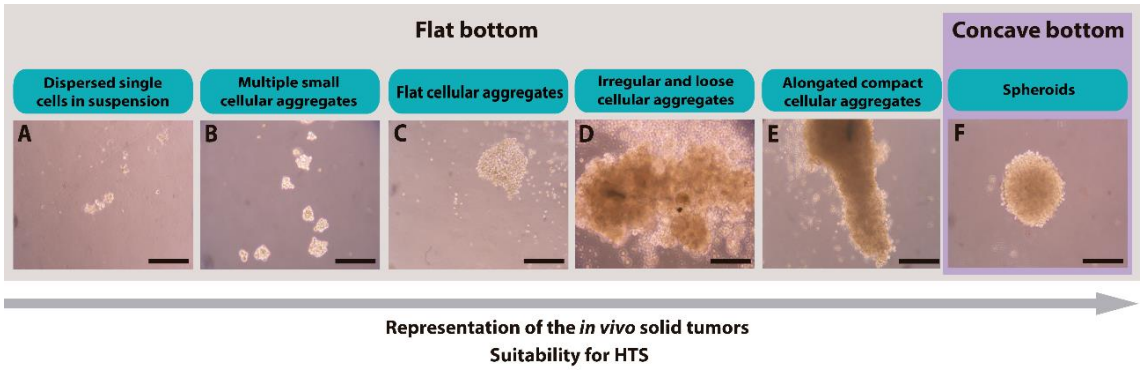

Figure 3.3. Classification of structures formed on flat non-adherent surfaces (*e.g.* Petri dishes or cell culture plates covered with a thin layer of non-adherent biomaterial (A-E)) and concave surfaces (*e.g.* cell culture plate bottoms covered with high amounts of non-adherent biomaterial and cell culture plates with U-shape bottoms (F)). Scale bar represents 200 µm.

On the other hand, the use of concave non-adherent surfaces, which are produced by increasing the volume of the non-adherent biomaterial solution added to each flat bottom well, usually leads to the formation of cellular aggregates with a more defined spherical-like shape [47, 60] - Figure 3.3 F. Gaskell and co-workers compared the formation of C3A hepatoma aggregates in poorly adherent flat surfaces and in 96-well cell culture plates coated with 100 µL of 1.5% (w/v) agarose (the agarose coating gives a U-shape design to the bottom of the culture plate wells) [60]. Authors verified that the aggregates attained on the non-adherent flat surfaces displayed an irregular, non-spherical structure with a poorly defined outer perimeter while well-defined spheroids were created on the agarose coated wells [60]. Similar results were also reported for HeLa cervical and MCF-7 breast cancer cells seeded on 24-well cell culture plates coated with 300 µL of 1.0% (w/v) agarose, *i.e.* spheroids with a defined and uniform spherical-shape were formed [47]. The concavity of the coating induces cells deposition in the center of the well due to the gravitational force or by submitting the plates to smooth centrifugation [97], ultimately leading to the formation of a single and well-defined spheroid per well [47, 97].

Lastly, V-shaped non-adherent wells can also mediate the formation of spheroids with a spherical shape. A recent study performed by Froehlich *et al.* demonstrated that MCF-7 breast

cancer spheroids attained a compact spherical-like shape when cells were seeded on Cellstar® V-shape 96-well plates coated with poly-HEMA [97]. Still, MCF-7 spheroids formed in wells with the U-bottom shape (Cellstar® Cell-Repellent Surface) displayed a more spherical shape than those formed on the V-shape surface, independently of the tested conditions [97].

3.4.3. Influence of cell type on spheroids formation

The cells capacity to form spheroids by LOT is not similar for all types of cells. Carlsson *et al.* studied the spheroids forming ability of 39 different human cell lines (malignant and normal) usually grown in monolayer or in suspension, to form spheroids by LOT. Authors noticed that 10 out of 12 normal cells and 16 out of 27 cancer cells were able to generate spheroids by LOT [98]. In this case, the cell lines that did not form spheroids remained as single cells (*e.g.* U-343-MGa glioma cells, U-2-OS sarcoma cells, U-1285 lung cancer cells, 769-P renal cancer cells), or formed flat cellular aggregates (*e.g.* U-296 lymphoid cells, SH-SY5Y neuroblastoma cells) or even long and large disorganized aggregates (*e.g.* U-118-MG glioma cells, IMR-32 neuroblastoma cells) [98]. The obtained results also demonstrated that spheroids formation is independent of the culture method used (monolayer or in suspension), since both types were able to form spheroids.

Moreover, cells ability to form spheroids by LOT is not correlated with the cells' tissue origin [98, 99]. For instance, some breast cancer cell lines are able to form spheroids (MCF-7, T47D, MDA-MB-435, MCF7-ADR) while others generate disorganized cellular aggregates composed of loosely packed cells (MDA-MB-231, MDA-MB-468, SKBR3 and MDA-MB-361) [99]. Nevertheless, some cell culture medium additives can also be used to facilitate cells aggregation through LOT, as it will be discussed in the section 3.4.6.

3.4.4. Control the spheroids size by using fine-tuning the initial number of cells

Spheroids size can be optimized by modulating the initial number of cells seeded on the non-adherent surfaces as observed by Ma *et al.* [62]. The authors seeded a different number of HeLa cells per well (62, 125, 250, 500 and 1000) to obtain spheroids by LOT in agarose (1% (w/v)) coated 96-well plates [62]. They verified that after 3 days of culture, the diameter of all spheroids increased overtime in a rate that was proportional to the initial number of cells seeded. In this way, spheroids produced with a higher initial cell number (1000 cells/well) were the first to attain sizes higher than 500 μm (approximately after 7 days of culture) [62]. Accordingly, Yamaguchi *et al.* also observed that the increase of the cell seeding density (100, 1000 and 10000 cells/well) in low cell-binding surfaces of 96-well plates, leads to an increase in the MSCs spheroids diameter [100]. Therefore, spheroids with higher diameters can be obtained when higher initial cell seeding densities are utilized [47, 60, 62].

3.4.5. Centrifugation and horizontal stirring to improve cellular aggregation

There are other factors such as centrifugation and horizontal stirring that can also contribute for cells aggregation, as well as for the formation of a unique spheroid per well by LOT. Ho *et al*. demonstrated that the addition of a centrifugation step (1000 g for 5 min) facilitates the formation of MCF-7 breast cancer spheroids by prompting the cellular aggregation in an initial stage [69]. Moreover, previous results obtained in our lab also demonstrated that the application of horizontal stirring, during 6 days, at 200 rotations per minute (RPM), improves the formation of HeLa cervical cancer spheroids by LOT, since it avoids cells spreading and allows the production of one spheroid per well with a regular spherical shape [47]. In fact, without any mechanical stirring, cells remained more disorganized along time. The horizontal stirring induces a closer physical contact between cells in the center of the well, leading to the formation of more cohesive cellular aggregates. Still, the centrifugation and the stirring must be optimized to promote cellular aggregation without inducing cells mechanical lysis.

3.4.6. Cell culture medium additives that are used to improve cellular aggregation

Some cell lines (*e.g.* MDA-MB-231, HepG2 and SK-OV-3) are unable to establish strong interactions between them, leading to the formation of loose cellular aggregates when seeded on non-adherent surfaces. These aggregates have a lack of physical diffusion barriers and do not display a layered organization. Therefore, they are not able to fully represent the features of *in vivo* solid tumors.

In this context, the addition of supplements (*e.g.* viscosity-increasing additives, ECM related components and others) to the culture medium has been explored for enhancing the construction of more compact cellular aggregates and spheroids by LOT (Table 3.4).

Methylcellulose, is a well-known crowding agent that supports the formation of spheroids from different cell lines. Froehlich *et al*. showed that the addition of 25% Methocel™ (The Dow Chemical Company) to the culture medium can facilitate the development of different breast cancer cells (MCF-7, MDA-MB-231 and SK-BR-3) spheroids by LOT [97]. In a similar way, Longati *et al*. verified that methylcellulose (0.24%) helps in the formation of PANC-1, BXPC3 and PSC spheroids by LOT (see Table 3.4 for further details) [18].

Table 3.4. Cell culture medium additives studied up to now for spheroids production through LOT.

Medium additives	Concentration(s) tested	Cell lines	Observation(s)	REF
Carboxymethyl cellulose	0.1-0.5% (w/v)	- Human osteoblasts (HOB); - Normal human dermal fibroblasts (NHDF); - Human dermal microvascular endothelial cells (HDME).	- Independently of the carboxymethyl cellulose concentration used, HOB and NHDF formed spheroids; - HDME spheroids were not produced.	[49]
Insulin	10 µg/mL	- Human breast cancer cells (MDA-361).	- MDA-361 cells are unable to form spheroids in the absence of cell culture medium supplemented with insulin.	[101]
Matrigel™	2% (w/v)	- Mouse mammary carcinoma cell line (4T1); - Murine embryonic fibroblasts (MEF).	- 4T1 cells only formed spheroids in cell culture medium supplemented with Matrigel™ and on surfaces coated with Matrigel™.	[102]
	3.5% (w/v)	- Human breast cancer cells (MCF-7, MDA-MB-231 and SK-BR-3).	- MCF-7 and MDA-MB-231 cells formed spheroids; - SK-BR-3 spheroids were not attained.	[97]
Methylcellulose	0.24% (w/v)	- Human pancreatic cancer cells (PANC-1, MiaPaCa2, BXPC3 and ASPC-1); - Human immortalized pancreatic stellate cells (PSCs).	- PANC-1 cells formed compact and spherical spheroids; - BXPC3 and PSC cells formed extremely compact and well-defined spheroids; - MiaPaCa2 cells did not form aggregates; - ASPC-1 or Capan-1 cells formed loose aggregates.	[18]
	0.24% (w/v)	- Human glioma cells (U343); - Immortalized murine glial precursor cells.	- U343 cells formed spheroids after 1-3 days of culture; - Immortalized murine glial precursor cells formed spheroids after 4-5 days of culture.	[103]
	20% (w/v)	- Human ovarian cancer cells (KGN, OVCA429 and OVCA433).	- All cell lines formed compact spheroids.	[104]
	25% (w/v) (Methocel™)	- Human breast cancer cells (MCF-7, MDA-MB-231 and SK-BR-3).	- MCF-7 cells formed spheroids; - MDA-MB-231 and SK-BR-3 cells just formed loose cellular aggregates.	[97]
Reconstituted basement membrane (rBM)	2.5% (w/v)	- Human breast cancer cells (MDA-MB-231).	- MDA-MB-231 cells formed spheroids with a spherical compact geometry.	[99]

Several ECM constituents (fibronectin, laminin, collagen type IV, heparin sulfate proteoglycans and chondroitin sulfate) and ECM protein mixtures (Matrigel™ and reconstituted basement membrane (rBM)) have also been investigated as additives for supporting spheroids formation by LOT [97, 99, 102]. Ivascu and Kubbies observed that MDA-MB-231 cells seeded on poly-HEMA coated surfaces (96-well plate) generate loose and easily disrupted cellular aggregates. In contrast, these cell lines formed spheroids with structural features similar to those of *in vivo* solid tumors, when they are cultured with medium supplemented with fibronectin, laminin, collagen type IV, sulfate proteoglycans or chondroitin sulfate [99]. However, collagen type I had a minor impact on the cohesivity of MDA-MB-231 aggregates, since it only increased the intercellular contacts between adjacent cells [99]. In contrast, when MDA-MB-231 cells were cultured in the presence of 2.5% rBM, cohesive spheroids with a defined geometry were generated after 24 h [99].

Moreover, Yuhas and Tarleton verified that the formation of MDA-361 breast cancer spheroids by LOT is an insulin concentration-dependent process, *i.e.* when cells were cultured with 10 µg/mL of insulin an exponential growth rate of ≈ 12 µm/day was observed (spheroids were not produced when lower concentrations of insulin were used) [101].

3.4.7. Prevent the evaporation-induced medium loss

The formation of spheroids by LOT can be affected by the medium evaporation effect, *i.e.* faster evaporation of the medium from the peripherical wells of the plate [105]. This phenomenon can have a huge impact on the growth, size and metabolism of spheroids, as well as on their response to therapeutics [68, 106].

In order to prevent the evaporation of liquids, self-adhesive plate sealers may be used. However, these sealers usually reduce the gas exchange (*e.g.* O_2/CO_2 exchange), which in turn can have an impact on several spheroids' properties (*e.g.* spheroids growth and cellular viability) and consequently on the screening assays outcome. Alternatively, spheroids development in the plate peripheral wells should be avoided (these wells may be filled with water) and incubators that have a more sensitive control over the environment humidity can be used for decreasing the problems associated with the medium evaporation effect (discussed in detail by Das *et al.* [68]).

3.5. Conclusion and Outlook

Up to now, several techniques have been used for spheroids production. Among them, LOT arises as one of the most promising approaches for the growth of cellular aggregates. Still, the traditional LOT, comprising spheroids formation on flat non-adhesive surfaces, has some

limitations like its lack of reproducibility. Therefore, various LOT technical developments have been investigated in order to improve the spheroids production and their suitability for HTS. Moreover, to produce more cohesive and spherical aggregates by LOT different non-adherent biomaterials and various amounts of these materials have been employed for coating the cell culture wells. Further, an increase in the cell seeding density allows the production of spheroids with higher diameters. Moreover, the type of cells and the presence of cell culture additives also have a huge impact the formation of spheroids by LOT. Such optimizations allowed to control of the size and shape of the cellular aggregates produced and also improved the reproducibility of the LOT, leading to the production of more uniform and spherical spheroids.

Overall, LOT improvements and troubleshooting (Table 3.5) open the possibility for obtaining reproducible spheroids at low cost, which is crucial for *in vitro* HTS of therapeutics aimed for cancer therapy.

Table 3.5. Troubleshooting guide for the main issues related to the spheroids production by LOT.

Stage	Issue	Troubleshooting(s)	REF(s)
Plate-coating procedure	Non-adherent biomaterials are hard to dissolve	- Agar and agarose solution are easily dissolved at high temperatures (> 80 ºC) or by autoclave; - Poly-HEMA can be dissolved in ethanol 95%. Do not use ethanol 100%.	[133, 136, 262, 263, 265]
	It takes several hours to dissolve poly-HEMA	- Put the poly-HEMA solution in a water bath at 65 ºC.	[264, 265]
	Poly-HEMA coating drying is slow (1 to 2 weeks at RT)	- Poly-HEMA drying time can be reduced to 48 h using an incubator at 37 ºC.	[264]
	The coating is not uniform	- Increase the volume of the coating solution; - Do not allow agarose to cool down below 60 ºC before the coating process; - Do not reheat the solutions.	[192, 213, 253]
	The coating has some cracks	- Do not store the cell culture platforms during long periods of time; - For long storage periods, it may be helpful to cover the coating with cell culture medium.	[192, 213]
	Plate-coating procedure is time-consuming	- Use commercial plates (*e.g.* PrimeSurface® culture plates (Sumitomo Bakelite), Lipidure® COAT Plates (NOF Corporation) and Nunc®Low Cell Binding Surface 96-well plate (Thermofisher)).	[136, 182]
Spheroids formation, growth and culture	Some cells (*e.g.* MDA-MB-231) cannot grow into spheroids by LOT	- Use cell culture medium additives (*e.g.* carboxymethyl cellulose, methylcellulose).	[195, 213, 271, 273, 275-278, 281]

	Various spheroids are formed on the non-adherent surface, *i.e.* spheroids are not produced individually	- Use cell culture plates (avoid the use of Petri dishes); - Use centrifugation to promote cells closeness; - Use an appropriate amount of agarose per surface area to guarantee the formation of a concave agarose surface.	[136, 192, 214, 271]
	Spheroids formed with non-spherical-like shapes	- Use concave bottoms (U- or V-shape).	[136, 192, 236]
	Spheroids formed with small diameters (< 500 µm)	- Increase the culture time; - Use higher cell seeding densities.	[136, 236, 238, 274]
	Inhomogeneous spheroid formation among the wells;	- Avoid cell culture medium evaporation by using different lids and different incubators.	[244, 280]
	Spheroids desegregation and detachment of cells from the external layers of the spheroids	- Avoid movement and monitoring of plates during the next 2 days after cell seeding; - Change the cell culture medium carefully; - Replace only 50% of the cell culture medium when doing spheroids maintenance.	[136, 192]

3.6. References

1. Edmondson, R., *et al.*, *Three-Dimensional Cell Culture Systems and Their Applications in Drug Discovery and Cell-Based Biosensors.* Assay and Drug Development Technologies, 2014. 12: 207-218.

2. Hickman, J. A., *et al.*, *Three-dimensional models of cancer for pharmacology and cancer cell biology: capturing tumor complexity in vitro/ex vivo.* Biotechnology Journal, 2014. 9: 1115-1128.

3. Breslin, S. and O'Driscoll, L., *Three-dimensional cell culture: the missing link in drug discovery.* Drug Discovery Today, 2013. 18: 240-249.

4. Chen, Y.-C., *et al.*, *Single cell dual adherent-suspension co-culture micro-environment for studying tumor-stromal interactions with functionally selected cancer stem-like cells.* Lab on a Chip, 2016. 16: 2935-2945.

5. Costa, E. C., *et al.*, *Evaluation of nanoparticle uptake in co-culture cancer models.* PLOS ONE, 2013. 8: e70072.

6. Hollmén, M., *et al.*, *Characterization of macrophage-cancer cell crosstalk in estrogen receptor positive and triple-negative breast cancer.* Scientific Reports, 2015. 5: 9188.

7. Skaper, S. D. and Facci, L., *Central nervous system neuron-glia co-culture models.* Methods in Molecular Biology, 2012. 846: 79-89.

8. Rose, K. A., *et al.*, *Co-culture of Hepatocytes and Kupffer Cells as an In Vitro Model of Inflammation and Drug-Induced Hepatotoxicity.* Journal of Pharmaceutical Sciences, 2016. 105: 950-964.

9. Xu, J. J., *et al.*, *Cellular Imaging Predictions of Clinical Drug-Induced Liver Injury.* Toxicological Sciences, 2008. 105: 97-105.

10. Bell, C. C., *et al.*, *Characterization of primary human hepatocyte spheroids as a model system for drug-induced liver injury, liver function and disease.* Scientific Reports, 2016. 6: 25187.

11. Dingle, Y.-T. L., *et al.*, *Three-Dimensional Neural Spheroid Culture: An In Vitro Model for Cortical Studies.* Tissue Engineering Part C: Methods, 2015. 21: 1274-1283.

12. Kurosawa, H., *Methods for inducing embryoid body formation: in vitro differentiation system of embryonic stem cells.* Journal of Bioscience and Bioengineering, 2007. 103: 389-398.

13. Costa, E. C., *et al.*, *3D tumor spheroids: an overview on the tools and techniques used for their analysis.* Biotechnology Advances, 2016. 34: 1427-1441.

14. Mehta, G., *et al.*, *Opportunities and challenges for use of tumor spheroids as models to test drug delivery and efficacy.* Journal of Controlled Release, 2012. 164: 192-204.

15. Friedrich, J., *et al.*, *Spheroid-based drug screen: considerations and practical approach.* Nature Protocols, 2009. 4: 309-324.

16. Yeon, S.-E., *et al.*, *Application of Concave Microwells to Pancreatic Tumor Spheroids Enabling Anticancer Drug Evaluation in a Clinically Relevant Drug Resistance Model.* PLOS ONE, 2013. 8: e73345.

17. Bjerkvig, R., Laerum, O. D., and Rucklidge, G. J., *Immunocytochemical characterization of extracellular matrix proteins expressed by cultured glioma cells.* Cancer Research, 1989. 49: 5424-5428.

18. Longati, P., *et al.*, *3D pancreatic carcinoma spheroids induce a matrix-rich, chemoresistant phenotype offering a better model for drug testing.* BMC Cancer, 2013. 13: 95.

19. Lawrenson, K., Grun, B., and Gayther, S. A., *Heterotypic Three-dimensional In Vitro Modeling of Stromal-Epithelial Interactions During Ovarian Cancer Initiation and Progression.* Journal of Visualized Experiments, 2012: e4206.

20. Khoei, S., *et al.*, *Evaluation of the Combined Effect of 2ME2 and (60)Co on the Inducement of DNA Damage by IUdR in a Spheroid Model of the U87MG Glioblastoma Cancer Cell Line Using Alkaline Comet Assay.* Cell Journal, 2011. 13: 83-90.

21. Sutherland, R. M., *et al.*, *A multi-component radiation survival curve using an in vitro tumour model.* International Journal of Radiation Biology and Related Studies in Physics, Chemistry and Medicine, 1970. 18: 491-495.

22. Sutherland, R. M., *et al.*, *Resistance to adriamycin in multicellular spheroids.* International Journal of Radiation Oncology, Biology, Physics, 1979. 5: 1225-1230.

23. Franko, A. J. and Sutherland, R. M., *Radiation Survival of Cells from Spheroids Grown in Different Oxygen Concentrations.* Radiation Research, 1979. 79: 454-467.

24. Kobayashi, H., *et al.*, *Acquired multicellular-mediated resistance to alkylating agents in cancer.* Proceedings of the National Academy of Sciences, 1993. 90: 3294-3298.

25. Chitcholtan, K., Sykes, P. H., and Evans, J. J., *The resistance of intracellular mediators to doxorubicin and cisplatin are distinct in 3D and 2D endometrial cancer.* Journal of Translational Medicine, 2012. 10: 38.

26. Rae, C. and Mairs, R. J., *Evaluation of the radiosensitizing potency of chemotherapeutic agents in prostate cancer cells.* International Journal of Radiation Biology, 2017. 93: 194-203.

27. Moreira, A. F., *et al.*, *Thermo- and pH-responsive nano-in-micro particles for combinatorial drug delivery to cancer cells.* European Journal of Pharmaceutical Sciences, 2017. 104: 42-51.

28. Kunz-Schughart, L. A., *et al.*, *The use of 3-D cultures for high-throughput screening: the multicellular spheroid model.* Journal of Biomolecular Screening, 2004. 9: 273-285.

29. Gaspar, V. M., *et al.*, *Folate-targeted multifunctional amino acid-chitosan nanoparticles for improved cancer therapy.* Pharmaceutical Research, 2015. 32: 562-577.

30. Carvalho, M. P., *et al.*, *Tumor spheroid assembly on hyaluronic acid-based structures: A review.* Carbohydrate Polymers, 2016. 150: 139-148.

31. Rimann, M. and Graf-Hausner, U., *Synthetic 3D multicellular systems for drug development.* Current Opinion in Biotechnology, 2012. 23: 803-809.

32. Shin, S., *et al.*, *Alginate-marine collagen-agarose composite hydrogels as matrices for biomimetic 3D cell spheroid formation.* RSC Advances, 2016. 6: 46952-46965.

33. Xu, X., *et al.*, *Recreating the Tumor Microenvironment in a Bilayer, Hyaluronic Acid Hydrogel Construct for the Growth of Prostate Cancer Spheroids.* Biomaterials, 2012. 33: 9049-9060.

34. Chaudhuri, J. B., *Methods and Protocols. Edited by John W. Haycock*. ChemBioChem, ed. J. W. Haycock. Vol. 12. 2011: John Wiley & Sons, Ltd. 1604-1605.

35. Gurski, L. A., *et al.*, *Hyaluronic Acid-Based Hydrogels as 3D Matrices for in Vitro Evaluation of Chemotherapeutic Drugs Using Poorly Adherent Prostate Cancer Cells.* Biomaterials, 2009. 30: 6076-6085.

36. Lin, R. Z. and Chang, H. Y., *Recent advances in three-dimensional multicellular spheroid culture for biomedical research.* Biotechnology Journal, 2008. 3: 1172-1184.

37. Lee, T. J., *et al.*, *Spinner-flask culture induces redifferentiation of de-differentiated chondrocytes.* Biotechnology Letters, 2011. 33: 829-836.

38. Friedrich, J., Ebner, R., and Kunz-Schughart, L., *Experimental anti-tumor therapy in 3-D: spheroids-old hat or new challenge?* International Journal of Radiation Biology, 2007. 83: 849-871.

39. Kim, J. B., *Three-dimensional tissue culture models in cancer biology.* Seminars in Cancer Biology, 2005. 15: 365-377.

40. Achilli, T.-M., Meyer, J., and Morgan, J. R., *Advances in the formation, use and understanding of multi-cellular spheroids.* Expert Opinion on Biological Therapy, 2012. 12: 1347-1360.

41. Helige, C., *et al.*, *Uterine natural killer cells in a three-dimensional tissue culture model to study trophoblast invasion.* Laboratory Investigation, 2001. 81: 1153-1162.

42. Yuhas, J. M., *et al.*, *A simplified method for production and growth of multicellular tumor spheroids.* Cancer Research, 1977. 37: 3639-3643.

43. Sutherland, R. M., McCredie, J. A., and Inch, W. R., *Growth of multicell spheroids in tissue culture as a model of nodular carcinomas.* Journal of the National Cancer Institute, 1971. 46: 113-120.

44. Deen, D. F., *et al.*, *Development of a 9L rat brain tumor cell multicellular spheroid system and its response to 1, 3-bis (2-chloroethyl)-1-nitrosourea and radiation.* Journal of the National Cancer Institute, 1980. 64: 1373-1382.

45. Zanoni, M., *et al.*, *3D tumor spheroid models for in vitro therapeutic screening: a systematic approach to enhance the biological relevance of data obtained.* Scientific Reports, 2016. 6: 19103.

46. Foty, R., *A Simple Hanging Drop Cell Culture Protocol for Generation of 3D Spheroids.* Journal of Visualized Experiments, 2011. 51: e2720.

47. Costa, E. C., *et al.*, *Optimization of liquid overlay technique to formulate heterogenic 3D co-cultures models.* Biotechnology and Bioengineering, 2014. 111: 1672-1685.

48. Carlsson, J. and Yuhas, J. M., *Liquid-Overlay Culture of Cellular Spheroids*, *Spheroids in Cancer Research*. 1984, Springer Berlin Heidelberg.

49. Metzger, W., *et al.*, *The liquid overlay technique is the key to formation of co-culture spheroids consisting of primary osteoblasts, fibroblasts and endothelial cells.* Cytotherapy, 2011. 13: 1000-1012.

50. Halldorsson, S., *et al.*, *Advantages and challenges of microfluidic cell culture in polydimethylsiloxane devices.* Biosensors and Bioelectronics, 2015. 63: 218-231.

51. Napolitano, A. P., *et al.*, *Scaffold-free three-dimensional cell culture utilizing micromolded nonadhesive hydrogels.* Biotechniques, 2007. 43: 494-500.

52. Costăchel, O., Fadei, L., and Badea, E., *Tumor cell suspension culture on non adhesive substratum.* Z. Krebsforseh., 1969. 72: 24-31.

53. do Amaral, J. B., *et al.*, *MCF-7 cells as a three-dimensional model for the study of human breast cancer.* Tissue Engineering Part C: Methods, 2011. 17: 1097-1107.

54. Mayer, B., *et al.*, *Multicellular gastric cancer spheroids recapitulate growth pattern and differentiation phenotype of human gastric carcinomas.* Gastroenterology, 2001. 121: 839-852.

55. Wen, Z., *et al.*, *A spheroid-based 3-D culture model for pancreatic cancer drug testing, using the acid phosphatase assay.* Brazilian Journal of Medical and Biological Research, 2013. 46: 634-642.

56. Lee, I., *et al.*, *The Effect of Taxol and Arsenic Trioxide in HT-29 Spheroid Cells.* Journal of Biomedical Science, 2006. 12: 153-160.

57. Kadletz, L., *et al.*, *Evaluation of spheroid head and neck squamous cell carcinoma cell models in comparison to monolayer cultures.* Oncology Letters, 2015. 10: 1281-1286.

58. Raghavan, S., *et al.*, *Comparative analysis of tumor spheroid generation techniques for differential in vitro drug toxicity.* Oncotarget, 2016. 7: 16948-16961.

59. Bilir, A., *et al.*, *Potentiation of cytotoxicity by combination of imatinib and chlorimipramine in glioma.* International Journal of Oncology, 2008. 32: 829-839.

60. Gaskell, H., *et al.*, *Characterization of a functional C3A liver spheroid model.* Toxicological Research, 2016. 5: 1053-1065.

61. Mikhail, A. S., Eetezadi, S., and Allen, C., *Multicellular tumor spheroids for evaluation of cytotoxicity and tumor growth inhibitory effects of nanomedicines in vitro: a comparison of docetaxel-loaded block copolymer micelles and Taxotere®.* PLOS ONE, 2013. 8: e62630.

62. Ma, H.-l., *et al.*, *Multicellular tumor spheroids as an in vivo-like tumor model for three-dimensional imaging of chemotherapeutic and nano material cellular penetration.* Molecular Imaging, 2012. 11: 487-498.

63. Lei, K. F., Lin, B.-Y., and Tsang, N.-M., *Real-time and label-free impedimetric analysis of the formation and drug testing of tumor spheroids formed via the liquid overlay technique.* RSC Advances, 2017. 7: 13939-13946.

64. Senavirathna, L. K., *et al.*, *Tumor Spheroids as an In Vitro Model for Determining the Therapeutic Response to Proton Beam Radiotherapy and Thermally Sensitive Nanocarriers.* Theranostics, 2013. 3: 687-691.

65. Scherer, K. M., *et al.*, *Three-dimensional imaging and uptake of the anticancer drug combretastatin in cell spheroids and photoisomerization in gels with multiphoton excitation.* Journal of Biomedical Optics, 2015. 20: 78003.

66. Hornung, A., *et al.*, *Toxicity of Mitoxantrone-loaded Superparamagnetic Iron Oxide Nanoparticles in a HT-29 Tumour Spheroid Model.* Anticancer Research, 2016. 36: 3093-3101.

67. Hornung, A., *et al.*, *Treatment Efficiency of Free and Nanoparticle-Loaded Mitoxantrone for Magnetic Drug Targeting in Multicellular Tumor Spheroids.* Molecules, 2015. 20: 18016-11830.

68. Das, V., *et al.*, *Reproducibility of Uniform Spheroid Formation in 384-Well Plates: The Effect of Medium Evaporation.* Journal of Biomolecular Screening, 2016. 21: 923-930.

69. Ho, W. Y., *et al.*, *Development of multicellular tumor spheroid (MCTS) culture from breast cancer cell and a high throughput screening method using the MTT assay.* PLOS ONE, 2012. 7: e44640.

70. Ingram, M., *et al.*, *Three-dimensional growth patterns of various human tumor cell lines in simulated microgravity of a NASA bioreactor.* In Vitro Cellular & Developmental Biology, 1997. 33: 459-466.

71. Keller, G. M., *In vitro differentiation of embryonic stem cells.* Current Opinion in Cell Biology, 1995. 7: 862-869.

72. Bhise, N. S., *et al.*, *A liver-on-a-chip platform with bioprinted hepatic spheroids.* Biofabrication, 2016. 8: 014101.

73. Ham, S. L., *et al.*, *Liquid-based three-dimensional tumor models for cancer research and drug discovery.* Bulletin of Experimental Biology and Medicine, 2016. 241: 939-954.

74. Tang, Y., Liu, J., and Chen, Y., *Agarose multi-wells for tumour spheroid formation and anti-cancer drug test.* Microelectronic Engineering, 2016. 158: 41-45.

75. Gaspar, V. M., *et al.*, *Bioreducible poly(2-ethyl-2-oxazoline)-PLA-PEI-SS triblock copolymer micelles for co-delivery of DNA minicircles and Doxorubicin.* Journal of Controlled Release, 2015. 213: 175-191.

76. Carlsson, J., *et al.*, *Protein-coated agarose surfaces for attachment of cells.* In Vitro, 1979. 15: 844-850.

77. Sgouros, G., Yang, W.-H., and Enmon, R., *Spheroids of prostate tumor cell lines.* Methods in Molecular Medicine, 2003: 79-88.

78. Dalen, H. and Burki, H. J., *Some observations on the three-dimensional growth of L5178Y cell colonies in soft agar culture.* Experimental Cell Research, 1971. 65: 433-438.

79. Huey-Wen Jeng, B., Feigal, M. R. J., and Messer, P. H. H., *Comparison of the cytotoxicity of formocresol, formaldehyde, cresol, and glutaraldehyde using human pulp fibroblast cultures.* Pediatric Dental Journal, 1987. 9: 295-300.

80. Demicheli, R., Pratesi, G., and Foroni, R., *The exponential-Gompertzian tumor growth model: data from six tumor cell lines in vitro and in vivo. Estimate of the transition point from exponential to Gompertzian growth and potential clinical implications.* Tumori, 1991. 77: 189-195.

81. Sarisozen, C., Abouzeid, A. H., and Torchilin, V. P., *The effect of co-delivery of paclitaxel and curcumin by transferrin-targeted PEG-PE-based mixed micelles on resistant ovarian cancer in 3-D spheroids and in vivo tumors.* European Journal of Pharmaceutics and Biopharmaceutics, 2014. 88: 539-550.

82. Casey, R. C., *et al.*, *Beta 1-integrins regulate the formation and adhesion of ovarian carcinoma multicellular spheroids.* The American Journal of Pathology, 2001. 159: 2071-2080.

83. Li, Q., *et al.*, *3D models of epithelial-mesenchymal transition in breast cancer metastasis: high-throughput screening assay development, validation, and pilot screen.* Journal of Biomolecular Screening, 2011. 16: 141-154.

84. Lu, M., *et al.*, *Construction of three-dimensional in vitro culture model of ovarian carcinoma and the study of its multicellular drug resistance.* Journal of Huazhong University of Science and Technology (Medical Science), 2006. 26: 741-743.

85. Jou, C.-H., *et al.*, *In vitro biocompatibility of three-dimensional chitosan scaffolds immobilized with chondroitin-6-sulfate.* Polymers for Advanced Technologies, 2008. 19: 377-384.

86. Xiang, X., *et al.*, *The Development and Characterization of a Human Mesothelioma In Vitro 3D Model to Investigate Immunotoxin Therapy.* PLOS ONE, 2011. 6: e14640.

87. Ivascu, A. and Kubbies, M., *Diversity of cell-mediated adhesions in breast cancer spheroids.* International Journal of Oncology, 2007. 31: 1403-1413.

88. Tong, J. Z., Bernard, O., and Alvarez, F., *Long-term culture of rat liver cell spheroids in hormonally defined media.* Experimental Cell Research, 1990. 189: 87-92.

89. Phung, Y. T., *et al.*, *Rapid Generation of In Vitro Multicellular Spheroids for the Study of Monoclonal Antibody Therapy.* Journal of Cancer, 2011. 2: 507-514.

90. Kuroda, Y., *et al.*, *Isolation, culture and evaluation of multilineage-differentiating stress-enduring (Muse) cells.* Nature Protocols, 2013. 8: 1391-1415.

91. Peshwa, M. V., *et al.*, *Kinetics of hepatocyte spheroid formation.* Biotechnology Progress, 1994. 10: 460-466.

92. Lai, J. Y. and Tu, I. H., *Adhesion, phenotypic expression, and biosynthetic capacity of corneal keratocytes on surfaces coated with hyaluronic acid of different molecular weights.* Acta Biomaterialia, 2012. 8: 1068-1079.

93. Carvalho, M. P., Costa, E. C., and Correia, I. J., *Assembly of breast cancer heterotypic spheroids on Hyaluronic Acid coated surfaces.* Biotechnology Progress, 2017. 33: 1346-1357.

94. Necas, J., *et al.*, *Hyaluronic acid (hyaluronan): a review.* Journal of Veterinary Medicine, 2008. 53: 397-411.

95. Toole, B. P., *Hyaluronan: from extracellular glue to pericellular cue.* Nature Reviews Cancer, 2004. 4: 528-539.

96. Achilli, T. M., *et al.*, *Multilayer spheroids to quantify drug uptake and diffusion in 3D.* Molecular Pharmaceutics, 2014. 11: 2071-2081.

97. Froehlich, K., *et al.*, *Generation of Multicellular Breast Cancer Tumor Spheroids: Comparison of Different Protocols.* Journal of Mammary Gland Biology and Neoplasia, 2016. 21: 89-98.

98. Carlsson, J., *et al.*, *Formation and growth of multicellular spheroids of human origin.* International Journal of Cancer, 1983. 31: 523-533.

99. Ivascu, A. and Kubbies, M., *Rapid generation of single-tumor spheroids for high-throughput cell function and toxicity analysis.* Journal of Biomolecular Screening, 2006. 11: 922-932.

100. Yamaguchi, Y., *et al.*, *Mesenchymal stem cell spheroids exhibit enhanced in-vitro and in-vivo osteoregenerative potential*. BMC Biotechnology, 2014. 14: 105.

101. Yuhas, J. M. and Tarleton, A. E., *Dormancy and spontaneous recurrence of human breast cancer in vitro*. Cancer Research, 1978. 38: 3584-3589.

102. Li, L. and Lu, Y., *Optimizing a 3D Culture System to Study the Interaction between Epithelial Breast Cancer and Its Surrounding Fibroblasts*. Journal of Cancer, 2011. 2: 458-466.

103. Hattermann, K., Held-Feindt, J., and Mentlein, R., *Spheroid confrontation assay: A simple method to monitor the three-dimensional migration of different cell types in vitro*. Annals of Anatomy, 2011. 193: 181-184.

104. Bilandzic, M. and Stenvers, K. L., *Assessment of Ovarian Cancer Spheroid Attachment and Invasion of Mesothelial Cells in Real Time*. Journal of Visualized Experiments, 2014. 87: e51655.

105. Berg, M., *et al.*, *Evaluation of liquid handling conditions in microplates*. Journal of Biomolecular Screening, 2001. 6: 47-56.

106. Faessel, H. M., *et al.*, *Parabolic growth patterns in 96-well plate cell growth experiments*. In Vitro Cellular & Developmental Biology, 1999. 35: 270-278.

Chapter 4

Introduction (part C)

3D tumor spheroids: an overview on the tools and techniques used for their analysis

This chapter is based on the publication entitled: 3D tumor spheroids: an overview on the tools and techniques used for their analysis, Biotechnology Advances, 2016, 34(8): 1427-1441.

4.1. Abstract

In comparison with two-dimensional (2D) cell culture models, three-dimensional (3D) spheroids are able to accurately mimic some features of solid tumors, such as their spatial architecture, physiological responses, secretion of soluble mediators, gene expression patterns and drug resistance mechanisms. These unique characteristics highlight the potential of 3D cellular aggregates to be used as *in vitro* models for screening new anticancer therapeutics, both at a small and large scale. Nevertheless, few reports have focused on describing the tools and techniques currently available to extract significant biological data from these models. Such information will be fundamental to drug and therapeutic discovery process using 3D cell culture models. The present chapter provides an overview of the techniques that can be employed to characterize and evaluate the efficacy of anticancer therapeutics in 3D tumor spheroids.

Keywords: 3D tumor spheroids; cancer therapy; *in vitro* models; methodologies; therapeutic screening.

4.2. Introduction

For many decades, 2D *in vitro* cultures, in which cells grow in a monolayer, have been used as a tool to evaluate the biological performance of bioactive molecules under investigation for use as therapeutics for different diseases like Parkinson's, diabetes or cancer [1]. The easy handling, cost-effectiveness, good reproducibility and ability to grow a myriad of different cell types made 2D cell cultures one of the most employed preclinical *in vitro* methodologies for drug development [1]. In addition, this type of cell culture system has also contributed to reducing the use of laboratory animal models. However, monolayers usually involve cell seeding on polystyrene surfaces, such as culture flasks (T-flasks) or Petri dishes, which are unable to reproduce the real complexity and 3D structure found in the human body.

In the particular case of solid tumors, monolayer cell cultures are unable to mimic the structure and drug resistance conferred by elements of the tumor microenvironment and its 3D organization [1, 2]. These aspects are responsible for the inaccurate assessment of the biological performance of therapeutics. Therefore, researchers are currently developing new *in vitro* cell culture systems that better reproduce *in vivo* tumors properties and that can simultaneously increase, in the future, the development of new treatments at the preclinical stage.

From this standpoint, 3D cell culture models such as spheroids have emerged as a promising platform for screening anticancer therapeutics, since they are able to more accurately mimic both the 3D structure of malignant tissue and also the cancer microenvironment to which the cells within the tumor are exposed (*e.g.* survival, proliferation, gene expression heterogeneity and multidrug resistance) [7, 285, 286].

Alongside with the development of spheroid cell culture models, well-established techniques and methods must be adapted as cutting-edge technologies emerge to fully characterize these complex cellular aggregates. Such characterization is required for extracting relevant biological data and for the standardization of techniques, methods and protocols for spheroid validation in preclinical assays [290, 291].

Therefore, this review compares the features of spheroids with those of *in vivo* solid tumors and also highlights the currently available techniques and methodologies (microscopy, flow cytometry, western blot, quantitative real-time reverse transcription polymerase chain reaction (qRT-PCR), colorimetric assays and mathematical models) used for the characterization of spheroid properties (*e.g.* size, growth, morphology, cellular organization, protein expression, cellular death, drug penetration, *etc.*).

4.3. Characterization of 3D tumor spheroids

Nowadays, a plethora of techniques are employed to study 3D tumor spheroids characteristics, such as the: i) morphology [3, 4]; ii) topography [3, 5]; iii) size [6, 7]; iv) cellular organization [8]; v) protein and gene expression [9, 10]; vi) cell cycle patterns [11-13]; and vii) invasive and metastatic potential of cancer cells. Additionally, these techniques have also been used to characterize the effect of anticancer therapeutics in 3D spheroids (*e.g.* penetration [14, 15] and cell death [4, 16, 17]). A detailed description of the techniques used to study each of these properties is described hereafter.

4.3.1. Optical microscopy as a tool to characterize 3D spheroids

Optical (*e.g.* bright field [17], dark field [18], differential interference contrast (DIC) [7], phase contrast [19] and fluorescence [7]) microscopic techniques are particularly valuable techniques for characterizing the size, morphology and internal organization of the spheroids (Figure 4.1).

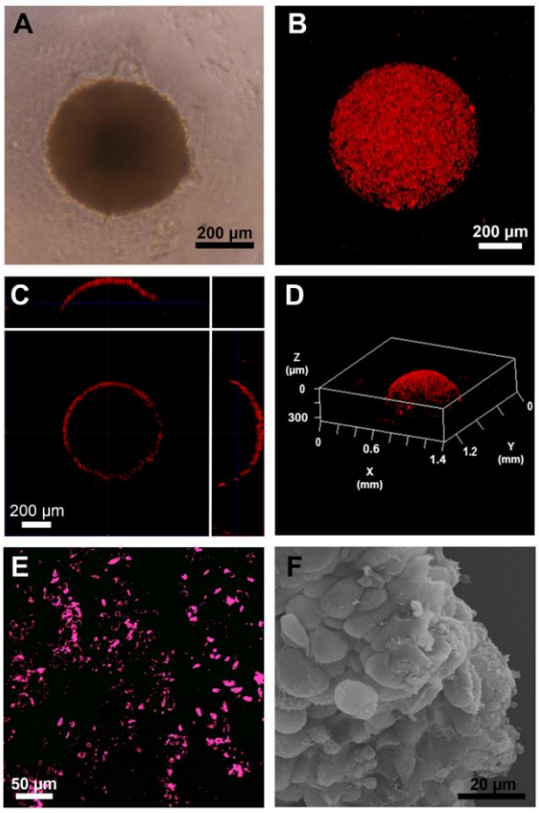

Figure 4.1. Micrographs of 3D mammospheres comprised by MCF-7 cells. A) Top view image of a spheroid acquired using phase contrast microscopy. B) Image of a 3D spheroid section obtained by confocal laser scanning microscopy (CLSM). C) Orthogonal projection of a 3D spheroid obtained by CLSM. D) 3D reconstruction of a CLSM image of a 3D tumor spheroid. E) Evaluation of E-cadherin expression in a 3D spheroid by CLSM. F) Scanning electron microscopy (SEM) image of the spheroid surface. Red channel: cell staining with wheat germ agglutinin (WGA)-Alexa Fluor® 594. Violet channel: E-cadherins stained with anti-E-cadherin Alexa Fluor® 647 conjugate.

Optical microscopes equipped with digital cameras are usually used to study the growth evolution of 3D tumor spheroids [7, 20, 21]. Also, this type of microscope allows for the observation and analysis of spheroid internal organization and the state of the cells in each layer. To accomplish this, antibodies that specifically target proteins (*e.g.* caspase-3, hypoxia-inducible factors (HIF) and Ki-67) or biomarkers (*e.g.* EF5 and pimonidazole) are used to characterize the cellular microenvironment (hypoxia) or state (proliferating, senescent or apoptotic), as represented in Figure 4.1 A. Furthermore, fluorescent microscopy is another type of optical microscopy that can be used to perform fluorescence-based live/dead assays to determine the distribution of dead and live cells within 3D spheroids. Calcein AM (Cal AM) and propidium iodide (PI) are commonly used stains for this purpose (Figure 4.2 C). In addition, other stains like Hematoxylin and Eosin (H&E), Toluidine Blue (TB) and Masson's Trichrome (MCT) can be used for histological analysis (Figure 4.2 B) and can also be monitored by optical microscopy.

In terms of the evaluation of the therapeutic effect in 3D spheroids, fluorescence microscopy is a very useful technique. It allows the evaluation of pharmaceutical dispersion within spheroids, when autofluorescent drugs are used (*e.g.* Doxorubicin (DOX) and Epirubicin). This technique has also been used to determine the distance that molecules are able to penetrate through a spheroid, both in its free form or encapsulated in a nanocarrier [22, 23].

Currently, confocal laser scanning microscopy (CLSM) is the most employed microscopic fluorescent modality to characterize spheroids. However, an analysis of the 3D cellular aggregates with high spatial resolution is challenging when this technique is used. CLSM does not support the visualization of thick specimens due to limited light penetration and the working distance of the commonly used objectives (*e.g.* water immersion objectives). In CLSM, spatial resolution is affected by the pinhole and by the type of the objective used. Scattering in thick specimens leads the illuminating beam to originate out of focus rays. Such a limitation may be surpassed by sectioning spheroids into thin slices (5-7 μm) [23]. In this particular case, spheroids staining can be performed before or after the slicing process. In 3D spheroid sections, the penetration of the staining agent (*e.g.* fluorescent dyes, antibodies) is not significantly hindered, but this does occur in intact spheroids. However, sample fractures may occur due to the sectioning procedures (described in detail elsewhere [24, 25]). Moreover, when cryosectioning is used, ice crystals that form during cryofixation can distort the initial spheroid morphology; thus, the usage of a cryoprotecting agent is required (*e.g.* 300 mM sucrose [25]).

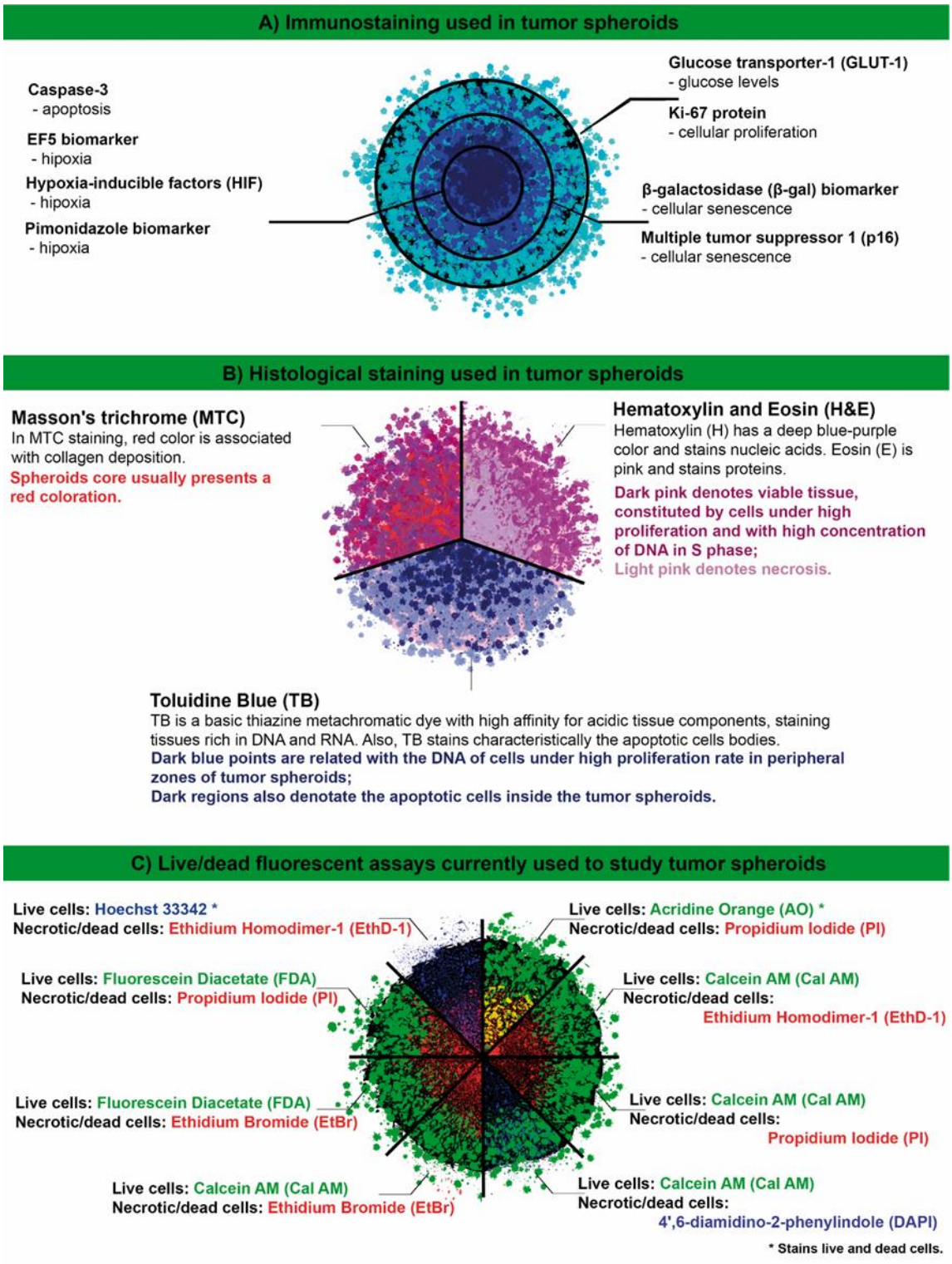

Figure 4.2. Assays usually used to visualize and distinguish the different layers of tumor spheroids using optical microscopy: immunostaining (A), histological staining (B) and live/dead assays (C).

In order to avoid the drawbacks associated with spheroid sectioning, different fluorescence-based techniques have been developed for imaging the cell layers present in the interior of 3D spheroids. Light sheet fluorescence microscopy (LSFM) [26, 27], a variant of LSFM - single (or selective) plane illumination microscopy (SPIM) [28, 29], two-photon microscopy (2PM) [30] and

multi-photon microscopy (MPM) [31] are examples of the techniques used for this propose - Figure 4.3.

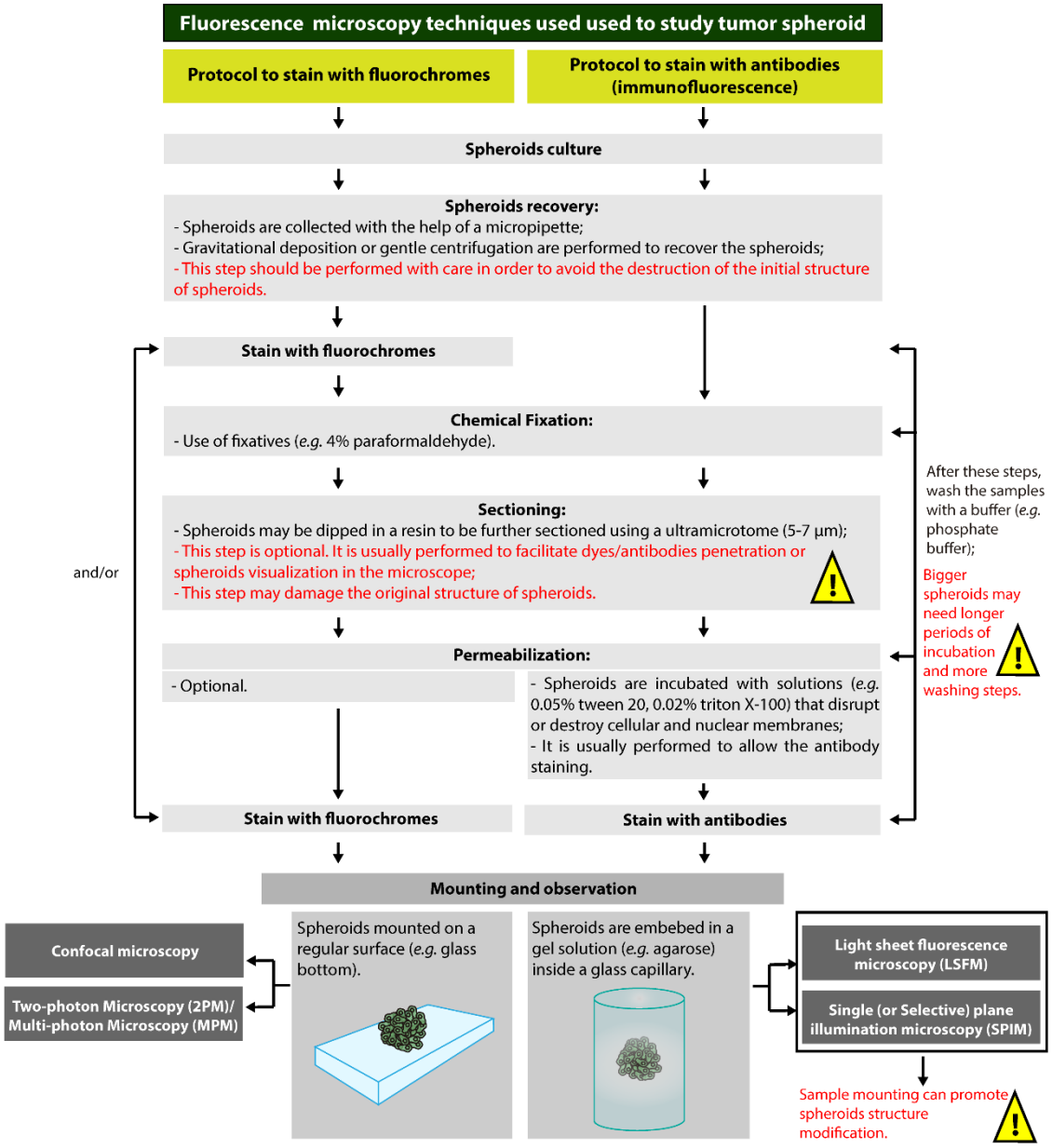

Figure 4.3. Summary of the experimental procedure used to prepare spheroids samples to be analyzed by confocal laser scanning microscopy (CLSM), light sheet fluorescence microscopy (LSFM), two-photon microscopy (2PM)/multi-photon microscopy (MPM) and single (or selective) plane illumination microscopy (SPIM).

4.3.2. Spheroid analysis by scanning electron microscopy (SEM) and transmission electron microscopy (TEM)

Electron microscopy (scanning or transmission) allows the acquisition of images of 3D spheroids with high magnification and resolution (revealing details at the nanoscale level). Among the

other applications, electron microscopy enables the observation of established cellular filopodial projections and other cellular structures (*e.g.* cytoskeleton) that are involved in cell-cell physical interactions [5, 7]. Furthermore, the loss of cell-cell physical interactions and the formation of holes in the spheroid surface due to cellular death promoted, for instance, by an anticancer treatment can also be studied using this type of microscopy [5].

High vacuum scanning electron microscopy (high vacuum SEM) is the most commonly used electron microscopy modality for 3D spheroid observation [5, 7, 32]. In Figure 4.1 F, an SEM image of the surface of a 3D spheroid is presented. Sample preparation for this type of microscopy involves four main steps: i) fixation (where the initial spheroid structure is preserved and stabilized in order to allow its manipulation and imaging); ii) dehydration (water in the sample is replaced by alcohols or acetone); iii) critical point drying (sample is completely dried, *i.e.* ethanol/acetone present in the sample is replaced by CO_2, which will later escape by evaporation from the sample); and iv) sample sputter coating with gold to allow imaging.

However, high vacuum SEM analysis is associated with two main issues, namely structure collapse during critical point drying [33] and the modification of spheroid morphology when the sample is sputtered coated with gold [17]. To overcome these issues related to gold coating, critical point drying or both steps, other types of SEM techniques can be used. Low vacuum SEM (where images are acquired with the sample under low vacuum), environmental SEM (where wet samples are used) [33, 34] and cryogenic SEM (where frozen samples are used) [35] constitute alternatives to conventional SEM.

Transmission electron microscopy (TEM) is another electron microscopy technique that has been widely applied for 3D spheroid analysis. For sample analysis, spheroids are initially chemically fixed, then dehydrated and sectioned into thin slices. However, although spheroid sectioning is usually performed after immersion in resins (*e.g.* epoxy) [17], specimen fractures may still occur. Finally, before observation by TEM, spheroid sections have to be negatively stained (*e.g.* 2% uranyl acetate [36]) to improve image contrast [17].

The most common application of TEM in spheroid analysis is related to the analysis of the penetration and distribution of nanoparticles within the spheroid [37].

4.3.3. Flow cytometry as a tool to characterize cell populations in 3D tumor spheroids

Flow cytometry is a technique where cells have to be in suspension for the individual analysis of each cell. Hence, spheroids in the native state cannot be used and cellular disaggregation has to be performed in order to obtain a single-cell suspension. To accomplish this, spheroids are collected, usually by centrifugation, and treated with enzymes (*e.g.* trypsin) or enzyme cocktails (*e.g.* Accutase® or Accumax®) that promote cellular detachment [13, 14, 38].

Particularly, Accutase® is less toxic and more effective than the other alternatives since it acts on a wide variety of cell-cell adhesion proteins [39]. Afterwards, cells are manipulated and stained using a similar procedure to that employed for 2D cell cultures [13, 14].

So far, flow cytometry has been used to quantify the cellular uptake of drugs and nanoparticles in spheroids and to evaluate their cytotoxic potential (*e.g.* quantification of apoptosis) [13, 17, 40-42]. However, flow cytometry may not be the most efficient technique to evaluate drug penetration and localization within the different layers of the spheroid, since this technique involves the disaggregation of spheroids before their analysis; once cells are in suspension, it is impossible to determine if the cells that contain the therapeutic in their intracellular compartments are from the peripheral cell layers or from the inner regions of the spheroid. To mitigate this limitation, Beaumont *et al.* proposed the use Hoechst dye to distinguish the inner and outer cells of a spheroid in flow cytometry experiments [43], as first described by Durand [44]. According to these authors, the staining of spheroid cells with Hoechst dye is time-dependent, so the outer cells are stained first [43, 44]. Therefore, the degree of Hoechst staining can be useful to indirectly estimate the penetration of therapeutics into the outer (stained with Hoechst) and inner (none Hoechst fluorescence) cell layers of the spheroid [43, 44].

Flow cytometry has also been used for tumor spheroid cell cycle pattern analysis (senescent and proliferative cells) [13]. For instance, Khaitan *et al.* [13] and Laurent *et al.* [12] used DNA fluorescent dyes that bind or intercalate with DNA during the different stages of the cell cycle. Specific fluorescent probes for DNA (*e.g.* PI, 4′,6-diamidino-2-phenylindole (DAPI), deep red anthraquinone 5 (DRAQ5) and Hoechst dyes) interact with DNA during S phase distinguishing senescent from proliferating cells (Figure 4.4). Furthermore, other probes can also be used to identify cells in different phases of the cell cycle (Figure 4.4), including S phase (*e.g.* 5-bromo-2'-deoxyuridine (BrdU) and 5-ethynyl-2'-deoxyuridine (EdU)), G1 phase (Fucci-red) and S-M phase (Fucci-green) [12, 13, 45]. These cell cycle dyes can also be used for fluorescence microscopy [12, 16, 46].

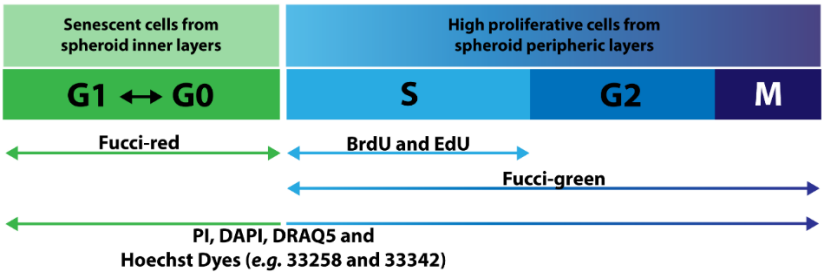

Figure 4.4. Fluorescent probes used to determine the cell cycle stage of cells within tumor spheroids by flow cytometry: i) Fucci-red probe can be used to identify cells in G1 phase; ii) Cells in S phase can be recognized using 5-bromo-2'-deoxyuridine (BrdU) or 5-ethynyl-2'-deoxyuridine (EdU); iii) Fucci-green can be used to mark cells in S-M phase; and iv) propidium iodide (PI), 4',6-diamidino-2-phenylindole (DAPI), deep red anthraquinone 5 (DRAQ5) and Hoechst dye can be used for cells in the G1/S-M phases.

Moreover, fluorescent probes or fluorescently labelled antibodies can also be used to target other cellular components or proteins of interest for flow cytometry-based analysis of other parameters (*e.g.* cellular death and gene expression) [13, 17, 23, 40-42].

4.3.4. Western blot and qRT-PCR as tools to characterize gene expression patterns in 3D tumor spheroids

Western blot (also called immunoblotting) and qRT-PCR are techniques widely used to evaluate the presence of proteins and gene expression patterns in 3D tumor spheroids, respectively. Western blot is used to evaluate the presence of specific proteins in cell lysates. To do so, cellular homogenates are obtained by harvesting 3D spheroids by chemical lysis, using a buffer that contains a detergent (*e.g.* sodium dodecyl sulfate (SDS)), sometimes in combination with mechanical lysis (*e.g.* sonication) [13, 47]. Lysis is performed to destroy the cell structure and release intracellular proteins from different subcellular compartments. Therefore, the lysis buffer should be selected in accordance with the location of the protein of interest (*e.g.* nucleus, cytoplasm or membrane). Moreover, spheroids, owing to their complexity and cellular density, may need a longer incubation period with the lysis buffer than 2D cell cultures, in order for all the cells to be lysed. Although western blot has been widely applied for 3D spheroids analysis, so far and to the best of our knowledge a specific experimental protocol for 3D cell cultures is not yet defined. Currently, only an increase of in lysis buffer volume for spheroid degradation has been described in comparison to 2D cell cultures [48]. The main advantage of western blot-based analysis is related to its sensitivity, since very low concentrations of proteins can be detected. However, western blot is a semi-quantitative method and should be complemented with a more quantitative analysis such as qRT-PCR. This technique is used for quantifying gene expression through the synthesis of complementary DNA (cDNA) transcripts from RNA. Spheroid sample preparation for qRT-PCR analysis is very similar to that required for western blot analysis, namely cellular aggregate disruption and the preparation of a cellular homogenate [49].

Western blot and qRT-PCR analysis of tumor spheroids allows the identification of different proteins that play essential roles in tumor progression (Table 4.1). Moreover, these techniques can also be used for the analysis of therapeutic efficacy by assessing the expression of pro-apoptotic (*e.g.* Bax) or anti-apoptotic markers (*e.g.* Bcl-2) [13, 50]. Furthermore, these techniques can also be used to verify the efficacy of gene therapy (*e.g.* RNA interference (RNAi)) in spheroids [51, 52].

Table 4.1. Proteins and genes usually analyzed by western blot and qRT-PCR in 3D tumor spheroids.

Proteins/genes analyzed		Technique	REF(s)
Adhesion related proteins	E-, N- and VE-cadherins	Western blot	[53-56]
		qRT-PCR	[10, 57]
	ß1-integrin	qRT-PCR	[10, 58]
	Vascular cell adhesion molecule 1 (VCAM-1)	qRT-PCR	[10]
Cellular proteins (cytoskeleton)	ß- and F-actin	Western blot	[56, 59]
		qRT-PCR	[57]
		qRT-PCR PCR	[60]
	Tubulin	Western Blot	[51]
Proteolytic enzymes	Cathepsin B	Western blot	[52]
	Matrix metalloproteinases (MMP-2, MMP-9 and MMP-14)	Western blot	[52, 56, 59, 61]
		qRT-PCR	[10]
Soluble Factors	Hypoxia-inducible factor 1-alpha (HIF-1α)	Western blot	[13, 62, 63]
	Transforming growth factor beta (TGF-ß)	Western blot	[64]
		qRT-PCR	[65]

4.3.5. Application of colorimetric techniques for 3D spheroids analysis

Colorimetric techniques for 3D tumor spheroid analysis are based on chemical assays that are usually used to access the viability of cells or to evaluate the cytotoxic effect of a therapeutic agent. Colorimetric assays applied to the examination of spheroids include the AlamarBlue® (resazurin) [66], Acid Phosphatase (APH) [23, 67], Lactate Dehydrogenase (LDH) [68], 3-(4,5-dimethylthiazol-2-yl)-5-(3-carboxymethoxyphenyl)-2-(4-sulfophenyl)-2H-tetrazolium (MTS) [23], 3-(4,5-dimethyl-2-thiazolyl)-2, 5-diphenyl-2H-tetrazolium bromide (MTT) [68] and 2-(2-methoxy-4-nitrophenyl)-3-(4-nitrophenyl)-5-(2,4-disulfophenyl)-2-tetrazolium (WST-8) assays [3, 69] – Table 4.2.

The majority of these assays are based on the enzymatic conversion of a solute within the subcellular compartments of viable cells (cytoplasm or mitochondria). The reaction product is quantified by measuring its absorbance (or fluorescence) at a specific wavelength (Table 4.2); usually, the value is proportional to the number of metabolically active cells [70]. However, special care needs to be taken in the analysis of the results obtained through these colorimetric assays, since the experimental protocols available are usually optimized for monolayer cultures. In spheroids, the limited mass transport may prevent a homogeneous distribution of the solute (mainly into the inner layers), which may lead to inaccurate results. Taking this into account, Valley and collaborators modified the original protocols in order to improve reagents penetration in 3D spheroids, mainly by submitting samples to horizontal stirring [71].

Table 4.2. Colorimetric assays used to characterize cellular viability within 3D spheroids.

Assay	Principle	Measurement	REF(s)
Alamar blue® (resazurin)	Metabolically active cells are able to reduce resazurin to resorufin mainly through mitochondrial enzymes (NADH dehydrogenase or NADPH dehydrogenase).	Fluorescence of resorufin (pink) is measured with an excitation wavelength of 540–570 nm and emission at 580–610 nm.	[66]
Acid phosphatase (APH)	Based on the quantification of cytosolic acid phosphatase activity. *p*-nitrophenyl phosphate is hydrolyzed by viable cells to *p*-nitrophenol via intracellular acid phosphatase.	The absorbance of *p*-nitrophenol (yellow product) is measured at 405 nm.	[23, 67]
Lactate dehydrogenase (LDH)	The LDH assay involves the conversion of lactate to pyruvate via the reduction of NAD^+ to NADH. Then, diaphorase uses NADH to reduce a tetrazolium salt to a formazan product.	The absorbance of formazan (red product) is measured at 450 nm.	[68]
MTS[a]	Reduction of MTS tetrazolium salt by NADPH dehydrogenases, present in the mitochondria of metabolic active cells, into a soluble formazan product.	The absorbance of formazan (brown product) is measured at 490 nm.	[23]
MTT[b]	Reduction of MTT tetrazolium salt by NADPH dehydrogenases, present in the mitochondria of metabolically active cells, into an insoluble formazan product.	The absorbance of formazan (brown product) is measured at 570 nm.	[68]
WST-8[c]	WST-8 is reduced by NADH dehydrogenase, present in the mitochondria of metabolically active cells, into a soluble formazan dye.	The absorbance of formazan (yellow product) is measured at 450 nm.	[3, 69]

[a] 3-(4,5-dimethylthiazol-2-yl)-5-(3-carboxymethoxyphenyl)-2-(4-sulfophenyl)-2H-tetrazolium;
[b] 3-(4,5-dimethyl-2-thiazolyl)-2, 5-diphenyl-2H-tetrazolium bromide;
[c] 2-(2-methoxy-4-nitrophenyl)-3-(4-nitrophenyl)-5-(2,4-disulfophenyl)-2-tetrazolium.

As an alternative to colorimetric assays, other spectroscopic techniques have been applied for cellular viability analysis within spheroids, including luminescence, tissue dynamic spectroscopy (TDS) [72], fourier transform infrared (FTIR) imaging [73] and proton induced X-ray emission (PIXE) [73]. These techniques allow the characterization of cellular population in spheroids by taking advantage of their inherent properties, namely cellular density and motility (TDS), the distribution of biologic elements such as DNA, adenosine triphosphate (ATP), proteins and metabolites (luminescence and FTIR imaging) and inorganic elements such as copper and zinc (PIXE). Nevertheless, the potential of these approaches for spheroids analysis is still poorly documented.

4.3.6. Mathematical modeling to predict 3D spheroids growth

The inherent properties of 3D tumor spheroids, specifically their i) round shape, ii) initial exponential growth, iii) growth plateau, iv) layered organization and v) gradient of nutrients, oxygen, pH and necrosis present in the spheroid core, have been used to develop mathematical models that are capable of extracting relevant biological data [74]. Based on these features, the first mathematical models developed for spheroid analysis were capable of predicting the initial exponential growth of spheroids (Exponential Growth Model - Equation 1) and the growth plateau (Gompertzian Function – Equation 2) - Figure 4.5.

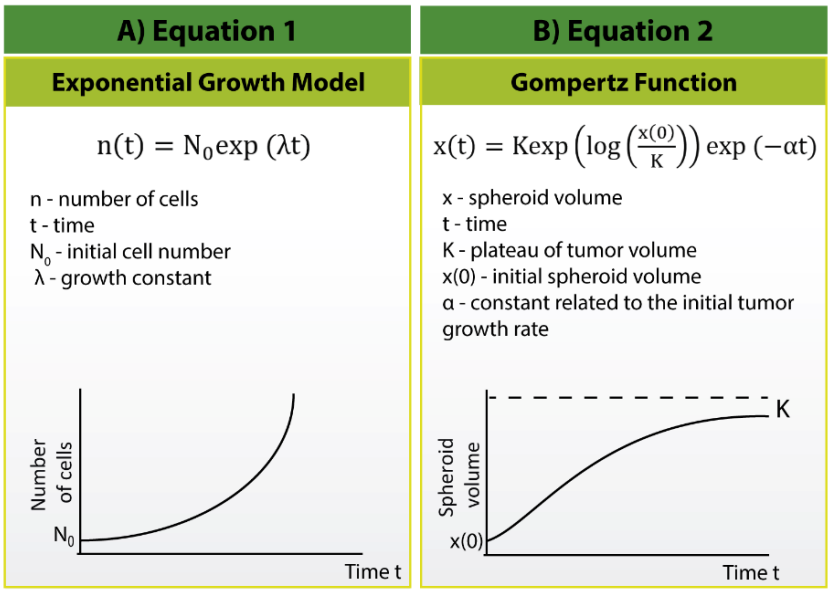

Figure 4.5. Mathematical models used to predict spheroids growth: Exponential Growth Model (A) and Gompertz function (B).

The Exponential Growth Model correlates the number of cells at time t (n(t)) with the initial cell number (N_0) and the growth constant (λ) [75] - see Figure 4.5 A for further details. The Gompertz function, first reported in the 60s by Laird [76], predicts spheroid growth (x(t)) by correlating the 3D spheroids volume (x) with the initial spheroid volume (x(0)) [77]. This model can predict the spheroid volume plateau (K) after extended periods of culture (t = ∞) - Figure 4.5 B.

Recently developed mathematical models are able to predict 3D spheroid growth in accordance with the gradient of nutrients, oxygen, pH and necrosis. In addition to these advances, improvements in image analysis software and image processing algorithms have provided the opportunity to better follow up and analyze spheroid growth. In this context, Piccinini *et al.* developed an automatic unsupervised method using MATLAB® (The MathWorks, Inc., MA, USA) to reconstruct microtissues 3D structure and calculate spheroids volume overtime using simple 2D microscopic images (*e.g.* widefield microscopic images) [78].

Besides the use of mathematical models to predict 3D tumor spheroid growth, other equations have been developed to analyze and predict the biological effect and penetration of different therapeutics (anticancer drugs and drug-loaded nanocarriers) in spheroids [15, 79-84]. Particularly, for nanoparticle-based therapies, some models are now capable of predicting nanoparticle penetration in spheroids according to nanoparticle size [15], half-life time in plasma [83], incubation time and the initial concentration [84].

4.4. Conclusion and Outlook

Currently, animal models are the only preclinical platform accepted by regulatory agencies for characterizing the full effect of a given anticancer therapy. In fact, animal use in the laboratory is the only suitable way of observing the overall effects of a treatment on a living organism. However, the application of *in vitro* models (2D and 3D) for the evaluation of therapeutics has been increasing in recent decades; these techniques avoid the cost and legal/ethical concerns regarding the use of animals in the laboratory.

Despite the absence of studies that demonstrate a direct correlation between the data obtained from 3D tumor spheroids and those gathered from cancer patients, many reports have shown that spheroids are the most appropriate *in vitro* model to represent the features of solid tumors, and moreover present a drug resistant environment when compared to 2D cell culture. However, embracing spheroid models in the search for new anticancer drug candidates (chemically synthetized, drug-loaded nanosized delivery systems, natural compounds, among others) during preclinical stages may be challenging due to the lack of techniques that ensure the reproducible large-scale production of cellular aggregates with uniform sizes and a spherical shape. Moreover, the lack of simple and affordable standardized assays and the scarcity of handling technologies/equipment for assessing therapeutic responses in spheroids are also limiting factors.

Additionally, a limited amount of information is provided in the literature about the protocols, techniques and technologies that can allow for a more harmonized analysis of the effects of new compounds on 3D spheroids structure, morphology, volume/size, cellular distribution, viability and gene expression patterns. Herein, a compilation of the approaches used so far, to characterize spheroids properties has been presented in order to fill the existing gap in the literature and to emphasize the huge potential that 3D tumor spheroids hold for drug evaluation purposes (Table 4.3).

Future improvements to 3D tumor spheroids models are expected in the future, namely the inclusion of the surrounding vasculature, immune system components and mechanical signals, or even the enhancement of their ability to capture the full biological approximation of the native tumor. Such advances may further encourage the pursuit of methodologies to extract valid biological information from 3D models and propel the incorporation of these platforms in the search for anticancer candidates.

Table 4.3. Summary of the main techniques and methodologies used to characterize the effect of anticancer therapeutics on 3D tumor spheroids.

Techniques/ methodologies	Parameter analyzed	Description	REF(s)
Optical and fluorescence microscopy	Size and growth	- Monitoring of spheroid size, area or volume.	[7, 20, 21]
	Cellular organization	- Observation of the live and dead cell distribution.	[7, 68, 85]
		- Observation of spheroids labelled with antibodies.	[16, 21, 86]
		- Observation of spheroids stained using simple histological protocols.	[14, 32, 67]
		- Observation of cell polarity.	[53, 54]
	Morphology	- Monitoring spheroid shape and symmetry.	[7, 16]
		- Monitoring spheroid disaggregation and/or morphological disruption in response to an anticancer treatment.	[5, 87, 88]
	Drug penetration	- Determination of the penetration and dispersion capacity of drugs.	[22, 23, 87]
	Cellular death	- Observation of the presence of specific markers of cellular death or cellular proliferation.	[23, 69, 89]
		- Identification of live or apoptotic cells.	[3, 90]
	Proteins expression	- Assessment of the expression of proteins before and after drugs administration.	[59, 91]
	Invasion/metastization of cancer cells	- Visualization and determination of spheroid cell invasion/metastatic capacity.	[51, 64, 92]
Scanning electron microscopy (SEM)	Topology	- Visualization of the spheroid surface and cell-cell physical interactions.	[5, 7, 23]
	Cellular death	- Visualization of the superficial destruction of spheroids.	[5, 7, 23]
Transmission electron microscopy (TEM)	Cellular organization	- Observation of specific characteristics of each spheroid layer.	[32, 93]
		- Observation of cell polarity.	[32]
		- Visualization of cell-cell physical interactions.	[94]
		- Observation of modifications to spheroid structures.	[5, 23, 95]
	Drugs penetration	- Determination of the penetration and dispersion capacity of the drugs and their presence in cellular compartments.	[36, 37]
	Cellular death	- Observation of the presence of cellular death markers.	[32, 94]
		- Observation of cell destruction and apoptosis in response to an anticancer treatment.	[32, 94]
	Cell cycle	- Identification of cells that are in mitosis.	[32]
	Invasion/metastization of cancer cells	- Visualization and determination of spheroid cell invasion/metastatic capacity.	[95]

Flow cytometry	Drug penetration/uptake	- Quantification of the percentage of cells in spheroids that internalized a drug.	[14, 42, 96]
	Cellular death	- Quantification of the percentage of live and dead cells.	[13, 17, 40-42]
		- Observation of mitochondrial status.	[13]
	Cell cycle	- Quantification of the percentage of proliferating and senescent cells.	[13]
		- Quantification of the percentage of cells in a specific stage of the cell cycle.	[12, 13]
		- Analysis of the influence of drugs on the cell cycle.	[12]
	Protein expression	- Quantification of the percentage of cells that express specific proteins.	[13, 23]
Western blot and qPCR	Cellular death	- Analysis of the expression of cellular death biomarkers.	[13]
	Protein expression	- Analysis of the expression of proteins.	[56, 59]
Ultraviolet/visible and fluorescence spectroscopy	Cellular death	- Determination of the metabolic viability of cells before and after drugs administration.	[3, 23, 66-69]
	Cellular organization	- Observation of the specific characteristics of each spheroids layer.	[72, 73]
Mathematical modelling	Size and growth	- Prediction of spheroid size, area or volume.	[75, 76, 97]
	Cellular organization	- Prediction of spheroid layer organization.	[98]
	Drug penetration	- Prediction of anticancer drug penetration.	[79-82]
		- Prediction of drug-loaded nanoparticle penetration.	[15, 83, 84]

4.5. References

1. Breslin, S. and O'Driscoll, L., *Three-dimensional cell culture: the missing link in drug discovery.* Drug Discovery Today, 2013. 18: 240-249.

2. Trédan, O., *et al.*, *Drug resistance and the solid tumor microenvironment.* Journal of the National Cancer Institute, 2007. 99: 1441-1454.

3. Kang, A., *et al.*, *Concave microwell array-mediated three-dimensional tumor model for screening anticancer drug-loaded nanoparticles.* Nanomedicine, 2015. 11: 1153-1161.

4. Desmaison, A., *et al.*, *Mechanical Stress Impairs Mitosis Progression in Multi-Cellular Tumor Spheroids.* PLOS ONE, 2013. 8: e80447.

5. Yao, H.-J., *et al.*, *The antitumor efficacy of functional paclitaxel nanomicelles in treating resistant breast cancers by oral delivery.* Biomaterials, 2011. 32: 3285-3302.

6. Evensen, N. A., *et al.*, *Development of a High-Throughput Three-Dimensional Invasion Assay for Anti-Cancer Drug Discovery.* PLOS ONE, 2013. 8: e82811.

7. Costa, E. C., *et al.*, *Optimization of liquid overlay technique to formulate heterogenic 3D co-cultures models.* Biotechnology and Bioengineering, 2014. 111: 1672-1685.

8. Amann, A., *et al.*, *Development of an Innovative 3D Cell Culture System to Study Tumour - Stroma Interactions in Non-Small Cell Lung Cancer Cells.* PLOS ONE, 2014. 9: e92511.

9. Härmä, V., *et al.*, *Quantification of Dynamic Morphological Drug Responses in 3D Organotypic Cell Cultures by Automated Image Analysis.* PLOS ONE, 2014. 9: e96426.

10. Chen, R., *et al.*, *Screening candidate metastasis-associated genes in three-dimensional HCC spheroids with different metastasis potential.* International Journal of Clinical and Experimental Pathology, 2014. 7: 2527-2535.

11. Lorenzo, C., *et al.*, *Live cell division dynamics monitoring in 3D large spheroid tumor models using light sheet microscopy.* Cell Division, 2011. 6: 22.

12. Laurent, J., *et al.*, *Multicellular tumor spheroid models to explore cell cycle checkpoints in 3D.* BMC Cancer, 2013. 13: 73.

13. Khaitan, D., *et al.*, *Establishment and characterization of multicellular spheroids from a human glioma cell line; Implications for tumor therapy.* Journal of Translational Medicine, 2006. 4: 12-12.

14. Carver, K., Ming, X., and Juliano, R. L., *Multicellular Tumor Spheroids as a Model for Assessing Delivery of Oligonucleotides in Three Dimensions.* Molecular Therapy - Nucleic Acids, 2014. 3: e153.

15. Goodman, T. T., *et al.*, *Spatio-temporal modeling of nanoparticle delivery to multicellular tumor spheroids.* Biotechnology and Bioengineering, 2008. 101: 388-399.

16. Cheng, G., *et al.*, *Micro-environmental mechanical stress controls tumor spheroid size and morphology by suppressing proliferation and inducing apoptosis in cancer cells.* PLOS ONE, 2009. 4: e4632.

17. Ma, H.-l., *et al.*, *Multicellular tumor spheroids as an in vivo-like tumor model for three-dimensional imaging of chemotherapeutic and nano material cellular penetration.* Molecular Imaging, 2012. 11: 487-498.

18. Huo, S., *et al.*, *Superior penetration and retention behavior of 50 nm gold nanoparticles in tumors.* Cancer Research, 2013. 73: 319-330.

19. Friedrich, J., *et al.*, *Spheroid-based drug screen: considerations and practical approach.* Nature Protocols, 2009. 4: 309-324.

20. Ivanov, D. P., *et al.*, *In vitro co-culture model of medulloblastoma and human neural stem cells for drug delivery assessment.* Journal of Biotechnology, 2015. 205: 3-13.

21. Mikhail, A. S., Eetezadi, S., and Allen, C., *Multicellular tumor spheroids for evaluation of cytotoxicity and tumor growth inhibitory effects of nanomedicines in vitro: a comparison of docetaxel-loaded block copolymer micelles and Taxotere®.* PLOS ONE, 2013. 8: e62630.

22. Gaspar, V. M., *et al.*, *Poly(2-ethyl-2-oxazoline)-PLA-g-PEI amphiphilic triblock micelles for co-delivery of minicircle DNA and chemotherapeutics.* Journal of Controlled Release, 2014. 189: 90-104.

23. Yeon, S.-E., *et al.*, *Application of Concave Microwells to Pancreatic Tumor Spheroids Enabling Anticancer Drug Evaluation in a Clinically Relevant Drug Resistance Model.* PLOS ONE, 2013. 8: e73345.

24. Langenbach, F., *et al.*, *Generation and differentiation of microtissues from multipotent precursor cells for use in tissue engineering.* Nature Protocols, 2011. 6: 1726-1735.

25. Vidi, P.-A., Bissell, M. J., and Lelièvre, S. A., *Three-dimensional culture of human breast epithelial cells: the how and the why*, *Epithelial Cell Culture Protocols*, S. H. Randell and L. M. Fulcher, Editors. 2013, Humana Press: Totowa, New Jersey. p. 193-219.

26. Bruns, T., *et al.*, *Preparation strategy and illumination of three-dimensional cell cultures in light sheet–based fluorescence microscopy.* Journal of Biomedical Optics, 2012. 17: 101518.

27. Pampaloni, F., Ansari, N., and Stelzer, E. H. K., *High-resolution deep imaging of live cellular spheroids with light-sheet-based fluorescence microscopy.* Cell and Tissue Research, 2013. 352: 161-177.

28. Cella Zanacchi, F., *et al.*, *Live-cell 3D super-resolution imaging in thick biological samples.* Nature Methods, 2011. 8: 1047-1049.

29. Swoger, J., Pampaloni, F., and Stelzer, E. H., *Imaging cellular spheroids with a single (selective) plane illumination microscope.* Cold Spring Harbor Protocols, 2014. 2014: 106-113.

30. Baek, S. K., *et al.*, *Photothermal treatment of glioma; an in vitro study of macrophage-mediated delivery of gold nanoshells.* Journal of Neuro-Oncology, 2011. 104: 439-448.

31. Hwang, Y.-J., *et al.*, *Multi-photon Imaging of Actin Filament Formation and Mitochondrial Energetics of Human ACBT Gliomas.* Photochem Photobiol, 2011. 87: 408-417.

32. Amaral, D. B. J., Urabayashi, S. M., and Machado-Santelli, M. G., *Cell death and lumen formation in spheroids of MCF-7 cells.* Cell Biology International, 2010. 34: 267-274.

33. Uroukov, I. S. and Patton, D., *Optimizing environmental scanning electron microscopy of spheroidal reaggregated neuronal cultures*. Microscopy Research and Technique, 2008. 71: 792-801.

34. Yoshida, D., *et al.*, *Novel approach to analysis of in vitro tumor angiogenesis with a variable-pressure scanning electron microscope: suppression by matrix metalloproteinase inhibitor SI-27*. Brain Tumor Pathology, 2001. 18: 89-100.

35. Dorst, N., *et al.*, *Analysis of cellular composition of co-culture spheroids*. Annals of Anatomy, 2014. 196: 303-311.

36. Goodman, T. T., Olive, P. L., and Pun, S. H., *Increased nanoparticle penetration in collagenase-treated multicellular spheroids*. International Journal of Nanomedicine, 2007. 2: 265-274.

37. Huang, K., *et al.*, *Size-dependent localization and penetration of ultrasmall gold nanoparticles in cancer cells, multicellular spheroids, and tumors in vivo*. ACS Nano, 2012. 6: 4483-4493.

38. Ivascu, A. and Kubbies, M., *Rapid generation of single-tumor spheroids for high-throughput cell function and toxicity analysis*. Journal of Biomolecular Screening, 2006. 11: 922-932.

39. Merten, O.-W., *Cell Detachment*, *Encyclopedia of Cell Technology*. 2003, John Wiley & Sons, Inc.

40. Frankel, A., *et al.*, *Lack of Multicellular Drug Resistance Observed in Human Ovarian and Prostate Carcinoma Treated with the Proteasome Inhibitor PS-341*. Clinical Cancer Research, 2000. 6: 3719-3728.

41. Trumpi, K., *et al.*, *Paired image- and FACS-based toxicity assays for high content screening of spheroid-type tumor cell cultures*. FEBS Open Bio, 2015. 5: 85-90.

42. Patra, B., *et al.*, *Drug testing and flow cytometry analysis on a large number of uniform sized tumor spheroids using a microfluidic device*. Scientific Reports, 2016. 6: 21061.

43. Beaumont, K. A., *et al.*, *Imaging- and Flow Cytometry-based Analysis of Cell Position and the Cell Cycle in 3D Melanoma Spheroids*. Journal of Visualized Experiments, 2015: e53486.

44. Durand, R. E., *Use of Hoechst 33342 for cell selection from multicell systems*. Journal of Histochemistry & Cytochemistry, 1982. 30: 117-122.

45. Muto, J., *et al.*, *RNA-binding protein Musashi1 modulates glioma cell growth through the post-transcriptional regulation of Notch and PI3 kinase/Akt signaling pathways*. PLOS ONE, 2012. 7: e33431.

46. Robertson, F. M., *et al.*, *Imaging and analysis of 3D tumor spheroids enriched for a cancer stem cell phenotype*. Journal of Biomolecular Screening, 2010. 15: 820-829.

47. Mahmood, T. and Yang, P.-C., *Western blot: technique, theory and trouble shooting*. North American Journal of Medicine and Science, 2012. 4: 429-434.

48. Mischiati, C., *et al.*, *Changes in protein expression in two cholangiocarcinoma cell lines undergoing formation of multicellular tumor spheroids in vitro*. PLOS ONE, 2015. 10: e0118906.

49. Fraga, D., Meulia, T., and Fenster, S., *Real-Time PCR*, *Current Protocols Essential Laboratory Techniques*, S. R. Gallagher and E. A. Wiley, Editors. 2008, John Wiley & Sons, Inc. p. 10.13.11–10.13.40.

50. Makhija, S., *et al.*, *Taxol-induced bcl-2 phosphorylation in ovarian cancer cell monolayer and spheroids.* International Journal of Oncology, 1999. 14: 515-521.

51. Pettee, K. M., *et al.*, *An mDia2/ROCK Signaling Axis Regulates Invasive Egress from Epithelial Ovarian Cancer Spheroids.* PLOS ONE, 2014. 9: e90371.

52. Lakka, S. S., *et al.*, *Inhibition of cathepsin B and MMP-9 gene expression in glioblastoma cell line via RNA interference reduces tumor cell invasion, tumor growth and angiogenesis.* Oncogene, 2004. 23: 4681-4689.

53. Härmä, V., *et al.*, *A Comprehensive Panel of Three-Dimensional Models for Studies of Prostate Cancer Growth, Invasion and Drug Responses.* PLOS ONE, 2010. 5: e10431.

54. Kenny, P. A., *et al.*, *The morphologies of breast cancer cell lines in three-dimensional assays correlate with their profiles of gene expression.* Molecular Oncology, 2007. 1: 84-96.

55. Kerjaschki, D., *et al.*, *Lipoxygenase mediates invasion of intrametastatic lymphatic vessels and propagates lymph node metastasis of human mammary carcinoma xenografts in mouse.* Journal of Clinical Investigation, 2011. 121: 2000-2012.

56. Meng, F., *et al.*, *Inhibition of DNA methyltransferases, histone deacetylases and lysine-specific demethylase-1 suppresses the tumorigenicity of the ovarian cancer ascites cell line SKOV3.* International Journal of Oncology, 2013. 43: 495-502.

57. Lin, R.-Z., *et al.*, *Dynamic analysis of hepatoma spheroid formation: roles of E-cadherin and β1-integrin.* Cell and Tissue Research, 2006. 324: 411-422.

58. Wartenberg, M., *et al.*, *Tumor-induced angiogenesis studied in confrontation cultures of multicellular tumor spheroids and embryoid bodies grown from pluripotent embryonic stem cells.* The FASEB Journal, 2001. 15: 995-1005.

59. de Sampaio, P. C., *et al.*, *A heterogeneous in vitro three dimensional model of tumour-stroma interactions regulating sprouting angiogenesis.* PLOS ONE, 2012. 7: e30753.

60. Larson, A. R., *et al.*, *Melanoma spheroid formation involves laminin-associated vasculogenic mimicry.* The American Journal of Pathology, 2014. 184: 71-78.

61. Rao, J. S., *et al.*, *Inhibition of invasion, angiogenesis, tumor growth, and metastasis by adenovirus-mediated transfer of antisense uPAR and MMP-9 in non-small cell lung cancer cells.* Molecular Cancer Therapeutics, 2005. 4: 1399-1408.

62. Tian, X., *et al.*, *Hypoxia-inducible factor-1α enhances the malignant phenotype of multicellular spheroid HeLa cells in vitro.* Oncology Letters, 2010. 1: 893-897.

63. Menrad, H., *et al.*, *Roles of hypoxia-inducible factor-1α (HIF-1α) versus HIF-2α in the survival of hepatocellular tumor spheroids.* Hepatology, 2010. 51: 2183-2192.

64. Naber, H. P., *et al.*, *BMP-7 inhibits TGF-β-induced invasion of breast cancer cells through inhibition of integrin β3 expression.* Cellular Oncology, 2012. 35: 19-28.

65. Doublier, S., *et al.*, *HIF-1 activation induces doxorubicin resistance in MCF7 3-D spheroids via P-glycoprotein expression: a potential model of the chemo-resistance of invasive micropapillary carcinoma of the breast.* BMC Cancer, 2012. 12: 4.

66. Walzl, A., *et al.*, *The Resazurin Reduction Assay Can Distinguish Cytotoxic from Cytostatic Compounds in Spheroid Screening Assays*. Journal of Biomolecular Screening, 2014. 19: 1047-1059.

67. Friedrich, J., *et al.*, *A reliable tool to determine cell viability in complex 3-d culture: the acid phosphatase assay*. Journal of Biomolecular Screening, 2007. 12: 925-937.

68. Ho, W. Y., *et al.*, *Development of multicellular tumor spheroid (MCTS) culture from breast cancer cell and a high throughput screening method using the MTT assay*. PLOS ONE, 2012. 7: e44640.

69. Zhang, X., *et al.*, *Induction of mitochondrial dysfunction as a strategy for targeting tumour cells in metabolically compromised microenvironments*. Nature Communications, 2014. 5: 3295.

70. Riss, T., *et al.*, *Cell viability assays*, *Assay Guidance Manual*. 2004, Eli Lilly & Company and the National Center for Advancing Translational Sciences.

71. Valley, M. P., *et al.*, *Abstract 3731: Luminescent cell health assays for tumor spheroid evaluation*. Cancer Research, 2014. 74: 3731.

72. An, R., *et al.*, *Phenotypic Profiling of Raf Inhibitors and Mitochondrial Toxicity in 3D Tissue Using Biodynamic Imaging*. Journal of Biomolecular Screening, 2014. 19: 526-537.

73. Zhang, J. Z., *et al.*, *The use of spectroscopic imaging and mapping techniques in the characterisation and study of DLD-1 cell spheroid tumour models*. Integrative Biology, 2012. 4: 1072-1080.

74. Mehta, G., *et al.*, *Opportunities and challenges for use of tumor spheroids as models to test drug delivery and efficacy*. Journal of Controlled Release, 2012. 164: 192-204.

75. Yoshida, D., *et al.*, *Modeling the development of metastases from primary and locally recurrent tumors: comparison with a clinical data base for prostatic cancer*. Cancer Research, 1993. 53: 2987-2993.

76. Laird, A. K., *Dynamics of tumour growth*. British Journal of Cancer, 1964. 13: 490-502.

77. Marušić, M., *et al.*, *Analysis of growth of multicellular tumour spheroids by mathematical models*. Cell Proliferation, 1994. 27: 73-94.

78. Piccinini, F., *et al.*, *Cancer multicellular spheroids: Volume assessment from a single 2D projection*. Computer Methods and Programs in Biomedicine, 2015. 118: 95-106.

79. Ward, J. P. and King, J. R., *Mathematical modelling of drug transport in tumour multicell spheroids and monolayer cultures*. Mathematical Biosciences, 2003. 181: 177-207.

80. Ward, J. and King, J., *Mathematical modelling of the effects of mitotic inhibitors on avascular tumour growth*. Computational and Mathematical Methods in Medicine, 1999. 1: 287-311.

81. Norris, E., King, J. R., and Byrne, H. M., *Modelling the response of spatially structured tumours to chemotherapy: Drug kinetics*. Mathematical and Computer Modelling, 2006. 43: 820-837.

82. Achilli, T. M., *et al.*, *Multilayer spheroids to quantify drug uptake and diffusion in 3D*. Molecular Pharmaceutics, 2014. 11: 2071-2081.

83. Chou, C.-Y., *et al.*, *Investigation of the Spatiotemporal Responses of Nanoparticles in Tumor Tissues with a Small-Scale Mathematical Model*. PLOS ONE, 2013. 8: e59135.

84. Gao, Y., *et al.*, *Predictive models of diffusive nanoparticle transport in 3-dimensional tumor cell spheroids*. The AAPS Journal, 2013. 15: 816-831.

85. Chan, H. F., *et al.*, *Rapid formation of multicellular spheroids in double-emulsion droplets with controllable microenvironment*. Scientific Reports, 2013. 3: 3462.

86. Mellor, H. R. and Callaghan, R., *Accumulation and distribution of doxorubicin in tumour spheroids: the influence of acidity and expression of P-glycoprotein*. Cancer Chemother Pharmacol, 2011. 68: 1179-1190.

87. Gaspar, V. M., *et al.*, *Folate-targeted multifunctional amino acid-chitosan nanoparticles for improved cancer therapy*. Pharmaceutical Research, 2015. 32: 562-577.

88. Tung, Y.-C., *et al.*, *High-throughput 3D spheroid culture and drug testing using a 384 hanging drop array*. Analyst, 2011. 136: 473-478.

89. McIntyre, A., *et al.*, *Carbonic anhydrase IX promotes tumor growth and necrosis in vivo and inhibition enhances anti-VEGF therapy*. Clinical Cancer Research, 2012. 18: 3100-3111.

90. Vorsmann, H., *et al.*, *Development of a human three-dimensional organotypic skin-melanoma spheroid model for in vitro drug testing*. Cell Death & Disease, 2013. 4: e719.

91. Wei, B., *et al.*, *Coaction of spheroid-derived stem-like cells and endothelial progenitor cells promotes development of colon cancer*. PLOS ONE, 2012. 7: e39069.

92. Souza, G. R., *et al.*, *Three-dimensional tissue culture based on magnetic cell levitation*. Nature Nanotechnology, 2010. 5: 291-296.

93. Folkman, J. and Hochberg, M., *Self-regulation of growth in three dimensions*. The Journal of Experimental Medicine, 1973. 138: 745-753.

94. Erguven, M., *et al.*, *Imatinib mesylate decreases the cytotoxic effect of roscovitine on human glioblastoma cells in vitro and the role of midkine*. Oncology Letters, 2012. 3: 200-208.

95. Kunz-Schughart, L. A., *et al.*, *Potential of fibroblasts to regulate the formation of three-dimensional vessel-like structures from endothelial cells in vitro*. American Journal of Physiology-Cell Physiology, 2006. 290: C1385-1398.

96. Durand, R. E., *Flow cytometry studies of intracellular adriamycin in multicell spheroids in vitro*. Cancer Research, 1981. 41: 3495-3498.

97. Ward, J. P. and King, J., *Mathematical modelling of avascular-tumour growth*. IMA Journal of Applied Mathematics, 1997. 14: 39-69.

98. Schaller, G. and Meyer-Hermann, M., *Multicellular tumor spheroid in an off-lattice Voronoi-Delaunay cell model*. Physical review. E, Statistical, nonlinear, and soft matter physics, 2005. 71: 051910.

Chapter 5

Introduction (part D)

Optical clearing methods: an overview of the techniques used for the imaging of 3D spheroids

This chapter is based on the publication entitled: Optical clearing methods: an overview of the techniques used for the imaging of 3D spheroids, Biotechnology and Bioengineering, 2019, 116: 2742– 2763.

5.1. Abstract

Spheroids have emerged as *in vitro* models that reproduce in a great extent the architectural microenvironment found in human tissues. However, the imaging of 3D cell cultures is highly challenging due to its high thickness, which results in a light scattering phenomenon that limits the light penetration. Therefore, several optical clearing methods, widely used in the imaging of animal tissues, have been recently explored to render spheroids with enhanced transparency. These methods are aimed to homogenize the microtissue refractive index (RI) and can be grouped into four different categories, namely i) simple immersion in an aqueous solution with high RI; ii) delipidation and dehydration followed by RI matching; iii) delipidation and hyperhydration followed by RI matching; and iv) hydrogel embedding followed by delipidation and RI matching. In this chapter, the main optical clearing methods, their mechanism of action, advantages and disadvantages are described. Furthermore, the practical examples of the optical clearing methods application for the imaging of 3D spheroids are highlighted.

Keywords: imaging; light scattering; optical clearing; optical microscopy; spheroids.

5.2. Introduction

In the early years of the 20th century, cell culture techniques (*i.e.* cell proliferation in environmentally controlled conditions) emerged as a powerful methodology to study and understand cells behavior within the human body [1]. Such approach allowed the characterization of the cellular differentiation, migration, proliferation, and mechanics, as well as their response to external *stimuli* (*e.g.* drugs, environment changes and mechanical stress) [1]. In this way, researchers could decipher the background of several *in vivo* processes, such as the tissue development and the pathophysiology of the diseases [1, 2]. Therefore, *in vitro* culture of cells is now broadly used in several fields, such as cancer research, tissue regeneration, gene therapy and drug screening, among others [3, 4].

In the literature, 2D cell cultures (*i.e.* the culture of cells as monolayers attached to a plastic or glass surface) are the most attractive for research purposes, due to its simplicity, reproducibility and low cost [4]. Nevertheless, different studies have been demonstrating that 2D cellular systems display biochemical profiles and bioactivities divergent from those observed *in vivo*, which is correlated with the lack of capacity of these cell culture models to reproduce the 3D cellular organization [4, 5]. For instance, Sandberg and Ernberg reported that ≈ 30% of the 7000 genes analyzed in different cell lines showed a statistically significant differential gene expression when compared to their original tissues [6]. Thus, 3D cell cultures, such as spheroids, have received great attention from the research community, as these *in vitro* models can represent more accurately the different properties of human tissues, such as liver [7], thyroid [8], cartilage [9], pancreatic tissue [10], cardiac muscle [11] or of solid tumors (*e.g.* breast, colon, pancreas, prostate, ovary, among others [12-19]). Spheroids are microtissues with a diameter within hundreds of micrometers to few millimeters that present a spatial architecture, cellular organization, cell-cell and cell-extracellular matrix interactions quite similar to those found in the human tissues (as reviewed in detail elsewhere [3, 20]).

On the other hand, the microscopy techniques (*e.g.* optical and fluorescence microscopy) arise as one of the easiest, low cost and safe methodologies for the analysis of *in vitro* samples [21]. Particularly, the fluorescence microscopy assumes great importance since it allows the observation of fluorescent markers that stain a specific area or molecule of interest within the cells [22]. Furthermore, the fluorescence microscopy also supports the acquisition of images with high-resolution of the subcellular structures when the cells are cultured as monolayers. However, the imaging of large 3D spheroids by fluorescence microscopy is challenging due to their thickness and to the light scattering phenomenon. The light scatter results from the mismatches between the cellular constituents refractive index (RI) that prompt the dispersion of the excitation light through the sample and thus limiting its penetration, or by decreasing the amount of emitted light that reaches the detector [23]. For this reason, it is difficult to obtain high-resolution images of intact spheroids, specially from its interior [24]. Therefore,

researchers often use thin slices of spheroids (5 – 7 μm) to obtain images at a submicron resolution by fluorescence microscopy [20, 22]. Notwithstanding, the spheroids sectioning is a laborious and time-consuming process that can permanently alter the spheroid initial structure (*e.g.* distort, disrupt, fold, compress or stretch) [23, 25]. Additionally, the post-acquisition 3D reconstruction of the slices performed using computer software may introduce artifacts in the images [23]. Another approach for the imaging of the deeper regions of intact spheroids is the utilization of optical sectioning microscopies, such as Confocal Laser Scanning Microscopy (CLSM), Multiphoton Microscopy (MPM; *e.g.* two-photon microscopy (2PM)) and Light-sheet Fluorescence Microscopy (LSFM; *e.g.* Single (or Selective) Plane Illumination Microscopy (SPIM)) (Table 5.1; reviewed in detail in [22, 26]).

Table 5.1. Comparison of the optical sectioning microscopy techniques that can be used for the imaging of 3D spheroids.

Technique	**Confocal laser scanning microscopy (CLSM)**	**Multi-photon Microscopy (MPM; *e.g.* Two-Photon Microscopy (2PM))**	**Light-sheet-based fluorescence microscopy (LSFM; *e.g.* Single (or Selective) Plane Illumination Microscopy (SPIM))**
Concept	• Optical sections are produced by scanning the sample point-by-point with a laser beam focused on the sample; • Uses a pinhole to exclude out-of-focus background fluorescence from detection.	• Uses localized nonlinear excitation to excite fluorescence only within a thin plane; • More than one photon is emitted by a pulsed infrared laser source at a time to excite a fluorophore.	• A sheet plane of light illuminates a plane within a sample; • The illumination is done perpendicularly to the direction of the imaging axis.
Optical sectioning	Yes	Yes	Yes
Light scatter influence	+++	+	+++
Penetration depth	≈ 100 μm	up to 1 mm	> 1 cm
Resolution	< micron	< micron	micron
Photodamage	+++	++	+
Handling	+	+	+++
Time	+++	++	+
Equipment cost	++	+++	+
REFs	[20, 21, 27-29]	[20, 21, 27-30]	[20, 21, 26-29, 31, 32]

+: low; ++: moderate; +++: high.

These microscopic techniques are capable of acquiring images of a thin single plane of the sample (so-called "*stack*") with minimal interference of the remaining parts of the sample. Then, the 3D reconstruction of different stacks allows the observation of a great part or even the totality of the sample [23]. In particular, LSFM is the fluorescence-based microscopy technique with the highest penetration depth (> 1 cm) and therefore has been broadly used for the imaging of intact spheroids [20, 21, 26-29, 31-35].

Alternatively, to perform the imaging of intact spheroids researchers can employ optical clearing methods before samples be analyzed by microscopy. These methods aim to reduce the light scattering phenomenon in the biological samples, rendering samples with an increased transparency that promotes a deeper imaging, as well as the cells structural and functional analysis (discussed hereafter).

5.3. Light scattering and tactics of optical clearing

Fluorescence imaging of biological samples is quite challenging due to the limited light penetration, which is influenced by the optical properties of the acellular and cellular sample's constituents. In this way, the light absorption by molecules, such as hemoglobin, myoglobin, and melanin, present in some tissues will reduce the light intensity that reaches both the deeper regions of the tissue (excitation light) and the detector (emitted light) [23]. Therefore, the samples bleaching allows to minimize or even prevent the light absorption by the endogenous pigments. In fact, different methodologies can be explored to reduce the light absorption by heme (major light absorber and the most abundant chromophore in the body): i) sample can be treated with hydrogen peroxide that oxidizes the pigment [36]; ii) samples washing with highly acidic or basic solutions that lead to the heme dissociation from hemoglobin [37]; and iii) sample incubation with aminoalcohols (*e.g.* N,N,N,N-tetrakis(2-hydroxypropyl) ethylenediamine) that elute the heme chromophore from hemoglobin [37].

On the other hand, the limited light penetration in tissues and spheroids can also be attributed to the non-homogeneous RI (*i.e.* how light propagates through a given substance compared to vacuum conditions) through the sample and consequent light refraction [23] - Table 5.2.

Table 5.2. Refractive index (RI) of several cellular components.

Cellular component	Refractive Index (RI)	REF(s)
Cell membrane	1.46	[38]
Cytoplasm	1.36 - 1.39	[39-41]
DNA	1.44	[38]
Lipids	1.39 - 1.48	[31, 38, 40]
Lysosome	1.6	[42]
Mitochondria	1.36 - 1.42	[40, 43]
Nucleus	1.36 - 1.39	[39, 41]
Proteins	1.38 - 1.43	[21, 38]
Water	1.33	[38]
Organelles	1.33 - 1.35	[31]

For instance, the cells' lipids and proteins present high RI values (≈ 1.44 and ≈ 1.43, respectively), while cells' cytoplasm presents the lower RI (≈ 1.35) [31, 37, 44]. These RI mismatches induce changes on the speed and angle of the light (visible and near-infrared (NIR) region) propagation, *i.e.* light refraction from molecules, membranes, organelles and cells [23] - Table 5.2. This phenomenon promotes the light scattering and it is the main cause of tissues opacity. The light dispersion through the sample difficult its penetration into deeper regions and decreases its intensity [45] - Figure 5.1.

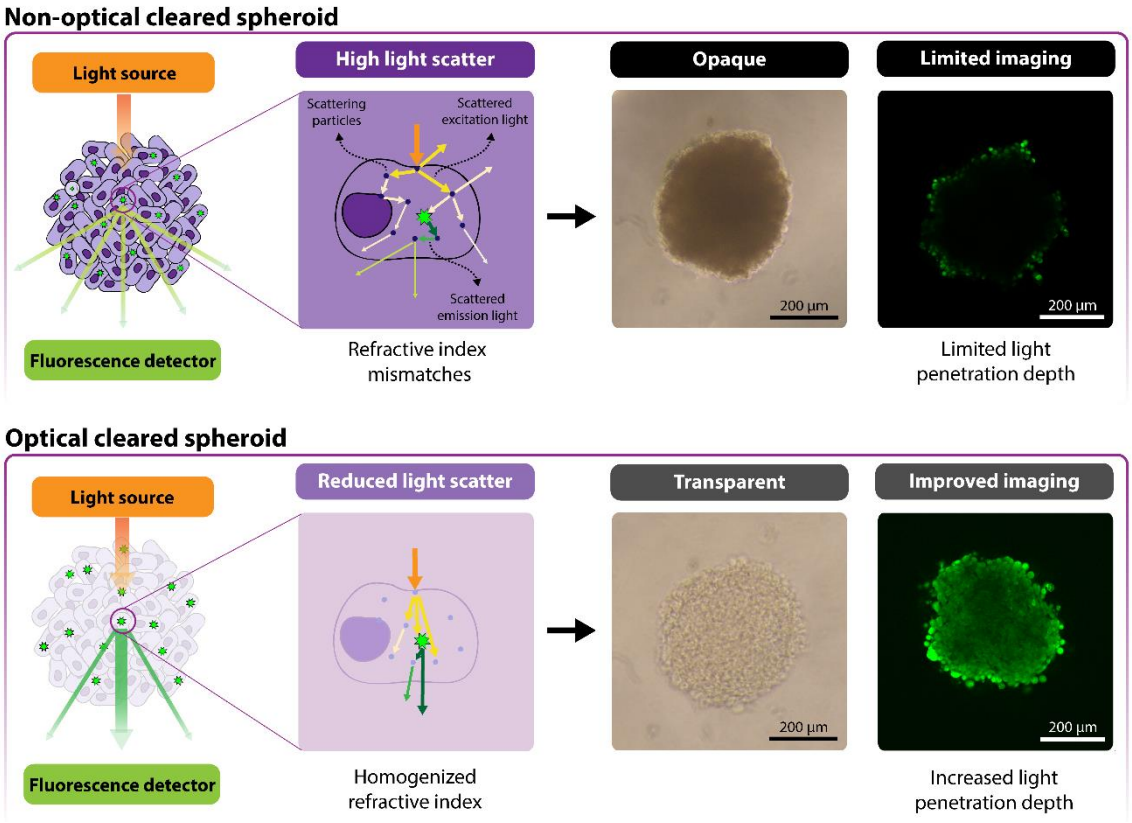

Figure 5.1. Representation of the light propagation in a non-cleared and cleared spheroid. A non-cleared spheroid has several mismatches in the refractive indexes (RI) of its constituents inducing the light scattering and consequently light dispersion through the spheroids, which results in opaque samples that do not allow deep imaging. A cleared spheroid has a transparent appearance due to the homogenization of the RI of its cellular constituents and consequently, light penetrates deeper in the spheroid making possible the imaging of the inner regions.

In this way, the light penetration is usually limited to a range of 100 - 150 µm, which is insufficient for the imaging of the spheroids whole volume [23, 46]. On the other hand, the fluorescence light resulting from the excited fluorophore can also be scattered and therefore it may not reach the detector with high intensity or indicate inaccurately its origin, which results in images with poor resolution and contrast [45]. Hence, several optical clearing approaches have been investigated in order to homogenize the RI across the sample and consequently reduce the light scattering phenomenon. This process renders 3D large biological

samples with higher transparency and therefore improves the light penetration, imaging depth and contrast, *i.e.* the majority of the light will attain the focus point and then the majority of the fluorescence light will be detected without suffering deviations in its path (Figure 5.1).

5.4. Classification of the optical clearing methods

Optical clearing methods are used to modify the optical properties of biological samples by removing, replacing and modifying some of its components, in order to match the overall RI. These methods can be divided into four major groups according to their basic procedures, as previously reported [44]: i) Simple immersion in an aqueous solution with high RI; ii) Delipidation and dehydration followed by RI matching; iii) Delipidation and hyperhydration followed by RI matching; and iv) Hydrogel embedding followed by delipidation and RI matching (Figure 5.2).

The clearing methods were originally developed for processing large samples obtained from animals (*e.g.* bone, brain, embryo, heart, intestine, kidney, lung, muscle, pancreas, spinal cord, spleen, testis, among others), as already reviewed in detail in [21, 23, 31, 37, 44, 47-52]. Herein, the basic concepts and mechanisms of the different clearing methods are presented, highlighting their application in the handling of spheroids samples. For sake of brevity, only the 3DISCO and its derivatives, BABB, CLARITY and its derivatives, *Clear*^{T}, *Clear*^{T2}, CUBIC, FocusClear™, Sca*l*e, SeeDB, Spalteholz's technique, and TDE (2,2′-thiodiethanol) will be described.

5.4.1. Simple immersion in an aqueous solution with high RI

This group includes the SeeDB, TDE, *Clear*^{T}, *Clear*^{T2} and FocusClear™ clearing methods. In these methods, biological samples are gradually cleared by immersing them in aqueous solutions that have a high RI (1.4 – 1.5) [44, 53] - Figure 5.2. Due to the osmotic pressure, the water content in the sample (that has low RI ≈ 1.33) will be passively replaced by the clearing solution. Therefore, the average RI of the sample will be homogenized to 1.4 -1.5 since the clearing solution RI value match that exhibited by proteins (RI ≈ 1.43) and lipids (RI ≈ 1.44) [31].

These immersion techniques are simple, easy to perform, and low-cost [21]. Additionally, the absence of detergents preserve the lipidic content of each sample, thus allowing the imaging of these structure using lipophilic tracer dyes (*e.g.* DiI and FM 1-43FX) [51]. Nevertheless, the preservation of the lipid content (which are one of the main factors responsible for light-scattering in biological tissues) restricts the sample transparency [52].

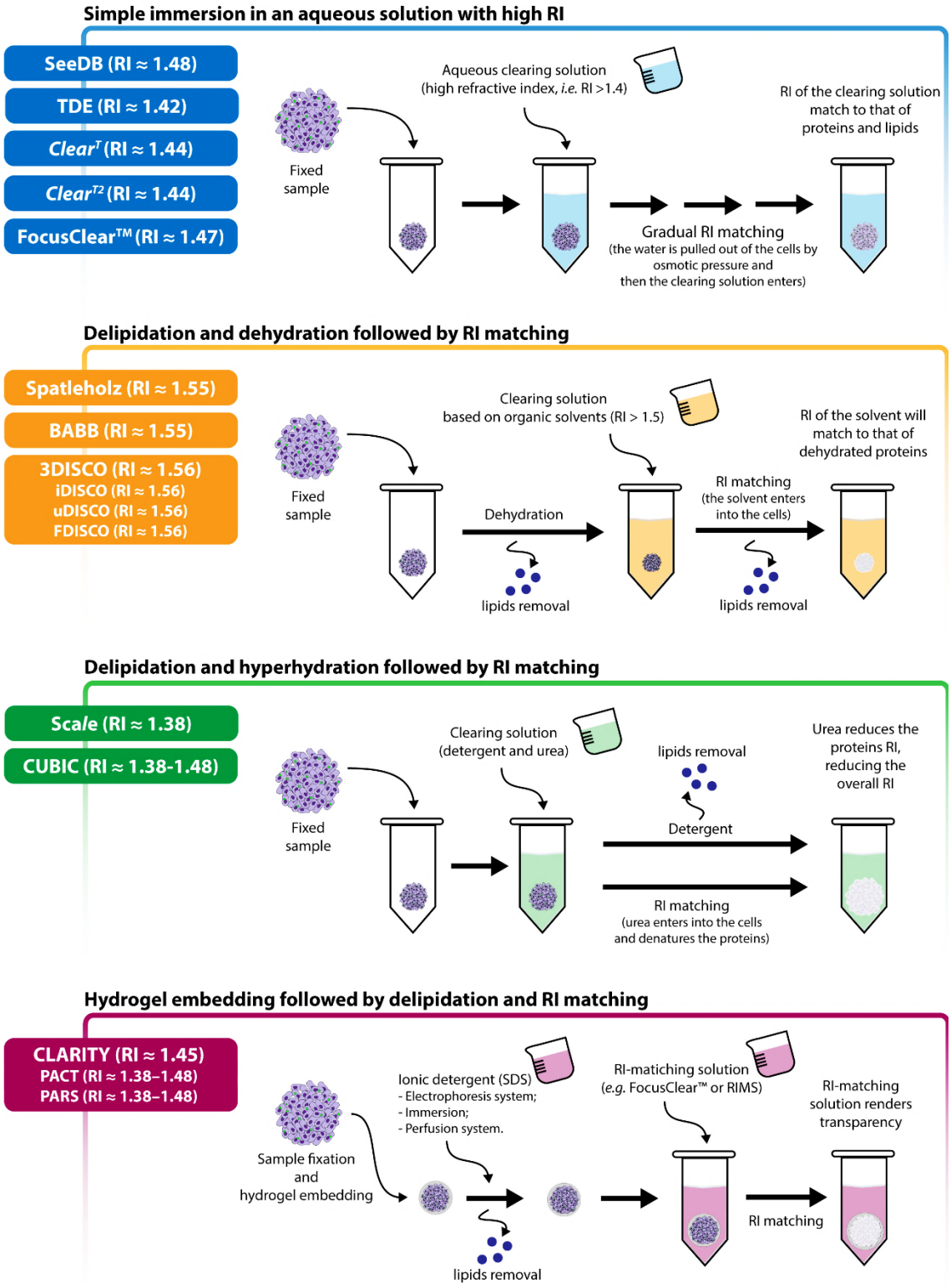

Figure 5.2. Overview of the four major groups of optical clearing methods: i) simple immersion in an aqueous solution with high refractive index (RI); ii) delipidation and dehydration followed by RI matching; and delipidation; iii) hyperhydration followed by RI matching; and iv) hydrogel embedding followed by delipidation and RI matching. The final sample RI generally obtained with each of the clearing methods is also displayed.

Furthermore, the incorporation of the aqueous clearing solution in the sample may induce an increase in the sample volume and consequently change its initial structure [23]. Such also impacts on the imaging of the whole spheroid due to the increased image acquisition time and postprocessing issues [49]. Lastly, since these methods rely on the passive diffusion of the solutions into the sample, the clearing process may need extensive incubation times depending on the sample size [44, 49].

5.4.1.1. SeeDB (See Deep Brain)

The RI of the biological samples' constituents can be homogenized by immersing them in sugar-based aqueous solutions that have a high RI. In this way, Ke *et al*. used fructose to develop the SeeDB method that was applied for the clearing of large mouse samples, like whole embryos and neonatal brains [54]. In SeeDB method, samples are successively immersed in 20, 40 and 60% (w/v) fructose aqueous solutions during 4 - 8 h, followed by their incubation in 80% fructose during 12 h and lastly in the SeeDB solution (RI ≈ 1.49 at 25 ºC; 115% (w/v) fructose and 0.5% (v/v) α-thioglycerol) during 24 h [54, 55]. The α-thioglycerol is used to avoid the Maillard browning discoloration derived from the reactive ketone group of fructose, which can lead to autofluorescence [56]. Grist *et al*. applied SeeDB to clear MCF-7 breast cancer spheroids with 370 ± 90 µm of diameter that were transfected with Fluorescent Ubiquitination-based Cell Cycle Indicator (Fucci) for imaging by using 2PM [46]. The clearing process was performed with the assistance of a microfluidic system, where spheroids were trapped. Then, clearing solutions (20, 40, 60, 80, 100 and 115% (w/v) fructose solutions with 0.5% (v/v) α-thioglycerol) were perfused through the microchannels using a syringe pump at a rate of approximately 20 µL/min. The results demonstrated that the method induces minimal reduction of the spheroids size, *i.e*. the ratio of spheroids area before and after the clearing was 1.02 [46]. This reduction is dependent on the flow rate used in the microfluidic channel, *i.e*. higher flow rates lead to higher shrinkage, which may be related to the fluidic compressive forces or to the osmotic pressure. The transparency was slightly improved since the light transmittance increased to about 5.5% in the cleared spheroids [46]. An analysis of the average Fucci fluorescence intensity as a function of penetration depth into the sample demonstrated that the SeeDB method allowed to image the spheroids at depths greater than 250 µm, while the imaging of non-cleared spheroid was limited to about 150 µm [46]. Nevertheless, the authors also observed that SeeDB solution increased the green fluorescence intensity of the spheroids [46], which was attributed to the formation of Maillard reaction products [57].

Boutin and Hoffman-Kim also applied the SeeDB method to clear rat adult neural stem cells (NSC) spheroids (mean diameter of 104.64 ± 22.01 µm) [58]. Authors embedded the spheroids in 20, 40 and 60% (w/v) fructose solutions (8 h each). Then, spheroids were immersed in 80% (w/v) and in 100% (w/v) fructose solutions (12 h each) and lastly during 24 h in 115% (w/v) fructose, with all solutions containing 0.5% (v/v) α-thioglycerol. The spheroids after the clearing process presented a moderate transparency in comparison to the non-cleared spheroids

(maintained in phosphate buffered saline (PBS)) [58]. Interestingly, despite being described that the SeeDB does not significantly influence the samples size [46, 54], these authors observed that the spheroids shrink (104.64 ± 22.01 *vs.* 76.2 ± 13.77 μm in diameter) occurred as a consequence of the clearing process [58]. Authors also observed that DAPI-labeled nuclei were difficult to distinguish. Furthermore, during execution of the experimental protocol, the use of highly viscous solutions made the spheroids manipulation difficult, which resulted in the loss of many samples during the assay [58]. Moreover, the viscosity of highly concentrated solutions of fructose also made challenging the acquisition of in-focus images containing both the spheroid and the background [58].

Alternatively, poor viscous clearing aqueous solutions with high RI can be obtained by using TDE, formamide (used in *Clear^{T}* and *Clear^{T2}* methods) or diatrizoic acid (used in FocusClear™ method), as discussed hereafter.

5.4.1.2. TDE

TDE is a non-toxic, cheap and water-soluble liquid displaying a low viscosity that has been widely used as a mounting media, since it has a RI (for 100% TDE the RI is 1.52) similar to that of typical immersion oils used in fluorescence microscopy [59, 60]. Moreover, TDE has also been used as a clearing agent, since it allows the control of the RI value by diluting it with water , *i.e.* 30, 60 and 97% (v/v) TDE:water solutions have RI ≈ 1.39, 1.45 and 1.52, respectively [61, 62]. Aoyagi *et al.* applied TDE solutions (30, 60 and 97% (v/v) in PBS) to clear mice brains and brain slices after their incubation for 6 h to 7 days, for improving the light penetration depth in both CLSM and 2PM [61]. TDE has also been applied for the clearing of spheroids. Paiè *et al.* applied TDE to clear H2B-mCherry (histone H2B fluorescent nuclear reporter protein) expressing spheroids with an average diameter of 300 μm [33]. For that purpose, authors dipped spheroids in different TDE solutions (25, 50 and 68% (v/v) in PBS) for 10 min each. Then, the high-throughput imaging of the spheroids was performed in an optofluidic lab-on-a-chip that integrates SPIM illumination and continuous sample delivery in a microfluidic channel. Briefly, after the clearing, the spheroids circulated at a constant speed (20 μm/s) in a microchannel containing a 0.1% (v/v) TDE solution and their imaging was performed quickly (50 ms acquisition time) while passing through the light sheet. Combining the use of TDE with SPIM, it was possible to acquire images of the entire spheroid with a subcellular resolution that allowed the clear identification of the cells' nuclei, the cell counting and the observation of the cell mitosis [33]. Furthermore, it was possible to perform the 3D rendering of the acquired images and consequently obtain a 360º detailed view of the spheroids [33].

5.4.1.3. *Clear^{T} and Clear^{T2}*

Formamide is a water-miscible polar solvent that was used for the first time by Kuwajima *et al.* in a method, termed *Clear^{T}*, for clearing mice tissues (whole brains, brain sections and embryos) [63]. In this method, samples are dipped in gradient solutions of formamide in water

(20 up to 95% (v/v) formamide) in order to homogenize the RI of the tissue to about 1.44 [23]. The sample incubation time in each solution varies according to the sample size, for example the clearing of whole brains took more than 2 days, while 20-1000 µm brain sections took less than 1 h.

The *Clear*^{T2} method is an adaptation of the *Clear*^{T} with the objective of avoiding the formamide-mediated quenching of the fluorescent protein dyes. In this way, the *Clear*^{T2} method described by Kuwajima *et al.* aimed to preserve the samples fluorescence by promoting the protein stabilization using polyethylene glycol (PEG) 8000 Da in combination with formamide [63, 64]. In brief, the clearing of the biological samples (mice whole brains, brain sections and embryos) was achieved through their immersion in graded series of formamide/PEG solutions (once in 25/10% (v/w) and then twice in 50/20% (v/w)) [63]. Similarly, the time of incubation in each solution depends on the sample size (clearing of the whole mouse brains takes ≈ 18 h, while 20 - 1000 µm sections require less than 2 h).

The *Clear*^{T2} method has been widely described for spheroids clearing [58, 65, 66]. Boutin and Hoffman-Kim used *Clear*^{T2} to process C6 glioma, primary cortical neuron and NSC spheroids by embedding them during 10 min in 25/10% (v/w) formamide/PEG 8000, followed by 5 min in 50/20% (v/w) formamide/PEG 8000 and lastly 60 min in 50/20% (v/w) formamide/PEG 8000 [58]. The authors observed that no significant changes occurred in the volume of the NSC spheroids, after their clearing through *Clear*^{T2}, *i.e.* the diameter of cleared spheroids was 99.77 ± 22.3 µm and 104.64 ± 22.01 µm for the non-cleared ones. Furthermore, the fluorescence signals of tracers (nucleus (DAPI)) and antibody immunostaining (Cadherin (Cy3), laminin (Dylight®488), nestin (Cy3), β-III tubulin (Cy3), S100 (Cy3)) were detectable by CLSM at all depths within spheroids as well as the fine features within the center of the spheroids [58]. The authors also described that prolonging the spheroid incubation time did not improve the clearing efficacy. Recently, the same research group also showed the applicability of the *Clear*^{T2} method for the imaging of immunostained spheroids composed of primary-derived postnatal rodent cortex cells by CLSM and MPM, in order to study *in vitro* the formation of endothelial cell capillary-like structures [65].

In another study, *Clear*^{T2} was used in conjunction with immunostaining and biochemical staining for the imaging of spheroids of PLHC-1, LNCaP and BEAS-2B cells by CLSM [66]. *Clear*^{T2} allowed the sharp visualization of the nuclear structure (Hoechst 33342) even in the center of the microtissue at depths superior to 75 µm along the z-axis, contrasting with the maximum depth of 30 µm in the non-cleared spheroids [66]. The method also allowed an improved imaging of the spheroids' E-cadherin cell-cell interactions (Alexa Fluor™ 647), as well as the reactive oxygen species (ROS) by using the CellROX® green assay [66].

5.4.1.4. FocusClear™

FocusClear™ is a non-toxic, ready to use clearing solution that was originally developed for the processing of fruit fly brains and now is commercialized by CelExplorer Labs (U.S. Pat. No. 6472216B1 and China Taiwan Patent No. 206390). FocusClear™ solution comprises a mixture of diatrizoic acid, the clearing agent, with dimethyl sulfoxide (DMSO), ethylenediaminetetraacetic acid, glucamine, ß-nicotinamide adenine dinucleotide phosphate, sodium diatrizoate and a derivative of polyoxyalkalene [21]. In the literature, it was already demonstrated that FocusClear™ can enhance the transparency of several types of biological tissues (*e.g.* mouse intestine [67] and mouse brain tissues [68]), as well as in spheroid samples [69]. Chen *et al.* reported the clearing of crypt spheroids composed of intestinal stem cells isolated from mice, with approximately 300 µm of thickness, by performing their immersion during 2 h in the FocusClear™ solution [69]. Optical light microscopic observation revealed that it was possible to observe that spheroids maintained in PBS were opaque and dark in their central regions, while the cleared spheroids were almost transparent [69]. In addition, the clearing process also allowed the visualization of the PI fluorescence signal across the spheroid by CLSM as well as the clear identification of the crypt spheroid shape and the protruded villi-crypt domains [69].

5.4.2. Delipidation and dehydration followed by RI matching

In order to expedite the clearing process, researchers developed methods based on the lipids removal through the use organic solvents, *i.e.* delipidation and dehydration, followed by RI matching methods (Spalteholz's technique, BABB, 3DISCO and its derivatives). These approaches usually require two major steps: i) initial dehydration of the sample; and ii) immersion of the samples in organic solvents (Figure 5.2). The initial dehydration step is usually performed using ethanol or methanol, since the solvents used in the following steps are not miscible with water [44]. During the dehydration step can also occur the removal of some lipids. After the water removal, the overall RI of the sample will increase since dehydrated proteins have a RI value > 1.5, which is higher than that of water and lipids (1.33 and 1.44, respectively) [23]. Therefore, in the second step, samples are immersed in an organic solvent with higher RI (> 1.5) to match the value of the dehydrated sample. Ideally, the organic solvents should also promote the removal of the remaining lipids since this will ensure a better homogeneous RI matching [23].
Although these methods result in improved transparencies in large samples in shorter periods of time, these approaches are well known for disrupting the fluorescence of some probes (*e.g.* GFP), due to the use of fixatives like ethanol, methanol and acetone as well as organic solvents that cause structural changes in the proteins [49]. Moreover, the samples dehydration can lead to their shrinkage, which can affect the fluorescence of some proteins. Fluorescent protein chromophores need water molecules to sustain their fluorescence emission [23]. This sample shrinkage occurs due to the loss of the 3D hydrogen-bonding networks between the water (70 – 80% of the samples) and the remaining intracellular constituents, an interaction that the

dehydrating agents cannot fully replicate [50]. Lastly, the organic solvents are toxic and can destroy the glues, as well as the equipment used in samples imaging.

5.4.2.1. Spalteholz's technique

The first optical clearing method based on organic solvents was described about a century ago by Spalteholz and it was developed to allow the histological analysis of large biological samples (*e.g.* entire organs and organ systems) [70]. This method included an initial sample fixation with formalin, followed by its bleaching with hydrogen peroxide (used to perform hemoglobin discoloration which is responsible for the biological tissues visible light absorption). Then samples were dehydrated, using series of alcohol concentrations, and immersed in a mixture of methyl salicylate and benzyl benzoate. Nevertheless, this method leads to samples shrinkage, browning, and also to the damage of the biological samples outer layers (2 – 3 cm), due to the formation of bubbles and cell death prompted by hydrogen peroxide [71-73]. Additionally, the Spalteholz method can also affect the fluorescence emission by protein dyes (*e.g.* GFP loses its fluorescence upon exposure to oxyradicals that are produced by the hydrogen peroxide) [71]. Therefore, this method has not been used for the clearing of 3D cell cultures but is the basis of other clearing methods aimed for the spheroids processing (described hereafter).

5.4.2.2. BABB

Inspired by the Spalteholz method, Dent *et al.* [74] and Dodt *et al.* [75] reported the application of benzyl alcohol/benzyl benzoate (BABB)-based optical clearing protocol (also known as Murray's clear). The BABB method was initially used to clear mice embryos and whole brains for allowing their imaging by ultramicroscopy. The method includes an initial dehydration step based on the samples' incubation for 1 day in each ethanol solution (*i.e.* 30, 50, 70, 80, 96 and twice in 100% (v/v) ethanol) with an additional 1 h in 100% (v/v) hexane to achieve the maximum dehydration. Then, the samples are incubated with the clearing solution of benzylalcohol/benzyl benzoate (1:2 (v/v)) during 2 days.

Wenzel *et al.* adapted the BABB method to clear spheroids of T47D, DLD1, DU145 and primary colon cancer cells with a mean diameter of ≈ 400 µm [76]. For that purpose, spheroids were initially dehydrated in ascending ethanol concentrations (50, 70, 85 and 99% (v/v); 5 min each) and then transferred to a benzyl alcohol/benzyl benzoate (1:1 (v/v)) solution. The authors demonstrated that the spheroids clearing allowed the visualization of the hypoxic (anti-pimonidazole antibody conjugated with FITC, a marker for hypoxia) and the dead cells (SYTOX™ Green stain for dead cells) in the inner regions of the spheroid, as well as the proliferative cells (Click-iT™ EdU Alexa Fluor™ 555) in their periphery using a custom build monolithic digital LSFM (mDSLM) [76]. Furthermore, the authors could evaluate the presence of dead cells in the spheroids core region after the administration of different compounds that target dormant cells (*e.g.* Antimycin, Cisplatin, Metformin, Paclitaxel, Rotenone and Staurosporine). These results

allowed the authors to confirm that the spheroids mimic the *in vivo* tumor microenvironment and additionally that this technique can be used in the high-throughput and high-content microscopy analysis for identifying substances that specifically target dormant cells in spheroids core regions [76].

Desmaison *et al*. also applied the BABB clearing and LSFM microscopy for the structural analysis of large HCT116 spheroids (average diameter of 650 µm) [34]. The clearing was performed through the sequential incubation of spheroids in 25, 50, 75 and 95% (v/v) ethanol solutions and lastly in BABB solution (benzyl alcohol:benzyl benzoate, 1:2 (v/v)). After the clearing, the authors demonstrated that the imaging of the PI stained cell nuclei in the deep interior regions of the spheroids could be performed with improved resolution and detail. The obtained results revealed that the shape of the cell nuclei and the cell division is influenced by the spheroid growth conditions, *i.e*. free growth over a non-adhesive surface *vs*. physically confined growth conditions (spheroids embedded in agarose) [34]. Similarly, Schmitz *et al*. applied the BABB clearing method and mDSLM to image DRAQ5 stained T47D spheroids (displaying diameters ranging from 150 µm to more than 500 µm) [77]. After the clearing procedure, the authors could perform the study of several parameters in spheroids, such as spheroids volume, number of cells and cell nucleus volume by using the automated nuclei segmentation and image computational analysis.

Smyrek and Stelzer applied the BABB method to clear U343 spheroids (average diameter of 600 µm) with the aim to optimize an immunofluorescence staining protocol for 3D cell biology [60]. The spheroids GM130 (cis-Golgi matrix protein), α-tubulin, and ß-catenin proteins were immunolabeled and the cell nucleus was stained with DAPI. For the clearing, spheroids were dehydrated with increasing concentrations of ethanol (30, 50, 70, 90, 96 and twice in 100% (v/v), 2 min each) and then transferred to the BABB solution (benzyl alcohol:benzyl benzoate, 1:2 (v/v)) until the transparency was attained [60]. After, the authors quantitatively analyzed the specificity and homogeneity of the stain, as well as the Alexa Fluor™ 568, Alexa Fluor™ 488, and DAPI signal intensity. Overall, the results demonstrated that the best protocol for the spheroids immunofluorescence labeling included: i) fixation of the spheroids during 15 min with 4% paraformaldehyde at room temperature (RT); ii) detergent-based permeabilization by Triton X-100, during 15 min, at RT; iii) blockage of unspecific binding sites with a solution of 0.1% bovine serum albumin, 0.2% Triton X-100, 0.05% Tween-20 and 10% goat serum for 1 hour at RT; iv) incubation of the first antibody at 37ºC during 18-24 h; v) incubation of the second antibody at 37ºC during 4 h; vi) dehydration and clearing by BABB during 15 min; and vii) imaging by mDSLM [60].

Although the utilization of the BABB clearing method can result in samples with high tissue transparency, the use of ethanol/methanol during the dehydration step still results in a reduction of the spheroids size, which can impact the analysis of the data extracted from these samples [60].

5.4.2.3. 3DISCO (3D imaging of solvent-cleared organs)

Since the ethanol dehydration step used in the BABB method results in the quenching of the proteins fluorescence [31, 78], Becker *et al*. investigated alternative chemicals (RI between 1.5 and 1.7) that could be used for samples dehydration [78]. The results obtained demonstrated that the utilization of tetrahydrofuran (THF) in brain hemispheres has a similar dehydration effect to that of ethanol, with the advantage of the background fluorescence intensity be considerable reduced and the intensity of the fluorescence signal be enhanced [78]. This solvent adaptation was termed the 3DISCO clearing method. In this procedure, the samples were initially dehydrated by using grading THF solutions (50, 70, 80% (v/v)) followed by their incubation in THF 100% (v/v), 1 to 3 times, dichloromethane, and then in dibenzylether [79]. The incubation time of the samples depends on its size, *i.e*. few hours for small organs (few millimeters in size) such as spinal cords, mammary glands or lymph nodes and a day for large organs such as the brain.

3DISCO protocol variations have been also developed, such as iDISCO (immunolabeling-enabled 3D imaging of solvent-cleared organs), uDISCO (ultimate 3D imaging of solvent-cleared organs), and FDISCO (DISCO with superior fluorescence preserving capability), that were described by Renier *et al*. [80], Pan *et al*. [81] and Qi *et al*. [82], respectively. In the iDISCO, samples are pre-treated with methanol, Triton X-100, and dimethyl sulfoxide (DMSO) to facilitate the antibody penetration and consequently improve the whole-organ immunolabeling [80]. On the other hand, the uDISCO was developed to significantly reduce the size of the samples (up to 65% of its original size) by using tert-butanol as a dehydration reagent, which can make possible the observation of large samples, with sizes up to the whole mouse body [81]. The FDISCO method allows to overcome the quenching of the fluorescent proteins that happens in the 3DISCO method by controlling the pH and temperature conditions during the clearing procedure [82].

Despite the 3DISCO and its modified methods being widely used for the clearing of several animal samples, its application in spheroids processing is yet to be described.

5.4.3. Delipidation and hyperhydration followed by RI matching

The delipidation and hyperhydration followed by RI matching methods (Sca*l*e and CUBIC) use solutions of urea (denaturing agent) and Triton X-100 (non-ionic detergents) for promoting the clearing of the samples (Figure 5.2). During this process, the detergents will remove the lipids that have high RI (≈ 1.44) and therefore reduce the sample overall RI. Furthermore, the urea will penetrate the cells denaturing the folded proteins (RI ≈ 1.43), which also reduces the sample RI [23]. Moreover, the urea also creates an osmotic gradient that will favor the water diffusion into the sample (hydration) and therefore homogenizes the overall RI value to ≈ 1.38 [23].

These methods are easy to perform and have a high clearing capacity, due to the removal of lipids from the sample, without leading to fluorescence quenching and toxicity problems associated with the solvent-based clearing methods [44]. Furthermore, this approach is also compatible with immunoblotting techniques (*e.g.* immunofluorescent labeling with antibodies) since the cellular membrane is permeable to the antibodies after its treatment with the detergent [83]. On the other hand, the samples can undergo hydration-induced expansion, which is undesirable during the analysis of the spheroids [44].

5.4.3.1. Sca*l*e

Hama *et al*. developed the Sca*l*e clearing method for the imaging of brain samples obtained from mice and patients [84]. These researchers initially observed that the use of 8 M urea solutions can improve the tissue transparency, but also results in a great tissue expansion. In this way, these authors tested different Sca*l*e solutions composed of urea, as well as Triton X-100 and glycerol with the objective to reduce the samples expansion and improve the tissue transparency. The Triton X-100 detergent was used to promote the lipids removal from the sample and therefore improve the sample transparency. Glycerol was added to counterbalance the urea-induced tissue expansion, assist the dehydration, and to target the lipophilic tissue regions. Among the different solutions investigated, the better clearing results were obtained when Sca*l*eA2 (4 M urea, 10% (w/v) glycerol and 0.1% (w/v) Triton X-100; RI ≈ 1.378) solution were used. However, the clearing took several weeks (*e.g.* more than 2 weeks for mouse embryos) and the samples became highly fragile, difficult to handle, and tissue swelling was still observed. Having this in mind, in a subsequent work this research group developed the Sca*l*eS clearing method, where solutions composed of urea (4 M), Triton X-100 (≤ 0.2% (v/v)) and sorbitol (20, 27, 36.4, and 40% (w/v)) were used [85]. The sorbitol replaced the glycerol due to its clearing properties and superior potential to reduce the sample volume expansion caused by urea.

Sca*l*e clearing solutions have also been employed for processing spheroid samples [58, 85]. Sca*l*eA2 solution (4 M urea, 0.2% (w/v) Triton X-100 and 10% (w/w) glycerol in water) was used to clear NSC spheroids (with an average diameter of 104.64 ± 22.01 µm) for imaging by CLSM [58]. In this work, a 2 times higher concentration of Triton X-100, in comparison to that described by Hama *et al*. [85], was used for improving the samples clearing. The spheroids clearing was achieved by performing 3 cycles of 24 h incubation with fresh Sca*l*eA2 solutions. Further, the authors observed that the realization of the Sca*l*eA2 protocol during longer periods did not improved the samples clearing. Moreover, the spheroids processing with the Sca*l*eA2 resulted in a size expansion to an average diameter of 139.2 ± 32.64 µm [58]. Lastly, the authors reported that the spheroids, in comparison to those incubated with PBS, become mechanically fragile after the clearing process.

In another study, the Sca*l*eSQ (one of the Sca*l*e solutions investigated by Hama et al. [85], composed of 9.1 M urea and 22.5% (w/v) sorbitol; RI ≈1.439) was used to clear MCF-7 breast cancer spheroids (diameter = 370 ± 90 µm) [46]. The method increased the average transmitted light intensity through the spheroids, *i.e.* the transmittance after the clearing increased 7.5%. Furthermore, the authors observed that the Sca*l*eSQ significantly increased the Fucci fluorescence intensity in the deeper regions of the spheroid and also the depth until each spheroid could be imaged (more than 250 µm deeper in the z-axis) by 2PM [46]. Nevertheless, the clearing solution induced the sample swelling, about 1.7-times higher spheroids area after the clearing and appear to mediate a shift in the color, *i.e.* the Fucci orange fluorescence (characteristic of the cells' nucleus in interphase stages of their cell cycle) appear more yellow [46].

5.4.3.2. CUBIC (Clear, Unobstructed Brain/Body Imaging Cocktails and Computational Analysis)

Another clearing method that uses urea and Triton X-100 (like the Sca*l*e solutions) is the CUBIC. This method was initially developed for the clearing of mouse whole-brain imaging with LSFM [86], and it involves the samples treatment with two clearing solutions, termed Sca*l*eCUBIC-1 (also known as reagent 1; 25% (w/w) urea, 25% (w/w) N,N,N',N'-tetrakis(2-hydroxypropyl) ethylenediamin and 15% (w/w) Triton X-100) and Sca*l*eCUBIC-2 (also known as reagent 2; 50% (w/v) sucrose, 25% (w/v) urea, 10% (w/v) 2,2′,2''-nitrilotriethanol and 0.1% (v/v) Triton X-100; RI ≈ 1.48). The amino alcohol N,N,N,N-tetrakis(2-hydroxypropyl) ethylenediamine in the reagent 1 solution was used as a tissue solubilizing agent which decolorizes blood and makes the organs much more transparent [87]. In brief, the CUBIC protocol was performed by immersing the whole-brain samples in the reagent 1 for 6-7 days (renewing the media after the first 3 days of incubation), then washing them several times with PBS followed by their incubation with 20% (w/v) sucrose in PBS and then a final immersion in the reagent 2 solution for 2-7 days.

Masson *et al.* applied the CUBIC clearing method to clear HCT116 spheroids (average diameter of 400 µm) in order to develop a high-resolution in-depth imaging approach of optically cleared thick spheroids using an adaptive SPIM [35]. For this purpose, spheroids were immersed with the reagent 1 solution for either 2 or 4 days (temperature 37 ºC), then samples were transferred into a fresh reagent 1 solution for additional 3 to 4 days. Then, spheroids were washed several times with PBS and incubated with 20% (w/v) sucrose and 50% (w/v) glycerol solution for a minimum of 2 hours. Lastly, spheroids were immersed in the reagent 2 solution with gentle shaking for 1 - 2 days, before the imaging. The optical clearing guaranteed high transparency and reduced the aberration patterns of the spheroids, contributing to the high-resolution in-depth imaging of the Alexa Fluor™ 594 (Click-iT™ EdU) and H2B-mCherry signals [35]. Moreover, authors demonstrated that, after the clearing procedure, the spheroids' images improved in quality, namely the fluorescence intensity and contrast.

5.4.4. Hydrogel embedding followed by delipidation and RI matching

The hydrogel embedding followed by delipidation and RI matching optical clearing methods comprehend the CLARITY and its derived approaches (*e.g.* PACT and PARS). These methods involve three major steps. The first step comprises the perfusion of the sample with a mixture of paraformaldehyde (or formaldehyde), acrylamide and bisacrylamide monomers (that form a polyacrylamide gel in the sample after its polymerization).Then, the lipids are removed from the sample-gel hybrid by using a solution of an ionic detergent, namely sodium dodecyl sulfate (SDS). Lastly, the hydrogel embedded samples are immersed on a RI-matching solution (*e.g.* FocusClear™) to render it transparency.

The gel will provide support for the biological structures in order to sustain their initial integrity, but it will also stabilize the proteins, nucleic acids and other small molecules by cross-linking them with the mesh of the gel [48]. Despite of the sample being immersed in a hydrogel, its porous nature makes possible the penetration and diffusion of exogenous macromolecules, such as immunolabeling dyes and fluorochromes [31]. Since CLARITY-based methods include the lipids removal, it is possible to achieve a great clearing in a similar way to other delipidation-based methods. However, due to the sample protection in a gel, the proteins concentration and folding is not affected in the same extent like when the methods containing harsh solvents or high concentrations of detergents. Additionally, since the lipids removal is performed by using SDS instead of organic solvents (like those used in the BABB and 3DISCO methods), the fluorescence is preserved (*e.g.* GFP fluorescence) [88].

5.4.4.1. CLARITY (Clear Lipid-exchanged Acrylamide-hybridized Rigid Imaging/Immunostaining/*In situ* Hybridization-compatible Tissue-Hydrogel) and derived methods

The original CLARITY method (also known as active CLARITY) was proposed in 2013 by Chung *et al.* to clear adult mouse whole brains and human brain samples of 500 μm in thickness [88]. Authors, initially infused a mixture of 4% (w/v) paraformaldehyde, 4% (w/v) acrylamide, 0.05% (w/v) bisacrylamide and 0.25% (w/v) 2,2'-azobis[2-(2-imidazolin-2-yl)propane] dihydrochloride (VA-044; thermal radical initiator) into the tissues. Then, after the hydrogel polymerization (3 h at 37° C), samples were subjected to an electric field potential (created by a custom electrophoresis system) and a 4% (w/v) SDS solution (1 or 2 days) to actively remove the lipidic content. Lastly, the samples were incubated in FocusClear™ (2 days for mouse brains and 1 day for human brain samples).

Nevertheless, the active CLARITY method requires specific equipment, as well as an expensive commercial RI-matching clearing solution (FocusClear™). Additionally, the strong electric field can change the molecular and structural integrity of the sample [44]. Therefore, several

CLARITY-derived methods emerged, such as PACT (passive clarity technique), PARS (perfusion-assisted agent release *in situ*) and others (reviewed in detail by [89] and [90]). The PACT and PARS methods use lower concentrations of fixatives and hydrogel monomers in conjugation with higher SDS concentrations (8% (w/v)), in order to facilitate and increase the passive diffusion of SDS into the sample and thus obtain a greater clearing without using the electrophoresis system. Additionally, both methods usually use RIMS (Refractive Index Matching Solution composed mainly of Histodenz or Sorbitol), which is a more economical RI-matching solution than FocusClear™ [91]. In the PACT method, sample-hydrogel hybrid is simply merged with a SDS solution, while in the PARS method the lipids removal is performed by perfusing continually the sample with the SDS solution [91].

CLARITY-based methods were also used to clear spheroids. Santisteban *et al*. used CLARITY and a microfluidic system to clear and image human derived adipose stem cells (hASC) spheroids (200 ± 50 µm in diameter) by CLSM [92]. In brief, after spheroids trapping in the chambers of the microfluidic chip, these were perfused with a solution of paraformaldehyde, acrylamide and bisacrylamide (4:4:0.25% (v/v)) for 1 h (replaced every 10 min). After 2 h of gel polymerization (VA-044 at 37ºC), the lipids were removed by using 0.14 M SDS solution (pH = 8.5) that was renewed every 30 min during a total of 3 days. All solutions (except the thermal radical initiator) were flushed with a flow rate of 2 µl/min using a flush time per chamber of 20 s. At last, X-Clarity™ (Logos Biosystems, USA) was introduced as mounting media to match the RI. The results demonstrated that the clearing time of the spheroids off-chip took 10 - 14 days, while this process was reduced to 2 days when a microfluidic system was used. Furthermore, authors also investigated the influence of the pH value in the media surrounding the hydrogel-embedded spheroids on the swelling and shrinkage of the gel [92]. These changes lead to the creation of an osmotic pressure and thus facilitate the lipids extraction form the spheroids. For that purpose, the hydrogel-embedded spheroids were subjected to incubation cycles (10 min) in SDS solution (pH 8.5) and phosphate buffer (pH 6.5). In these conditions, the clearing time was reduced to 5 h. Lastly, authors confirmed that the osmotic pump cycles did not perturb the nuclear structure and the proteins position, which was studied by labeling the cell nucleus (DAPI), the mitochondria (anti-COX IV antibody labeled with Alexa Fluor™ 647), and cytoplasm (anti-GAPDH labeled with Atto488™) [92]. Nevertheless, the authors observed that the spheroids shrank to 150 µm in diameter after the clearing process [92].

Chen and co-workers also investigated the application of a microfluidic technology to clear whole intact spheroids (*e.g.* MCF-7 spheroids with 250 µm of diameter and GFP-expressing U87MG spheroids with diameter of 450 µm) using a CLARITY-based method and perform imaging by CLSM [93]. Upon spheroids loading in the microfluidic system, a solution of 2 – 8% (w/v) acrylamide, 4% (w/v) formaldehyde, and 2.5% (w/v) of VA-044 was infused at 600 - 800 µL/h through the spheroids for 20 min. After 2 h of gel polymerization (37 °C), 8% (w/v) SDS was infused at 800 µL/h during 5 - 10 min. Lastly, RIMS (88% (w/v) Iohexol, 2.5% (w/v) 1,4-

diazabicyclo[2.2.2]octane, 50 mM sodium borate, and 0.01% (w/v) sodium azide) was infused into the spheroids (800 µL/h for tumor spheroids) during 10–15 min. Authors observed that without the acrylamide treatment, the spheroid structure is deformed due to the fluidic forces applied during the clearing process [93]. Moreover, increasing the acrylamide concentration decreases the extent of tissue shrinkage (*e.g.* 80 to 90% of the spheroids initial volume was maintained when used 8% (w/v) acrylamide). On the other hand, SDS solution flow led to the lipophilic dye (DiO) fluorescence loss but simultaneously did not affect the spheroids stain with Transferrin-647 as well as facilitated the spheroids staining with DAPI and Phalloidin-488 [93]. The results obtained also demonstrated that the imaging depth was increased by 150% for MCF-7 spheroids (labelled with CellTracker™ Red), and 250% for U87MG-GFP spheroids, when compared to the non-cleared spheroids. Furthermore, authors also verified that the CLARITY-based method performed in the microfluidic system could be used for live/dead imaging of the spheroids treated with drugs (doxorubicin, imatinib, or sunitinib) and using LIVE/DEAD® Fixable Near-IR Dead Cell Stain.

5.5. Conclusion and Outlook

For more than 100 years, optical clearing methods have been used for the clearing of large biological samples obtained from animals. These methods have been developed to fulfill the following two major premises: i) provide high transparency without affecting the initial structure and size of the sample; and ii) preserve endogenous and exogeneous fluorescence (*e.g.* immunofluorescence), which is fundamental for the analysis of the proteins of interest.

More recently, optical clearing methods started to be explored for allowing the whole imaging of large 3D spheroids, as reviewed in this chapter (Table 5.3). Till nowadays, SeeDB, TDE, *Clear*^{T2}, FocusClear™, BABB, Sca*l*e, CUBIC and CLARITY optical clearing methods have been used for spheroids imaging under different types of microscopes (2PM, adaptive SPIM, CLSM, LSFM and mDSLM). Nevertheless, there is several other optical clearing methods (*e.g.* 3DISCO, FRUIT, PRESTO and SWITCH) that are yet to be investigated in spheroids.

With the future efforts, it will be possible to obtain of a high-throughput-compatible approach to combine clearing, high-content imaging, and analysis of spheroids. Thus, optical clearing methods will contribute significantly to the widespread use of spheroids in the evaluation of different cellular events in normal and diseased human tissues.

Table 5.3. Overview of the optical clearing methods applied for the imaging of spheroids.

Method	Reagent(s)	Time[a]	Spheroids cells	Spheroids diameter (µm)	Microscopy Technique	Observation(s)[b]	REF
Simple immersion in an aqueous solution with high RI							
SeeDB	• Fructose; • α-thioglycerol.	< 1 h	• MCF-7 human breast cancer.	370	MPM (2PM)	• Clearing was performed with the assistance of a microfluidic device; • Spheroids size is minimally reduced; • Transparency is slightly improved; • Allow more than 250 µm of image depth; • Nuclei blur is less extent; • Fluorescence intensity (green autofluorescence) is increased.	[46]
		72 h	• Rat adult neural stem cells (NSC).	104	CLSM	• Leads to spheroids shrinkage; • Moderate transparency; • Allows the imaging of the whole spheroid; • Difficult handling of the viscous clearing solutions.	[58]
TDE	• 2,2′-thiodiethanol (TDE).	30 min	• Tissue spheroids.	300	LSFM (SPIM)	• High-throughput imaging at subcellular level is performed; • Detailed imaging of the whole spheroid.	[33]
Clear^{T2}	• Formamide; • Polyethylene glycol (PEG; 8000 Da).	75 min	• C6 rat glioma; • Primary cortical neurons; • Rat adult neural stem cells (NSC).	104	CLSM	• Longer incubation times does not improve the clearing; • Spheroids size was not affected; • Allows up to ≈ 100 µm of image depth; • Imaging in the spheroids interior is improved.	[58]
		75 min	• PLHC-1 human liver cancer; • LNCaP human prostate cancer; • BEAS-2B human lung epithelium.	n.a.	CLSM	• Imaging depth is augmented; • Imaging in the spheroids interior is improved.	[66]
FocusClear™	• FocusClear™ solution.	2 h	• Intestinal stem cells isolated from mice.	≈ 300	CLSM	• Transparency is improved; • Imaging performed with high-resolution.	[69]

Delipidation and dehydration followed by RI matching							
BABB	• Benzyl alcohol; • Benzyl benzoate; • Ethanol.	> 20 min	• T47D human breast cancer; • DLD1 human colorectal cancer; • DU145 human prostate cancer; • Primary human colon cancer cells.	≈ 400	mDSLM	• Clear imaging of spheroids hypoxic, dead, and proliferative cells.	[76]
		n.a.	• HCT116 human colorectal cancer.	650	LSFM	• Imaging depth is improved; • Imaging performed with high-resolution.	[34]
		n.a.	• T47D human breast cancer.	150 - 500	mDSLM	• Allows the acquisition of high-quality images of intact spheroids at cellular resolution;	[77]
		> 14 min	• U343 human glioblastoma.	≈ 600	mDSLM	• Transparency is improved; • Occurs spheroids shrinkage.	[60]
Delipidation and hyperhydration followed by RI matching							
Sca*l*e	• Glycerol; • Triton X-100; • Urea.	72 h	• Rat adult neural stem cells (NSC).	104	CLSM	• Double concentration of Triton X-100 improves the clearing; • Longer incubations times does not improve the clearing; • Transparency is improved; • Occurs spheroids expansion; • Spheroids become mechanically fragile.	[58]
	• Sorbitol; • Urea.	< 1 h	• MCF-7 human breast cancer cells.	370	MPM (2PM)	• Transparency is improved; • Occurs spheroids expansion; • Nuclei blur is less extent; • Allows more than 250 μm of image depth; • Fluorescence intensity is increased; • Occurs fluorescence shift.	[46]
CUBIC	• 2,2′,2′′-nitrilotriethanol; • Glycerol; • N,N,N',N'-tetrakis(2-hydroxypropyl) ethylenediamine; • Triton X-100; • Sucrose; • Urea.	≈ 6 - 10 d	• HCT116 human colorectal cancer.	400	adaptive SPIM	• Transparency is improved; • Allows the acquisition of high-resolution in-depth images; • Improved image quality in terms of peak intensities and contrast.	[35]

Hydrogel embedding followed by delipidation and RI matching							
CLARITY	• Acrylamide; • Bisacrylamide • VA-044 • SDS • X-Clarity™	2 d	• Human derived adipose stem cells (hASC)	200	CLSM	• Clearing was performed with the assistance of a microfluidic device; • Transparency is improved; • Leads to spheroids shrinkage; • Nuclear structure and the proteins position are not disturbed; • Fluorescence intensity is acquired in the entire spheroid; • Clearing time is reduced to 5 h by alternating the pH in the surrounding hydrogel-embedded spheroids.	[92]
	• Acrylamide • VA-044 • RIMS(Iohexol, 1,4-diazabicyclo[2.2.2]octane, sodium borate and sodium azide)	< 5 h	• MCF-7 human breast cancer cells; • MDA-MB-435 human melanoma cells; • B16F10 murine melanoma cells (endogenously expressing tdTomato); • U87MG human glioblastoma cells (endogenously expressing GFP); • HUVEC human umbilical vein endothelial cells.	250 and 450	CLSM	• Clearing was performed with the assistance of a microfluidic device; • Transparency is improved; • Spheroids not embedded in the gel are deformed by the fluidic forces; • Higher concentrations of acrylamide allow better preservation of spheroids structure; • DiO fluorescence is lost during spheroids treatment with SDS, while this process does not affect the spheroids stain with Transferrin-647 and facilitated the spheroids stain with DAPI, and Phalloidin-488; • Imaging depth is improved by 150% for MCF-7 spheroids, and 250% for U87MG-GFP spheroids; • Method is compatible with live/dead imaging of drug treated spheroids.	[93]

n.a.: not available; [a]: Time spent in the clearing process, excluding the spheroids fixation time; [b]: Information available about the clearing technique.

5.6. References

1. Souza, A., *et al.*, *Advances in cell culture: more than a century after cultivating cells.* Journal of Biotechnology and Biomaterials, 2016. 6: 1-4.

2. Hudu, S. A., *et al.*, *Cell Culture, Technology: Enhancing the Culture of Diagnosing Human Diseases.* Journal of Clinical and Diagnostic Research, 2016. 10: DE01-DE05.

3. Duval, K., *et al.*, *Modeling Physiological Events in 2D vs. 3D Cell Culture.* Physiology, 2017. 32: 266-277.

4. Kapałczyńska, M., *et al.*, *2D and 3D cell cultures – a comparison of different types of cancer cell cultures.* Archives of Medical Science, 2018. 14: 910-919.

5. Edmondson, R., *et al.*, *Three-Dimensional Cell Culture Systems and Their Applications in Drug Discovery and Cell-Based Biosensors.* Assay and Drug Development Technologies, 2014. 12: 207-218.

6. Sandberg, R. and Ernberg, I., *The molecular portrait of in vitro growth by meta-analysis of gene-expression profiles.* Genome Biology, 2005. 6: R65.

7. Yoon No, D., *et al.*, *3D liver models on a microplatform: well-defined culture, engineering of liver tissue and liver-on-a-chip.* Lab on a Chip, 2015. 15: 3822-3837.

8. Cirello, V., *et al.*, *Multicellular spheroids from normal and neoplastic thyroid tissues as a suitable model to test the effects of multikinase inhibitors.* Oncotarget, 2017. 8: 9752-9766.

9. Jukes, J. M., *et al.*, *Endochondral bone tissue engineering using embryonic stem cells.* Proceedings of the National Academy of Sciences, 2008. 105: 6840-6845.

10. Lumelsky, N., *et al.*, *Differentiation of embryonic stem cells to insulin-secreting structures similar to pancreatic islets.* Science, 2001. 292: 1389-1394.

11. Kehat, I., *et al.*, *Human embryonic stem cells can differentiate into myocytes with structural and functional properties of cardiomyocytes.* Journal of Clinical Investigation, 2001. 108: 407-414.

12. Hamilton, G., *Multicellular spheroids as an in vitro tumor model.* Cancer Letters, 1998. 131: 29-34.

13. Khawar, I. A., *et al.*, *Three Dimensional Mixed-Cell Spheroids Mimic Stroma-Mediated Chemoresistance and Invasive Migration in hepatocellular carcinoma.* Neoplasia, 2018. 20: 800-812.

14. Lazzari, G., *et al.*, *Multicellular spheroid based on a triple co-culture: A novel 3D model to mimic pancreatic tumor complexity.* Acta Biomaterialia, 2018. 78: 296-307.

15. Ham, S. L., *et al.*, *Three-dimensional tumor model mimics stromal - breast cancer cells signaling.* Oncotarget, 2018. 9: 249-267.

16. Ham, S. L., *et al.*, *Engineered Breast Cancer Cell Spheroids Reproduce Biologic Properties of Solid Tumors.* Advanced Healthcare Materials, 2016. 5: 2788-2798.

17. Suga, H., *et al.*, *Self-formation of functional adenohypophysis in three-dimensional culture.* Nature, 2011. 480: 57-62.

18. Eiraku, M., *et al.*, *Self-organizing optic-cup morphogenesis in three-dimensional culture*. Nature, 2011. 472: 51-56.

19. Eiraku, M., *et al.*, *Self-organized formation of polarized cortical tissues from ESCs and its active manipulation by extrinsic signals*. Cell Stem Cell, 2008. 3: 519-532.

20. Costa, E. C., *et al.*, *3D tumor spheroids: an overview on the tools and techniques used for their analysis*. Biotechnology Advances, 2016. 34: 1427-1441.

21. Genina, E. A., Bashkatov, A. N., and Tuchin, V. V., *Tissue optical immersion clearing*. Expert Review of Medical Devices, 2010. 7: 825-842.

22. Graf, B. W. and Boppart, S. A., *Imaging and analysis of three-dimensional cell culture models*. Methods in Molecular Biology, 2010. 591: 211-227.

23. Richardson, D. S. and Lichtman, J. W., *Clarifying Tissue Clearing*. Cell, 2015. 162: 246-257.

24. Achilli, T.-M., Meyer, J., and Morgan, J. R., *Advances in the formation, use and understanding of multi-cellular spheroids*. Expert Opinion on Biological Therapy, 2012. 12: 1347-1360.

25. Langenbach, F., *et al.*, *Generation and differentiation of microtissues from multipotent precursor cells for use in tissue engineering*. Nature Protocols, 2011. 6: 1726-1735.

26. Santi, P. A., *Light sheet fluorescence microscopy: a review*. Journal of Histochemistry and Cytochemistry, 2011. 59: 129-138.

27. Marques, P. E., *et al.*, *Understanding liver immunology using intravital microscopy*. Journal of Hepatology, 2015. 63: 733-742.

28. Combs, C. A. and Shroff, H., *Fluorescence Microscopy: A Concise Guide to Current Imaging Methods*. Current Protocols in Cell Biology, 2017. 79: 2.1.1-2.1.25.

29. Benninger, R. K. P. and Piston, D. W., *Two-Photon Excitation Microscopy for the Study of Living Cells and Tissues*. Current Protocols in Cell Biology, 2013. 4: Unit 4.11.11-24.

30. Zipfel, W. R., Williams, R. M., and Webb, W. W., *Nonlinear magic: multiphoton microscopy in the biosciences*. Nature Biotechnology, 2003. 21: 1369-1377.

31. Feuchtinger, A., Walch, A., and Dobosz, M., *Deep tissue imaging: a review from a preclinical cancer research perspective*. Histochemistry and Cell Biology, 2016. 146: 781-806.

32. Reynaud, E. G., *et al.*, *Light sheet-based fluorescence microscopy: more dimensions, more photons, and less photodamage*. HFSP Journal, 2008. 2: 266-275.

33. Paiè, P., *et al.*, *Selective plane illumination microscopy on a chip*. Lab on a Chip, 2016. 16: 1556-1560.

34. Desmaison, A., *et al.*, *Impact of physical confinement on nuclei geometry and cell division dynamics in 3D spheroids*. Scientific Reports, 2018. 8: 8785.

35. Masson, A., *et al.*, *High-resolution in-depth imaging of optically cleared thick samples using an adaptive SPIM*. Scientific Reports, 2015. 5: 16898.

36. Azaripour, A., *et al.*, *A survey of clearing techniques for 3D imaging of tissues with special reference to connective tissue*. Progress in Histochemistry and Cytochemistry, 2016. 51: 9-23.

37. Susaki, Etsuo A. and Ueda, Hiroki R., *Whole-body and Whole-Organ Clearing and Imaging Techniques with Single-Cell Resolution: Toward Organism-Level Systems Biology in Mammals*. Cell Chemical Biology, 2016. 23: 137-157.

38. Bigio, I. J. and Bown, S. G., *Spectrroscopic sensing of cancer and cancer therapy: Current status of translational research*. Cancer biology & therapy, 2004. 3: 259-267.

39. Choi, W., *et al.*, *Tomographic phase microscopy*. Nature Methods, 2007. 4: 717-719.

40. Zhang, Q., *et al.*, *Quantitative refractive index distribution of single cell by combining phase-shifting interferometry and AFM imaging*. Scientific Reports, 2017. 7: 2532.

41. Bassnett, S., *On the mechanism of organelle degradation in the vertebrate lens*. Experimental Eye Research, 2009. 88: 133-139.

42. Wilson, J. D., Cottrell, W. J., and Foster, T. H., *Index-of-refraction-dependent subcellular light scattering observed with organelle-specific dyes*. Journal of Biomedical Optics, 2007. 12: 014010.

43. Haseda, K., *et al.*, *Significant correlation between refractive index and activity of mitochondria: single mitochondrion study*. Biomedical Optics Express, 2015. 6: 859-869.

44. Seo, J., Choe, M., and Kim, S. Y., *Clearing and Labeling Techniques for Large-Scale Biological Tissues*. Molecules and Cells, 2016. 39: 439-446.

45. Keereweer, S., *et al.*, *Optical Image-Guided Cancer Surgery: Challenges and Limitations*. Clinical Cancer Research, 2013. 19: 3745-3754.

46. Grist, S. M., *et al.*, *On-chip clearing of arrays of 3-D cell cultures and micro-tissues*. Biomicrofluidics, 2016. 10: 044107.

47. Zhu, D., *et al.*, *Recent progress in tissue optical clearing*. Laser & Photonics Reviews, 2013. 7: 732-757.

48. Silvestri, L., *et al.*, *Clearing of fixed tissue: a review from a microscopist's perspective*. Journal of Biomedical Optics, 2016. 21: 081205.

49. Lee, E., Kim, H. J., and Sun, W., *See-Through Technology for Biological Tissue: 3-Dimensional Visualization of Macromolecules*. International Neurourology Journal, 2016. 20: S15-22.

50. Tainaka, K., *et al.*, *Chemical Principles in Tissue Clearing and Staining Protocols for Whole-Body Cell Profiling*. Annual Review of Cell and Developmental Biology, 2016. 32: 713-741.

51. Yu, T., *et al.*, *Optical clearing for multiscale biological tissues*. Journal of Biophotonics, 2018. 11: 1-13.

52. Tuchin, V. V., *Tissue optics and photonics: light-tissue interaction*. Journal of Biomedical Photonics & Engineering, 2015. 1: 98-134.

53. Ariel, P., *A beginner's guide to tissue clearing*. The International Journal of Biochemistry & Cell Biology, 2017. 84: 35-39.

54. Ke, M.-T., Fujimoto, S., and Imai, T., *SeeDB: a simple and morphology-preserving optical clearing agent for neuronal circuit reconstruction.* Nature Neuroscience, 2013. 16: 1154-1161.

55. Ke, M. T. and Imai, T., *Optical clearing of fixed brain samples using SeeDB.* Current Protocols in Neuroscience, 2014. 66: Unit 2.22.

56. Dills, W. L., Jr., *Protein fructosylation: fructose and the Maillard reaction.* The American Journal of Clinical Nutrition, 1993. 58: 779s-787s.

57. Berke, I. M., *et al.*, *Seeing through Musculoskeletal Tissues: Improving In Situ Imaging of Bone and the Lacunar Canalicular System through Optical Clearing.* PLOS ONE, 2016. 11: e0150268.

58. Boutin, M. E. and Hoffman-Kim, D., *Application and assessment of optical clearing methods for imaging of tissue-engineered neural stem cell spheres.* Tissue Engineering Part C: Methods, 2015. 21: 292-302.

59. Staudt, T., *et al.*, *2,2'-thiodiethanol: a new water soluble mounting medium for high resolution optical microscopy.* Microscopy Research and Technique, 2007. 70: 1-9.

60. Smyrek, I. and Stelzer, E. H. K., *Quantitative three-dimensional evaluation of immunofluorescence staining for large whole mount spheroids with light sheet microscopy.* Biomedical Optics Express, 2017. 8: 484-499.

61. Aoyagi, Y., *et al.*, *A Rapid Optical Clearing Protocol Using 2,2′-Thiodiethanol for Microscopic Observation of Fixed Mouse Brain.* PLOS ONE, 2015. 10: e0116280.

62. Costantini, I., *et al.*, *A versatile clearing agent for multi-modal brain imaging.* Scientific Reports, 2015. 5: 9808.

63. Kuwajima, T., *et al.*, *ClearT: a detergent- and solvent-free clearing method for neuronal and non-neuronal tissue.* Development, 2013. 140: 1364-1368.

64. Rawat, S., Raman Suri, C., and Sahoo, D. K., *Molecular mechanism of polyethylene glycol mediated stabilization of protein.* Biochemical and Biophysical Research Communications, 2010. 392: 561-566.

65. Boutin, M. E., *et al.*, *A three-dimensional neural spheroid model for capillary-like network formation.* Journal of Neuroscience Methods, 2018. 299: 55-63.

66. Kabadi, P. K., *et al.*, *Into the depths: Techniques for in vitro three-dimensional microtissue visualization.* BioTechniques, 2015. 59: 279-286.

67. Fu, Y.-Y., *et al.*, *A microtome-free 3-dimensional confocal imaging method for visualization of mouse intestine with subcellular-level resolution.* Gastroenterology, 2009. 137: 453-465.

68. Moy, A. J., *et al.*, *Optical properties of mouse brain tissue after optical clearing with FocusClear.* Journal of Biomedical Optics, 2015. 20: 95010.

69. Chen, Y., *et al.*, *Application of Three-Dimensional Imaging to the Intestinal Crypt Organoids and Biopsied Intestinal Tissues.* The Scientific World Journal, 2013. 2013: 624342.

70. Spalteholz, W., *Über das Durchsichtigmachen von menschlichen und tierischen Präparaten und seine theoretischen Bedingungen, nebst Anhang: Über Knochenfärbung*. 1914: S. Hirzel.

71. Alnuami, A. A., *et al.*, *Oxyradical-induced GFP damage and loss of fluorescence.* International Journal of Biological Macromolecules, 2008. 43: 182-186.

72. Steinke, H. and Wolff, W., *A modified Spalteholz technique with preservation of the histology.* Annals of Anatomy, 2001. 183: 91-95.

73. Cumley, R. W., Crow, J. F., and Griffen, A. B., *Clearing Specimens for the Demonstration of Bone.* Stain Technology, 1939. 14: 7-11.

74. Dent, J. A., Polson, A. G., and Klymkowsky, M. W., *A whole-mount immunocytochemical analysis of the expression of the intermediate filament protein vimentin in Xenopus.* Development, 1989. 105: 61-74.

75. Dodt, H. U., *et al.*, *Ultramicroscopy: three-dimensional visualization of neuronal networks in the whole mouse brain.* Nature Methods, 2007. 4: 331-336.

76. Wenzel, C., *et al.*, *3D high-content screening for the identification of compounds that target cells in dormant tumor spheroid regions.* Experimental Cell Research, 2014. 323: 131-143.

77. Schmitz, A., *et al.*, *Multiscale image analysis reveals structural heterogeneity of the cell microenvironment in homotypic spheroids.* Scientific Reports, 2017. 7: 43693.

78. Becker, K., *et al.*, *Chemical Clearing and Dehydration of GFP Expressing Mouse Brains.* PLOS ONE, 2012. 7: e33916.

79. Erturk, A., *et al.*, *Three-dimensional imaging of solvent-cleared organs using 3DISCO.* Nature Protocols, 2012. 7: 1983-1995.

80. Renier, N., *et al.*, *iDISCO: a simple, rapid method to immunolabel large tissue samples for volume imaging.* Cell, 2014. 159: 896-910.

81. Pan, C., *et al.*, *Shrinkage-mediated imaging of entire organs and organisms using uDISCO.* Nature Methods, 2016. 13: 859-867.

82. Qi, Y., *et al.*, *FDISCO: Advanced solvent-based clearing method for imaging whole organs.* Science Advances, 2019. 5: eaau8355.

83. Mattei, B., *et al.*, *Membrane permeabilization induced by Triton X-100: The role of membrane phase state and edge tension.* Chemistry and Physics of Lipids, 2017. 202: 28-37.

84. Hama, H., *et al.*, *Scale: a chemical approach for fluorescence imaging and reconstruction of transparent mouse brain.* Nature Neuroscience, 2011. 14: 1481-1488.

85. Hama, H., *et al.*, *ScaleS: an optical clearing palette for biological imaging.* Nature Neuroscience, 2015. 18: 1518-1529.

86. Susaki, E. A., *et al.*, *Whole-brain imaging with single-cell resolution using chemical cocktails and computational analysis.* Cell, 2014. 157: 726-739.

87. Tainaka, K., *et al.*, *Whole-body imaging with single-cell resolution by tissue decolorization.* Cell, 2014. 159: 911-924.

88. Chung, K., *et al.*, *Structural and molecular interrogation of intact biological systems.* Nature, 2013. 497: 332–337.

89. Jensen, K. H. R. and Berg, R. W., *Advances and perspectives in tissue clearing using CLARITY.* Journal of Chemical Neuroanatomy, 2017. 86: 19-34.

90. Du, H., *et al.*, *Advances in CLARITY-based tissue clearing and imaging*. Experimental and Therapeutic Medicine, 2018. 16: 1567-1576.

91. Yang, B., *et al.*, *Single-cell phenotyping within transparent intact tissue through whole-body clearing*. Cell, 2014. 158: 945-958.

92. Silva, S. T., *et al.*, *Rapid spheroid clearing on a microfluidic chip*. Lab on a Chip, 2018. 18: 153-161.

93. Chen, Y. Y., *et al.*, *Clarifying intact 3D tissues on a microfluidic chip for high-throughput structural analysis*. Proceedings of the National Academy of Sciences, 2016. 113: 14915-14920.

Chapter 6

Research Work 1

Clear^T immersion optical clearing method for intact 3D spheroids imaging through confocal laser scanning microscopy

This chapter is based on the publication entitled: Clear^T immersion optical clearing method for intact 3D spheroids imaging through confocal laser scanning microscopy, Optics & Laser Technology, 2018, 106: 94-99.

6.1. Abstract

Spheroids are three-dimensional (3D) *in vitro* platforms that fill the gap between the two-dimensional (2D) cell cultures and animal models on the therapeutics development pipeline. Yet, the methods and equipment used in the *in vitro* assays are optimized for the analysis of cells cultured as monolayers. For instance, confocal laser scanning microscopy (CLSM) does not allow the observation of thick intact spheroids due to light penetration issues. To overcome this limitation, spheroids treatment with clearing agents started to be explored. Herein, we demonstrate for the first time the application of *Clear*^{T} clearing method for the imaging of propidium iodide (PI) stained spheroids by CLSM. The results demonstrate that the *Clear*^{T} is a reversible clearing method that does not influence the structure of the spheroid and significantly improved the PI signal penetration depth in about 43%. Additionally, *Clear*^{T} also enhanced the cells imaging within the spheroid by increasing the cross-penetration depth in 46.6% at 100 µm of depth. Overall, the results show that *Clear*^{T} method may allow the improvement of the CLSM accuracy on the evaluation of the cellular death within spheroids prompted by therapeutics.

Keywords: *Clear*^{T}; confocal microscopy; formamide; propidium iodide; spheroids.

6.2. Introduction

2D cell cultures (monolayers of cells) have been extensively used to evaluate the toxicity and therapeutic efficacy of compound's libraries during the *in vitro* preclinical phase of the drug discovery process [1]. Afterwards, therapeutics are evaluated on animal models (mice, monkey, fishes, among others). However, 2D cell cultures are unrealistic representations of the *in vivo* conditions and a large number of ineffective drugs proceed to the *in vivo* assays. Altogether, these issues have been delaying and limiting the drug discovery process [1], which makes evident the urgent need to use more reliable models of human tissues, such as 3D cell culture models, to test the drug candidates before the animal experimentation be performed.

Spheroids are 3D cell culture models capable of reproducing the human solid tumors features, by mimicking their 3D structure, cellular organization, extracellular matrix (ECM) proteins deposition, gene expression and drug resistance profile (reviewed in [2]). During the last decades, these models have been applied to evaluate the efficacy of drugs [3], radiation [4] and nanotherapeutics [5, 6] in cancer therapy. However, despite of the increase of spheroids use for therapeutics analysis, most of the assays and equipment are developed and optimized for the analysis of cells cultured in a monolayer. In this regard, fluorescence microscopy arises as one of the main techniques used to evaluate the therapeutics distribution within the spheroids or even the cellular death in response to a potential therapeutic. For instance, Jyoti *et al.* described the use fluorescence microscopy to study the liposomes' cytotoxicity towards tumor-endothelial cell spheroids through the analysis of the PI dye fluorescence (DNA stain that only stains cells with a compromised cellular membrane) [7].

Some microscopes, namely light sheet fluorescence microscopy (LSFM) allow the imaging of intact spheroids since the penetration depth of the equipment is greater than 1 cm [8-10]. Still, CLSM equipment, which is commonly available in different laboratories, is the most used approach for spheroids analysis (size, morphology, expression of proteins and therapeutics and nanotherapeutics efficacy) [5, 6, 11, 12]. However, generally CLSM does not allow the imaging of samples with thickness bigger than 100 µm [13-15]. Therefore, since spheroids usually present diameters superior to few hundreds µm, the observation of intact spheroids through CLSM is very limited and thus spheroids must be sliced to allow their imaging [13, 14]. Still, the sectioning of the spheroids is time-consuming, organic solvents dependent, can introduce artifacts and sometimes presents limited efficacy due to the destruction of the spheroids initial structure [2].

To overcome such issues, clearing methods started to be recently explored in the spheroids analysis in order to increase the samples transparency by reducing light scattering and, consequently, improve the signal penetration depth [13, 14, 16-27]. These clearing methods can be grouped in solvent (*e.g.* BABB and 3DISCO), simple immersion (*e.g. Clear*^{T} and SeeDB)

and hyperhydration (*e.g.* Sca*l*e) based approaches (reviewed by Richardson and Lichtman [13]). Among these methods, *Clear*^{T} clearing method is organic-solvent free and easy to handle, *i.e.* samples are cleared by immersing the samples on gradient solutions of formamide. This method was reported for the first time in 2013 by Kuwajima *et al.*, that successfully cleared mouse brain and head tissues samples [18]. Nevertheless, the use of *Clear*^{T} for the clearing of spheroids was not yet investigated. In this work, the effect of using the *Clear*^{T} method in the imaging of PI stained spheroids through CLSM was studied. The obtained results demonstrated that the *Clear*^{T} method significantly improves the imaging of the spheroids in comparison with the non-cleared spheroids (spheroids that were maintained in phosphate-buffered saline (PBS) solution). In future works, the use of *Clear*^{T} may facilitate the visualization and analysis of cellular death induced by therapeutics in the spheroids.

6.3. Materials and Methods

6.3.1. Materials

Normal Human Dermal Fibroblasts (NHDF) were bought from PromoCell (C-12302, Labclinics, S.A.; Barcelona, Spain). Dulbecco's Modified Eagle's Medium F-12 (DMEM-F12), formamide (99.6%), paraformaldehyde (PFA), PBS, trypsin and ethylenediaminetetraacetate (EDTA) were purchased from Sigma-Aldrich (Sintra, Portugal). Agarose was obtained from Grisp (Porto, Portugal). Cell culture plates, T-flasks and other culture plastics were obtained from ThermoFisher Scientific (Porto, Portugal). Cell imaging plates were acquired from Ibidi GmbH (Munich, Germany). Fetal bovine serum (FBS) was obtained from Biochrom AG (Berlin, Germany). PI was purchased from Invitrogen (Carlsbad, CA, USA).

6.3.2. Methods

6.3.2.1. Cells maintenance

NHDF were grown in DMEM-F12, supplemented with 10% (v/v) FBS and 1% streptomycin and gentamycin, at 37 ºC, in a humidified atmosphere with 5% CO_2. When cells confluence was attained, they were recovered by using 0.25% trypsin (1:250) and EDTA 0.1% (w/v) [12].

6.3.2.2. Spheroids assembly

Hydrogel structures with round-bottom microwells were produced by placing agarose 2% (w/v in H_2O) in micromolds (3D Petri Dish®, Microtissues Inc., Providence RI, US) [28]. Spheroids production was initialized by seeding $1x10^6$ NHDF cells per agarose structure.

Afterwards, cells were grown for 6 days to allow the spheroids formation through cellular aggregation. During this period, spheroids were maintained in DMEM-F12, supplemented with

10% (v/v) FBS and 1% streptomycin and gentamycin, in a humidified atmosphere at 37 ºC with 5% CO_2.

6.3.2.3. Spheroids fixation and staining with PI

Whole spheroids were recovered from the agarose structures and then fixed with PFA 4% (w/v in PBS) (freshly prepared to minimize its autofluorescence) during 24 h, at 4 ºC [23]. Subsequently, spheroids were washed 3 times with PBS and stained with 1 mL of PI at a concentration of 10 µg/mL, during 24 h, in a shaker plate at 100 rotations per minute (RPM), as previously performed in our group [12, 29]. The excess of PI dye was removed by washing the spheroids with PBS.

6.3.2.4. Spheroids clearing by *Clear*^{T}

Spheroids were cleared by using the *Clear*^{T} method [18]. Briefly, formamide solutions (20, 40, 80 and 95% (v/v in PBS)) were freshly prepared. Subsequently, whole spheroids were immersed in increasing concentrations of formamide, *i.e.* samples were incubated for 5 min in 20, 40, 80 and 95% formamide solutions followed by a last incubation step of 15 min in formamide 95%. After, the clearing process, the spheroids were transferred to µ-slide 8-well imaging plates (Ibidi GmbH, Germany) for further analysis through CLSM. For comparative purposes, non-cleared spheroids, *i.e.* spheroids that were maintained on PBS, were also obtained.

6.3.2.5. Imaging of whole spheroids by optical microscopy and CLSM

Optical images of intact non-cleared and *Clear*^{T} cleared spheroids were acquired with a Carl Zeiss Axio Imager A1 inverted microscope equipped with an AxioVision camera.

CLSM images of intact non-cleared and *Clear*^{T} cleared PI stained spheroids were acquired by using a Zeiss LSM 710 AxioObserver confocal laser scanning microscope (Carl Zeiss SMT, Inc., Oberkochen, Germany). All the fluorescence images were obtained using the same equipment settings for comparison purposes. The images were acquired using a 20x air objective (Plan-Apochromat 20x/0.8 M27, working distance = 0.55 mm) and a confocal aperture of 1 Airy disk. Further, laser power and master gain were kept constant during the images acquisition. PI was visualized with a 514 nm Argon laser. Z-stacks were collected with 5 µm intervals.

6.3.2.6. Optical and CLSM images analysis

Optical and CLSM images of spheroids were analyzed by using an image processing program designed for scientific purposes - ImageJ, National Institutes of Health [30].

The influence of *Clear*^{T} method on spheroids' morphology was indirectly evaluated by the analysis of the spheroids diameter before and after each immersion step in the formamide solutions, as previously described elsewhere [12, 19]. The ability of the *Clear*^{T} method to turn spheroids transparent after each immersion cycle in the formamide solutions was observed by

the optical microscopic images of spheroids placed on a crosshatched background [18, 26]. The preservation of the PI fluorescence signal after the use of the *Clear*^{T} method was determined as described in literature [21, 27, 31]. In brief, the corrected total cell fluorescence (CTCF) of the CLSM maximum intensity Z-projections with a thickness of 100 µm (total of 20 Z-stacks) was measured.

The penetration depth of PI signal in Z-axis was determined by multiplying the number of stacks with PI fluorescence (stacks with fluorescence intensity in the spheroids area higher than the fluorescence intensity of the background) by the stacks thickness (5 µm) [22, 32]. Thus, this parameter is a measure of how deep in the Z-axis it is possible to acquire PI fluorescence signal.

The determination of the PI cross-section imaging depth (PI fluorescence inside the spheroid) was performed at 25, 50, 75 and 100 µm of depth (Z-axis). This analysis was performed by counting the number of pixels with fluorescence in the spheroid region [33, 34]. For such, the gray value of each pixel was determined (gray value equal to zero corresponds to pixels with no PI fluorescence; gray value higher than 0 corresponds to pixels with PI fluorescence) [33, 34]. Additionally, plot profiles that demonstrate the PI fluorescence intensity along the spheroid were performed at penetration depth of 100 µm, as previously described in other works [24, 25].

All the data were compared and/or normalized to that obtained for non-cleared spheroids (control).

6.3.2.7. Statistical analysis

Data was expressed as mean values ± standard deviation (SD). The statistical analysis was performed by using unpaired t test. A value of $p < 0.05$ was considered statistically significant. Data analysis was performed in GraphPad Prism v.6.0 software (Trial version, GraphPad Software, CA, USA).

6.4. Results and Discussion

The observation of thick samples through CLSM has been hindered by the low penetration depth of the confocal equipment as well as by light scattering effects [35]. In biological samples, light scattering occurs due to the reflection or refraction phenomena induced by the cellular constituents (*e.g.* cellular membrane and organelles). To improve the imaging of thick samples, *Clear*^{T} can be used to reduce the scattered light in the samples, turning the samples more transparent and improving the imaging penetration depth [13]. In the *Clear*^{T} method, spheroids' scattering light is reduced through the equilibration of the overall refractive index (RI) of the

sample [17]. In brief, the water content of the cells is replaced by formamide through an osmotic gradient [13]. This process reduces light refraction since the formamide RI (1.44) is similar to the RI of the fixed cells (≈ 1.50) [13].

Therefore, in this work, the *Clear*^{T} applicability in the CLSM imaging of PI-stained NHDF spheroids was investigated. For this purpose, the influence of the *Clear*^{T} on the spheroids size, transparency, PI fluorescence penetration depth (Z-axis) and cross-section diffusion was analyzed.

6.4.1. Influence of *Clear*^{T} on spheroids size

Clearing methods can induce size variations on spheroids, leading to incorrect interpretations due to changes in samples initial morphology [13, 27]. Therefore, spheroids size after each immersion in the *Clear*^{T} solutions was measured. In Figure 6.1 A, it is possible to observe that the spheroids immersion in the formamide solutions does not induce significant changes on their diameter. After the clearing method, spheroids presented a 407 ± 27 μm of diameter, while those that were not cleared displayed a diameter of 378 ± 47 μm. This observation is in agreement with literature, since the *Clear*^{T} method has been described as not having any influence on the size of embryonic mouse brain tissues [18]. In fact, the modifications on spheroids size were not significant once the *Clear*^{T} method does not include dehydration by using organic solvents like methanol (that can induce the samples shrinking) or hydration (that expands the sample) steps [13].

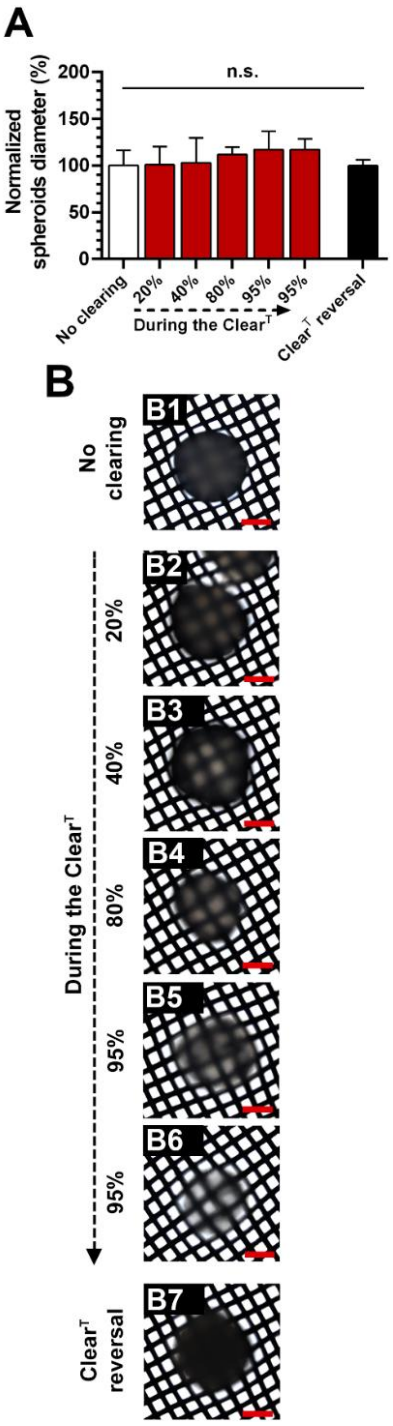

Figure 6.1. Influence of *Clear*^{T} method on NHDF spheroids size and transparency. Normalized diameter of non-cleared spheroids, spheroids during the *Clear*^{T} method and spheroids after clearing reversal (A). Optical microscopy images of spheroids placed on crosshatched backgrounds to show their transparency (B). Scale bars correspond to 200 µm. n = 7, *p < 0.05, n.s. – non-significant.

6.4.2. Influence of *Clear*^{T} on spheroids transparency

Spheroids transparency prompted by the *Clear*^{T} method was observed by acquiring optical microscopy images of spheroids placed on a crosshatched background (Figure 6.1 B). As demonstrated in Figure 6.1, the non-cleared spheroids remained opaque (Figure 6.1 B1), while

the spheroids incubation in *Clear*^{T} solutions with increasing content of formamide turned them gradually more transparent (the highest transparency was observed after spheroids incubation with all the formamide solutions, *i.e.* 20 plus 40 plus 80 plus 95 and plus 95% (Figure 6.1 B2-B6).

6.4.3. *Clear*^{T} reversibility

The evaluation of the *Clear*^{T} reversibility was performed by analyzing the recovery of the cleared spheroids' size and transparency after their incubation with PBS during 30 min [18]. This analysis is fundamental to ensure that the spheroids can be restored to their initial conditions and then be used for further studies like immunohistochemistry [18, 22]. Moreover, such reversibility also ensures that the samples were not chemically modified by the solvents used in the clearing method [22]. The analysis of the spheroids' size after incubation in the saline solution demonstrated that the spheroids' diameter remained unchanged (Figure 6.1 A). However, the cleared spheroids incubated with the saline solution turned opaquer, indicating that the transparency can be reversed (Figure 6.1 B7). In this way, the performed *Clear*^{T} method does not chemically affect the spheroids.

6.4.4. Fluorescence intensity after the use of *Clear*^{T}

Some of the currently available clearing methods are not capable of preserving the fluorescence intensity signal of tissue samples. Such difficult the observation of samples by fluorescence microscopy and also leads to wrong interpretations, like on those studies where fluorescently labeled proteins are analyzed. In the literature, this phenomenon has been reported for several clearing methods including the BABB [36], ClearSee [24], Sca*l*e [24], SeeDB [22] and even the *Clear*^{T} [18]. For instance, the use of formamide solutions to clear embryos diminished the green fluorescent protein (GFP) intensity [18]. However, until now, there are no reports in the literature addressing if the PI fluorescence signal in spheroids is affected by the *Clear*^{T} method. Therefore, the non-cleared and cleared spheroids fluorescence intensity of maximum projections (100 µm) CLSM images were measured, as previously described [21, 27, 31]. Although the *Clear*^{T} method appears to reduce the PI fluorescence intensity, the differences between the non-cleared and cleared spheroids were not statistically significant (Figure 6.2 A). Still, it should be taken into account that formamide may destabilize proteins conformation and decreases the water content in the cells, which may affect the acquired fluorescence signal (water is necessary to maintain the emission from the majority of fluorescent proteins) [13, 18].

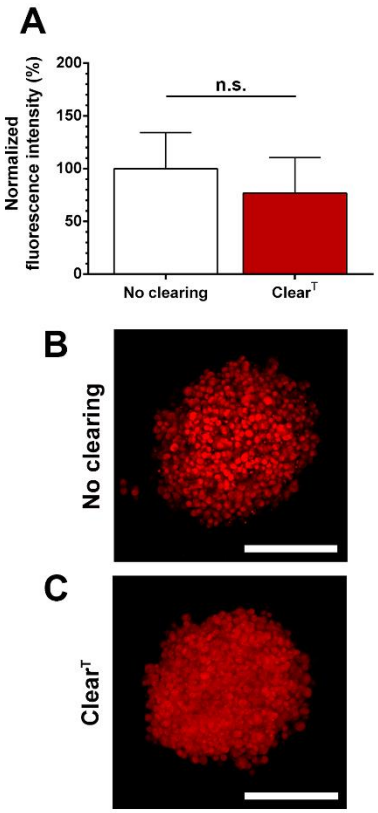

Figure 6.2. Fluorescence analysis of PI stained NHDF spheroids. Fluorescence intensity of *Clear*^{T} cleared spheroids normalized to the average of the non-cleared spheroids fluorescence intensity (A). Maximum intensity projections CLSM images with a thickness of 100 µm; scale bars correspond to 200 µm (B-C). Scale bars correspond to 200 µm. n = 7, *p < 0.05, n.s. – non-significant.

6.4.5. Penetration imaging depth and cross-section imaging depth of PI stained *Clear*^{T} cleared spheroids

As observed in Figure 6.1 B, the *Clear*^{T} method improves the transparency of the spheroids. Samples' transparency is inversely correlated to the scattered light and thus the *Clear*^{T} method has great potential to improve the PI signal penetration depth (Z-axis) [13]. In Figure 6.3, the normalized PI signal penetration depth on CLSM images of cleared and non-cleared spheroids was compared.

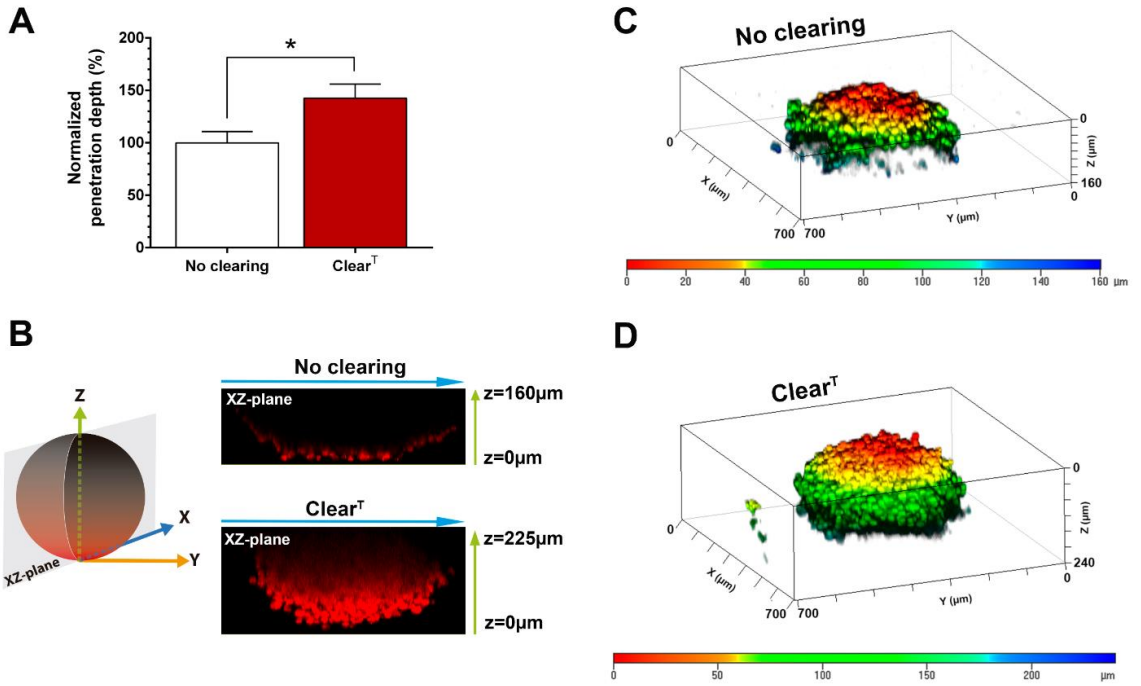

Figure 6.3. CLSM imaging of non-cleared and *Clear*^{T} cleared PI stained NHDF spheroids. Penetration depth along the Z-axis of PI signal in *Clear*^{T} cleared spheroids normalized to the average PI penetration depth in non-cleared spheroids (A). PI fluorescence in XZ-plane (sagittal plane) of the spheroids (B) and depth coding (C-D) CLSM images of non-cleared and cleared spheroids. n = 7, *p < 0.05, n.s. – non-significant.

The results show that the signal penetration depth on the cleared spheroids was about 43% higher than that on the non-cleared spheroids (207.72 ± 19.54 *vs.* 145.71 ± 15.66 µm) - Figure 6.3 A. Despite this improvement, the imaging of the entire structure of the spheroids is still not achieved, once the spheroids have large diameters (407 ± 27 µm). However, the *Clear*^{T} method significantly improves the imaging of spheroids through CLSM. In fact, by using this clearing method, the acquired fluorescence is not circumscribed to the superficial "shell" of the spheroid since it allows the imaging of deeper layers of the spheroid (Figure 6.3 B). Consequently, it is possible to perform a more complete analysis of the spheroid structure as shown on 3D projection images (Figure 6.3 C and D), which may even allow the imaging of the complete structure of spheroids with diameters under 200 µm.

Cross-section imaging depth measurements were also performed to further evaluate the *Clear*^{T} method influence on spheroids imaging through CLSM. For this purpose, the PI fluorescence area in different spheroids cross-section depths along the Z-axis (25, 50, 75 and 100 µm) was measured (Figure 6.4 A).

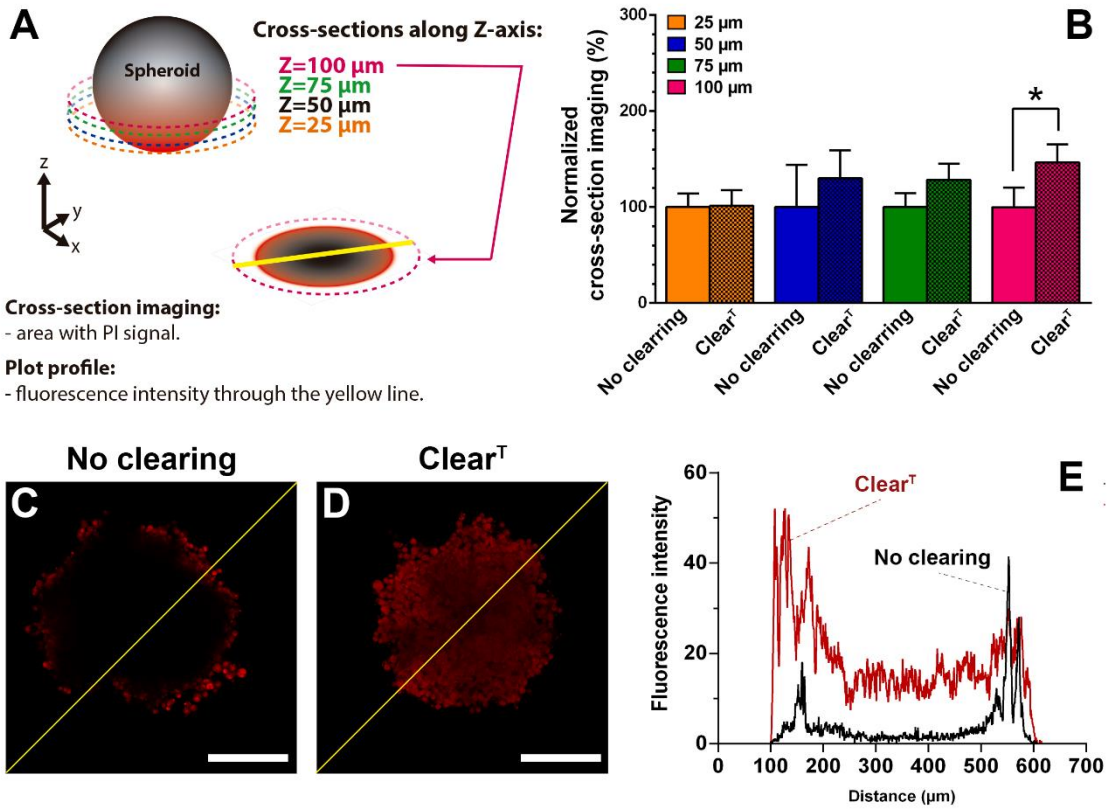

Figure 6.4. PI cross-section imaging depth in non-cleared and *Clear*^{T} cleared NHDF spheroids. Scheme representing the cross-sections selected along the Z-axis for the analysis of the cross-section imaging depth (A). Cleared spheroids PI cross-section imaging depth along the Z-axis (25, 50, 75 and 100 µm) normalized to the average PI cross-section imaging depth in non-cleared spheroids (B). CLSM images of the PI fluorescence in the core of the non-cleared (C) and cleared spheroids (D) at penetration depth of 100 µm, and respective plot profiles (traced using the yellow line) (E). Scale bars correspond to 200 µm. n = 7, *p < 0.05, n.s. – non-significant.

The results demonstrate that the PI signal in the cleared spheroids' cross-sections appeared to be higher, being possible to observe the cells within the microtissues' structure (Figure 6.4 B and D). Further, this result was more evident at 100 µm of depth in the Z-axis, since at this point the cross-section imaging depth was 46.6% higher than that of the non-cleared spheroids (Figure 6.4 B). Plot profiles also support these observations by showing that the PI fluorescence intensity in the core of the cleared spheroid, at penetration depth of 100 µm, was higher than that observed in the non-cleared ones (Figure 6.4 C-E).

6.5. Conclusion

Optical clearing approaches have been employed to improve the 3D microcopy of thick sample, like embryos, mouse brains, skin and other tissues. In this work, the application of the *Clear*^{T} method for the imaging of PI stained spheroids through CLSM was investigated. The obtained

results demonstrated that this simple and organic solvent-free clearing method can improve the imaging of intact bigger spheroid. Overall, the *Clear*^{T} method avoids the use of time-consuming and sample disrupting techniques for the imaging of spheroids' interior regions as well as improved significantly the imaging penetration depth and cross-section depth in intact PI labeled spheroids. In future works, the use of *Clear*^{T} may facilitate the visualization and analysis of the cellular death induced by therapeutics in the spheroids.

6.6. References

1. Breslin, S. and O'Driscoll, L., *Three-dimensional cell culture: the missing link in drug discovery*. Drug Discovery Today, 2013. 18: 240-249.

2. Costa, E. C., *et al.*, *3D tumor spheroids: an overview on the tools and techniques used for their analysis*. Biotechnology Advances, 2016. 34: 1427-1441.

3. Sutherland, R. M., *et al.*, *Resistance to adriamycin in multicellular spheroids*. International Journal of Radiation Oncology, Biology, Physics, 1979. 5: 1225-1230.

4. Sutherland, R. M., *et al.*, *A multi-component radiation survival curve using an in vitro tumour model*. International Journal of Radiation Biology and Related Studies in Physics, Chemistry and Medicine, 1970. 18: 491-495.

5. Gaspar, V. M., *et al.*, *Folate-targeted multifunctional amino acid-chitosan nanoparticles for improved cancer therapy*. Pharmaceutical Research, 2015. 32: 562-577.

6. Moreira, A. F., *et al.*, *Thermo- and pH-responsive nano-in-micro particles for combinatorial drug delivery to cancer cells*. European Journal of Pharmaceutical Sciences, 2017. 104: 42-51.

7. Jyoti, A., *et al.*, *An in vitro assessment of liposomal topotecan simulating metronomic chemotherapy in combination with radiation in tumor-endothelial spheroids*. Scientific Reports, 2015. 5: 15236.

8. Bruns, T., *et al.*, *Preparation strategy and illumination of three-dimensional cell cultures in light sheet–based fluorescence microscopy*. Journal of Biomedical Optics, 2012. 17: 101518.

9. Pampaloni, F., Ansari, N., and Stelzer, E. H. K., *High-resolution deep imaging of live cellular spheroids with light-sheet-based fluorescence microscopy*. Cell and Tissue Research, 2013. 352: 161-177.

10. Santi, P. A., *Light sheet fluorescence microscopy: a review*. Journal of Histochemistry and Cytochemistry, 2011. 59: 129-138.

11. Gong, X., *et al.*, *Generation of Multicellular Tumor Spheroids with Microwell-Based Agarose Scaffolds for Drug Testing*. PLOS ONE, 2015. 10: e0130348.

12. Costa, E. C., *et al.*, *Optimization of liquid overlay technique to formulate heterogenic 3D co-cultures models*. Biotechnology and Bioengineering, 2014. 111: 1672-1685.

13. Richardson, D. S. and Lichtman, J. W., *Clarifying Tissue Clearing*. Cell, 2015. 162: 246-257.

14. Graf, B. W. and Boppart, S. A., *Imaging and analysis of three-dimensional cell culture models*. Methods in Molecular Biology, 2010. 591: 211-227.

15. St Croix, C. M., Shand, S. H., and Watkins, S. C., *Confocal microscopy: comparisons, applications, and problems*. Biotechniques, 2005. 39: S2-S5.

16. Costantini, I., *et al.*, *A versatile clearing agent for multi-modal brain imaging*. Scientific Reports, 2015. 5: 9808.

17. Silvestri, L., *et al.*, *Clearing of fixed tissue: a review from a microscopist's perspective*. Journal of Biomedical Optics, 2016. 21: 081205.

18. Kuwajima, T., *et al.*, *ClearT: a detergent- and solvent-free clearing method for neuronal and non-neuronal tissue*. Development, 2013. 140: 1364-1368.

19. Boutin, M. E. and Hoffman-Kim, D., *Application and assessment of optical clearing methods for imaging of tissue-engineered neural stem cell spheres*. Tissue Engineering Part C: Methods, 2015. 21: 292-302.

20. Silvestri, L., *et al.*, *Micron-scale resolution optical tomography of entire mouse brains with confocal light sheet microscopy*. Journal of Visualized Experiments, 2013: e50696.

21. Grist, S. M., *et al.*, *On-chip clearing of arrays of 3-D cell cultures and micro-tissues*. Biomicrofluidics, 2016. 10: 044107.

22. Ke, M.-T., Fujimoto, S., and Imai, T., *SeeDB: a simple and morphology-preserving optical clearing agent for neuronal circuit reconstruction*. Nature Neuroscience, 2013. 16: 1154-1161.

23. Ke, M.-T., Fujimoto, S., and Imai, T., *Optical clearing using SeeDB*. Bio-protocol, 2014. 4: e1042.

24. Kurihara, D., *et al.*, *ClearSee: a rapid optical clearing reagent for whole-plant fluorescence imaging*. Development, 2015. 142: 4168-4179.

25. Masson, A., *et al.*, *High-resolution in-depth imaging of optically cleared thick samples using an adaptive SPIM*. Scientific Reports, 2015. 5: 16898.

26. Song, E., *et al.*, *Optical clearing assisted confocal microscopy of ex vivo transgenic mouse skin*. Optics & Laser Technology, 2015. 73: 69-76.

27. Yu, T., *et al.*, *Rapid and prodium iodide-compatible optical clearing method for brain tissue based on sugar/sugar-alcohol*. Journal of Biomedical Optics, 2016. 21: 081203.

28. Napolitano, A. P., *et al.*, *Scaffold-free three-dimensional cell culture utilizing micromolded nonadhesive hydrogels*. Biotechniques, 2007. 43: 494-500.

29. Carvalho, M. P., Costa, E. C., and Correia, I. J., *Assembly of breast cancer heterotypic spheroids on Hyaluronic Acid coated surfaces*. Biotechnology Progress, 2017. 33: 1346-1357.

30. Rasband, W. S., *ImageJ*. http://rsbweb. nih. gov/ij/, 2008.

31. Klaka, P., *et al.*, *A novel organotypic 3D sweat gland model with physiological functionality*. PLOS ONE, 2017. 12: e0182752.

32. Decroix, L., *et al.*, *Tissue clearing for confocal imaging of native and bio-artificial skeletal muscle*. Biotechnic & Histochemistry, 2015. 90: 424-431.

33. Chubinskiy-Nadezhdin, V. I., Negulyaev, Y. A., and Morachevskaya, E. A., *Simvastatin induced actin cytoskeleton disassembly in normal and transformed fibroblasts without affecting lipid raft integrity*. Cell Biology International, 2017. 41: 1020-1029.

34. Lipskaia, L., *et al.*, *SERCA2a gene transfer prevents intimal proliferation in an organ culture of human internal mammary artery*. Gene Therapy, 2013. 20: 396-406.

35. Svoboda, K. and Yasuda, R., *Principles of Two-Photon Excitation Microscopy and Its Applications to Neuroscience*. Neuron, 2006. 50: 823-839.

36. Yushchenko, D. A. and Schultz, C., *Geklärte Gewebeproben für die optische Anatomie*. Angewandte Chemie, 2013. 125: 11151-11154.

Chapter 7

Research Work 2

Polyethylene glycol molecular weight influences the *Clear^{T2}* optical clearing method for spheroids imaging by confocal laser scanning microscopy

This chapter is based on the publication entitled: Polyethylene glycol molecular weight influences the Clear^{T2} optical clearing method for spheroids imaging by confocal laser scanning microscopy, Journal of Biomedical Optics, 2018, 23(5):1-11.

7.1. Abstract

Some fluorescence microscopy techniques, like confocal laser scanning microscopy (CLSM), have a limited penetration depth. Consequently, the visualization and imaging of three-dimensional (3D) cell cultures, such as spheroids, using these methods can be a significant challenge. Therefore, to improve the imaging of 3D tissues, optical clearing methods have been optimized to render transparency to the opaque spheroids. In this work, the influence of the polyethylene glycol (PEG) molecular weight (MW) used in the *Clear*^{T2} method for the imaging of propidium iodide (PI) stained spheroids was investigated. The results demonstrated that the *Clear*^{T2} clearing method contributes to spheroids transparency and to the preservation of PI fluorescence intensity for all the PEG MW used (4000, 8000 and 10000 Da). Further, the *Clear*^{T2} method performed using PEG 4000 Da allowed a better PI signal penetration depth and cross-section depth. Overall, the optimization of PEG MW can improve the imaging of intact spheroids by CLSM. Further, this work may also contribute to increase the application of 3D cell culture models by the pharmaceutical industry for the high-throughput screening of therapeutics.

Keywords: *Clear*^{T2}; confocal microscopy; polyethylene glycol; propidium iodide; spheroids.

7.2. Introduction

During the preclinical drug development phase, compound libraries must be thoroughly tested. For this purpose, cells cultured as monolayers on flat surfaces are the gold-standard model used to evaluate the effectiveness and safety of the therapeutics in development [1]. Still, this type of cell culture model has been associated with lack of correspondence between the results obtained *in vitro* and those obtained in *in vivo* or in clinical trials [1-3]. Therefore, there has been an increasing need to improve the reliability of the *in vitro* methodologies in the high through screening of new drugs. To address this issue, 3D cell culture models have been developed. In the 70s, 3D cellular aggregates - spheroids - started to be produced with the aim of mimicking the features of solid tumors, such as cellular organization, cell-cell and cell-extracellular matrix (ECM) interactions, gene expression profile and drug resistance mechanisms (reviewed in detail in [4, 5]).

Despite the advantages of 3D cell cultures, performing experiments on spheroids introduces new challenges since the methodologies and the equipment currently used for therapeutics screening are only optimized for cells cultured as monolayers. Fluorescence microscopy, such as light sheet fluorescence microscopy (LSFM), two-photon microscopy multiphoton microscopy and single (or selective) plane illumination microscopy have demonstrated an excellent performance in the *in vitro* analysis of therapeutics on spheroids [4, 6, 7]. Still, most laboratories are equipped with CLSM apparatus, which has been used to determine spheroids' size [8], morphology [9], internal cellular organization [10, 11], expression of proteins (*e.g.* α-tubulin and E-cadherins) [10, 12], as well as to evaluate the penetration and efficacy of therapeutics (*e.g.* drugs and delivery systems) in the spheroid [8, 13-15]. However, taking into account that spheroids are thick opaque samples with diameters between few hundred micrometers to few millimeters, the observation of whole spheroids by CLSM is hindered by the low penetration depth of this equipment (usually less than 100 μm) [4, 6, 16]. This handicap is usually surpassed by slicing the spheroids into thin sections (3-7 μm) [17, 18]. However, the sectioning of spheroids is a laborious and time-consuming process that depends on organic solvents and can induce the disruption of the initial morphology of the spheroid (due to the introduction of structural artifacts) [4, 19, 20].

Another approach that has been employed to facilitate the imaging of 3D thick samples is the use of optical clearing methods. These clearing techniques have been applied in the deep imaging of embryos and mouse tissues (*e.g.* brain, skin and skeletal muscle) [21-25], and more recently started to be applied in the imaging of spheroids [26, 27]. In general, the optical clearing methods reduce the light scattering induced by the cells and make the samples more transparent, thus enhancing light penetration and, consequently, the images quality [6].

The clearing methods developed so far include the 3DISCO, ACT-PRESTO, BABB, *Clear*^{T}, *Clear*^{T2}, CLARITY, CUBIC, FocusClear™, FRUIT, iDISCO, PACT/PARS, RTF, Sca*l*e, Sca*l*eA2, Sca*l*eS, Sca*l*eU2, SeeDB, SeeDB2, TDE, uDISCO, among others (reviewed by Azaripour *et al.* [25], Tainaka *et al.* [28], Richardson *et al.* [6] and Seo *et al.* [29]). In 2013, *Clear*^{T2} was described for the first time by Kuwajima and collaborators [22]. Compared to the other methods, the *Clear*^{T2} is quicker and it does not use detergents or organic solvents. The *Clear*^{T2} protocol involves the immersion of the samples in aqueous solutions with increasing concentrations of formamide and PEG [22]. These clearing solutions will promote the replacement of the water inside the cells by the aqueous solutions of formamide and PEG until an equilibrium is reached, while maintaining the sample hydrated, reducing the overall refractive index (RI) of the sample and improving samples' transparency [6, 22, 29, 30]. On the other side, PEG is used to maintain the integrity and stability of the fluorescently labeled elements (*e.g.* proteins), thus avoiding the fluorescence quenching prompted by the formamide [6, 22, 29, 30].

So far, PEG with a MW of 8000 Da has been used in the *Clear*^{T2} method [22, 26]. Still, some studies demonstrated that PEG with other MW can also be used to stabilize proteins [31, 32]. In this way, disclosing the optimal PEG MW for spheroids clearing by *Clear*^{T2} may improve their analysis through CLSM and their potential for high throughput screening of therapeutics. Herein, the influence of the PEG MW (4000, 8000 and 10000 Da) used in the *Clear*^{T2} method in the imaging of PI stained spheroids was investigated. For this purpose, PI was selected since it is commonly applied for spheroids analysis and it was also used in other works, where clearing methods were investigated [10, 33-37]. After imaging whole non-cleared and cleared spheroids through optical and CLSM, images were analyzed to characterize the effect of the *Clear*^{T2} method variations on spheroids' morphology, transparency, fluorescence, imaging penetration depth and cross-section imaging depth.

7.3. Materials and Methods

7.3.1. Materials

Normal human dermal fibroblasts (NHDF) were bought from PromoCell (Labclinics, S.A.; Barcelona, Spain). Cell imaging plates were acquired from Ibidi GmbH (Ibidi, Munich, Germany). Agarose was purchased from Grisp (Porto, Portugal). Cell culture plates, T-flasks and cell culture consumables were obtained from ThermoFisher Scientific (Porto, Portugal). Dulbecco's Modified Eagle's Medium F-12 (DMEM-F12), formamide (≥ 99.5%), paraformaldehyde (PFA), phosphate-buffered saline (PBS), trypsin and ethylenediaminetetraacetate (EDTA), PEG 4000, 8000 and 10000 Da were purchased from Sigma-Aldrich (Sintra, Portugal). Fetal bovine serum (FBS) was obtained from Biochrom AG (Berlin, Germany). PI was purchased from Invitrogen (Carlsbad, CA, USA).

7.3.2. Methods

7.3.2.1. Cell Line maintenance and NHDF spheroids production by micromolding

NHDF were cultured in DMEM-F12, with 10% (v/v) FBS and 1% streptomycin and gentamycin, inside an incubator with a humidified atmosphere at 37 ºC and 5% CO_2 [10]. After cells attained confluence, they were recovered by using 0.25% trypsin (1:250) and EDTA 0.1% (w/v).

Spheroids were fabricated by using agarose structures with spherical microwells to guide the cells self-assembly [38]. The agarose structures were produced by placing 2% (w/v) agarose solution on 3D Petri Dish® templates (Microtissues Inc., Providence RI, US) [13]. Before use, the agarose structures were placed in 12-well cell culture plates and sterilized by ultraviolet (UV) radiation. NHDF cells were then seeded by using $1x10^6$ cells per agarose structure, prompting the formation of 81 spheroids. Spheroids were maintained in culture with DMEM-F12 (10% (v/v) FBS and 1% streptomycin and gentamycin) at 37 ºC in a humidified atmosphere with 5% CO_2.

7.3.2.2. Whole NHDF spheroids fixation and staining with PI

Spheroids used in the experiments grew for 6 days. After this period, whole spheroids were recovered and then subjected to a chemical fixation process that encompasses spheroids incubation with PFA 4% (w/v) during 24 h, at 4 ºC [10]. The PFA solution was freshly prepared to minimize its autofluorescence [39]. After fixation, the spheroids were washed three times with PBS and then labeled with 1 mL of PI (10 µg/mL in H_2O), as previously described [10, 11]. After 24 h of spheroids incubation with the fluorescent probe on a plate shaker at 100 rotations per minute (RPM), spheroids were washed 3 times with PBS to remove the excess of PI.

7.3.2.3. Whole spheroids clearing by using the *Clear*^{T2} method

The *Clear*^{T2} clearing method variations (*Clear*^{T2}*/4*, *Clear*^{T2}*/8* and *Clear*^{T2}*/10* that use PEG with a MW of 4000, 8000 and 10000 Da, respectively) were performed accordingly to previous works [22, 26] - see Figure 7.1 for the pipeline overview of the method.

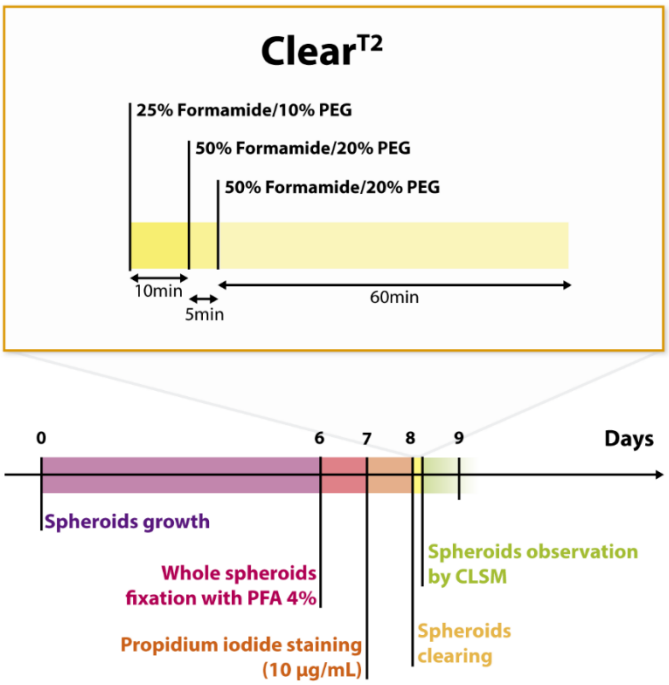

Figure 7.1. Pipeline overview of the spheroids formation, labeling with the PI and clearing with *Clear*^{T2}. The *Clear*^{T2} clearing procedure was performed by using PEG with different MW: *Clear*^{T2}*/4* (PEG 4000 Da), *Clear*^{T2}*/8* (PEG 8000 Da) and *Clear*^{T2}*/10* (PEG 10000 Da).

Initially, whole PI stained spheroids were immersed in a 25% formamide/10% PEG solution during 10 min. Afterward, spheroids were immersed in 50% formamide/20% PEG solution during 5 min and lastly in another 50% formamide/20% PEG solution during 1 h. PEG 4000, 8000 and 10000 Da were used to prepare the solutions used in the *Clear*^{T2}*/4*, *Clear*^{T2}*/8* and *Clear*^{T2}*/10* method, respectively. All *Clear*^{T2} methods were performed at room temperature (RT) using a plate shaker at 100 RPM.

For comparative purposes, some spheroids were only immersed in PBS instead of the clearing solutions (non-cleared PI stained spheroids). Moreover, non-stained spheroids were subjected to *Clear*^{T2} methods (cleared non-stained spheroids) to evaluate the influence of the method in the spheroids' autofluorescence.

After the clearing of the intact spheroids, samples were transferred to µ-slide 8-well imaging plates (Ibidi GmbH, Germany) for imaging experiments.

7.3.2.4. Whole spheroids imaging by optical and CLSM

To observe any possible changes in spheroids size and transparency due to the clearing method, optical microscopy images were acquired by using Olympus CX41 inverted optical microscope equipped with an Olympus SP-500 UZ digital camera and a Carl Zeiss Axio Imager A1 inverted microscope equipped with an AxioVision camera.

Images of intact NHDF spheroids were also acquired through CLSM using a Zeiss LSM 710 AxioObserver laser scanning confocal microscope (Carl Zeiss SMT, Inc., Oberkochen, Germany). For comparative purposes, all the samples were analyzed using the same equipment settings. The objective used was a 20x air objective (Plan-Apochromat 20x/0.8 M27, working distance = 0.55 mm). The size of the confocal aperture was 1 Airy disk and Z-stacks were collected with 5 µm intervals. Laser power and master gain were kept constant during image acquisition. PI was visualized with a 514 nm Argon laser. All the analysis described hereafter were performed by using an image processing program designed for scientific analysis – ImageJ, National Institutes of Health [40].

7.3.2.5. Measurement of the spheroids area and transparency

Spheroids area before and after the clearing process, and after clearing reversal was determined by analyzing optical microscopy images (Olympus CX41 inverted optical microscope equipped with an Olympus SP-500 UZ digital camera), as previously demonstrated in our work [10]. In brief, the area of spheroids was selected in the image by using a threshold and then the area of the spheroids was determined by converting the area in pixels to µm^2 values (Figure 7.2).

The transparency of the spheroids before and after clearing, as well as after the clearing reversal was observed by placing the spheroids on a grill that will serve as a crosshatched background to show relative differences in transparency (as performed previously [21, 22, 26, 35, 36, 41]). Then, optical microscopy images were acquired by using a Carl Zeiss Axio Imager A1 inverted microscope equipped with an AxioVision camera.

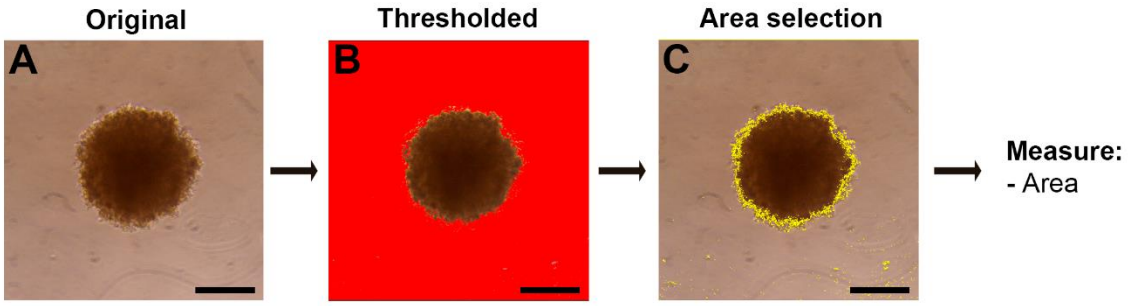

Figure 7.2. Schematic representation of the procedures used for the measurement of the spheroids area through optical microscopic images. Scale bars correspond to 200 µm.

7.3.2.6. Measurement of PI fluorescence intensity

The determination of the PI fluorescence levels in the spheroids was performed as previously described by Yu *et al.* [35] and Grist and Nasseri [42]. Initially, a maximum intensity z-projection of the CLSM image with a thickness of 50 and 100 µm (10 and 20 Z-stacks, respectively) was performed (Figure 7.3 A).

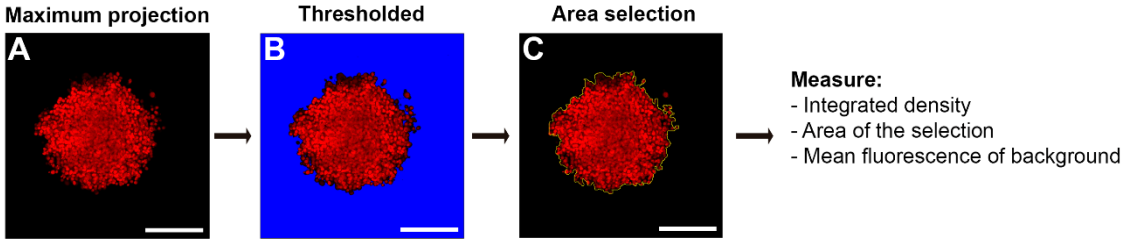

Figure 7.3. Schematic representation of the procedures used in the analysis of CLSM images to evaluate the spheroids PI fluorescence intensity by calculating the CTCF. Scale bars correspond to 200 µm.

Then, the spheroid area was selected by applying a threshold (Figure 7.3 B and C). Afterward, the integrated density (ID), the selected area (SA) and the mean fluorescence of the background (MFB; region without fluorescence) were measured. These values were then used to determine the PI fluorescence intensity through the calculation of the corrected total cell fluorescence (CTCF) [43] - Equation (1).

$$\mathrm{CTCF} = \mathrm{ID} - (\mathrm{SA} \times \mathrm{MFB}) \qquad (1)$$

The results were compared and normalized to those obtained for non-cleared PI stained spheroids (spheroids that were only treated with PBS).

7.3.2.7. Measurement of the PI imaging depth and cross-section imaging depth

The imaging depth of PI was determined by multiplying the number of stacks with PI fluorescence signal by the Z-stacks thickness (5 µm).

The determination of the PI cross-section imaging depth was performed by calculating the mean gray value of the spheroid selected area at 25, 50, 75 and 100 µm of penetration depth (Figure 7.4 A-C). The mean gray value is a relation between the number of pixels with color in a selected area and the intensity of this color. When the mean gray value is equal to 0, it corresponds to pixels without color (no fluorescence). Mean gray values between 1-250 corresponds to pixels with color and higher mean gray value correspond to higher color intensity.

The results were compared and normalized to those obtained for non-cleared PI stained spheroids (spheroids that were only treated with PBS).

Additionally, similarly to previous works [41, 44], the cross-section imaging depth of PI in the spheroids was analyzed by tracing plot profiles, *i.e.* a graph of the pixels fluorescence intensities along a line traced in the spheroid (Figure 7.4 D). The plot profiles were obtained at 75 µm of penetration depth.

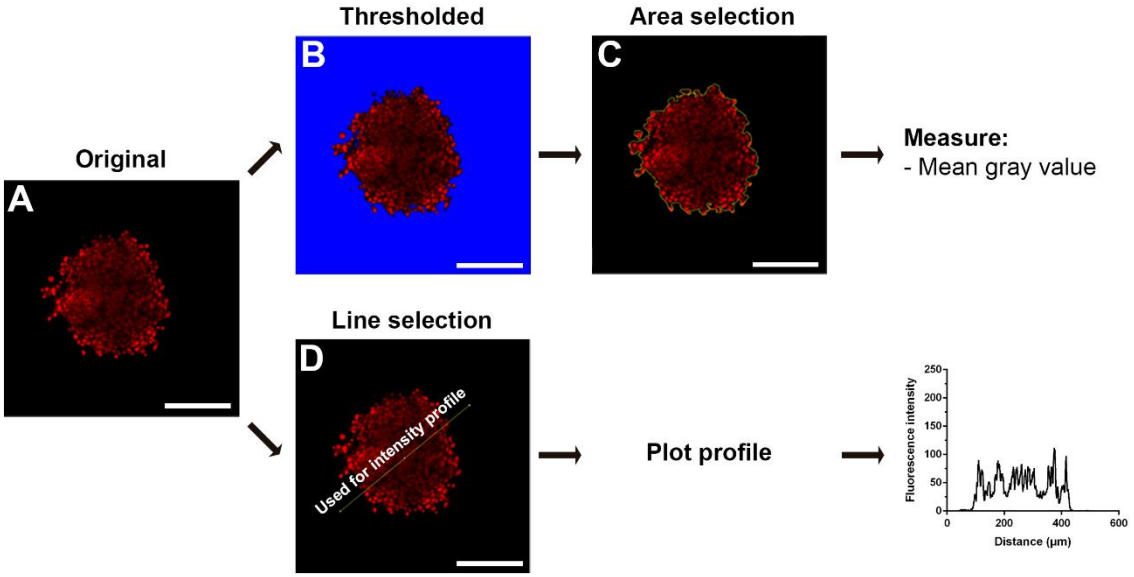

Figure 7.4. Schematic representation of the procedures used to analyze the PI cross-section imaging depth by the determination of mean gray value and plot profile. Scale bars correspond to 200 µm.

7.3.2.8. Statistical analysis

Data was expressed as mean values ± standard deviation (SD). The statistical analysis was performed by using one-way ANOVA test. A value of $p < 0.05$ was considered statistically significant. Data analysis was performed in GraphPad Prism v.6.0 software (Trial version, GraphPad Software, CA, USA).

7.4. Results and Discussion

In this study, spheroids composed of NHDF cells were chosen due to their superior capacity to maintain their structure and integrity during the clearing process, as previously demonstrated by our group [10]. Such approach bypasses interferences of spheroids' low cohesiveness on their structure and size during the clearing method.

Spheroids were produced by seeding cells on non-adhesive concave microwells, resulting in the formation of reproducible 3D spherical cellular aggregates with a diameter of 396.17 ± 28.72 µm, after 6 days of culture. After spheroids' fixation, they were stained with PI, a red-fluorescent stain that has been widely used for the evaluation of spheroids cellular viability through fluorescence microscopy and also in other works for optimizing the clearing methods [10, 33-37]. Then, whole spheroids were cleared by immersing them in formamide/PEG solutions (MW: 4000 Da (*Clear*^{T2}*/4*), 8000 Da (*Clear*^{T2}*/8*) or 10000 Da (*Clear*^{T2}*/10*)) and then they were observed through optical and CLSM.

7.4.1. *Clear*^{T2} clearings do not influence spheroids' size and enhance their transparency

A suitable clearing method must preserve samples' size and structure in order to allow the study of its initial morphology [35]. Additionally, the clearing method should not increase samples' dimensions, since larger samples require longer imaging times and they may also become unsuited for whole imaging through CLSM [6]. Therefore, the effect of *Clear*^{T2} methods in the preservation of the spheroids' morphology was evaluated by comparing the area of the cleared spheroids with that of the non-cleared spheroids (Figure 7.5).

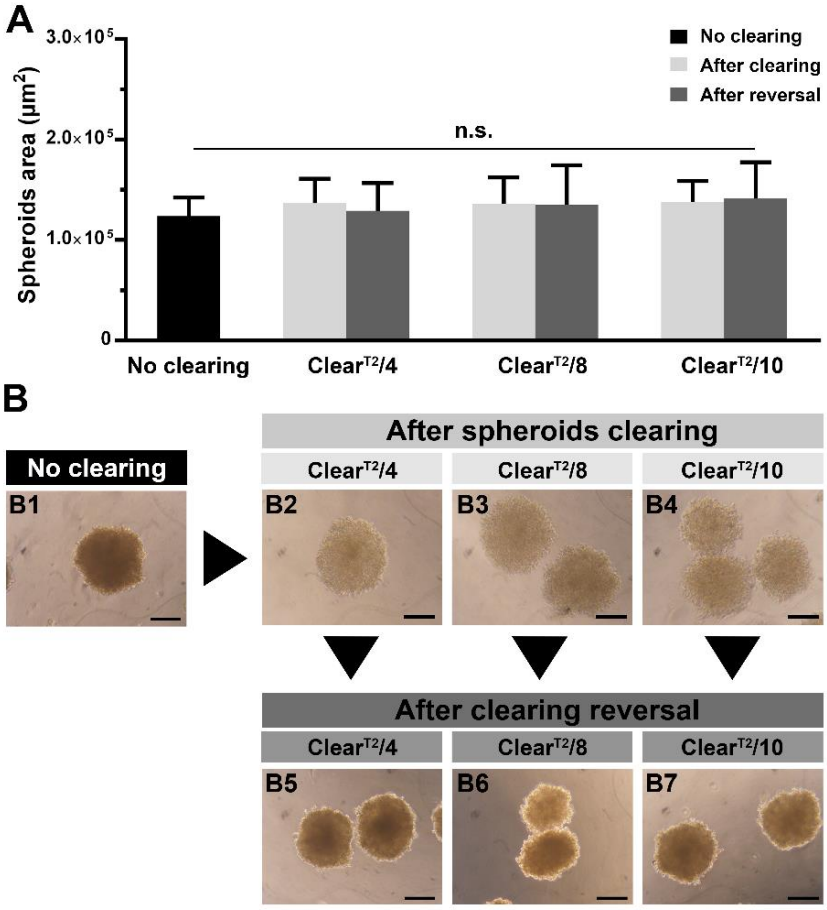

Figure 7.5. Influence of *Clear*^{T2} methods on NHDF spheroids size. Area measurements (A) and optical microscopy images (B) of non-cleared spheroids, spheroids cleared using *Clear*^{T2}*/4*, *Clear*^{T2}*/8* or *Clear*^{T2}*/10* methods, and spheroids after reversing the clearing process. Scale bars correspond to 200 µm. n = 8, *p < 0.05, n.s. – non-significant.

The mean area of the spheroids cleared by *Clear*^{T2}*/4*, *Clear*^{T2}*/8* and *Clear*^{T2}*/10* increased by 10.35, 9.91 and 10.11%, respectively, when compared to that of the non-cleared spheroids (Figure 7.5 A). The slight increase of spheroids' size was not statistically significant, which demonstrates that all the *Clear*^{T2} methods did not induce any significant changes on the spheroids' morphology and that PEG MW does not affect spheroids' size during the clearing procedure (Figure 7.5). Similar results were obtained in other studies, which demonstrated that

the *Clear*^{T2} method performed with PEG 8000 Da did not induce significant volume changes on brain sections [22] or on spheroids [26]. In fact, morphological and volumes changes are mostly associated to organic solvent-based clearing methods, which use benzylalcohol/benzylbenzoate (*e.g.* BABB) or dichloromethane/dibenzylether (*e.g.* 3DISCO and iDISCO) [6].

The capacity of the *Clear*^{T2} clearing methods to enhance the transparency of spheroids was also observed in the optical microscopy images, as previously reported in the literature [21, 22, 26, 35, 36, 41]. The results demonstrated that, independently of the PEG MW used in the clearing process, all spheroids become gradually more transparent after each immersion step in the clearing solutions (Figure 7.6). In fact, the transparency of the spheroids did not seem differ between the different *Clear*^{T2} methods variations. Such is explained by the fact that formamide is the main agent responsible for rendering transparency to the cells [6, 45], and that all the samples were immersed in solutions containing the same concentration of formamide.

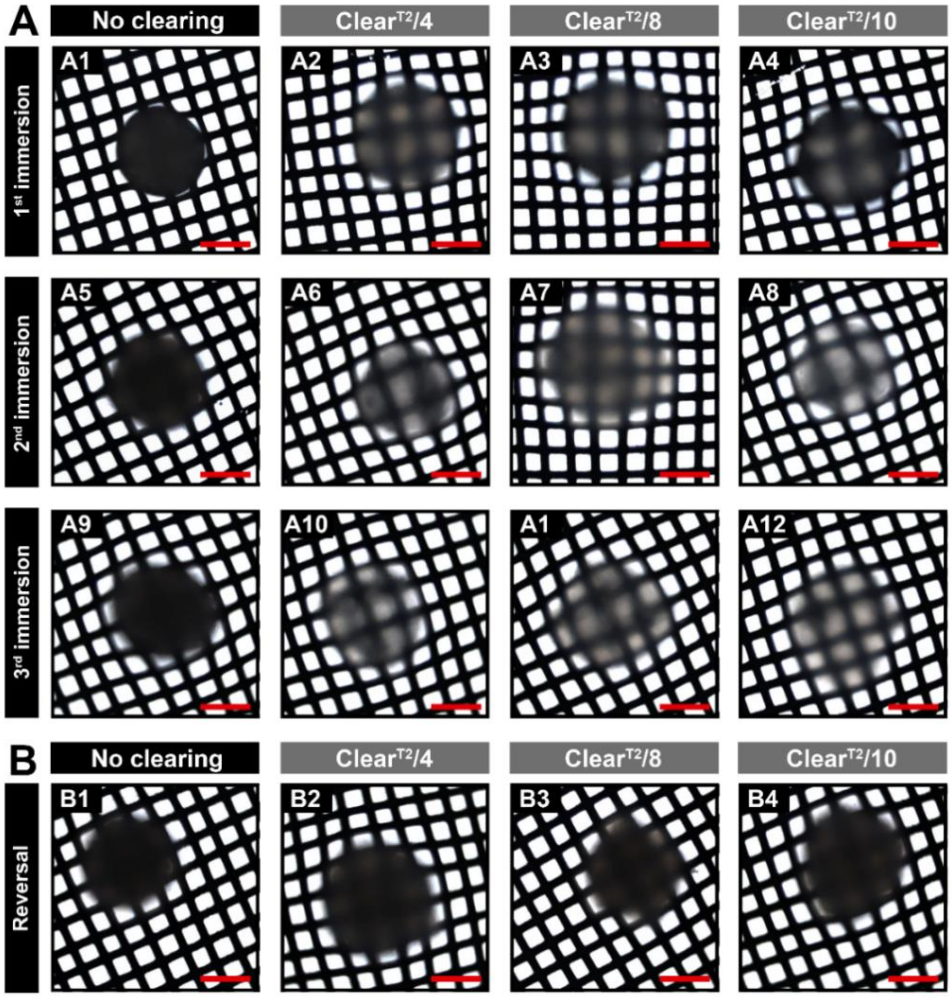

Figure 7.6. NHDF spheroids transparency after the *Clear*^{T2} methods. Optical transparency of non-cleared spheroids, and cleared spheroids with *Clear*^{T2}*/4*, *Clear*^{T2}*/8* and *Clear*^{T2}*/10* (A). Spheroids transparency after clearing reversal with PBS during 30 min (B). Spheroids were imaged on crosshatched backgrounds to show relative differences in transparency. Scale bars correspond to 200 µm.

7.4.2. *Clear*^{T2} clearing methods are reversible

The reversibility of the clearing methods, *i.e.* if the cleared samples can return to their original morphology and non-transparency, is also important for the application of spheroids in therapeutics screening [22, 23]. According to Ke *et al.*, the reversibility of the clearing method also enables the analysis of the same samples by other techniques (*e.g.* immunohistochemistry) [23]. Additionally, non-reversible clearing methods may be indicative that the sample is chemically modified during its treatment, leading to unrealistic interpretations [23].

Kuwajima *et al.* already demonstrated that the *Clear*^{T2} method that uses PEG 8000 Da can be reversed by immersing samples of mice embryos in PBS [22]. Herein, it was evaluated if PEG with other MW have any influence in the clearing reversal process of the spheroids. For this purpose, the size and transparency of the cleared spheroids were also evaluated after immersion in a PBS solution during 30 min. Independently of the *Clear*^{T2} method used, all spheroids maintained their original size (Figure 7.5 A) and were able to return to their non-transparent state (Figure 7.6). Therefore, the results indicate that the PEG MW does not influence the *Clear*^{T2} reversibility and/or that it does not induce permanent modifications on spheroids' general structure.

7.4.3. *Clear*^{T2} methods preserve the PI fluorescence intensity

The clearing process should not affect negatively the fluorescence intensity of the samples, *i.e.* clearing methods must preserve the fluorescence intensity in order to allow their imaging through fluorescence microscopy. In previous studies, it was demonstrated that some clearing methods, such as BABB [46] and Sca*l*e [41], lack in the preservation of the probes fluorescence intensity due to the fluorescence quenching effect. Such effect was also observed in tissues that were only cleared with formamide (*Clear*^{T} method) [22]. This result may be explained by protein denaturation caused by formamide [6]. In order to surpass this drawback, PEG was added to the formamide solutions to stabilize proteins' structure and maintain their fluorescence. Kuwajima *et al.* reported that the addition of PEG 8000 Da to formamide resulted in the preservation of the fluorescence of proteins, immunohistochemistry labeling and dye tracers (*e.g.* 1,1'-dioctadecyl-3,3,3',3'-tetramethylindocarbocyanine perchlorate (DiI)) [22]. Still, in other studies it was demonstrated that the use of PEG 8000 Da did not contribute to preserve the fluorescence intensity of PI within mice brain sections [35].

Therefore, we investigated the influence of the PEG MW on the *Clear*^{T2} capacity to preserve the fluorescence intensity of labeled spheroids. For this purpose, the fluorescence of the PI stained non-cleared and *Clear*^{T2}*/4*, *Clear*^{T2}*/8* and *Clear*^{T2}*/10* cleared spheroids was determined as previously described elsewhere [35]. From the analysis of the maximum projection images (thickness equal to 50 and 100 µm) - Figure 7.7 A, it was possible to verify that all the *Clear*^{T2} methods under investigation, were able to preserve the fluorescence of the PI (Figure 7.7 B and C).

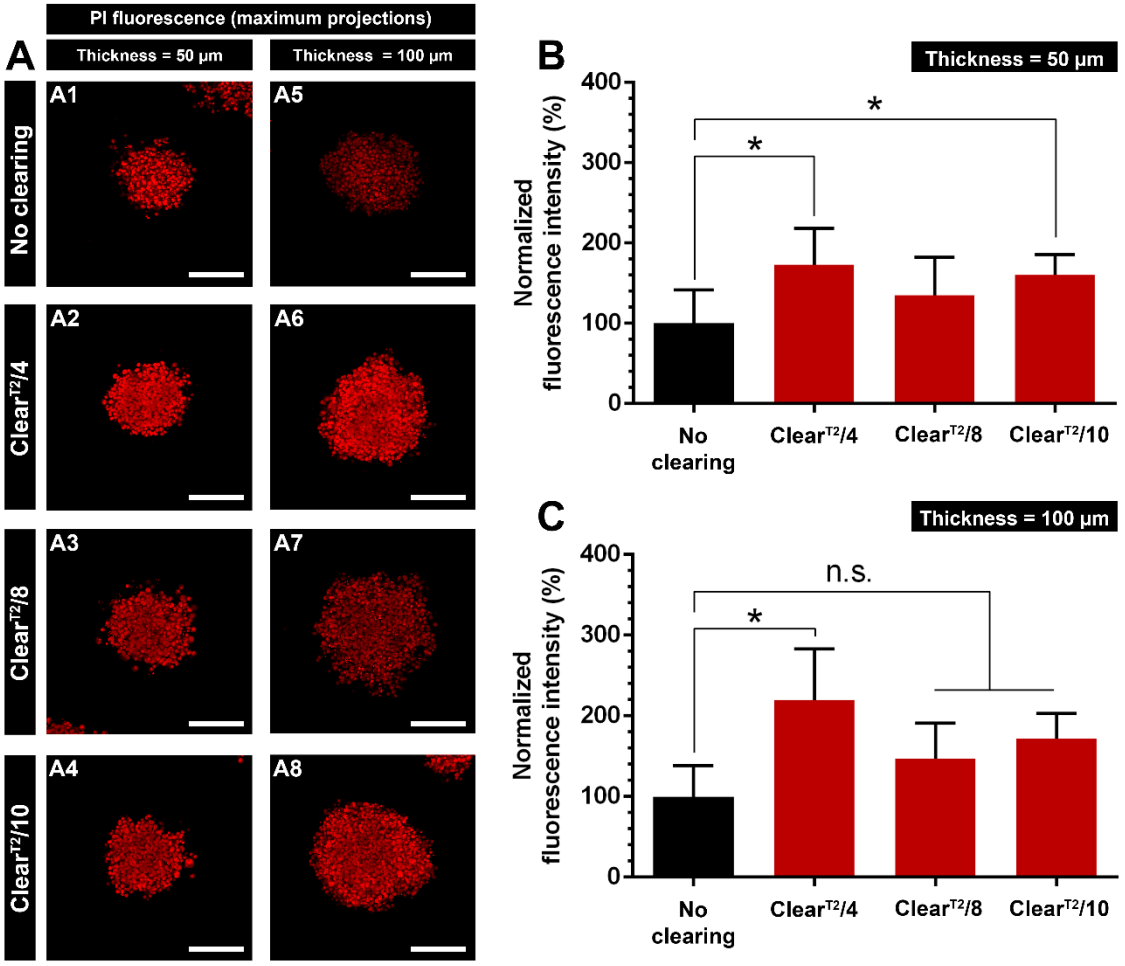

Figure 7.7. Influence of *Clear*^{T2} methods on NHDF spheroids PI fluorescence intensity. CLSM images of PI stained non-cleared and *Clear*^{T2}*/4*, *Clear*^{T2}*/8* and *Clear*^{T2}*/10* cleared spheroids (A). Each image is a maximum projection of the Z-stacks (thickness: 50 and 100 µm). Analysis of the fluorescence intensity of the spheroids stained with PI for the maximum projections of 50 µm (B) and 100 µm (C) of thickness. Scale bars correspond to 200 µm. n = 5, *p < 0.05, n.s. – non-significant.

However, among the *Clear*^{T2} methods variations, *Clear*^{T2}*/4* demonstrated a significantly higher capacity to preserve the PI fluorescence, even at deep penetration depths (Figure 7.7 B and C). Importantly, this improved fluorescence intensity was not prompted by the autofluorescence of the clearing solutions constituents, since all the solutions used in the various *Clear*^{T2} methods have a transmittance of ≈ 100% from 400-800 nm (the absorbance peaks of the PEG polymers-formamide solutions occurs below 400 nm and according to literature PEG has absorbance below 400 nm [47, 48]) - Figure 7.8.

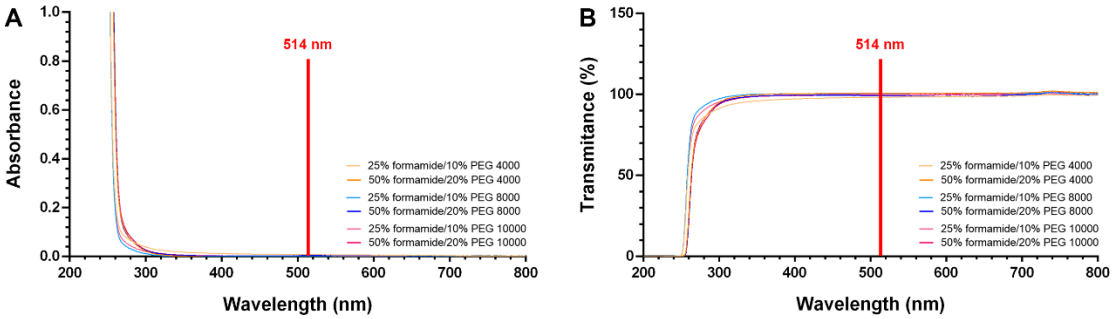

Figure 7.8. Absorbance (A) and transmittance (B) of the solutions used on the *Clear*^{T2}*/4*, *Clear*^{T2}*/8* and *Clear*^{T2}*/10* clearing methods.

In other words, the clearing solutions are permissive to the PI excitation laser light (514 nm) and the emitted fluorescence (550-750 nm) is not absorbed by the solutions (Figure 7.8). Moreover, non-stained cleared spheroids did not present fluorescence signals when analyzed in the same conditions used for PI stained spheroids (Figure 7.9).

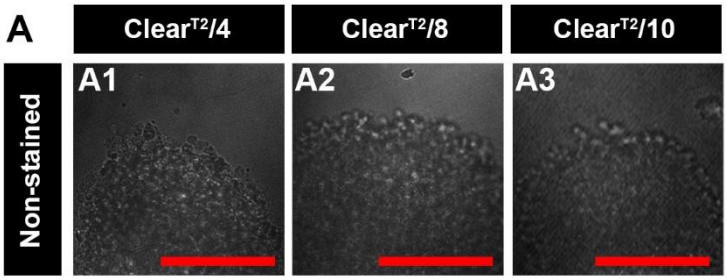

Figure 7.9. Autofluorescence of cleared non-stained spheroids. Differential interference contrast (DIC) merged with fluorescence images (red channel) of non-stained *Clear*^{T2}*/4* (A1) *Clear*^{T2}*/8* (A2) and *Clear*^{T2}*/10* (A3) cleared spheroids. Images correspond to a z-tack at a penetration depth of 25 µm Scale bars corresponds to 200 µm.

7.4.4. PI imaging depth and cross-section imaging are significantly improved by using the *Clear*^{T2}*/4* method

The fluorescence signal depth in CLSM is limited by the equipment (*e.g.* the working distance of the commonly used objectives) and also by the scattering phenomena between the specimen and the excitation and emission photons [4, 6]. Consequently, CLSM is more prone to be used for the imaging of thin samples (*e.g.* 2D cultures or sliced tissues). Nevertheless, in order to improve the imaging of whole thick samples (*e.g.* spheroids) by CLSM and avoid the handicaps associated with samples sectioning [4, 19, 20], the reduction of the light scattering by using optical clearing methods has been investigated [16]. To accomplish that, some clearing methods (*e.g.* Sca*l*e) remove the cellular lipids which are the main source of light scattering [6, 21]. On the other hand, clearing methods such as the Clear^{T2} reduce the inhomogeneity of the light scatter by equilibrating the RI throughout the sample [6]. In the *Clear*^{T2} method, the formamide and PEG aqueous solutions have a RI ≈ 1.44 that will match with the overall RI of the fixed tissue (RI ≈ 1.50) [6, 29, 49].

To study the possible improvement in the imaging depth after spheroids clearing by *Clear*^{T2} methods and the PEG MW influence on this process, the penetration depth of the PI fluorescence signal was measured and presented in Figure 7.10. The results show that the *Clear*^{T2}*/4* improved significantly the penetration depth of the PI signal (Figure 7.10 B and C). In fact, the use of PEG 4000 Da allowed to detect PI signal up to 211.67 ± 16.81 µm, while the PEG 8000 and 10000 Da only enabled the acquisition of a signal up to 183.89 ± 14.13 and 176.43 ± 11.44 µm, respectively.

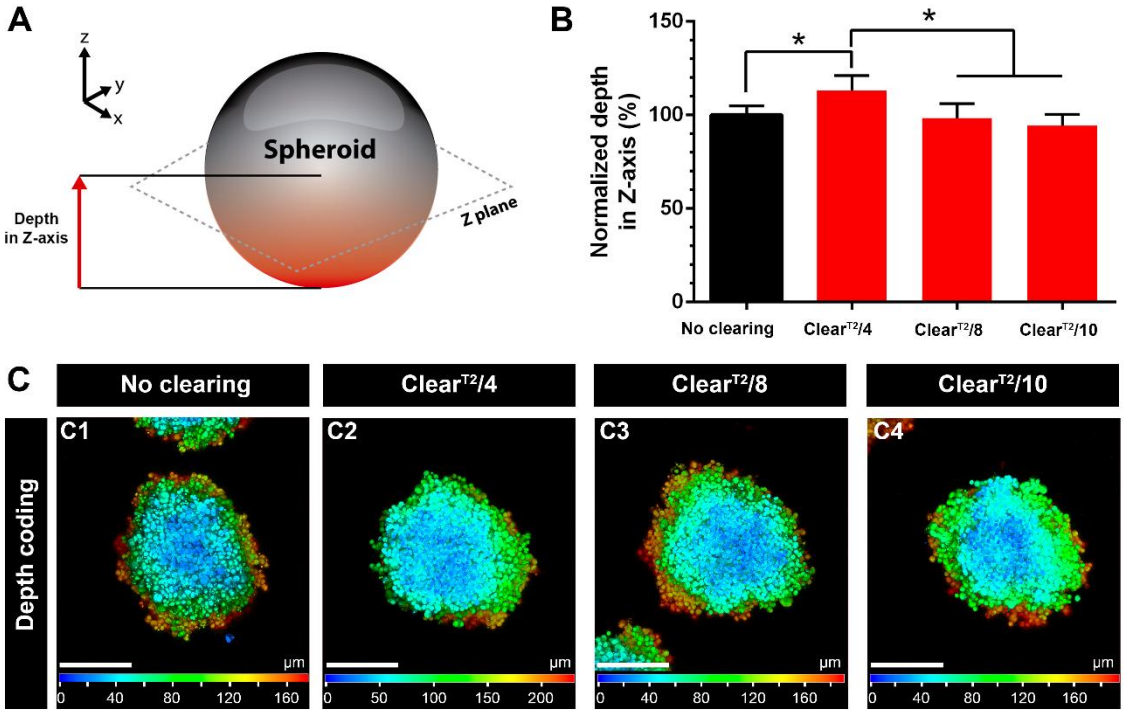

Figure 7.10. Quantitative representation of PI imaging depth in the NHDF spheroids. Schematic representation of the penetration depth measured in the spheroids (A). Penetration depth of PI fluorescence signal (B) and depth coding CLSM images of non-cleared (C1) and *Clear*^{T2}*/4* (C2), *Clear*^{T2}*/8* (C3) and *Clear*^{T2}*/10* (C4) cleared spheroids. Scale bars correspond to 200 µm. n = 5, *p < 0.05, n.s. – non-significant.

The cross-section imaging depth was also analyzed to demonstrate the influence of the *Clear*^{T2} clearing method, as well as the PEG MW in the PI stained spheroids observation by CLSM. This evaluation was performed to determine which method is more suitable for acquiring fluorescence from the interior of the spheroid. In comparison to the non-cleared spheroids, spheroids cleared with *Clear*^{T2} methods allowed the acquisition of images from PI stained cells that were in the interior of the spheroid (Figure 7.11), such is even more evident at the penetration depth of 100 µm (Figure 7.11 B).

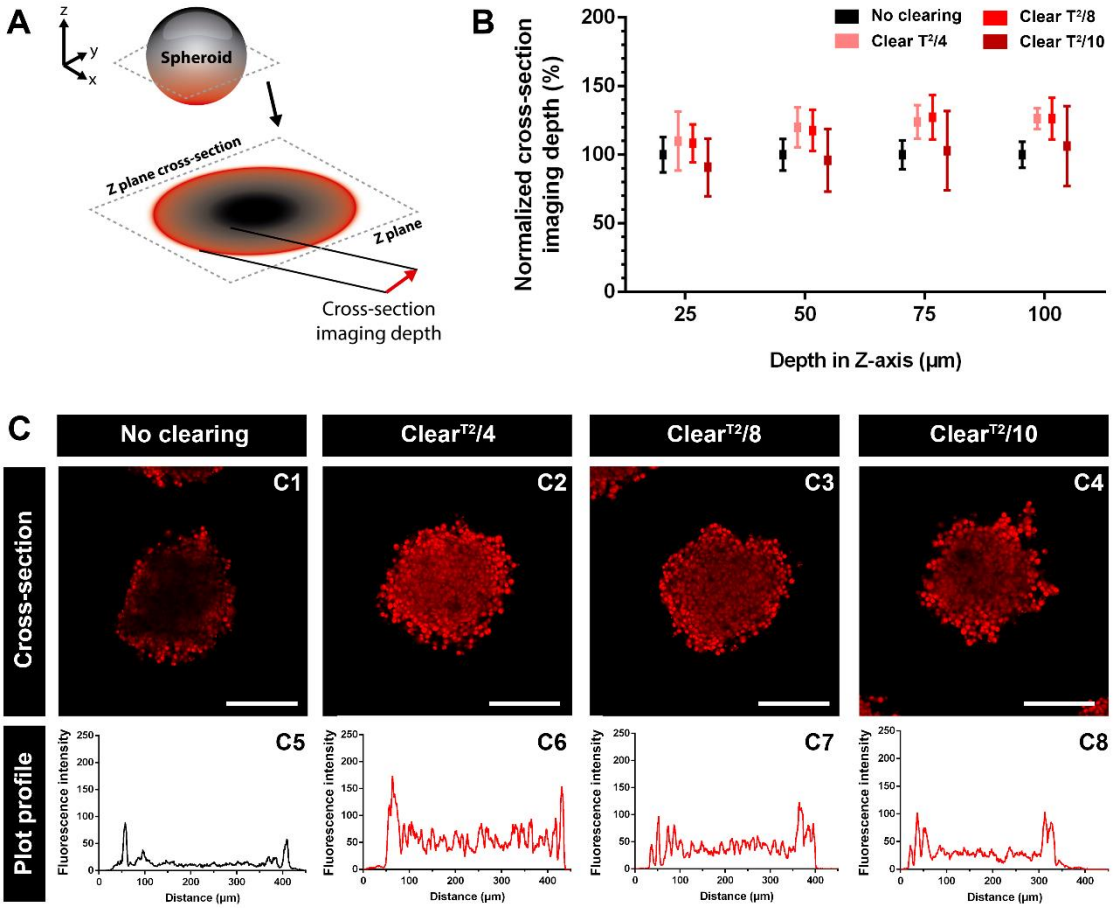

Figure 7.11. NHDF spheroids PI cross-section imaging depth analysis. Schematic illustration of the spheroids PI cross-section imaging depth measurements (A). Spheroids PI cross-section imaging depth analysis (B). Cross-section CLSM images of non-cleared (C1) and *Clear*^{T2}*/4* (C2), *Clear*^{T2}*/8* (C3) and *Clear*^{T2}*/10* (C4) cleared spheroids. Plot profiles of CLSM images of the non-cleared (C5) and *Clear*^{T2}*/4* (C6), *Clear*^{T2}*/8* (C7) and *Clear*^{T2}*/10* (C8) cleared spheroids. CLSM images correspond to a z-tack at a penetration depth of 75 µm. Scale bars correspond to 200 µm. n = 5, *p < 0.05, n.s. – non-significant.

At this penetration depth, the spheroids fluorescence signal in the cross-section improved 24.95 ± 7.50, 24.95 ± 15.07 and 6.31 ± 29.11% when cleared with *Clear*^{T2}*/4*, *Clear*^{T2}*/8* and *Clear*^{T2}*/10*, respectively. To corroborate these observations, plot profiles of the non-cleared and cleared spheroids CLSM cross-section images at 75 µm of penetration depth (Z-axis) were performed (Figure 7.11 C). These graphs display the color intensity of the pixels throughout the spheroid cross-section. As observed in Figure 7.11 C1-C4, without the use of a clearing method, the fluorescence observed within spheroids' core is limited. On the other side, the *Clear*^{T2}*/4* clearing method allowed a better observation of the spheroid´s interior and also the attainment of a higher PI fluorescence intensity, when compared to the other *Clear*^{T2} methods variations (Figure 7.11 C5-C8).

This improved imaging capacity of the *Clear*^{T2}*/4* method may be linked to the smaller size of the polymer chain of PEG 4000. Such may facilitate the PEG distribution and penetration throughout the spheroid and, consequently, the stabilization of the fluorescence probe in

deeper regions, thus allowing a better imaging. In fact, large molecules penetrate slowly into the tissues [50] and lower molecular weights are generally associated with higher diffusion coefficients [51]. Moreover, the use of PEG with a low MW may further contribute to a quicker establishment of the water balance between the clearing solution and the spheroids, leading to an improved penetration of the clearing agent through the spheroid caused by the osmotic pressure [52-55]. In future works, it may be interesting to use PEG with smaller MW (*e.g.* PEG 400 Da) to assess if they further improve the clearing efficacy of the *Clear*^{T2} method.

7.5. Conclusion

Clearing methods have been used to allow the observation and analysis of thick tissue samples and more recently spheroids by fluorescence microscopy, such as CLSM. In this work, we investigated for the first time the influence of PEG MW on *Clear*^{T2} clearing method ability to improve the imaging of PI stained NHDF spheroids. In general, all the Clear^{T2} methods variations (*Clear*^{T2}*/4*, *Clear*^{T2}*/8* and *Clear*^{T2}*/10*) allowed to obtain transparent spheroids without influencing their original size. Compared to the other *Clear*^{T2} methods, the *Clear*^{T2}*/4* improved the imaging of the spheroids in what concerns i) fluorescence intensity preservation, ii) penetration depth and iii) cross-section imaging depth. Such allows us to conclude that the use of PEG 4000 Da can be an improved alternative to the conventional *Clear*^{T2}*/8* methodology for the imaging of thick samples through fluorescence microscopy techniques, namely in the observation of the spheroids' necrotic core or the cellular death induced by a therapeutic molecule by using PI fluorescent staining. Ultimately, this work may contribute to the translation of analytical techniques, commonly used for in 2D cell cultures, to 3D cell cultures and therefore support the application of these models in the pharmaceutical industry.

7.6. References

1. Fennema, E., *et al.*, *Spheroid culture as a tool for creating 3D complex tissues.* Trends in Biotechnology, 2013. 31: 108-115.

2. Achilli, T.-M., Meyer, J., and Morgan, J. R., *Advances in the formation, use and understanding of multi-cellular spheroids.* Expert Opinion on Biological Therapy, 2012. 12: 1347-1360.

3. Breslin, S. and O'Driscoll, L., *Three-dimensional cell culture: the missing link in drug discovery.* Drug Discovery Today, 2013. 18: 240-249.

4. Costa, E. C., *et al.*, *3D tumor spheroids: an overview on the tools and techniques used for their analysis.* Biotechnology Advances, 2016. 34: 1427-1441.

5. Mehta, G., *et al.*, *Opportunities and challenges for use of tumor spheroids as models to test drug delivery and efficacy.* Journal of Controlled Release, 2012. 164: 192-204.

6. Richardson, D. S. and Lichtman, J. W., *Clarifying Tissue Clearing.* Cell, 2015. 162: 246-257.

7. Smyrek, I. and Stelzer, E. H. K., *Quantitative three-dimensional evaluation of immunofluorescence staining for large whole mount spheroids with light sheet microscopy.* Biomedical Optics Express, 2017. 8: 484-499.

8. Gong, X., *et al.*, *Generation of Multicellular Tumor Spheroids with Microwell-Based Agarose Scaffolds for Drug Testing.* PLOS ONE, 2015. 10: e0130348.

9. Sirenko, O., *et al.*, *High-Content Assays for Characterizing the Viability and Morphology of 3D Cancer Spheroid Cultures.* Assay and Drug Development Technologies, 2015. 13: 402-414.

10. Costa, E. C., *et al.*, *Optimization of liquid overlay technique to formulate heterogenic 3D co-cultures models.* Biotechnology and Bioengineering, 2014. 111: 1672-1685.

11. Carvalho, M. P., Costa, E. C., and Correia, I. J., *Assembly of breast cancer heterotypic spheroids on Hyaluronic Acid coated surfaces.* Biotechnology Progress, 2017. 33: 1346-1357.

12. Camões, S., *et al.*, *Human neonatal mesenchymal stem cell spheroids-conditioned medium accelerates skin regeneration.* Toxicology Letters, 2015. 2: S376-S377.

13. Gaspar, V. M., *et al.*, *Folate-targeted multifunctional amino acid-chitosan nanoparticles for improved cancer therapy.* Pharmaceutical Research, 2014: 562-577.

14. Moreira, A. F., *et al.*, *Thermo- and pH-responsive nano-in-micro particles for combinatorial drug delivery to cancer cells.* European Journal of Pharmaceutical Sciences, 2017. 104: 42-51.

15. Jeong, S.-Y., *et al.*, *Co-Culture of Tumor Spheroids and Fibroblasts in a Collagen Matrix-Incorporated Microfluidic Chip Mimics Reciprocal Activation in Solid Tumor Microenvironment.* PLOS ONE, 2016. 11: e0159013.

16. Svoboda, K. and Yasuda, R., *Principles of Two-Photon Excitation Microscopy and Its Applications to Neuroscience.* Neuron, 2006. 50: 823-839.

17. Zhang, X., *et al.*, *Induction of mitochondrial dysfunction as a strategy for targeting tumour cells in metabolically compromised microenvironments*. Nature Communications, 2014. 5: 3295.

18. Yeon, S.-E., *et al.*, *Application of concave microwells to pancreatic tumor spheroids enabling anticancer drug evaluation in a clinically relevant drug resistance model*. PLOS ONE, 2013. 8: e73345.

19. Langenbach, F., *et al.*, *Generation and differentiation of microtissues from multipotent precursor cells for use in tissue engineering*. Nature Protocols, 2011. 6: 1726-1735.

20. Vidi, P.-A., Bissell, M. J., and Lelièvre, S. A., *Three-dimensional culture of human breast epithelial cells: the how and the why*, *Epithelial Cell Culture Protocols*, S. H. Randell and L. M. Fulcher, Editors. 2013, Humana Press: Totowa, New Jersey. p. 193-219.

21. Hama, H., *et al.*, *Scale: a chemical approach for fluorescence imaging and reconstruction of transparent mouse brain*. Nature Neuroscience, 2011. 14: 1481-1488.

22. Kuwajima, T., *et al.*, *ClearT: a detergent- and solvent-free clearing method for neuronal and non-neuronal tissue*. Development, 2013. 140: 1364-1368.

23. Ke, M.-T., Fujimoto, S., and Imai, T., *SeeDB: a simple and morphology-preserving optical clearing agent for neuronal circuit reconstruction*. Nature Neuroscience, 2013. 16: 1154-1161.

24. Decroix, L., *et al.*, *Tissue clearing for confocal imaging of native and bio-artificial skeletal muscle*. Biotechnic & Histochemistry, 2015. 90: 424-431.

25. Azaripour, A., *et al.*, *A survey of clearing techniques for 3D imaging of tissues with special reference to connective tissue*. Progress in Histochemistry and Cytochemistry, 2016. 51: 9-23.

26. Boutin, M. E. and Hoffman-Kim, D., *Application and assessment of optical clearing methods for imaging of tissue-engineered neural stem cell spheres*. Tissue Engineering Part C: Methods, 2015. 21: 292-302.

27. Chen, Y. Y., *et al.*, *Clarifying intact 3D tissues on a microfluidic chip for high-throughput structural analysis*. Proceedings of the National Academy of Sciences, 2016. 113: 14915-14920.

28. Tainaka, K., *et al.*, *Chemical Principles in Tissue Clearing and Staining Protocols for Whole-Body Cell Profiling*. Annual Review of Cell and Developmental Biology, 2016. 32: 713-741.

29. Seo, J., Choe, M., and Kim, S. Y., *Clearing and Labeling Techniques for Large-Scale Biological Tissues*. Molecules and Cells, 2016. 39: 439-446.

30. Feuchtinger, A., Walch, A., and Dobosz, M., *Deep tissue imaging: a review from a preclinical cancer research perspective*. Histochemistry and Cell Biology, 2016. 146: 781-806.

31. Morgenstern, J., *et al.*, *Effect of PEG molecular weight and PEGylation degree on the physical stability of PEGylated lysozyme*. International Journal of Pharmaceutics, 2017. 519: 408-417.

32. Treetharnmathurot, B., *et al.*, *Effect of PEG molecular weight and linking chemistry on the biological activity and thermal stability of PEGylated trypsin.* International Journal of Pharmaceutics, 2008. 357: 252-259.

33. Kessel, S., *et al.*, *Real-time viability and apoptosis kinetic detection method of 3D multicellular tumor spheroids using the Celigo Image Cytometer.* Cytometry A, 2017. 91: 883-892.

34. Galateanu, B., *et al.*, *Impact of multicellular tumor spheroids as an in vivo-like tumor model on anticancer drug response.* International Journal of Oncology, 2016. 48: 2295-2302.

35. Yu, T., *et al.*, *Rapid and prodium iodide-compatible optical clearing method for brain tissue based on sugar/sugar-alcohol.* Journal of Biomedical Optics, 2016. 21: 081203.

36. Epp, J. R., *et al.*, *Optimization of CLARITY for Clearing Whole-Brain and Other Intact Organs.* eNeuro, 2015. 2: ENEURO.0022-0015.2015.

37. Fretaud, M., *et al.*, *High-resolution 3D imaging of whole organ after clearing: taking a new look at the zebrafish testis.* Scientific Reports, 2017. 7: 43012.

38. Napolitano, A. P., *et al.*, *Scaffold-free three-dimensional cell culture utilizing micromolded nonadhesive hydrogels.* Biotechniques, 2007. 43: 494-500.

39. Ke, M.-T., Fujimoto, S., and Imai, T., *Optical clearing using SeeDB.* Bio-protocol, 2014. 4: e1042.

40. Rasband, W. S., *ImageJ.* http://rsbweb. nih. gov/ij/, 2008.

41. Kurihara, D., *et al.*, *ClearSee: a rapid optical clearing reagent for whole-plant fluorescence imaging.* Development, 2015. 142: 4168-4179.

42. Grist, S. M., *et al.*, *On-chip clearing of arrays of 3-D cell cultures and micro-tissues.* Biomicrofluidics, 2016. 10: 044107.

43. Klaka, P., *et al.*, *A novel organotypic 3D sweat gland model with physiological functionality.* PLOS ONE, 2017. 12: e0182752.

44. Masson, A., *et al.*, *High-resolution in-depth imaging of optically cleared thick samples using an adaptive SPIM.* Scientific Reports, 2015. 5: 16898.

45. Yu, T., *et al.*, *RTF: a rapid and versatile tissue optical clearing method.* Scientific Reports, 2018. 8: 1964.

46. Yushchenko, D. A. and Schultz, C., *Geklärte Gewebeproben für die optische Anatomie.* Angewandte Chemie, 2013. 125: 11151-11154.

47. Lasagni, A., *et al. Rapid fabrication of biocompatible hydrogels microdevices using laser interference lithography. in* Bioengineered and Bioinspired Systems IV, SPIE Europe Microtechnologies for the New Millennium, 2009.

48. Jayaramudu, T., *et al.*, *Preparation and characterization of poly(ethylene glycol) stabilized nano silver particles by a mechanochemical assisted ball mill process.* Journal of Applied Polymer Science, 2016. 133: 43027.

49. Hou, B., *et al.*, *Scalable and DiI-compatible optical clearance of the mammalian brain.* Frontiers in Neuroanatomy, 2015. 9: 19.

50. Kiernan, J. A., *Formaldehyde, formalin, paraformaldehyde and glutaraldehyde: what they are and what they do.* Microscopy today, 2000. 1: 8-12.

51. Zhu, D., *et al.*, *Recent progress in tissue optical clearing.* Laser & Photonics Reviews, 2013. 7: 732-757.

52. Oliveira, L., *et al.*, *Optical clearing mechanisms characterization in muscle.* Journal of Innovative Optical Health Sciences, 2016. 9: 1650035.

53. Tuchin, V. V., *et al.*, *Light propagation in tissues with controlled optical properties.* Journal of Biomedical Optics, 1997. 2: 401-418.

54. Carneiro, I., *et al.*, *Water Content and Scatterers Dispersion Evaluation in Colorectal Tissues.* Journal of Biomedical Photonics & Engineering, 2017. 3: 040301.

55. Carneiro, I., *et al.*, *Simple multimodal optical technique for evaluation of free/bound water and dispersion of human liver tissue.* Journal of Biomedical Optics, 2017. 22: 125002.

Chapter 8

Concluding Remarks and Future Trends

8.1. Concluding Remarks and Future Trends

The mortality rate associated with cancer still remains very high. To revert this situation, several preclinical and clinical trials are currently being performed by multidisciplinary teams. In the preclinical trials, 2D cell cultures are known as the gold standard *in vitro* model. Nevertheless, these cell cultures are unable to fully represent the human tumors properties, such as cellular organization and functionalities. Therefore, they are not able to realistically predict the therapeutic outcome potential of compounds in human tumors.

Having this in mind, researchers begin to develop 3D cell culture models, like spheroids, that are more prone to mimic human solid tumors and therefore allow the researchers to exclude, in an early stage, a great number of unsuitable therapeutic candidates that otherwise would have to be tested on animal models.

Although, the analysis of the therapeutics' effect on spheroids is still challenging due to the limited availability of protocols, techniques and equipment required to perform such assays. In this regard, the analysis of spheroids by CLSM is unsatisfactory due to its inability to image large samples due to light scattering phenomenon that decreases the light penetration. To overcome this drawback spheroids can be cut into thin slices. However, this procedure is very time-consuming, organic solvent dependent, and can also compromise the initial structure of the spheroids.

Alternatively, optical clearing methods, that were originally developed and optimized to image biological samples obtained from animals, can be explored for improving the imaging of spheroids by CLSM. These methods are used to homogenize the RI across the sample for improving their transparency as well as reducing the light scattering phenomenon.

Till nowadays, SeeDB, TDE, *Clear*^{T2}, FocusClear™, BABB, Sca*l*e, CUBIC and CLARITY optical clearing methods have been used for enhancing the quality of spheroids imaging. In this thesis, the *Clear*^{T} method was used for the first time for the analysis of spheroids and the *Clear*^{T2} was optimized to improve the imaging of dead cells within spheroids by CLSM.

Overall, both *Clear*^{T} and *Clear*^{T2} methods prompted spheroids transparency without affecting their initial structure since no significant differences on spheroids' size were noticed between the cleared and non-cleared spheroids. Furthermore, the *Clear*^{T} method did not impact significantly on the fluorescence of the PI, while the *Clear*^{T2} method performed using PEG 4000 Da improved significantly the intensity of the PI signal. Such results demonstrate that PEG can indeed stabilize the PI-DNA interactions. Moreover, the analysis of the influence of the clearing methods tested on the PI imaging depth and cross-section imaging depth revealed that both

methods can improve the imaging of the entire spheroids, *i.e.* the PI signal was acquired deeper within spheroid and more PI signal was detected in the interior of the spheroids.

Based on these observations, the *Clear*^{T} and *Clear*^{T2} methods may be used to further enhance the imaging of the cellular death in spheroids. Such is fundamental for the development of new anticancer compounds. Moreover, these methods may also be helpful for the tracking of therapeutics (*e.g.* drugs and nanoparticles) penetration and dispersion in spheroids, which is crucial for increasing the application of these models by the pharmaceutical industry.

In the near future, other optimizations of the *Clear*^{T} and *Clear*^{T2} methods can be pursued in order to achieve a 360º detailed view of the spheroids in a lower period of time by CLSM. To accomplish that, the correlation between spheroids' size and clearing solutions incubation times may be investigated, in order to determine the optimal period of time required to achieve RI homogenization in spheroids of specific diameters. On the other hand, since the clearing capacity of the methods is influenced by the location and concentration of the clearing agent in the sample, it would be interesting to investigate physical or chemical procedures that are able to enhance the clearing agent penetration. The use of an electrical field or other agitation conditions during the spheroids incubation into the clearing solutions may be hypothesized for enhancing clearing agents' entrance into the spheroids.

Furthermore, the development of optical clearing methods that can allow the imaging of the cells without damaging or killing them will impact on the realization of time-course experiments. In fact, all the clearing methods described so far induce damage on cells (*e.g.* cells fixation and organic solvents utilization). Therefore, it is crucial to identify a RI-matching agent that does not harm the spheroids. In recent studies, Iodixanol has been investigated as a non-toxic medium supplement and RI-matching agent that improves the image quality in live-imaging experiments involving primary cell cultures, planarians, zebrafish and human cerebral organoids.

The development of an unharmful optical clearing method will also open several possibilities in terms of the therapeutic applications, *i.e.* an increased light penetration in cleared tissues may be useful for photo-based therapies, as well as for drug-delivery monitoring.

Lastly, further investigations may also allow the application of other clearing methods, that up to now have not been used for spheroids analysis, like 3DISCO.